FORSCHUNGSZENTRUM JÜLICH GmbH

Institut für Chemie und Dynamik der Geosphäre 4: Erdöl und Organische Geochemie

The generation and migration of sulphur-rich petroleums in a low-maturity carbonate source rock sequence from Italy

Rolando di Primio

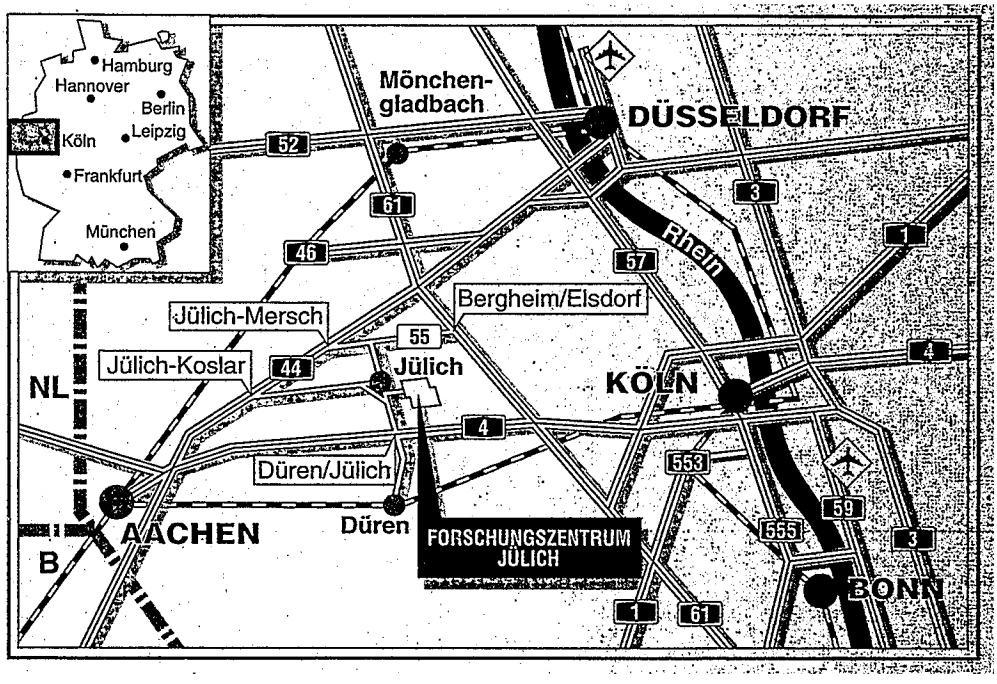

Berichte des Forschungszentrums Jülich ; 3110
ISSN 0944-2952
Institut für Chemie und Dynamik der Geosphäre 4:
Erdöl und Organische Geochemie Jül-3110
D38 (Diss. Universität Köln)

Zu beziehen durch: Forschungszentrum Jülich GmbH · Zentralbibliothek
D-52425 Jülich · Bundesrepublik Deutschland
Telefon: 02461/61-6102 · Telefax: 02461/61-6103 · Telex: 833556-70 kfa d

The generation and migration of sulphur-rich petroleums in a low-maturity carbonate source rock sequence from Italy

Rolando di Primio

Zusammenfassung

Auf der Basis eines interdisziplinären Ansatzes wurden die Genese und Migration von Schwerölen am Beispiel eines niedrig reifen karbonatischen Muttergesteins der Trias Italiens untersucht. Dabei sind organisch-geochemische, sedimentpetrographische und petrophysikalische Methoden an Proben aus vier verschiedenen Bohrungen, in denen das Muttergestein in unterschiedlichen Tiefen angetroffen worden war, angewendet worden.

In der untersuchten Muttergesteinsformation wurden vier Lithofazien unterschieden: Mudstones/Wackestones, Laminite, Tonsteine und Dolomite. Die Mudstones und Wackestones enthielten auch Stylolithe und Lösungssäume, die gesondert beprobt wurden.

Die Mudstone/Wackestone Lithofazies war durch geringe Mengen an organischem Material (∅ TOC=0.28%) und einem Kerogen vom Typ II charakterisiert. Laminite, Stylolithe und Lösungssäume enthielten in der Regel höhere Mengen an organischem Material (∅ TOC=1.2%) und waren durch ein Kerogen Typ II-S charakterisiert. Die Tonsteine enthielten die höchsten Mengen an organischem Material (∅ TOC=8.9 %) und enthielten, in der Regel, ein Kerogen Typ I-S. Die Dolomite waren durchweg mit Schweröl imprägniert und fungierten als intraformationelle Reservoire.

Die Muttergesteinsformation wurde in einem „Tidal Flat" Milieu mit erhöhten Salinitäten abgelagert. Dabei wurde die Mudstone/Wackestone Lithofazies im subtidalen Bereich, die Laminite und Tonsteine im intertidalen, und die Dolomite im supratidalen Bereich abgelagert. Die hohen Gehalte an organischem Material waren durch das ungehinderte Wachstum von Algenmatten im intertidalem Bereich bedingt. Der hohe organische Schwefelgehalt der Kerogene ist durch das Fehlen von Eisen im karbonatisch/evaporitischem Ablagerungsraum zu erklären. Die Reduktion von Sulphat zu Schwefelwasserstoff durch anaerobe Microorganismen führt zu einem Überangebot an H_2S im Porenwasser des Systems. Dieser Überschuß führt entweder zu der Reaktion von Schwefelwasserstoff mit Eisen(II) zu Pyrit, oder bei fehlendem Eisen zum Einbau von Schwefel in die organische Substanz. Die Inkorporation von Schwefel, gepaart mit einer intensiven bakteriellen Aufarbeitung der abgelagerten Algenmatten, führte in den Tonsteinen zur Entstehung von einem schwefelreichen und wasserstoffreichen Kerogen Typ I-S.

Die Reife des Muttergesteins in den vier Bohrungen wurde mittels Rock-Eval Tmax; einer Reihe von Komponenten aus der Gruppe der aromatischen Kohlenwasserstoffe (Methylphenantrene, Methyldibenzothiophene), und mit Hilfe von Hopan- und Steranisomerisierungsverhältnissen (gesättigte Kohlenwasserstoffe) bestimmt. Durch diese Methoden konnte festgestellt werden, daß die Muttergesteinsformation in allen Bohrungen eine Reife

unter 0.5% Vitrinitreflexion besaß. Mit zunehmender Teufe, von 2000 bis 4500 m, wurde zwar eine geringe Reifezunahme festgestellt, die aber nicht quantifiziert werden konnte.

Alle Lithofazien waren durch hohe Extraktgehalte charakterisiert. Diese sind das Produkt einer frühen Erdölgenese durch preferentielle Spaltung von C-S oder S-S Bindungen im Kerogen. Die experimentelle Simulation der Erdölgenese mit Kerogenen der Muttergesteinsformation (Typ I-S und II-S) erlaubte die Bestimmung von reaktionskinetischen Parametern, die die Schwerölgenese beschreiben. Die maximale Schwerölgeneserate aus schwefelreichen organischem Material wurde demnach durch eine Aktivierungsenergie von 53 kcal und einem Frequenzfaktor von $3*10^{18}$ 1/min charakterisiert. Unter geologischen Bedingungen bedeutet dies, daß bei Heizraten von 0.53 bis 53°/Ma die stärkste Genese von schwerem, schwefelreichem Öl bei Temperaturen zwischen 110° und 125°C stattfindet.

Die früh generierten Schweröle waren durch eine Prädominanz von schwefelhaltigen Verbindungen gekennzeichnet. Diese Komponenten, die vor allem bei der Pyrolyse von dem organischen Material entstanden, wurden gezielt untersucht, um Fazies- oder Reifeindikatoren zu finden. Drei verschiede Komponentenverhältnisse wurden gefunden, die möglicherweise als solche Indikatoren verwendet werden können. Dabei handelt es sich um das Verhältnis von 2,3-Dimethylthiophen zu 2,3,5-Trimethylthiophen (2,3/2,3,5 Ratio) als Faziesindikator; das Verhältnis von Thiophenen mit geradlinigem Kohlenstoffgerüst zu Thiophenen mit steroidalen Kohlenstoffgerüst als Indikator für eine bakterielle Überprägung, und das Verhältnis von Isopropylthiophen zu 2,3,4-Trimethylthiophen als Reifeindikator. Diese Komponenten-verhältnisse müßen allerdings noch anhand von anderen Probensequenzen bestätigt und kalibriert werden.

Die im natürlichem System generierten Kohlenwasserstoffe sind auch zum Teil abgegeben worden. Die Expulsion von Erdöl erfolgte in Form eines Ölphasenflusses ohne erkennbare Fraktionierungseffekte. Die Expulsionseffizienz war dabei von der Versenkungstiefe des Muttergesteins abhängig. Die Abhängigkeit von Druck und Expulsionseffizienz konnte auch experimentell nachgewiesen werden.

Eine Massenbilanzierung der Genese und Expulsion von Kohlenwasserstoffe aus der untersuchten Muttergesteinsformation ergab folgende Ergebnisse: Insgesamt wurde etwa 20% des verfügbaren organischen Materials in Kohlenwasserstoffe umgewandelt. Davon wurde aus Stylolithen und Lösungssäumen 30 bis 80% abgegeben (in Abhängigkeit der Teufe), aus den Tonsteinen erfolgte die höchste Abgaberate mit einem Durchschnitt von 70%. Mudstone/Wackestone Proben und Laminite waren nur in untergeordnetem Maße an der Expulsion von Kohlenwasserstoffen beteiligt.

Contents

Acknowledgements

This study would not have been possible without the support given by AGIP S.p.A., San Donato Milanese (Italy), and the Institute for Petroleum and Organic Geochemistry (ICG-4), Research Center Jülich (Germany). The author gratefully acknowledges the assistance of AGIP staff members Dr. M. A. Chiaramonte, Dr. A. Riva, F. Mosca, O. Borromeo, Dr. K. Leischner and B. Maragna.

The author would like thank Prof. D. Leythaeuser for suggesting the topic of this dissertation and for his and Prof. D.H. Welte's support and advice during my time at ICG-4. Very special thanks are due to Dr. B. Horsfield for his constant interest, encouragement and assistance in the course of this dissertation.

Thanks for analytical support are due to M. Radke, R.G. Schaefer, H.J. Schenk and R. Littke. The technical assistance by F. Leistner, A. Ropertz, H. Willsch, S. de Waal, W. Laumer, U. Disko, H. Hardelauf, A. Richter, E. Biermans, W. Benders, H. Schnitzler, R. Harms, J. Hoeltkemeier, and F.J. Keller is greatfully acknowledged.

I would like to thank my freinds and colleagues at ICG-4 for the great time we had.

This thesis would never have been completed without the help and support provided by my parents, thanks for the invaluable assistance.

Finally, I want to thank my wife, Bettina, and my daughters Teresa and Alena, who somehow always managed to get my mind off scientific problems as soon as I got home.

Abbreviations

A	Pre-exponential factor
ARO	Aromatic compounds
As	Asphaltenes
CPI	Carbon Preference Index
DMT	Dimethylthiophene
DNR	Dimethylnaphthalene Ratio
DPR	Dimethylphenanthrene Ratio
E	Activation energy (kcal/mol)
ENR	Ethylnaphthalene Ratio
FID	Flame Ionisation Detector
GC	Gas Chromatography
GC/MS	Gas Chromatography/Mass Spectrometry
GOR	Gas-Oil Ratio
HC	Hydrocarbon
HECD	Hall Electrolytic Conductivity Detector (HALL®)
HI	Hydrogen Index
HPLC	High Performance Liquid Chromatography
ITR	Isoprenoid-Thiophene Ratio
LHCPI	Light Hydrocarbon Preference Index
MDR	Methyldibenzothiophene Ratio
MNR	Methylnaphthalene Ratio
MPI	Methylphenathrene Index
MPLC	Medium Pressure Liquid Chromatography
MPR	Methylphenanthrene Ratio
MSSV	Microscale sealed vessel (pyrolysis)
MT	Methylthiophene
NSO	Heteroatomic compounds
OI	Oxygen Index
OSC	Organic Sulphur Compounds
OSHP	Open System Hydrous Pyrolysis
PI	Production Index
PyGC	Pyrolysis Gas Chromatography
REE	Relative Expulsion Efficiency
Ro	Vitrinite reflectance
SAT	Saturated compounds
SEM	Scanning Electron Microscope
SOM	Soluble Organic Matter
TC	Total Carbon
TMT	Trimethylthiophene
TNR	Trimethylnaphthalene Ratio
TOC	Total Organic Carbon

1 Introduction

Carbonate rocks are unique in that they serve both as source beds and as reservoir rocks for numerous oil and gas fields, some of which are among the largest in the world (e.g. Middle East, Mexico, western Canada). Their importance as reservoirs is underscored by the fact that they contain around 46 percent of the oils in the giant oil fields of the world (Carmalt and St. John, 1986). Carbonate-evaporitic and carbonate-siliceous rocks are the putative sources of large quantities of immature to marginally mature, usually non-biodegraded heavy oil deposits (Fu Jia Mo et al., 1984; Powell, 1984; Zumberge, 1984; Tannenbaum and Aizenshtat, 1985). Even some lacustrine source deposits designated as "oil shales", such as the Green River Formation, Uinta basin, are in terms of their lithology carbonate-dominated source beds (Tissot and Welte, 1984). Despite their significant economic importance, some controversy persists concerning the effectiveness of carbonate rocks as major sources of petroleum. This is probably due to the fact that carbonate source rocks have, as compared to shales, generally lower contents of organic matter, lower degrees of sediment compactability (which provides a driving force for petroleum expulsion), and lower presumed catalytic activity due to the scarcity of clay minerals (Palacas, 1983). Early workers therefore assumed that carbonates were not suitable as petroleum source rocks (Owen, 1964; Hunt, 1967). In the past decades geological and geochemical evidence provided by a multitude of authors has proved the efficacy of carbonate and carbonate-evaporitic rock types as sources of petroleum (among others: Grabowski, 1984; Oehler, 1984; Palacas et al., 1984; Powell, 1984; ten Haven et al., 1988; Palacas, 1989; Sassen and co-workers, 1987, 1988, 1990).

One of the main differences between shales and carbonates lies in their diagenetic evolution during burial. The porosity reduction in clastic sediments is dominated by sediment compaction and physical rearrangement of mineral grains while chemical processes control the porosity and permeability reduction in carbonates (Scholle and Halley, 1985). The initial porosity of carbonate muds is comparable to porosities observed in clastic sediments. Up to a depth of around 300 m these sediments compact in a similar fashion. With increasing depth of burial chemical diagenesis becomes more important. Carbonate dissolution and reprecipitation as well as recrystallisation are important processes during diagenesis of carbonates because they control the distribution and concentration of originally disseminated organic matter and other non-carbonate material such as clay minerals. Organic matter incorporated into a carbonate mud does not participate in the pressure solution process. Due to its insoluble nature, organic matter (together with clay minerals, pyrite, quartz grains, etc.) is enriched at the sites of pressure solution (stylolites, solution seams, fitted fabrics) thus forming zones of enhanced

hydrocarbon potential (di Primio, 1990; Leythaeuser et al., in press). This process can ultimately result in a lithologic unmixing on centimetre to meter scales by removing carbonate from one place and precipitating it in another (Scholle and Halley, 1985; Ricken, 1986).

The processes and efficiencies of hydrocarbon generation and migration have been studied in great detail in source rocks of siliciclastic lithologies. The generation of hydrocarbons from kerogen throughout the oil window has been demonstrated (e.g. Tissot et al., 1975; Leythaeuser et al., 1980b) and mass-balanced (Rullkötter et al., 1988) and the kinetic parameters of these reactions have been determined by a variety of methods (Ungerer and Pelet, 1987; Quigley et al. 1987; Burnham et al., 1988; Schaefer et al., 1990). The processes and effects of petroleum expulsion have been documented in great detail (Jones, 1978; McAuliffe, 1978; Momper, 1978; Mackenzie et al., 1987; Leythaeuser et al., 1988a, 1988b; Stainforth and Reinders, 1990; Leythaeuser and Poelchau, 1991; Ropertz, 1994).

The generation and expulsion of hydrocarbons in carbonate source rocks is much less well understood. While a fairly large amount of information has meanwhile been accumulated regarding the geochemical characterisation of carbonate source rocks by means of typical biomarkers or oil compositions (Palacas et al., 1984; Powell, 1984; Tannenbaum and Aizenshtat, 1985; Orr, 1986; ten Haven et al., 1988; Palacas, 1989; Sinninghe Damsté et al., 1989, 1993), few maturity and migration studies have been undertaken (Grabowski, 1984; Palacas et al., 1984; Sassen et al., 1987; di Primio, 1990; Leythaeuser et al., in press).

Carbonate source rocks have been considered to generate and expel heavy, NSO-rich oils at low levels of thermal maturity (Grabowski, 1984; Palacas, 1984; Tannenbaum and Aizenshtat, 1985). These so called heavy or extra-heavy crude oils and bitumens are petroleum or petroleum-like liquids or semisolids occurring naturally in porous and fractured media.

A definition of heavy or extra-heavy crude oils or bitumens was proposed by a working group consisting of petroleum geologists from the petroleum industry and governmental institutions during the second international conference on the future of heavy crude and tar sands in Venezuela, 1982. The working group reached the conclusion that viscosity should be used to differentiate between crude oils and bitumens, subsequently density should be used to differentiate among extra-heavy crude oils, heavy crude oils, and other crude oils (Martinez, 1982).

According to the agreement of the Venezuelan working group bitumens have viscosities greater that 10000 mPa*s, while crude oils have viscosities less than or equal to 10000 mPa*s. These viscosities are gas-free as measured and referenced to original reservoir temperature. Extra-heavy crude oils have densities greater than 1000 kg/m^3 at 15.6°C (60°F) and atmospheric pressure (API gravities less than 10°). Heavy crude oils have densities from 934

to 1000 kg/m^3 (API gravities from 20° to 10°) inclusive. Crude oils with densities less than 934 kg/m^3 (API gravities greater than 20°) may be classified as medium, light, or other crude oils.
Heavy and extra-heavy crude oil and bitumen occurrences are widespread, being known on all continents except Antarctica, at depths of up to 4000 meters, in rocks of various lithologies and ages, and under all climatic regimes both on and offshore (Martinez, 1982).
Heavy and extra-heavy crude oils are generally considered to be the result of degradation (biodegradation, oxidation) of normal oils in the reservoir. The Athabasca oil sands are a typical example for this kind of degraded oils. Non-biodegraded heavy oils are considered to be the products of early petroleum generation of oil-prone, sulphur-rich kerogens (Baskin and Peters, 1992). Oils of this type are found for example in the southern USA, Venezuela, Italy and West Africa (Tissot and Welte, 1984; Baskin and Peters, 1992; Mattavelli et al., 1993).
Early hydrocarbon generation from sulphur-rich kerogens is controlled by the abundance of weak heteroatomic bonds in the kerogen which break under lower thermal stress than the more ubiquitous carbon-carbon bonds (Tannenbaum and Aizenshtat, 1984; Orr, 1986; Baskin and Peters, 1992). Among the first to associate early oil generation with sulphur-rich kerogens were Granch and Posthuma (1974), who proposed that heavy oils from the Maracaibo basin in Venezuela were early generation products from the sulphur-rich La Luna source rocks (Cretaceous). Bostick et al. (1978), Walker et al. (1983) and Tannenbaum and Aizenshtat (1984) noted that oil generation from the Monterey formation and from Senonian shales, both of which are characterised by elevated sulphur contents, occurred at anomalously low temperatures. Lewan (1985) and Hunt (1991) derived lower activation energies for petroleum generation reactions from sulphur-rich kerogens (as compared to kerogens with low amounts of organic sulphur), and attributed them to the high heteroatom contents. While this theory of early heavy oil generation from sulphur-rich kerogens due to preferential cleavage of weak heteroatom bonds is relatively well founded (see Baskin and Peters, 1992 and references therein) only two sets of data (from Lewan, 1985, which was used again by Hunt et al., 1991, and from Tissot et al., 1987) exist on the kinetics of this kind of bond-cracking reaction.
It is generally assumed that heavy, viscous oils are incapable of migrating long distances, in fact Tissot and Welte (1984) state that "in a sense, heavy oil accumulations provide their own seal" due to their high viscosity which makes them immobile at permeabilities where normal oils can readily migrate.
The generation and migration of heavy oils from sulphur-rich carbonate-evaporitic source rocks is thus still a poorly understood subject in petroleum geochemistry.

1.1 Objectives

Problems in explaining the origin of heavy oils in a petroliferous area of Italy, and especially problems with respect to modelling the onset of petroleum generation and migration in this same area led to the initiation of the present study.

The specific goals of this study, which was performed at the Institute of Chemistry and Dynamics of the Geosphere 4: Petroleum and Organic Geochemistry (ICG-4) of the Forschungszentrum Jülich GmbH (KFA) and in co-operation with AGIP S.p.A. Italy, were as follows:

- to identify and possibly quantify the processes leading to the generation and migration of the heavy, sulphur rich oils produced in one of the oil fields of the study area;
- to establish for a known carbonate source rock sequence of the study area a chemical mass balance for the hydrocarbon generation and expulsion processes throughout the entire liquid window with special emphasis on the generation and migration of heavy oils;
- to elucidate the compositional effects associated with oil expulsion, i.e. to compare, especially, molecular patterns of reservoired oils with those of: i) residual oils left in the source rock after expulsion, and ii) the expelled oil calculated from mass balance considerations;
- to establish molecular criteria characterising the chemical maturity stages of carbonate source rocks. While chemical maturity parameters are well known and widely used for shale source rocks, the maturity assessment of carbonate source rocks needs to be improved;
- to test previously established concepts for recognition of petroleum generation and migration in carbonate source rocks (di Primio, 1990; Leythaeuser et al., in press);
- to obtain geological, chemical and petrophysical data pertinent to the development of pore fluid overpressures and fractures by: i) measurements of natural samples, and ii) controlled laboratory experiments.

In order to fulfil the above outlined objectives the present study followed two basic approaches:

a.) Geochemical analysis of natural systems: recognise the effects of petroleum generation and migration processes using detailed microscopical, sedimentological, organic geochemical and fluid inclusion studies of the core samples of this carbonate source rock sequence subjected to a wide range of burial depths.

b.) Experimental simulation: conduction of controlled laboratory experiments including hydrous pyrolysis, microscale sealed vessel (MSSV) pyrolysis and high-pressure high-

temperature generation/expulsion experiments using the least mature samples of the same source rock sequence.

The basic concepts for this AGIP/KFA co-operation were developed on the basis of the results of a previous study of similar objectives, however, for another petroliferous basin in Italy (di Primio, 1990; Leythaeuser et al., in press). The main results of these studies can be summarised as follows:

- The carbonate source rock studied had a heterogeneous internal distribution of organic matter, which resulted largely from an internal redistribution of carbonate by pressure solution processes.
- The diagenetic concentration process together with mechanical compaction led to the formation of a three dimensional kerogen network, which is an important prerequisite for effective petroleum generation and expulsion.
- Carbonate dissolution and reprecipitation during chemical compaction led to a distinct reduction of porosity in the limestone portions directly adjacent to dissolution sites. Solution seams and stylolites were thus surrounded by tightly cemented rims.
- Effects of petroleum migration were recognised on a molecular level based on mass balances between selected sample pairs (limestone and corresponding solution seam or stylolite).
- Petroleum expulsion occured initially in a lateral direction, following the orientation of solution seams and stylolites, into fractures.

1.2 Geological and Geochemical Background

For proprietary reasons no details on the location or of the stratigraphy of the study area can be given. The geological evolution of this region, from reservoir and source rock deposition up to the present, plays a crucial role in the timing of both hydrocarbon generation and expulsion processes. It is therefore presented below using coded formation names.

The study area is part of a petroliferous basin situated in the Mediterranean Sea. It is fundamentally seen as part of the African continental margin that played the role of foreland during the Tertiary Alpine compression. This basin is one of the tectonic troughs which, during the Lias, were part of a complex geographic pattern along the African margin of the opening Tethys. The basin now belongs to a plateau, partly engaged in continental subduction under southeast verging nappes. The plateau resulted from a bulge of the subducting African plate. It is a structurally high area, sloping to the west and south, with exposures of mainly Tertiary limestones and Miocene-Pliocene volcanics. The subsurface of this region consists primarily of carbonate rock sequences and ranges from Triassic to late Miocene age. It indicates the persistence of basin facies during its geologic history (Sestini and Flores, 1984).

The present structure of the Plateau is characterised by intense east-northeast, northeast, and west-northwest faulting, dissecting gentle Upper Cretaceous and Pliocene anticlines which serve as traps for oil (Brosse et al., 1989). West of the plateau, the foreland margin slopes under sediments and olistostromes of the European continental margin.

This area has been extensively explored by oil drilling; the achieved knowledge allows a paleogeographic history reconstruction that is represented as a lithostratigraphic sketch in Figure 1 (after Novelli *et al.*, 1988).

During the Mesozoic the study area underwent, along with other periadriatic regions, a geological evolutionary trend typical of a passive continental margin. Throughout the Norian the area was characterised by carbonate sedimentation, represented by tidal-flat dolomites and dolomitic limestones, which today form the principal reservoir strata of this region (Formation A). At the end of the Rhaetian, the carbonate platform began to break up due to transcurrent faulting, this lead to the deposition of euxinic lagoonal facies of the source rock Formation B in Rhaetian and marl-shale sequences with a distinctly lower hydrocarbon potential of the Formation C in Early Hetangian, where tectonic activity severely affected the Triassic platform, giving rise to the development of basinal conditions which continued until the Bathonian.

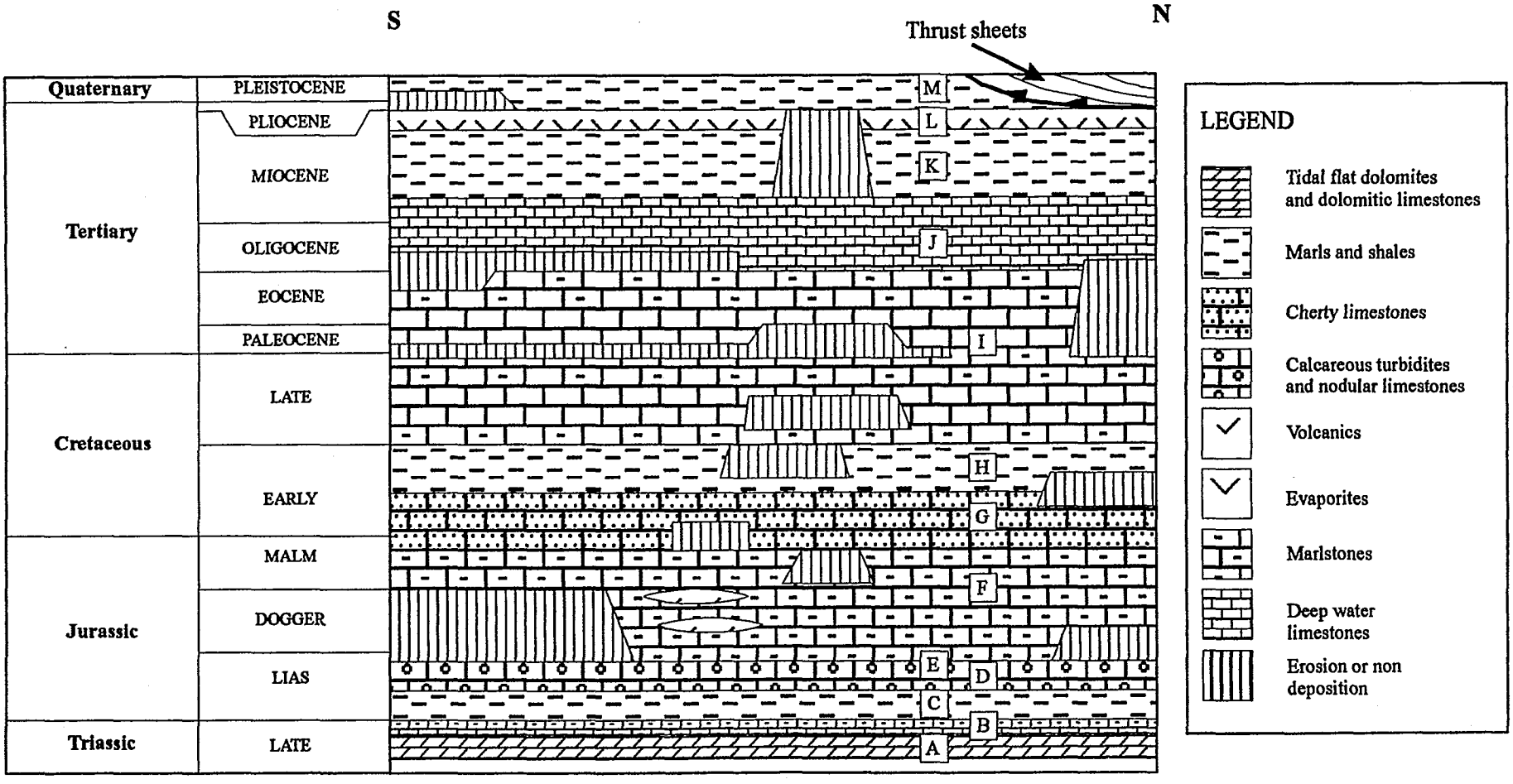

Figure 1: Lithostratigraphic sketch of the study area (after Novelli et al., 1988).

The early development of the Alpine Tethys, in response to the opening of the central-southern Atlantic (Dewey et al., 1973), caused rapid crustal subsidence and drowning of the Triassic-Liassic carbonate platform.

In the Sinemurian to Pliensbachian calcareous turbidites and nodular limestones (Formations D and E) followed, due to the continuation of subsidence.

During Toarcian-Tithonian, synsedimentary tectonics caused the facies variations observed in the Formation F and volcanic activity, represented by large local seamounts.

The cherty limestones of the Formation G characterised pelagic sedimentation that is common in the Tethys. Pelagic sedimentation continued during Early Cretaceous, giving rise to the sedimentation of marly limestones of the Formation H.

Starting from Albian there was a resumption of the tectonic activity, accompanied by high sedimentation rates, slumpings and calcareous-turbiditic-pelagic sequences (Formation I) and volcanism.

The beginning of the Tertiary was marked by generally regressive conditions, with frequent and prolonged periods of emersion, which explains the lack of Paleocene and Eocene sediments.

The deposition of carbonates of the Formation J (Oligocene-Langhian) took place in deeper marine conditions which continued during Serravallian (Formation K). During the Messinian salinity crisis, the evaporites of the Formation L were deposited.

The Pliocene marked the beginning of a transgression with the sedimentation of marls and clays of the Formation M and the development of a new trough. The evolution of this foredeep was accompanied by a piling of allochthonous nappes from the European continental margin due both to gravitational and compressional forces, resulting in a rapid burial of the northern part of the basin. As a consequence the source rock formation in this part of the basin was also buried extremely rapidly (the overthrusting began less than a million years ago). The actual source rock depths in each individual well are therefore also the maximum burial depths.

The petroleum types found in the basin studied range from light oils in the southeast to heavy asphaltic oils in the northwest. Explaining the occurrence of these heavy oils in this region posed the main question of the present study, whereby major emphasis was placed on elucidating the mechanisms of heavy oil generation and migration.

This region has been the object of several geochemical studies in the past (Brosse et al., 1989; Novelli et al., 1988), the results of which are summarised in the following:

- Novelli et al. (1988) demonstrated, using gas-chromatograms of the saturated HC fraction, isoprenoid/n-alkane ratios and GC/MS analysis of terpanes and aromatic steroid hydrocarbons, that immaturity and not biodegradation was responsible for the low API

density of the oils. Additionally they carried out systematic geochemical analyses on the different lithostratigraphic units which indicated that the Formation B was the main source rock of the oils present in the study area.

- The presence of immature oils in the area was attributed to the fact that a major portion of the early generated heavy asphaltene rich oils could have been expelled from the source rock during an early stage of oil generation, due to high expulsion efficiency (Novelli et al., 1988). This high expulsion efficiency was probably due to the concurrence of different factors: high heating rate, fast subsidence and overpressuring, the contemporary development of Tertiary tectonics and the carbonate nature of the source rock.
- Novelli et al. (1988) calculated in a three dimensional basin modelling study that the generation of hydrocarbons in Formation B occurred mainly over the last 5 ma. The massive hydrocarbon generation during this time was caused by the development of a foredeep basin located in front of the thrust sheets. The burial rate was very fast and accompanied by high heating rates (over 10°C/ma). Onset of oil generation was calculated to have occurred at 0.5% Ro and peak generation at 0.65% Ro. Determination of the HC generation history and the type and amount of HC's generated was perfomed in this study using the HC generation potential of the source rock formation, which was computed using the kinetic equations of Tissot and Espitalié (1975) and assuming a type II to type III kerogen.
- Detailed source rock geochemistry was performed by Brosse et al. (1989) who encountered numerous layers with high TOC values and fair petroleum potentials in Formation B, and thus considered it as a good source rock. They observed a large diversity in the organic carbon contents and in petroleum potential. High TOC concentrations were associated with intrinsically high petroleum generative qualities (high Rock-Eval HI values). The kerogens exhibited variability in oxygen content which allowed a classification oxygen-rich and oxygen-poor. The two groups of kerogens had somewhat different kinetic parameters of cracking. Nevertheless both had the ability to deliver oil early in thermal maturation.
- Brosse et al (1989) also differentiated four main facies types in the Formation B (massive carbonates, marls and shales, laminites and dolomites) in which kerogens of types I and II occurred. The marls and shales were noticed to contain less free hydrocarbons (S1/TOC or SOM/TOC) than the laminites and massive carbonates although no geochemical parameter was specific to any sedimentary facies observed at a core scale.

1.3 Samples

The 70 samples handled here were selected from 244.5 meters of cores from four wells in which the source rock formation has been buried to increasing depths. The aim of sampling was to analyse both petrographic and organic geochemical characteristics on the same scale. Major emphasis was placed on the choice of proper samples to be analysed. The set of samples can be considered to be representative of the various lithofacies encountered in the source rock formation (Formation B). The main lithofacies encountered in the examined cores are the following: 1) metric beds of massive light grey to grey-brown mudstones and wackestones which sometimes contained pressure solution features such as stylolites and solution seams, 2) centimetre to meter thick black shales, 3) carbonate and argillaceous laminites consisting of milimetric alternations of mudstone-wackestone, dark mudstones and clays, 4) fine to medium grained white dolostones with fracture or vuggy porosity and dolomitic breccias with macroscopically visible signs of oil impregnation.

As in the previous study (di Primio, 1990; Leythaeuser et al., in press) the carbonate source rock of this new study area is also characterised by a heterogeneous internal distribution of organic matter, which in part results from an internal redistribution of carbonate by pressure solution processes. As a consequence TOC-contents can, as recognised in the previous study, be expected to be higher in solution seams and stylolites as compared to the adjacent micritic carbonate. Samples containing solution seams and stylolites were therefore also taken for analysis.

Representative samples of the main lithofacies of each well were taken, as were two samples of heavy oils produced from the wells 8 and 17.

For this study a depth sequence of the source rock formation was required under the assumption that present depth represents an approximation of the maturity level. This approach was necessary because of the scarcity of vitrinite particles (AGIP, unpublished data). AGIP offered sample material from a total of 24 wells from which 4 wells, numbered 4, 8, 17 and 24, with cored source rock intervals around depths of 2500, 3000, 2000, and 4400 m respectively (Fig. 2) were selected for sampling according to the availability and quality of cored source rock sections. The wells were selected along a profile of around 15 km length (Fig. 3), whereby wells 8 and 24 are located in the region where autochthonous series are overthrust by allochthonous ones (Fig. 3, 4).

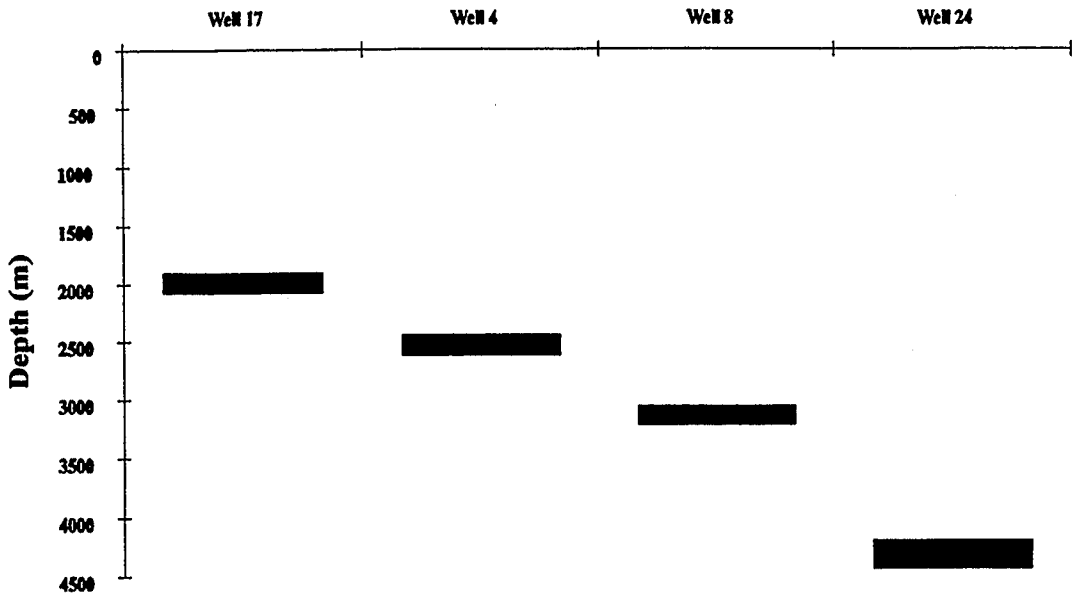

Figure 2: Present burial depth of the studied source rock formation in each well

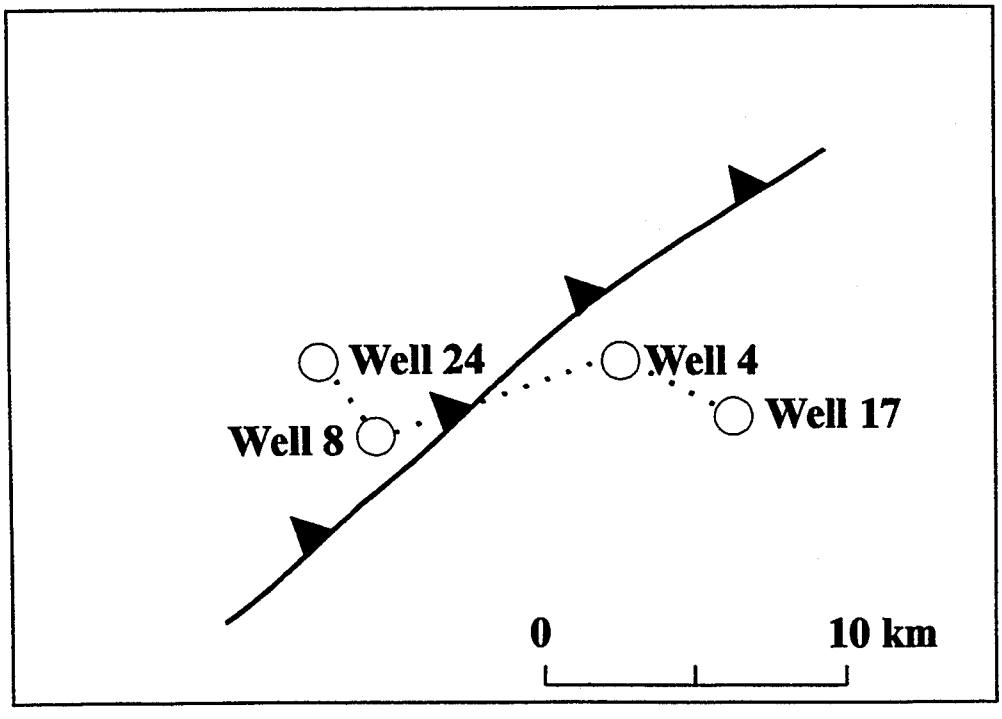

Figure 3: Sketch of the well locations in relation to the overthrust front.

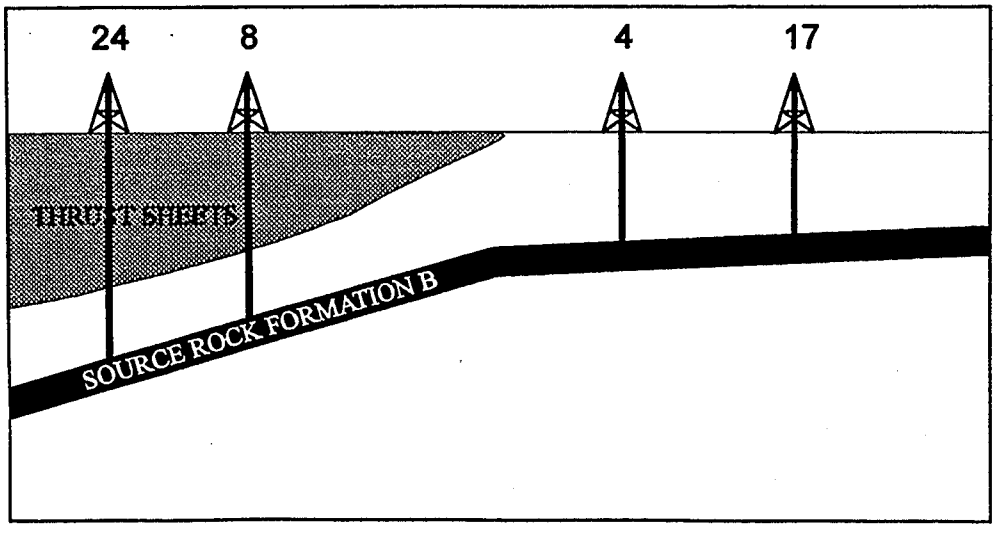

Figure 4: Schematic cross section connecting the sampled wells.

During the sampling care was taken to ensure that representative examples of each lithofacies were selected. The total sample series consisted of:

15 shale samples

17 oil impregnated samples (dolomitic breccias and fractured carbonates)

9 laminites

13 micritic limestone samples

9 solution seam/stylolite samples

2 oil samples

The cored intervals of the source rock formation represented varying portions of the total formation thickness of each well: in Well 4, 29 %; in Well 8, 92 %; in Well 17, 22 %; and in Well 24 only 3 %. Core sample control was obviously best in Well 8.

The laminites and shale samples from well 17 had been coated with wax by AGIP in order to prevent sample disintegration. The wax coatings were removed with a steel brush, but contamination could not be completely ruled out as seen later.

For wells No. 4, 8, and 17, where the cored interval was assumed to be representative of the lithologic composition of the entire source rock formation interval, a quantification of the distribution of the lithofacies was performed (Fig. 5). The relative proportion of each lithology type of the total source rock thickness of each well are presented in this figure.

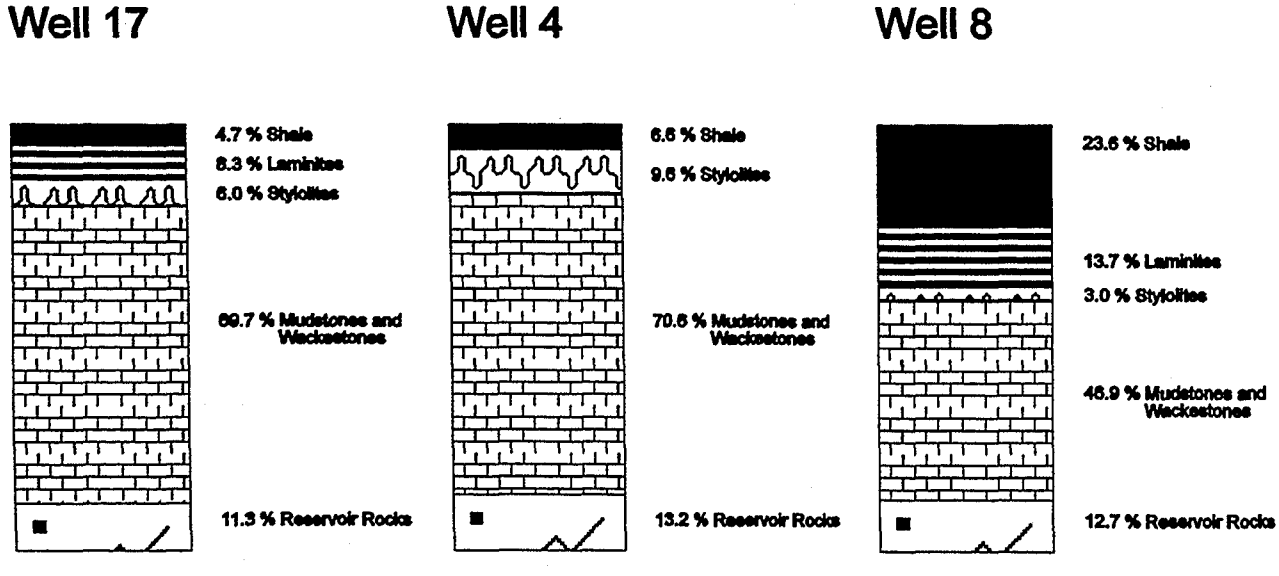

Figure 5: Lithofacies distribution in the cored intervals of Wells 17, 4 and 8.

1.4 Methodology

The methods applied in this study are depicted in Figure 6 and described in detail in the following pages.

1.4.1 Sedimentary petrology

A detailed petrographic study was performed with the aim to determine the depositional environments which lead to the sedimentation of the four main lithofacies described above. 40 **thin sections** were prepared to determine the mineralogical and morphological characteristics of the individual lithofacies.

1.4.2 Organic Petrology

For **microscopic studies**, 45 samples were selected representing the four lithofacies listed above. A slab of each sample was embedded in epoxy resin. One side of the resultant block, with the sample oriented perpendicular to bedding, was polished using successively finer abrasives, and then polished using 0.05 µm aluminum powder dispersed in water.

Macerals were classified according to Stach et al. (1982) into liptinites, vitrinites and inertinites by observation in blue light fluorescence (wavelength: 400 nanometer) and reflected white light.

Vitrinite reflectance could not be measured because of the lack of vitrinite particles in the sediments in general and, when present, due to the small size and often observed alteration (dark rims, inhomogeneous structure) of the vitrinite particles by oxidation prior to deposition.

1.4.3 Microthermometry

For selected samples containing calcite cemented fractures thin sections for **fluid inclusion analysis** were prepared. The microthermometric analyses were performed using a LINKAM (THM 600) heating-cooling stage. Only the homogenisation temperatures were measured due to the metastable character of the inclusion fluids.

1.4.4 Analysis of the soluble organic matter

A modified **flow blending** technique (Radke et al., 1978) was used to extract the ground sediment samples with a mixture of dichloromethane and methanol (99:1 v/v) as solvent. Total extracts were separated into saturated hydrocarbons, aromatic hydrocarbons, and heterocompounds by **medium pressure liquid chromatography** (Radke et al., 1980).

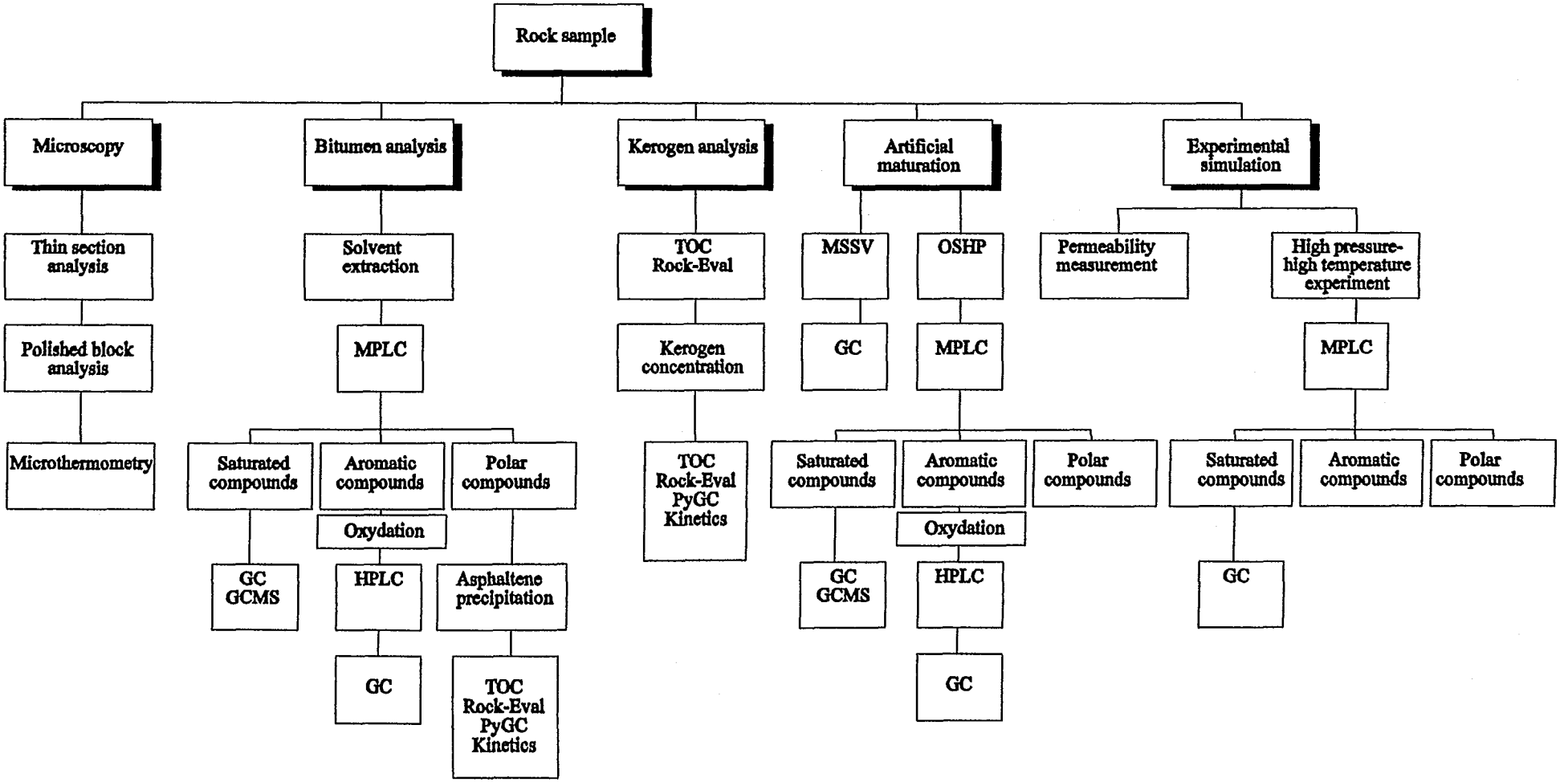

Figure 6: Analytical flowchart

The **saturated hydrocarbons** were analysed using a Hewlett-Packard 5710A gas chromatograph equipped with a fused silica capillary column of 60 m length, 0.35 mm internal diameter, coated with phenyl(5%)-vinyl(1%)-methyl(94%)-silica of 0.28 μm film thickness. The oven temperature was programmed to rise from 80°C to 300°C at 2°C/min. Helium was used as carrier gas. Sample introduction was performed by a programmed-temperature injection system. The split ratio was about 1:100. Selected n-alkanes and isoprenoids were quantified by internal standardisation with 5-α androstane applied prior to extraction.

The **aromatic hydrocarbon** fractions were analysed by a Hewlett-Packard 5731A gas chromatograph equipped with a programmed-temperature injection system (KAS) and a fused silica Ultra #2 capillary column of 50 m length, 0.20 mm internal diameter, coated with cross-linked poly-methyl(95%)-phenyl(5%)siloxane of 0.33μm film thickness. The temperature was programmed to rise from 120°C (hold 2 min.) to 310°C at 3°C/min. Helium was used as the carrier gas. Selected naphthalenes, phenanthrenes, and benzothiophenes were quantified by internal standardisation using 1-Phenylhexane, 1-Phenylheptane, 1,8-Dimethylnaphthalene, 1-Phenylnaphthaline, 1-Ethylpyrene, and 1-Butylpyrene applied prior to extraction. Due to high amounts of sulphur-aromatic compounds, which occluded the naphthalenes and phenanthrenes, the sulphur compounds in the aromatic fractions had to be oxidised using 3-chloro-peroxybenzoic acid (10x amount, 10 minutes, 40°C). The oxidised sulphur compounds were removed by adding water to the aromatics dissolved in dichloromethane. The acid, including the oxidised sulphur compounds, dissolves in water making its separation from the aromatics dissolved in dichloromethane possible. The desulfurized aromatic fraction was then separated into carbon ring classes by **High Performance Liquid Chromatography** (HPLC, Radke, 1981) and then analysed by gas chromatography with coupled Flame Ionisation and HALL® electrolytic conductivity detectors on the gas chromatograph described above. This sulphur removal technique was developed in this study.

Biological marker distributions were obtained by gas chromatography/mass spectrometry. Mass fragmentography work was done using a VC 7070E mass spectrometer coupled with a Carlo Erba model 4160 gas chromatograph. The GC was equipped with a 50 m fused silica column of 0.25 mm internal diameter coated with chemically bound CP Sil CB (OV-1 equivalent) of 0.4 μm film thickness. The oven temperature was programmed to rise from 110°C at 3°C/min to 320°C. Helium was used as carrier gas. In the mass spectrometer the ionisation energy was 70 eV, the emission current 200μA. Source temperature was 220°C. Multiple ion monitoring and metastable ion monitoring were performed with 1.3 s cycle time, with the residence time depending on the number of ions selected.

Asphaltenes were obtained from source rock bitumens and whole oils by precipitation using a minimum of 40-fold excess of n-heptane as compared to the extract volume. The solution was heated to 70°C for 1 hour and then filtered. The insoluble residue was washed repeatedly with n-heptane. Insoluble compounds, by definition asphaltenes, were washed from the filter with dichloromethane and concentrated by evaporation of the solvent.

1.4.5 Gas Analysis

Gases generated during hydrous pyrolysis were analysed by a Carlo Erba 4160 (HS) equipped with an automatic injection system and an OV-1 50 m fused silica capillary column with 0.32 mm internal diameter and 1.06 µm film thickness, followed by a 50 m SE 54 fused silica capillary column with 0.32 mm internal diameter and 1.05 µm film thickness. Hydrogen was used as carrier gas. 250 ml gas volume were injected automatically. The temperature of the injector was 125°C. The oven temperature was held isothermal at 33°C.

1.4.6 Kerogen Analysis

Total carbon (TC) determinations were made with a LECO IR-112 carbon analyser. The same instrument was used for **total organic carbon** (TOC) measurements after removal of carbonate with hydrochloric acid. **Carbonate** contents were calculated by subtracting TOC from TC (total non-organic carbon) and multiplying by the atomic proportion of carbon to the corresponding carbonate molecule as shown below, the result is expressed as percent calcium carbonate or dolomite:

In the case of calcium carbonate $CaCO_3$/C -> (40+12+3*16)/12=8.33

(TC-TOC)*8.33=X% Calcium carbonate

In the case of dolomite $Ca,Mg(CO_3)_2$ /C -> ((40+24)/2+12+3*16)/12=7.66

(TC-TOC)*7.66=X% Dolomite

Rock-Eval pyrolysis was performed with a Rock-Eval II-type instrument. Samples of ground whole rock, kerogen concentrates or asphaltenes weighing up to 100 mg are thermally distilled at 300°C for 3-4 minutes, followed by programmed pyrolysis at 25°C/min to 550°C, both in a helium atmosphere. Products released from the sample are detected by a flame ionisation detector (FID), which senses any organic compounds, and a thermal conductivity detector (TCD), which detects carbon dioxide. This method measures the amounts of products released during two heating steps, whereby TCD detection is applied during the second heating stage (up to 390°C), thus three peaks are generated during the measurement of one sample. The first peak (S1) represents milligrams of hydrocarbons that can be thermally distilled from one gram

of the rock. The second peak (S2) represents milligrams of hydrocarbons generated by pyrolytic degradation of the kerogen in one gram of rock. The third peak (S3) represents milligrams of carbon dioxide generated from one gram of rock during temperature programming up to 390°C, and is analysed by thermal conductivity detection (TCD). During pyrolysis, the temperature is monitored by a thermocouple. The temperature at which the maximum amount of S2 hydrocarbon is generated is called Tmax.

The hydrogen index (HI) corresponds to the quantity of pyrolyzable organic compounds (or "hydrocarbons", HC) measured as FID-signal corresponding to S2 normalised to the total organic carbon in the sample (mg HC/g TOC). The oxygen index (OI) corresponds to the quantity of carbon dioxide measured as TCD-signal corresponding to S3 normalised to the TOC (mg CO_2/g TOC). The production index (PI) is defined as the ratio S1/(S1+S2).

Kerogen concentrates were obtained by acid treatment of the extracted rock powder using hot hydrochloric and hydrofluoric acids. The kerogen concentrates were analysed by pyrolysis gas chromatography (PyGC), multistep pyrolysis gas chromatography (multi-step PyGC), micro-scale sealed-vessel pyrolysis gas chromatography (MSSV).

The **pyrolysis gas chromatography** system used was of a design similar to that described by Horsfield (1989). Up to 2 mg of each sample were heated in a flow of helium; only isolated kerogens were used to avoid mineral matrix effects (Horsfield and Douglas, 1980). Products released over the temperature range <300°C (ambient to 300°C at ballistic heating rate, 300°C for 10 min) were vented. Either one step PyGC or multi-step PyGC was then carried out. Pyrolysis products were collected in a cryogenic trap (liquid nitrogen cooling) from which they were then liberated by ballistic heating (held at 300°C). Analysis was made using a Hewlet Packard 5731A gas chromatograph equipped with a fused silica column of 25 m length, 0.32 mm internal diameter, BP-1 coating of 1µm thickness. The oven temperature was programmed from 40°C to 320°C at 8°C/minute. Alkane-alkene couplets, selected aromatic compounds and sulphur compounds were quantified by external standardisation. One step pyrolysis products were released over the temperature range 300 - 600°C (40°C/minute). Selected samples were analysed in three pyrolysis stages. In these multi-step experiments, three gas chromatograms, and, hence three sets of analytical data were obtained for each sample. The first set was collected between 300 - 375°C (40°C/min, held constant during the analysis and then cooled to ambient), the second set between 375 - 450°C (40°C/min, ambient to 450°C, held constant during the analysis and then cooled to ambient), and the third set between 450 - 600°C (40°C/min, ambient to 600°C, held constant during the analysis and then cooled to ambient).

Kinetic parameters were derived from open system pyrolysis experiments using the method of Schaefer et al. (1990). The apparatus consists of a high-temperature furnace (CM Furnaces

Inc., Bloomfield, NJ., USA) equipped with a quartz sample tube which is connected to a flame ionisation detector. Pyrolysis is performed on the finely ground, pre-extracted kerogen samples, or on asphaltene fractions. During pyrolysis a constant argon flow (45 ml/min) is maintained in order to transport the pyrolysis products from the sample to the detector. The linear heating rates (0.1, 0.7 and 5 K/min) are controlled by a thermocouple just above the sample. The calibration of the pyrolysis yield is achieved by external standardisation with known amounts of high-molecular-weight hydrocarbons.

1.4.7 Artificial maturation experiments

For each **MSSV** (micro-scale sealed vessel) experiment a commercially-produced glass capillary tube (100 µl) is flexed (120° angle), trimmed to approximately 40 µl volume, then sealed at one end using a flame. Pre-cleaned glass beads (80-120 mesh) are added up to the level of the elbow within the sealed arm of the tube. Between 1 and 5 mg of kerogen or asphaltenes is weighed into the elbow portion of the tube. The internal volume is then reduced to about 10 µl by filling the remainder with thermally pre-cleaned glass beads. Sample aliquots are artificially matured in batches using an oven designed for gas chromatography. Isothermal heating at 270°, 290°, 310°, 330°, and 350°C for 72 hours was employed for each sample. The contents of each tube are analysed using a system which consits of a purpose-built sample holder, a programmable pyrolysis furnace, a heated on-off split, a trap packed with glass beads that can be cooled cryogenically, a heated transfer zone and a gas chromatograph. After introduction of the tube into the sample holder a five minute purge cycle (300°C) is used to clean the outer surface. Produced effluents are vented during this time by means of the on-off split. The tube is then cracked open by piston action of the sample holder with the split in the off position. Products are swept from the heated zone (300°C) by helium flow and condensed using the liquid nitrogen-cooled trap. After ballistic heating of the trap (direct induction), gas chro2matographic analysis is performed using the method described for routine PyGC analysis. Products produced by the pyrolysis methods were detected using coupled flame ionisation (FID) and HALL® electrolytic conductivity detectors and quantified using an external butane standard.

One artificial maturation experiment was conducted using **open system hydrous pyrolysis** (OSHP; Krooss, 1993). 100 g of coarsely broken source rock sample were placed in a stainless steel autoclave (450 ml), the residual volume was filled with destilled water. A stepwise isothermal heating program starting at 230° C going up to 350° C at 22 MPa (220 bar) was used. The temperature was increased in steps of 10° C and held constant for 72 hours in each

heating step. Sampling of gas and liquid products was performed at the end of each isothermal interval.

1.4.8 Experimental simulation

A **high pressure - high temperature** triaxial flow cell (Hanebeck, 1994) was used for the experimental simulation of hydrocarbon generation and expulsion processes in natural source rock samples. In this flow cell a cylindrical rock sample, sandwiched between two porous stainless steel plates, is placed between two pistons which excert a controlled axial pressure. Sample and pistons are surrounded by a temperature resistant two-layered sleeve to which radial confining pressure can be applied. Additional conduits inside the pistons are used to control the fluid pressures on the upper and lower side of the sample. The entire flow cell can be heated under controlled pressure conditions to temperatures up to 350°C. Fluid and confining pressures in excess of 300 bar can be applied while the lithostatic pressure is limited mainly by the mechanical stability of the rock sample.

Generated oils were extracted from the source rock sample by soxhlet extraction (24 hours, dichloromethane as solvent). Expelled oils were washed of the surface of the source rock sample with dichloromethane, and added to the oil ultrasonically extracted from the pores of the metal plates.

Permeability measurements were performed using a modified high pressure - high temperature flow cell (Krooss et al., 1994). In this arrangement no lithostatic pressure was applied. A pressure gradient was applied to the selected fluid phase (usually distilled water, in one case whole oil) and the flux across the rock sample monitored by recording the amount of fluid collected at the outlet of the pressure regulator at the low pressure side of the flow cell.

2 Results

2.1 Characterisation of the source rock formation

2.1.1 Lithologic characterisation

The source rock formation was deposited in a tidal flat carbonate facies (AGIP internal report) and consists according to detailed petrographic examinations (a total of 40 samples were analysed by thin section and polished section microscopy using white and UV light) of four principal lithofacies each of which is described below.

Except for the laminites, all facies are present in each of the sampled wells. The fact that laminites were missing in wells 4 and 24 does not mean that they do not occur in these wells. The relatively small sections of the source rock which were cored must not necessarily be representative of the entire formation. This is specially the case for well 24, where the cored section represents only 3 % of the total source rock thickness.

2.1.1.1 Carbonate mudstones and wackestones

The limestones of the source rock formation consist mainly of a light to dark grey mudstone-wackestone with rare occurences of Ostracods and fossil fragments. The mudstones are characterised by a micritic texture sometimes containing microdolospar (rhombohedric crystals) suggesting an early, partial dolomitisation. The matrix is micritic to microsparitic and shows no macro- or microscopic evidence of porosity. The wackestones are similar to the mudstones but include more or less abundant lithoclasts mainly composed of laminite debris. The distribution of the lithoclasts follows the bedding. Thin calcarenites and synsedimentary breccias were also observed in the wackestones. These different textures indicate a low to moderate depositional energy on a probably inclined bottom. The thickness of the micritic limestones ranges between a few centimetres up to over 4 meters.

This lithofacies probably resulted from long-lasting periods of carbonate production and deposition. The sedimentary environment was probably shallow, subtidal and unfavourable for the development of benthic species, especially because of a constant reworking in a current- and channel-dominated environment.

The carbonate matrix is characterised by an almost complete absence of structured organic matter.

At irregular intervals solution seams and stylolites are found in the carbonate matrix. They consist of clay, organic matter, pyrite, silt and sometimes dolomite. Fractures often originate in these layers and are either directly related to the pressure solution process (tension gashes) or to hydrocarbon generation as discussed below. Stylolite amplitudes reached in certain cases up

to 4 cm. The thickness of the insoluble residue of solution seams was never larger than 3 cm. Solution seams and stylolites were a subordinate feature of the source rock sequence analysed in this study. The thickness of pressure solution influenced layers as described in Fig. 5 includes not only the insoluble residue of stylolites and solution seams, but also the limestone portions between individual pressure solution features. Thus the total thickness of only the stylolite and solution seam fillings are much lower than inferred from Fig. 5.

The identifiable organic matter particles encountered in solution seams and stylolites consist of yellow alginites and liptodetrinites and sometimes blood-red chlorophyllinites, embedded either in a yellow-brown fluorescing bituminous groundmass or in dark brown, clay mineral-rich, insoluble residue of the stylolites or solution seams. The liptinite particles are oriented parallel to bedding and are always fully compacted. A typical wackestone with solution seams is shown in Plate 1a.

2.1.1.2 Laminites

Carbonate laminites consist of light to dark grey mudstone-wackestone with parallel to low angle oblique laminations made of dark micrite layers including organic matter, pyrite and shale, and light microspar layers (recrystallised micrite). The laminae are laterally constant in thickness at the scale of the examined core. In some samples the lamination is well defined in the hand specimen, but poorly visible in thin section. Pseudomorphosed evaporite crystals, gypsum and anhydrite crystals in the sediment were noticed by AGIP-petrographers in this laminite type. Enhanced salinities can therefore be postulated for carbonate laminites.

The microstructure of the light and dark laminae is sparitic and micritic respectively, suggesting a depositional grain-sorting, or different diagenetic evolutions.

A second type of laminite is characterised by irregular alternating clear and dark laminae and by the presence of cellular alignments, fenestrae and bird's eyes. It is recognisable by comparison with recent or ancient stromatolites as being composed of microbial-mats which were deposited in an intertidal environment (Kenig et al., 1989). This type of laminite was described by AGIP sedimentologists, but was not encountered in the sample selection analysed in this study.

Argillaceous laminites were also observed. They were composed of regularly alternating laminae rich in dark clay and light microsparitic carbonate laminae. The carbonate was, according to reports from AGIP, composed of calcite, calcite plus dolomite, or aragonite, which is uncommon for a sediment of this age (Triassic). The aragonite observed in some samples corresponds to the original mineralogical composition of the mud precipitated. These argillaceous laminites could result from several depositional conditions: either tidalites or

seasonal deposits in deeper environments. Argillaceous laminites were observed to evolve from pure shale layers and grade into pure limestones.

Laminite thicknesses range from several centimetres up to 1 meter.

The carbonate laminites as well as the microbial-mat laminites were probably deposited in an intertidal, moderate energy environment. In contrast the argillaceous laminites seem not to be linked to emergence of the sediment or to tidal induced sediment displacement. Their interpretation as seasonal deposits is more probable (AGIP internal report).

Carbonate laminites are almost devoid of microscopically visible organic matter. The organic matter of the argillaceous laminites shows a relatively high content of bituminous groundmass and small amounts of figurated liptinites. Plate 1b shows a carbonate laminite at core scale.

2.1.1.3 Shales

Dark grey to black shales show a fine lamination due to red, orange or yellow organic flakes arranged parallel to bedding. They contain clay minerals, carbonate nodules, pyrite, quartz silt and phosphate fragments. The clay minerals are mainly illite (20-40%), interlayered minerals (35-55%), chlorite (0-7%), and kaolinite (15-25%, AGIP internal report). Fossils reported by AGIP petrologers include diverse pelecypoda and radiolaria indicating marine depositional conditions. The shales are normally 30 to 70 cm thick, in a few cases shale layers of 1.5 to 2 m thickness were observed.

The organic matter of the shales as seen by UV microscopy consits mainly of an orange brown bituminous groundmass and yellow fluorescing liptodetrinites as shown in the photomicrograph in Plate 2a. A subordinate part of the organic matter consists of yellow and red alginites and blood red chlorophyllinite particles (Plate 2a-d). Microscopical analysis of extracted kerogen concentrates revealed yellow-brown fluorescing particles with a fibrous structure (Plate 2e-f). These seem to have been occluded by the bituminous groundmass, which was at least partially removed by solvent extraction.

The occurrence of chlorophyllinite in sediments is usually limited to shallow depths and is a sign of immaturity of the organic matter. Its occurrence at depths in excess of 4000 m indicates that the burial of the source rock formation must have been extremely fast.

The high proportion of bituminous groundmass in the shale samples makes a direct identification of the depositional environment difficult. But, the sediment structure, the high organic content, and the observed fibrous structures in the kerogen concentrates can be interpreted as originating from microbial mats. Kenig et al. (1989) described microbial mats in a modern hypersaline carbonate lagoon environment of Abu Dhabi. They recognised that the upper intertidal zone along the landward side of the inner lagoon is the favourable site for

extensive development of microbial mats. They form an microbial belt at the periphery of the lagoon, where they may be followed laterally without interruption for at least twenty kilometres. These microbial mats were seen to form massive beds of up to 55 cm thickness with TOC contents of up to 7 %.

Sedimentological analyses by AGIP showed that, as a rule, the top of metric limestone layers was abruptly overlain by the shale units described here. The change from the shale layers to laminites and then limestones was observed to be more or less gradual. These facts indicate that either climatic or tectonic events were the cause for the abrupt change from subtidal to a lagoonal, intertidal depositional environment. After deposition of the shales, carbonate sedimentation increased (transgression) first diluting and later drowning the microbial mat environment. The transgression and drowning of the microbial mat environment seems to have been gradual as indicated by the occurrence of laminites which grade into limestones at the top of the shales. Plate 1c shows the abrupt transition from carbonate lithofacies in the left side of the displayed core to shale lithofacies in the right side.

2.1.1.4 Oil impregnated limestones

These samples consist of either fractured and oil-impregnated limestones, fine to medium grained white dolostone with vuggy or fracture porosity, or of dolomitic breccia made of medium to coarse grained dolopackstone in a matrix of fine to medium grained dolomite.

All dolomite facies are the result of either deposition in an open, well oxygenated tidal flat or of the resedimentation from the tidal flat to an adjacent deeper lagoon or basinal area.

The oil and bitumen impregnations show a dull yellow fluorescence colour. Particulate organic matter is absent. Plate 1d shows a fractured and oil impregnated dolostone at core scale.

2.1.2 Organic richness

2.1.2.1 Total organic carbon content

A basic parameter for source rock characterisation concerns the organic richness as monitored by measurement of the organic carbon content (% TOC). TOC data of all samples are listed in Table 1. TOC ranges and mean values in the source rock formation vary only between the different lithofacies and not between the individual wells. The TOC data is thus presented for each of the analysed lithofacies.

The highest TOC values are observed for shale samples where the organic carbon contents range between 3.74 % and 27.60 % (Table 2). Laminites, solution seams and stylolites have TOC contents between 0.34 % and 3.14 %. TOC contents of stylolite and solution seam samples were calculated using the method described by Leythaeuser et al. (in press) which is

based on the assumption that all carbonate has been removed by pressure solution (Table 1). These calculated TOC data range between 8.41 % and over 60 % TOC (Table 1). All carbonate mudstone/wackestone samples have less than 1 % TOC (Table 2).

A comparison of this data to the organic carbon threshold value of 0.3 % TOC for potential carbonate source rocks stated by Tissot and Welte (1984) indicates that, except for the impregnated and reservoir-rock samples, all lithofacies have source potential.

2.1.3 Kerogen quality

2.1.3.1 Rock-Eval

The quality of the organic matter in all lithofacies types of the source rock was assessed by Rock-Eval analysis (Tables 1 and 2). Rock Eval data of the source rock formation show meaningful variations only between the different lithofacies and not between the individual wells. This observation is obvious e.g. from Tmax values (Table 1). An increase of the Tmax values with depth as expected is not observed. The Tmax data range of each well is comparable to that of any other well, indicating that the organic matter in the rocks of all wells is in the same maturity range. The Rock-Eval data are, therefore, discussed below for the individual lithofacies combining samples from all wells.

The S1 parameter, measured by Rock-Eval, represents that fraction of the original genetic potential which has been effectively transformed into hydrocarbons. The quantity S2 represents the residual genetic potential which has not yet been used to generate hydrocarbons. Both S1 and S2 values are influenced by the amount and type of organic matter present in the rock sample. Measured S1 and S2 values are listed in Table 1. Maximum, minimum and average values calculated for the individual lithofacies present in the source rock are shown in Table 2. The shale samples have the highest genetic potential (S1 + S2; Tissot and Welte, 1984, page 511) with an average of around 70 mg HC/g rock indicating an excellent source rock potential. The yield of the combined S1 + S2 of laminites and solution seam/stylolite samples reached values of around 5 - 10 mg HC/g rock, which according to Tissot and Welte (1984, pages 511-513) indicates good to excellent source rock potential. The average genetic potential of the mudstone/wackestone samples lies below 1 mg HC/g rock and is thus negligible.

In general the source rock lithofacies analysed contain hydrogen rich, oil prone kerogen of type I to type II. This is indicated by hydrogen index (HI) values ranging from 400 to over 800 mg HC/g TOC for samples with more than 1% TOC (Table 1). Plotting the HI values versus TOC contents (Fig. 7) shows that samples below 1 % TOC reveal a very broad range of HI values (0 to 500 mg HC/g TOC). Peters (1986) had noticed that for argillaceous rocks containing less than 0.5 wt. % TOC, HI values are likely to be too low because of the mineral matrix effect i.e.

adsorption of pyrolytic organic compounds on mineral surfaces. Samples in excess of 1 % TOC are believed to give realistic HI values.

The individual lithofacies show characteristic hydrogen index ranges. Solution seams, stylolites and laminites have hydrogen indices between 179 and 730 mg HC/g TOC. The average HI for these lithofacies are 538 and 441 mg HC/g TOC respectively indicating the predominance of a type II kerogen. The hydrogen indices of shale samples vary between 317 and 933 mg HC/g TOC with an average of 742 (Table 2). This high average hydrogen index is indicative of a hydrogen-rich kerogen, predominantly of type I (Tissot and Welte, 1984). Carbonate mudstones and wackestones display a HI range from 70 to 517 mg HC/g TOC with an average of 239 mg HC/g TOC.

Oxygen indices (OI, mg CO_2/g TOC) could not be measured due to apparatus malfunction.

The production index values (PI, S1/(S1+S2)) are, due to impregnations, highest in the reservoir rocks and in the fractured source rocks (Table 1, 2). All other lithofacies have low PI values, which can be interpreted either as an indication of immaturity (low S1 due to non generation) or of effective petroleum expulsion (Espitalié et al., 1977).

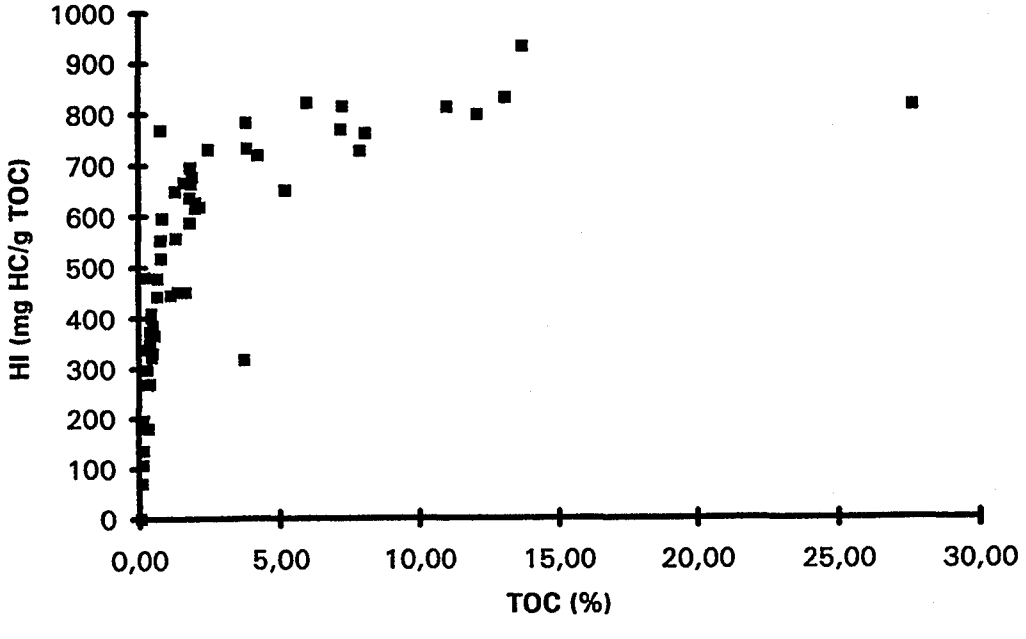

Figure 7: Plot of whole rock hydrogen index versus TOC for all samples analysed.

Since the hydrogen index can be influenced by mineral matrix effects, kerogen concentrates of 28 samples were made from extracted source rock samples and analysed by Rock-Eval. The results of this analysis are shown in Table 3 and plotted in the HI vs. OI diagram in Figure 8. The hydrogen index values of the kerogen concentrates analysed range from 380 to 931 mg HC/g TOC (Table 3). The lowest HI values were measured for mudstone and wackestone samples while the highest were measured for shales. As shown in Figure 8 the organic matter in the source rock formation includes type I and type II kerogens with a predominance of kerogen type I in the shales and kerogen type II in the mudstones and wackestones, in the laminites, and in some solution seams and stylolites (Figure 8). In certain solution seams (samples E 33366/2, E 33407/2, E 33433/2) predominantly kerogen type I occurs (Table 3). The oxygen index (OI) remains below 25 mg CO_2/g TOC in all samples. Tmax of the samples still shows a relatively large range of variation between 398°C and 430°C.

2.1.3.2 Elemental analysis

Elemental analysis of the kerogen concentrates allowed the calculation of atomic H/C and O/C ratios (Table 4) which, when plotted in a Van Krevelen diagram show, that the chemical composition of the kerogens is relatively heterogeneous (Fig. 9). A relatively large field of the diagram, between the typical evolution pathways for kerogens type I and type II is occupied by the data points. The atomic O/C ratio is in some cases very high, reaching values of almost 0.3 (Fig. 9). A high O/C ratio is commonly attributed to type III kerogens derived from higher land plant vegetation (Tissot and Welte, 1984). The occurrence of immature kerogens with high H/C and high O/C ratios is at the same time very unusual and difficult to explain. The distinction of kerogen types is made according to the theory that high H/C ratios are due to high contents of aliphatic structures, whereas high O/C ratios are due to high proportions of oxygen-bearing functional groups in the kerogen. According to the results of the elemental analysis all these structural elements could be present in the kerogens analysed.

Elemental analysis of the kerogen concentrates made a quantification of organic-bound sulphur possible (Table 4). By measuring the amount of iron in the kerogen concentrates and assuming that all the iron is pyritic, an estimation of the content of pyrite-bonded sulphur is obtained. By simple subtraction, an estimate of the organic sulphur content of the kerogen is possible. The sulphur content of the kerogens is best described by the atomic S_{org}/C ratio, which ranges between 0.03 and 0.10 for the kerogen concentrates analysed (Table 4). According to Orr (1986) an S_{org}/C ratio of over 0.04 indicates a sulphur-rich kerogen. The values shown in Table 4 reveal that the majority of the kerogens analysed (both of type I and II) are extremely rich in organic sulphur. Thus, kerogens of type I-S (Sinninghe Damsté et al., 1993), type II-S

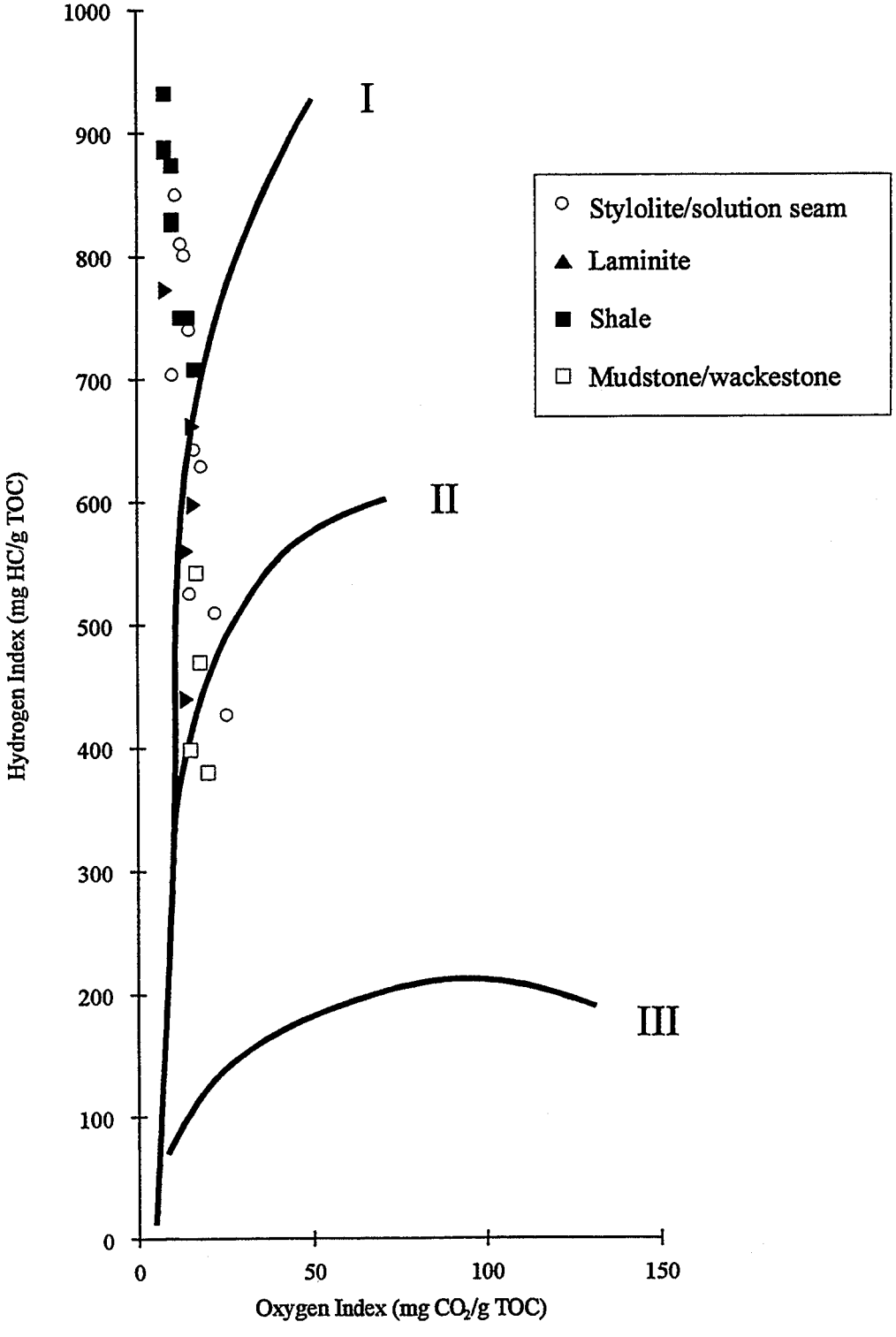

Figure 8: Plot of kerogen hydrogen index versus oxygen index showing values of the different source lithofacies as well as maturation pathways of the different kerogen types.

(Orr, 1986), and the common type II are present in the source rock formation analysed in this study. Contributions of free sulphur to the calculated organic-bound sulphur can be excluded since free sulphur was removed from the powdered source rock by addition of small sheets of copper to the source rock-solvent sludge.

The location of the data points in the van Krevelen diagram (Fig. 9) is independent of the lithofacies or of the wells from which the samples where taken. In the HI vs. OI diagram of the data of the kerogen concentrates is also spread between both kerogen evolution pathways (Fig. 8). These results would normally indicate that the source rock formation contains predominantly a kerogen type I/II. However, Tissot and Welte (1984) pointed out that at maturities less than 0.6 % vitrinite reflectance, the maturation pathways of kerogens in the Van Krevelen diagram are such that the types of kerogen are distinguished principally by the value of the atomic H/C ratio. Similarly, in the HI vs. OI diagram kerogen types I and II are distinguished mainly by HI values. Therefore, a kerogen with a hydrogen index of above 900 mg HC/g TOC or a H/C above 1.5 contains definitely a type I kerogen, while a HI of below 600 mg HC/g TOC and an H/C of 1.2 defines a kerogen as being of type II independent of the corresponding oxygen index or O/C ratio.

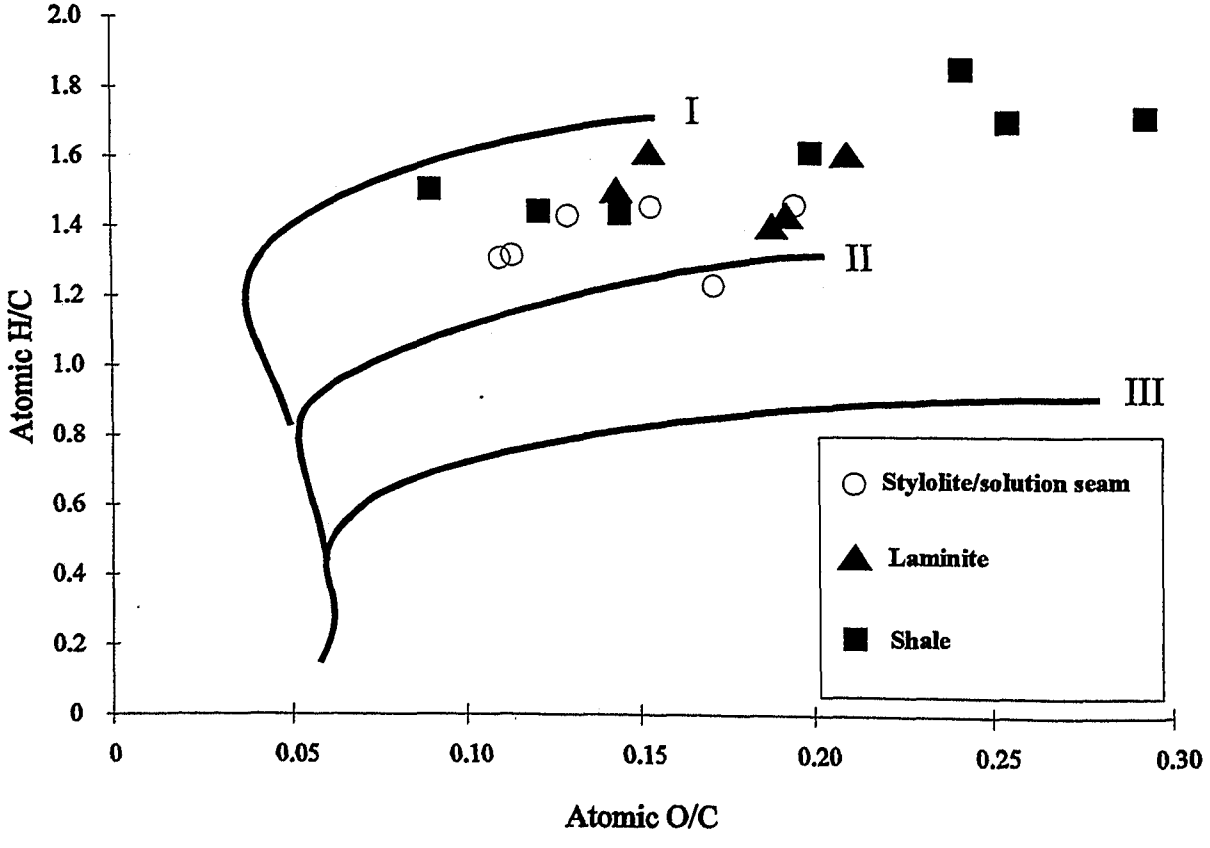

Figure 9: Plot of kerogen atomic H/C versus O/C showing values of the different source lithofacies as well as maturation pathways of the different kerogen types.

Using these interpretation guidelines the organic richness and kerogen quality data allow a first characterisation of the source rock qualities. The shales generally have the highest TOC contents and the highest hydrogen indices. They contain predominantly a type I-S kerogen and are excellent oil prone source rocks. The laminites, solution seams and stylolites have lower TOC contents and usually contain a type II-S kerogen. The carbonate mudstones and wackestones are, due to their low TOC contents in comparison with the remaining lithofacies, poorer quality source rocks with a kerogen type II.

2.1.3.3 Organic petrology

The amount and composition of the organic matter in the source rock formation varies only between the different lithofacies and not between the individual wells.

Each lithofacies has a distinct assemblage of particulate organic matter. The **carbonate mudstones and wackestones** are characterised by an almost complete absence of organic matter particles. In a few cases liptodetrinite, minuscule vitrinite particles and inertodetrinite were observed. The liptinitic particles showed a yellow fluorescence colour.

The organic content of the **solution seams, styolites** and **carbonate laminites** is composed mainly of a yellow-brown fluorescing bituminous groundmass. Individual liptinites, alginites as well as liptodetrinite (red, orange-brown or bright yellow fluorescence), are embedded in this groundmass. Vitrinite particles are rare and, when found, are very small and show signs of oxidation, indicating reworking and transport in an oxic water column. Inertinite is present in small amounts in the form of inertodetrinite.

Argillaceous laminites contain higher amounts of bituminous groundmass with orange-brown fluorescence. Liptinites are present in the form of liptodetrinites with a distinct yellow-orange fluorescence or as well preserved red alginites. The yellow fluorescing liptodetrinite, with particle sizes below 10µm, is mainly composed of elongated structures which are comparable to the marine *Nostocopsis* algae described by Mädler (1968) and Teichmüller and Ottenjahn (1977). An exact determination of these algal structures was impossible due to their small size so they were included into the liptodetrinite group. Virtually no vitrinite or inertinite particles were found in these samples.

The **shales** show the highest organic content. The main part of the organic matter is in form of a reddish-brown fluorescing bituminous groundmass. Liptodetrinites with yellow fluorescence (possibly *Nostocopsis* see above) are the next major component followed by blood-red fluorescing chlorophyllinite-rich layers and individual particles. The microbial mats were in some cases eroded and redeposited as indicated by the occurrence of chlorophyllinite-rich lithoclasts, which are generally marginally oxidised (black rims of the chlorophyllinite-rich

lithoclast shown in Plate 2b) and are thus easily detectable under the microscope. Red algae are often found between the chlorophyllinite-rich layers. They generally occur in groups of three or more individual algae (Plate 2c). In one case a sporinite with yellow-orange fluorescence was observed (plate 2d). Vitrinite and inertinite particles (fusinite, semifusinite and inertodetrinite) are minor contributors to the organic matter. They are sometimes found enriched in very thin layers (one particle thick) at the boundaries of, or in the microbial-mat structures (Plate 2g-h). Vitrinites are generally small, more or less rounded and marginally oxidised indicating reworking and transport in an oxic medium.

2.1.3.4 Microscopic evidence of hydrocarbon migration

Clear signs of hydrocarbon migration were noticed in samples of all wells predominantly in the vicinity of laminites, solution seams and stylolites. Such signs are represented by yellow fluorescing oil impregnated fractures and micro-fractures. Photomicrographs of impregnated fractures are shown in the Plate 3. Most of these fractures seem to be tectonically induced. Plate 3a shows a swarm of parallel fractures initiating in a dark laminae. In this case the impregnation of these fractures by oil is not indicated by fluorescence due to the magnification used, but was observed at higher magnification. Two generations of fractures are observed in this case and are pointed out by arrows in Plate 3a.

In Plate 3b a series of oil impregnated fractures originates at the edge of a solution seam. These fractures represent an oil impregnated network connecting several stylolites.

Calcite cemented fractures were in some cases reopened and subsequently impregnated by petroleum as demonstrated by the fluorescing fracture border in Plate 3c.

Shale samples also showed visible signs of oil migration. Plate 3d (sample E 33401, shale) shows a series of fractures and open porosity which is completely oil filled. A higher magnification view of a fracture which leads directly to this porous zone is shown in Plate 3e. Signs of rock matrix fluidisation are noticeable at this magnification. The fracture is filled with a fluorescing groundmass as well as clay particles and pyrite which are oriented parallel to the fracture walls. The texture in the fracture indicates soft rock deformation. These observations in the shale layers may be explained by the high organic matter contents monitored in the shales (4 to 27 % TOC) which, during hydrocarbon generation, could lead to such high oil saturation levels that the source rock reacted more like a mud than like a lithified rock. Similar microscopic indications of hydrocarbon migration were also observed in other shale samples.

2.1.4 Determination of palaeotemperatures by analysis of aqueous fluid inclusions

During the process of crystal growth and fracture healing in sedimentary rocks, small quantities of the surrounding fluid, either gaseous or liquid, can be trapped in individual crystals in the form of fluid inclusions. Analysis of these fluid inclusions allows the estimation of the temperature at the time when the inclusion was sealed.

The geothermometric use of fluid inclusions is based on the differential shrinkage of the fluid phase and the host mineral during cooling from the moment of enclosure to the time of observation. Since the fluid shrinks more than the mineral, a bubble in the fluid is usually observed at surface temperatures. Heating the sample up to the temperature where the bubble disappears (i.e. the fluid inclusion homogenises) reverses the process and provides a rough estimate of the temperature of enclosure. This temperature must, in most cases, be corrected according to the pressure at the time of trapping and to the fluid inclusion composition in order to give more accurate filling temperatures (Roedder, 1984).

The interpretation of temperature data from fluid inclusion analysis is further complicated by mechanical processes affecting the host mineral which lead to changes in the inclusion volume or composition. The reaction of the host mineral to an increase in the inclusion volume due to heating usually results in either a plastic deformation (stretching) or a fracturing (decrepitation) of the mineral. Both processes can result in a re-equilibration of the homogenisation temperature to the temperature conditions of the time when stretching or decrepitation occurred. In any of these cases the homogenisation temperature represents then an approximation of the maximum temperature which the host mineral has been subjected to and not the original temperature of enclosure.

The theoretical aspects of fluid inclusion analysis and the respective methods of interpretation are reviewed in the publications of Burrus (1987) and Mullis (1987).

2.1.4.1 Homogenisation temperatures

Aqueous fluid inclusions present in calcite healed fractures of the source rock formation analysed in this study were analysed in order to estimate the filling temperature and, if possible, the maximum temperature to which the sediment had been exposed. Four fractured samples, one from each well, were selected for fluid inclusion analysis because of the high probability of fluid inclusion occurence in calcite-healed fractures. Thin sections of 80μm thickness and polished on both sides were analysed by a microscope equipped with a heating-cooling stage.

Only the samples from wells 8 and 24 had aqueous fluid inclusions which were large enough to be measured. Both samples had enormous amounts of inclusions in calcite healed fractures, but almost all of these were empty. Only a few very small inclusions showed the typical aqueous

phase and gas bubble. Both the empty and full inclusions were characterised by cracks radiating outwards from the inclusion into the host mineral. In the case of the empty inclusions it can be assumed that the decrepitation of the inclusions lead to the loss of the enclosed phase. The empty inclusions were useful only as evidence that a sufficiently high pressure differential between inclusion content and host crystal had been achieved that fracturing and loss of fluid content was possible.

The pressure difference necessary for decrepitation of fluid inclusions depends on the inclusion size. Therefore small inclusions are more resistant to changes in internal pressure than larger inclusions (Roedder, 1984). Decrepitation of fluid inclusions does not always lead to the loss of the inclusion filling. In some cases the expansion from internal pressure will cause a microfracture to develop into the surrounding crystal that does not extend to the surface. The volume increase represented by this cracking relieves the pressure until the fracture can no longer propagate (stretching). The enclosed fluids re-equilibrate during this process to the new conditions. In this case the homogenisation temperature monitored by fluid inclusion analysis represents an approximation of the temperature which lead to the formation of the microfracture. Usually this temperature is close to the maximum temperature to which the sample was exposed.

The amount of differential stress necessary for fluid inclusion deformation depends on the tensile strength and number of slip systems in the crystalline structure of the host mineral. Reported data (Ulrich and Bodnar, 1988) indicate that quartz will stretch at an internal pressure of 1000 bar and that sphalerite, barite and fluorite will stretch at internal pressures as low as 200 bar. A pressure increase of this size may be achieved by only a 5°C increase in temperature for a single-phase, water-filled inclusion (Prezbindowski and Tapp, 1991). In addition to temperature increase shear stresses associated with tectonic activity also have the potential to facilitate fluid inclusion deformation by lowering the internal pressure necessary for inclusion deformation.

Thus, the small size of the inclusions, the presence of microfractures radiating into the host mineral, occurrence of vast amounts of decrepitated inclusions and the tectonic setting of the source rock analysed indicated that homogenisation temperatures derived from the analysis of the inclusions in samples from wells 8 and 24 are probably close to the maximum temperature to which these samples have been exposed.

Four fluid-bearing inclusions were detected and analysed in samples from well 8 and three in well 24. Each inclusion was heated until homogenisation occurred and then cooled back to ambient temperature five times, in order to obtain a reliable homogenisation temperature value. The measured homogenisation temperatures as well as the mean temperature values for each

inclusion and for each sample are listed in Table 5. The mean homogenisation temperatures of aqueous fluid inclusions from wells 8 and 24 were determined as 75.3°C and 72.8°C respectively. A correction of the temperatures according to inclusion filling salinity and enclosure pressure could not be performed due to difficulties in recognising the freezing temperature of the inclusions.

Depression of the freezing point of aqueous inclusions is a measure of the total solutes in the fluid, and permits an estimation of the salt concentrations in inclusions. Information about the salinity of the inclusion is necessary for the calculation of the temperature correction for a given pressure (Roedder, 1984). Hence, lack of salinity data implies difficulties in correcting the temperature according to the estimated pressure at the time of inclusion filling.

In the case of the inclusions analysed in this study, freezing temperatures varied by as much as 15°C. This fact is indicative of a so called "metastable behaviour" of the inclusion. Metastability occurs when the trapped fluid was very clean and free of solid nuclei (Roedder, 1984). This fluid composition can lead to elimination of the vapour bubble upon freezing and delayed renucleation upon heating. The temperatures of renucleation derived from metastable inclusions are then erroneously high.

The homogenisation temperatures determined in the samples from wells 8 and 24 must, therefore, be used without correction for salinity or pressure. The morphology of the inclusions indicated decrepitation and stretching, thus the temperatures derived from these inclusions can be assumed to be close to the maximal thermal stress applied to the host minerals (Leischner, 1994 and references therein). The samples from both wells showed relatively uniform temperatures between 72°C and 75°C. Thus, the rocks from both wells have, according to this data, been subjected to approximately the same maximum temperatures during burial.

2.1.5 Characterisation of the soluble organic matter

Analysis of the soluble organic matter (SOM) was performed in order to obtain geochemical information regarding the primary biological contributors to the organic matter, the degree of thermal maturation which the organic matter has been subjected to during burial, and to recognise hydrocarbon migration effects. A further goal was the correlation of the source rock bitumens to oils produced from adjacent layers.

2.1.5.1 SOM yields and compound class composition

The composition of the soluble organic matter of a source rock is mainly controlled by the type of organic matter and its maturity. The general trend of variations of SOM ratios with increasing thermal evolution is well known in the form of hydrocarbon generation curves with depth, as established for different basins (Tissot and Welte, 1984). The wide depth range sampled in this study was expected to allow the recognition of a hydrocarbon generation curve.

The amounts of soluble organic matter extracted from each individual sample are listed in Table 6. Fig. 10 shows a depth plot of the minimum, average, and maximum values for the carbon normalised extract yields. Macroscopically impregnated samples were excluded from the minimum, average and maximum value calculation. A HC generation curve was not observed in Fig. 10. The average values for each well are all in the range of more or less 100 mgSOM/gTOC. Minimum values remain constant with depth. The same can be said for the maximum values with the exception of well 8, where two samples reached values of over 350 mgSOM/gTOC (Table 6).

The uniform SOM ratio with depth is also consistent with the fact that all wells are in the same maturity range. The composition of the bitumen will, therefore, be discussed according to the main lithofacies and regardless of their well origin.

The individual and average extract yields of the different lithofacies are listed in Tables 6 and 7. The reservoir rock samples and the samples with macroscopically discernible signs of impregnation show, as expected, the highest carbon normalised SOM yields ranging from 67 to 1660 mg/g TOC and an average of 715 mgSOM/gTOC. Mudstone and wackestone samples and laminated lithofacies have extract yields ranging between 49 and 373 mgSOM/gTOC and averages of 204 and 220 mgSOM/gTOC respectively. Solution seams, stylolites and shale samples have extract yields ranging between 54 and 173 mgSOM/gTOC and average values of almost 100 mgSOM/gTOC (Tables 6, 7).

The soluble organic matter is characterised by a low proportion of hydrocarbons (usually < 30 %, Tables 8, 9) which is consistent with the low maturity of the samples. The average

compound class composition remains remarkably uniform for all lithofacies (Table 9, Fig. 11). Only the reservoir rock samples show a noticeable enrichment in asphaltenes as compared to the other lithofacies. The produced oil samples show higher proportions of hydrocarbons, reaching nearly 40 % in the petroleum of Well 8 (Fig. 12, Table 9). The asphaltene contents of both oils are remarkably high while the NSO fraction is lower as compared to the source rock extracts.

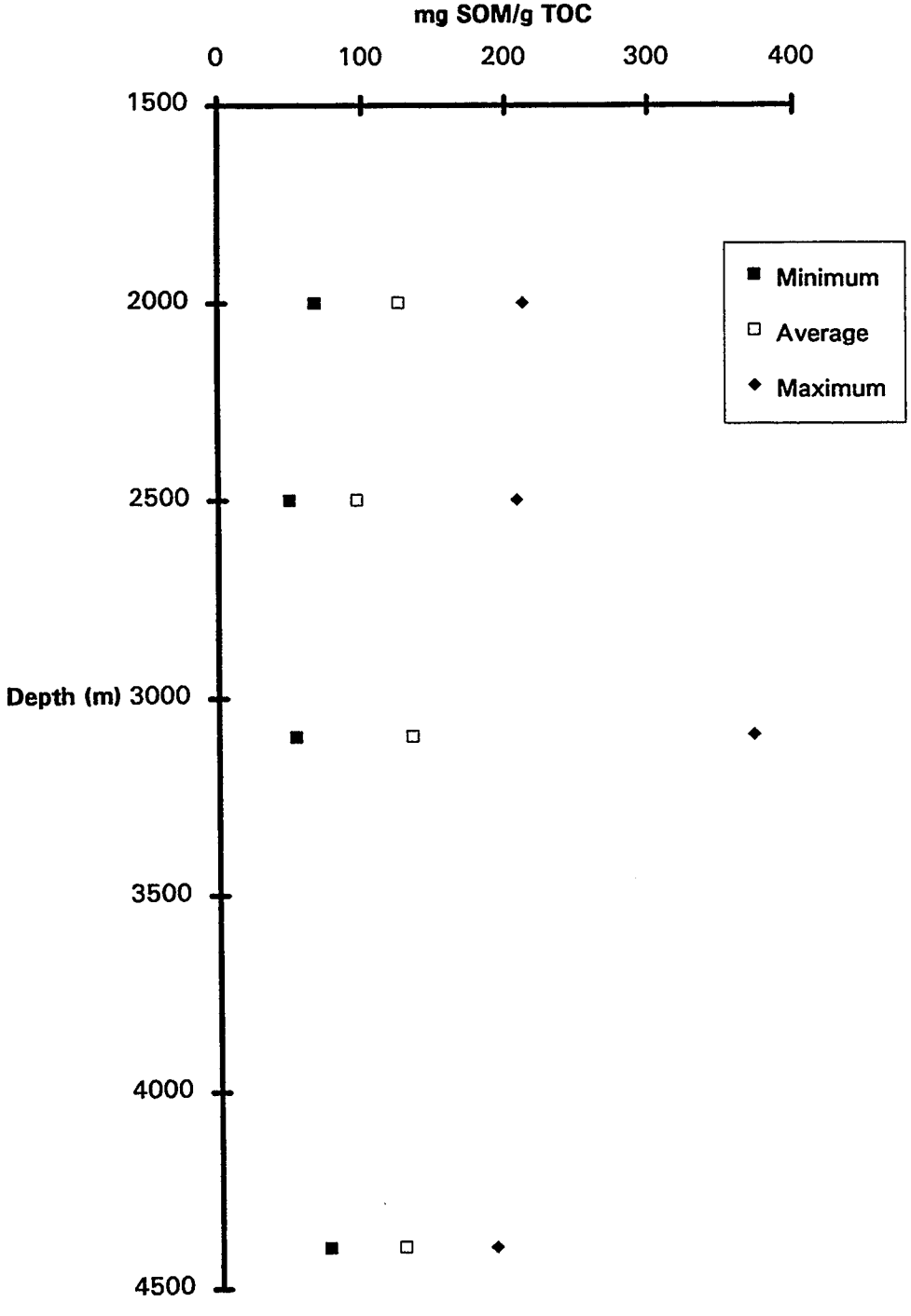

Figure 10: Minimum, average and maximum soluble organic matter yields of samples from the four wells analysed plotted versus sample depth.

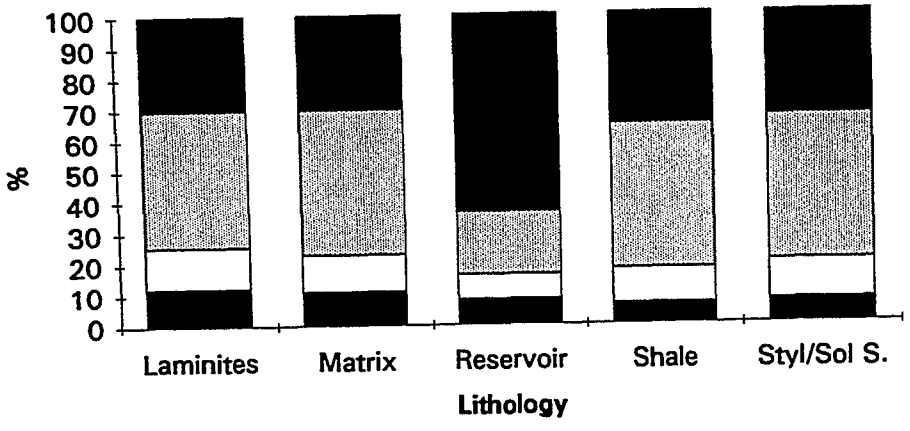

Figure 11: Average compound class composition of each lithofacies sampled (legend as in Fig. 12).

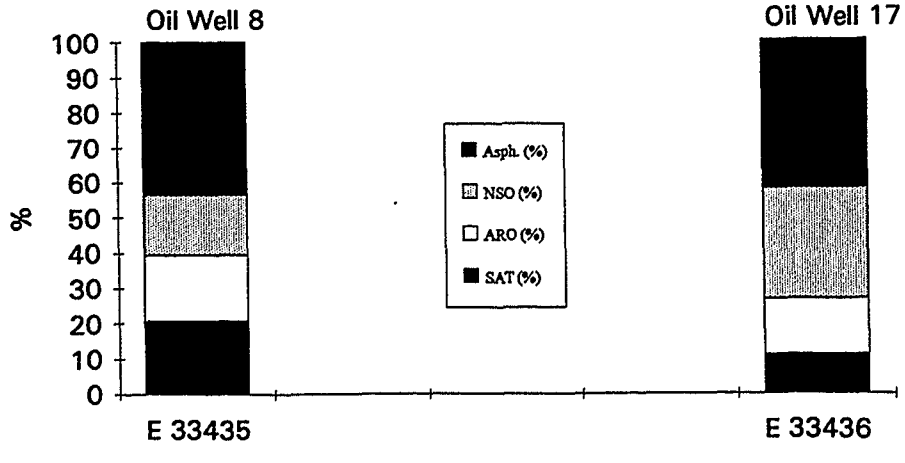

Figure 12: Compound class composition of the two crude oil samples analysed in this study.

2.1.5.2 Saturated hydrocarbons

The saturated compounds of 64 rock samples and two oils from the source rock formation were analysed quantitatively by gas chromatography. The results are listed in Tables 10 and 11. All source rock samples analysed show similar characteristics: High amounts of steroids and triterpenoids (e.g. Figs. 13, 14), an odd over even predominance of the n-alkanes and a pristane/phytane ratio normally lower than 1 (Tables 10, 11). Individual lithofacies cannot be recognised by any kind of typical "fingerprint" of, for example, their n-alkane or isoprenoid distributions. All samples possess comparable compound distributions bearing witness to the homogeneous nature of the soluble organic matter. Only when the relative amounts of the individual compound classes of the saturated hydrocarbon fraction (n-alkanes, isoprenoids and biomarkers) of the main source lithofacies are compared can a first, very general, distinction be made:

Mudstone and wackestone samples are characterised by higher contents of isoprenoids and n-alkanes relative to biomarkers, a typical example of the saturated hydrocarbon fraction for a mudstone sample is E 33388 (Fig 13). Shales, laminites, solution seams and stylolites show high contents of pristane and phytane, lower amounts of n-alkanes and a higher proportion of biomarkers than mudstone/wackestone samples. A prime example for this distribution is sample E 33407/2 (Fig. 14).

The dominant n-alkanes are usually n-C_{15} and n-C_{17}, which according to the literature can be attributed to marine algae (Youngblood etal., 1971).

The isoprenoids pristane and phytane are generally found in higher concentrations than the neighbouring alkanes in the source rock extracts. Phytane dominates in almost all cases over pristane. The pristane/phytane ratio of the samples analysed is normally between 0.9 and 0.2 indicating a reducing depositional environment (Didyck et al., 1978). Some mudstone/wackestone and stylolite/solution seam samples show a predominance of pristane over phytane (Table 10).

The saturated compounds of the two oils analysed have widely differing characteristics. The oil sample from Well 17 has a relatively large proportion of biomarkers and an odd over even preference in the n-C_{23} to n-C_{31} range (Fig. 15). This indicates that the oil of Well 17 is of relatively low maturity (Tissot and Welte, 1984). The saturated compounds in the oil produced from Well 8 show a much more mature signature (Fig. 16); biomarkers are almost absent and no odd over even preference of the n-alkanes can be seen. The n-alkane distribution is dominated by short chain compounds peaking at n-C_{15}. The only similarity between the two oils analysed is the dominance of phytane over pristane.

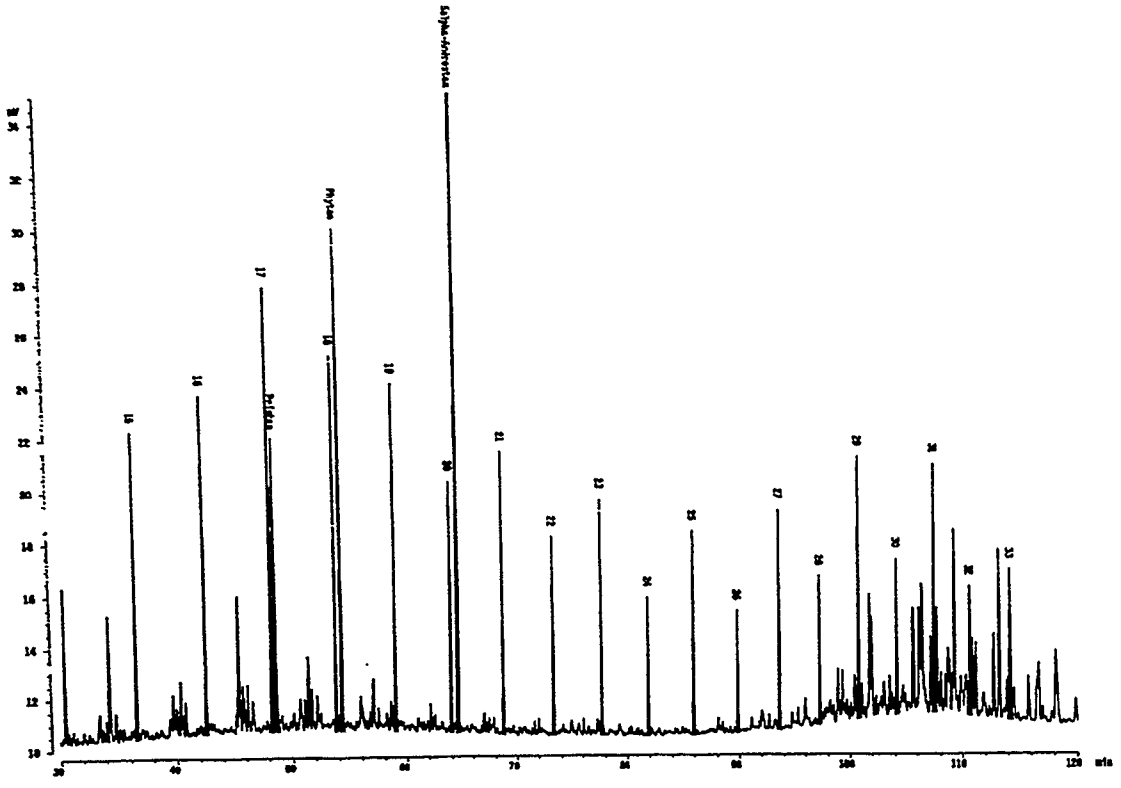

Figure 13: GC-trace of the saturated hydrocarbons of mudstone sample E 33388, well 8, 3092 m. 5a - Androstane was added as an internal standard.

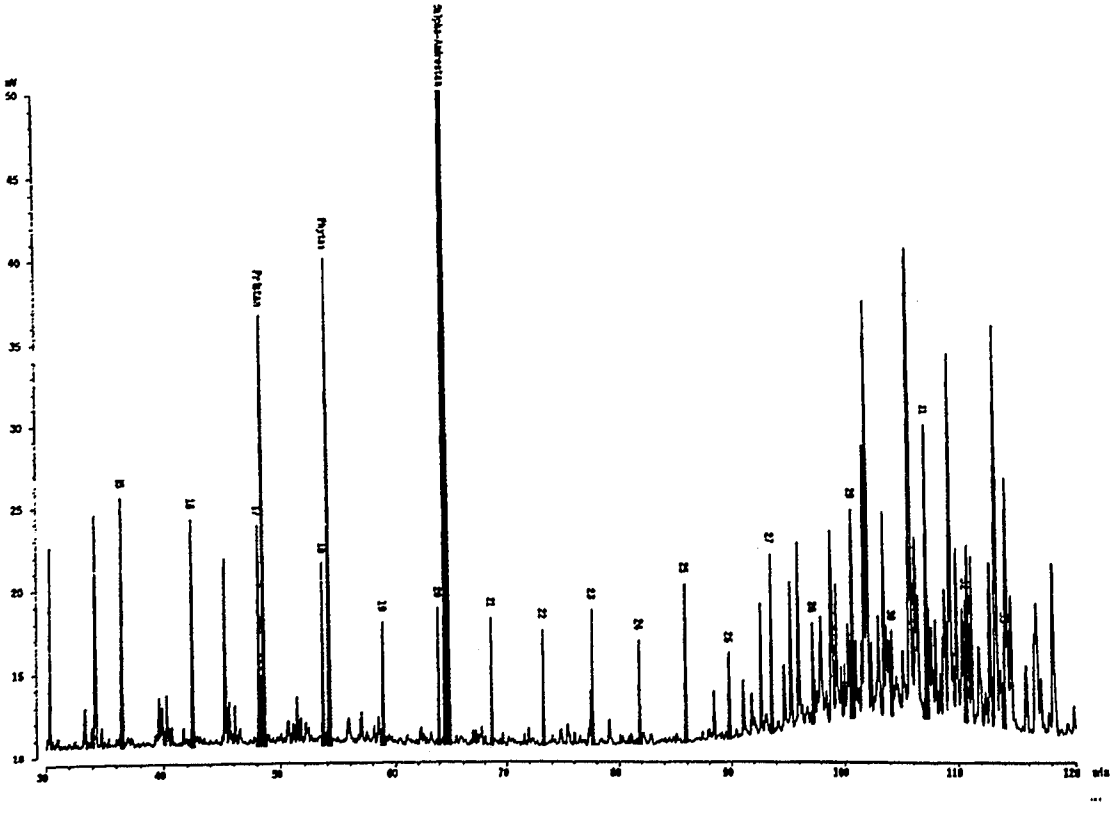

Figure 14: GC-trace of the saturated hydrocarbons of solution seam sample E 33407/2, well 8, 3136 m. 5a - Androstane was added as an internal standard.

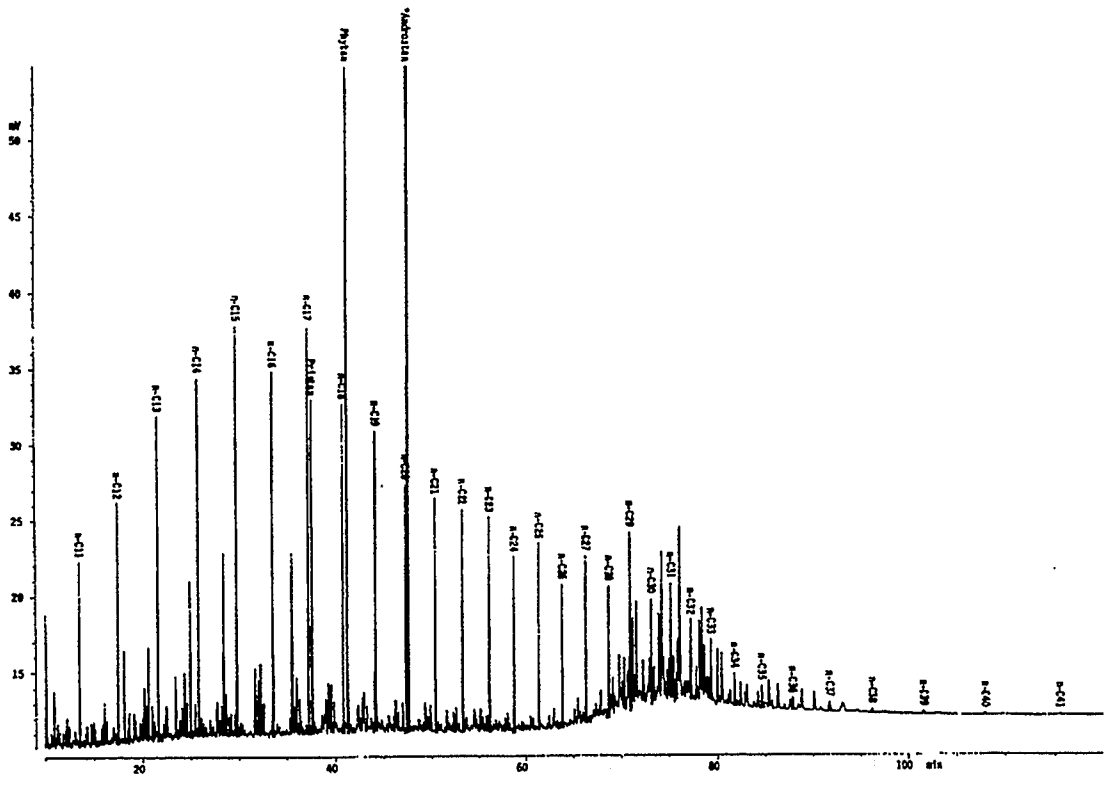

Figure 15: GC-trace of the saturated hydrocarbons of the crude oil from well 17. 5a-Androstane was added as an internal standard.

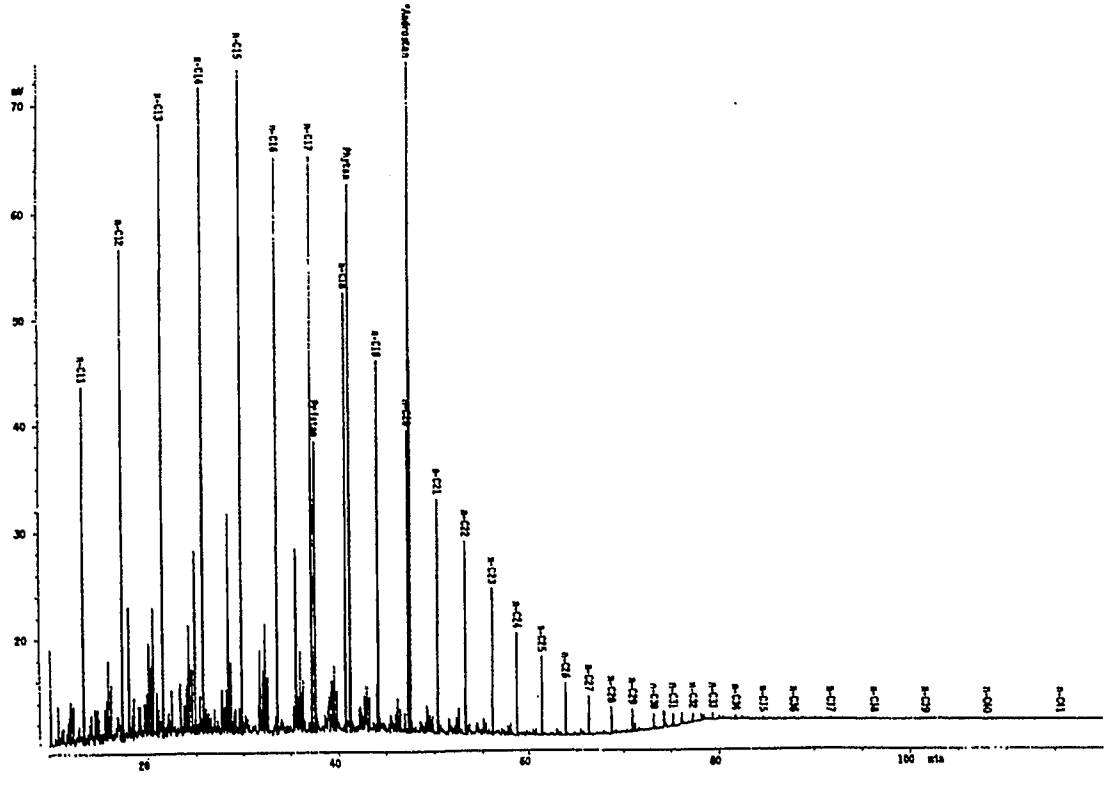

Figure 16: GC-trace of the saturated hydrocarbons of the crude oil from well 8. 5a-Androstane was added as an internal standard.

2.1.5.3 Biomarkers

Biomarkers are lipid-derived compounds that can be traced to particular biological precursor molecules. Consequently, they are capable of providing specific information regarding depositional environment, maturation, migration and biodegradation of source rocks or petroleum (Seifert and Moldowan, 1986). Many biological marker molecules are metastable, in constant evolution with respect to geological time and temperature. The degree of thermodynamic re-equilibration can be monitored by ratios of biomarker compounds of different stability, which allow an estimation of source rock or petroleum maturity (Ensminger et al., 1977; Seifert and Moldowan, 1978; Seifert and Moldowan, 1980). Ratios of certain saturated and aromatic biomarker compounds are some of the most commonly applied thermal maturity indicators. These indicators result from two types of reactions: a) cracking reactions (including aromatisations), or b) isomerisations at certain asymmetric carbon atoms. While both types of indicators are used, isomerisations are more commonly applied (Peters and Moldowan, 1993). The two most commonly used isomerisations are those involving hydrogen atoms at the C_{22} position in the hopanes and the C_{20} position in the steranes, both of which were determined for the source rocks in this study.

The biomarkers represent almost always a relatively large proportion of the saturated hydrocarbon fraction of the samples analysed (i.e. Figs. 13, 14). The distribution of C_{30}- to C_{35}- homohopanes is always dominated by C_{30} hopane. Relatively high contents of C_{33}- and C_{35}- homohopanes in some samples (i.e. E 33374, fractured mudstone, E 33391, shale, Fig. 17, Table 12) are indicative of a reducing depositional environment (Peters and Moldowan, 1993; ten Haven et al. 1988). An interesting feature observed is the dominance of C_{34} homohopane over C_{33} and C_{35} hopanes in some samples (i.e. Fig. 18a, stylolite sample E 33369/2, 18b, stylolite sample E33431/1, Table 12). A C_{34}-homohopane predominance was also noted by Moldowan et al. (1992) in an oil from an anoxic to slightly suboxic hypersaline source rock from Yugoslavia, but he did not propose a link to a specific precursor or to a depositional environment.

Gammacerane is almost always present but in varying amounts. Although oils and bitumens with high gammacerane ratios can often be traced to hypersaline depositional environments, there are exceptions to this rule (Peters and Moldowan, 1993). Thus, the presence of gammacerane in the samples analysed cannot be interpreted as a clear indication of hypersaline conditions.

Hopane maturity determinations calculated from the C_{32} hopanes (C_{32} 22S/(22S+22R)) showed relatively low maturities for the Wells 17, 4 and 24 and a large variability independent of the analysed lithofacies or kerogen type in Well 8 (Fig. 19). The strong variations in this

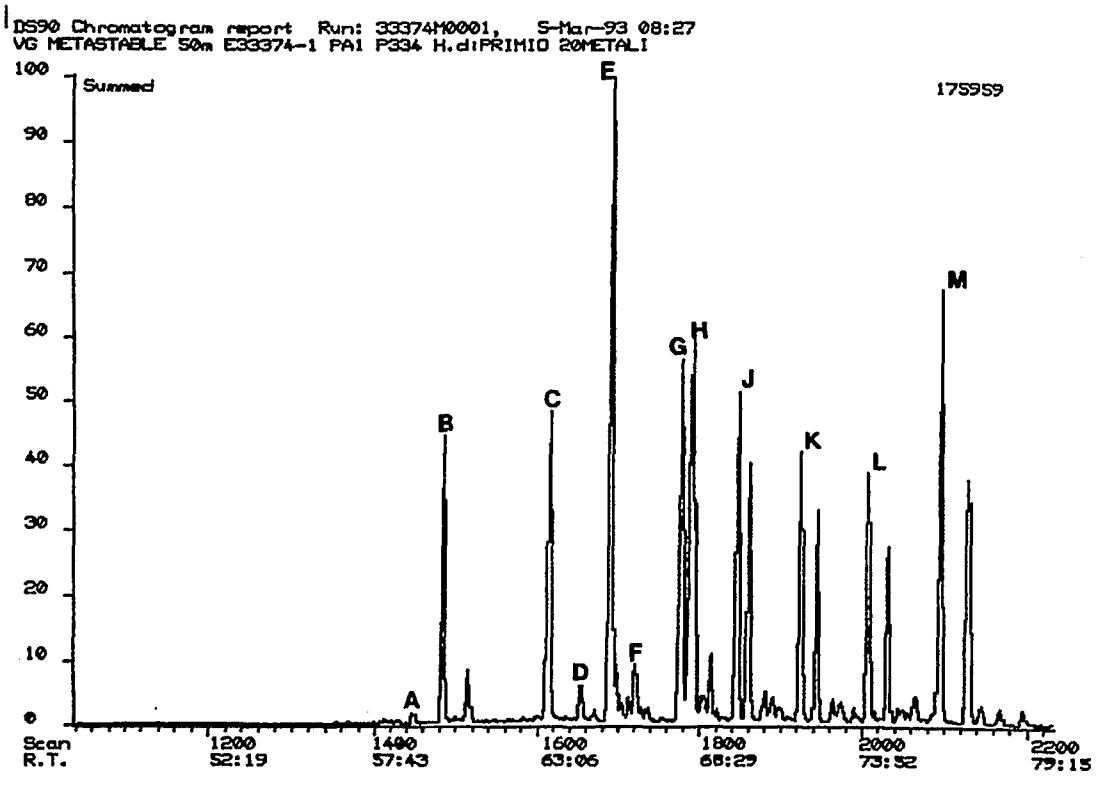

Figure 17a: Hopane distribution pattern in fractured mudstone sample E 33374, well 4, 2613 m. See appendix for peak identification.

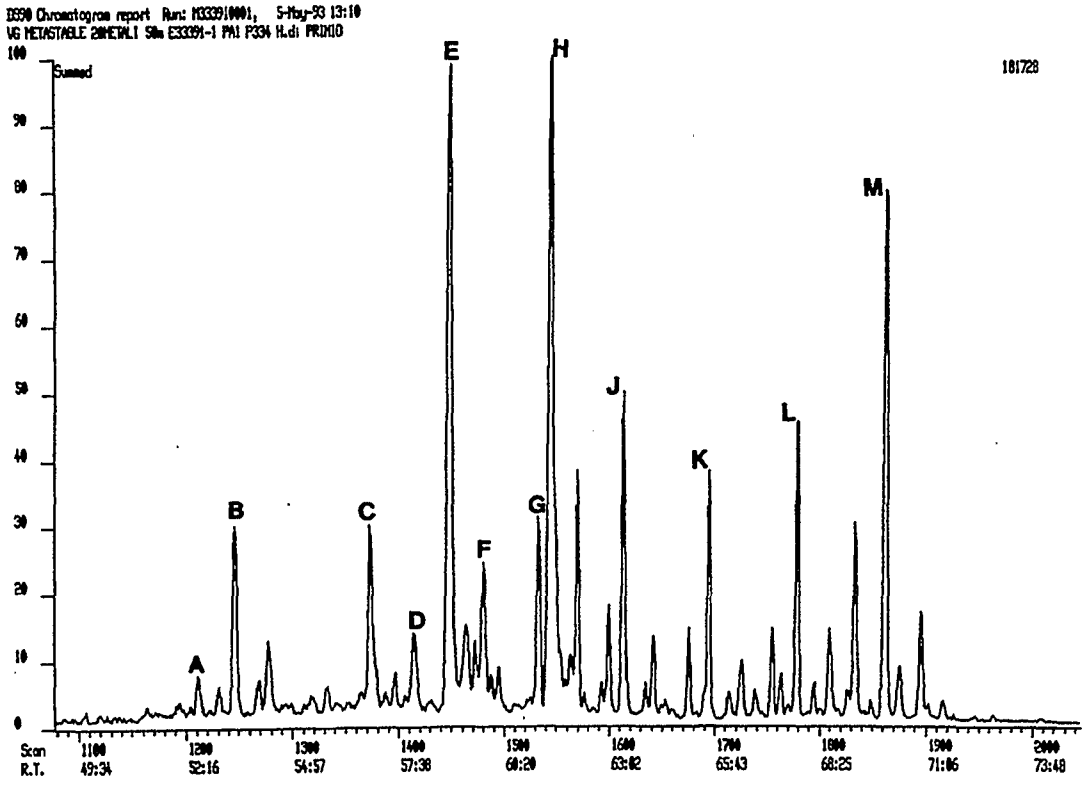

Figure 17b: Hopane distribution pattern in shale sample E 33391, well 8, 3103 m. See appendix for peak identification.

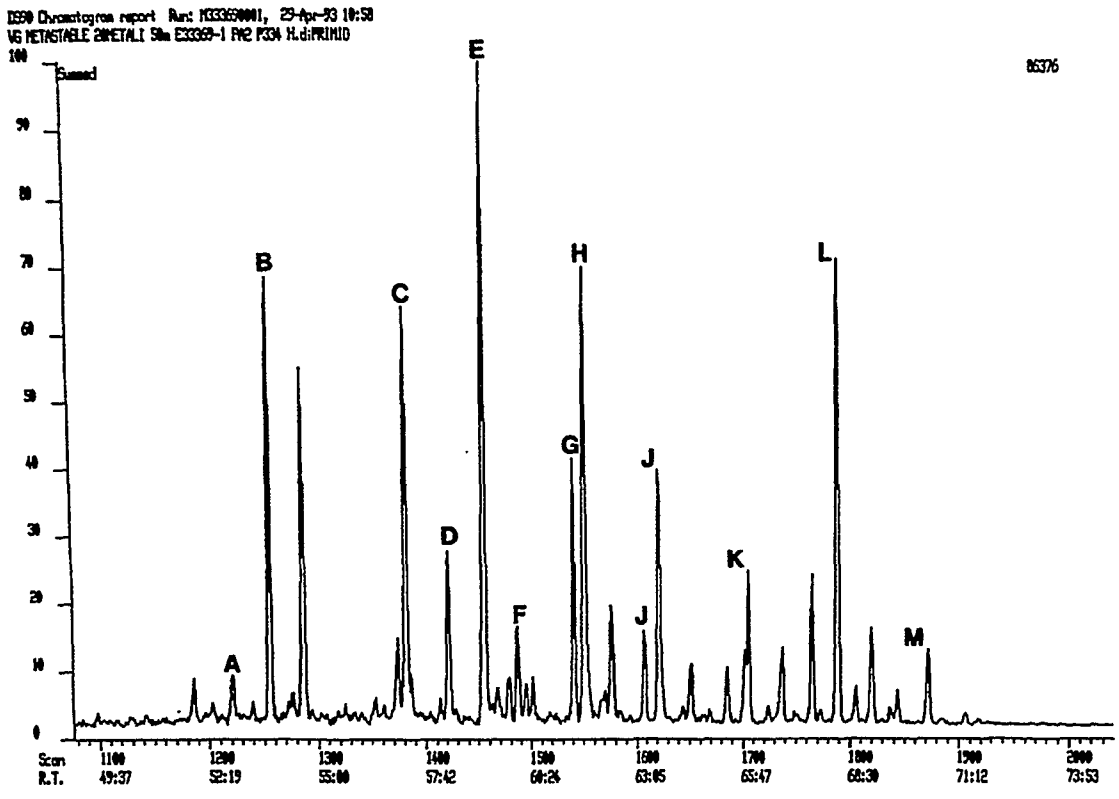

Figure 18a: Hopane distribution pattern of stylolite sample E 33369/2, well 4, 2553 m. See appendix for peak identification.

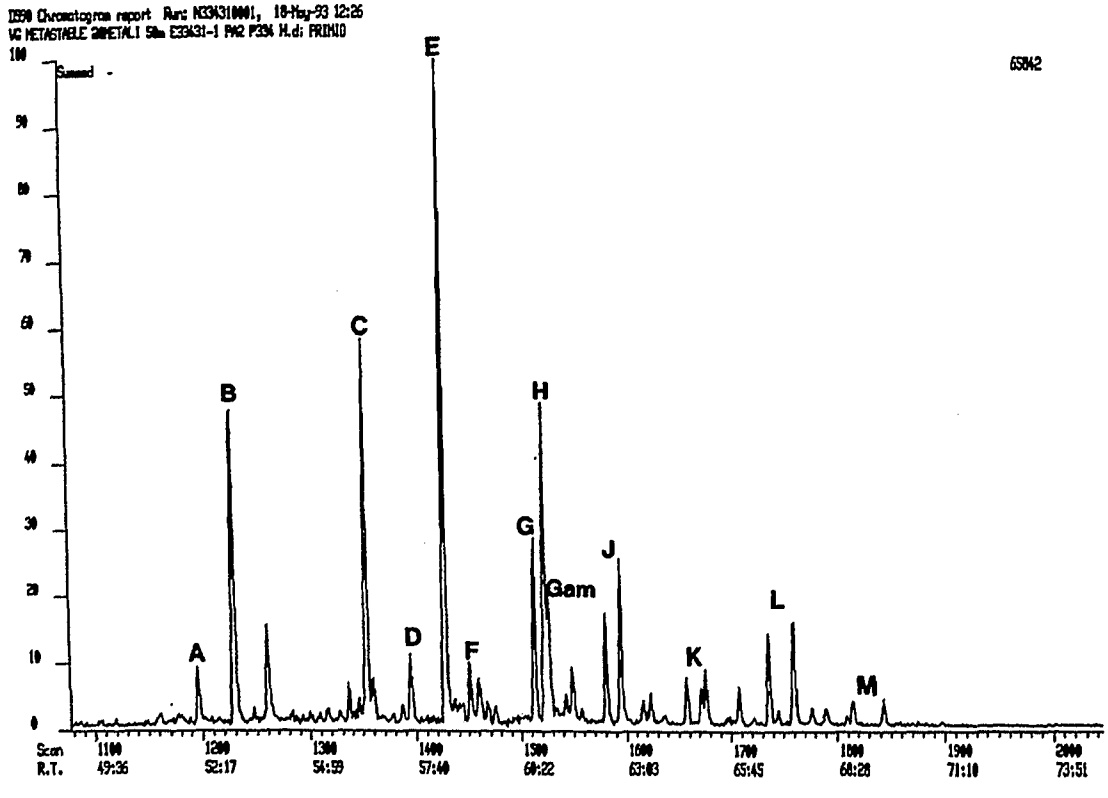

Figure 18b: Hopane distribution pattern of stylolite sample E 33431/1, well 24, 4437 m. See appendix for peak identification.

ratio in Well 8 may be due to impregnation of certain source rock intervals with a higher maturity petroleum. The values range normally from 0.2 to 0.4 for the samples from Wells 17, 4, and 24 (Fig. 19). Well 8 shows a distribution of the C_{32} 22S/(22S+22R) ratios between 0.15 up to 0.6.

The 22S and 22R forms of C_{32} hopane are in equilibrium in the oil produced from the dolomites underlying Well 8. The extended hopanes in the oil sample from Well 17 have not yet reached equilibrium. This is shown by a C_{32} 22S/(22S+22R) value of less than 0.5, which is an interesting fact since extended hopanes in oils have generally reached equilibrium (Waples and Machihara, 1991). Two reservoir rock and one solution seam sample of well 4, which showed elevated maturities according to the hopane ratios (Fig. 19) that correlated well with the maturities monitored by C_{29} 20S/(20S+20R) sterane isomerisation ratio, can be assumed to be impregnated by a migrated oil.

The maturities, as indicated by sterane isomerisation, show a certain degree of variation but can generally be classified as low (Fig. 19). The C_{27} 20S/(20S+20R) ratios range generally between 0.1 and 0.3, independent of sample lithofacies or well, and indicate vitrinite reflectance values of around 0.5 % Ro (Waples and Machihara, 1991). The oil sample from well 8 (E 33435) shows the highest C_{27} 20S/(20S+20R) value of all samples analysed (Fig. 19), which implies that the oil sample is of higher maturity than the source rock samples. C_{27} 20S/(20S+20R) values of well 4 (Fig. 19) show a large discrepancy between the reservoir rock samples and the source rock samples (with exception of the solution seam E 33366/2). This relationship was, as stated above, assumed to indicate an impregnation of the reservoir samples by an oil of higher maturity.

The C_{27} and C_{29} steranes dominate the mass spectra indicating both a marine and land plant influence as proposed by Huang and Meinschein (1979). The terrestrial origin of C_{29} steranes has lately been questioned. Specially the occurrence of C_{29} sterols in lower Palaeozoic and Precambrian sediments has lead to the conclusion that there must be unproved marine sources of this sterane (Volkman, 1986, 1988). Nichols et al. (1990) showed that large amounts of C_{29} sterols are produced by marine diatoms during the spring bloom in cold Antarctic waters. Matsumoto et al. (1982) and Fowler and Douglas (1987) suggest that C_{29} steranes could be derived from cyanobacteria (blue-green algae). Despite these recent advances in the understanding of sterane distributions any simplistic interpretation of C_{27}-C_{29} sterane distributions, especially in terms of palaeoenvironment, is still risky.

The regular steranes/17α(H)-hopanes ratio reflects input of eukaryotic (mainly algae and higher plants) versus prokaryotic (bacteria) organisms to the source rock. In general high concentrations of steranes combined with high sterane/hopane ratios seem to typify marine

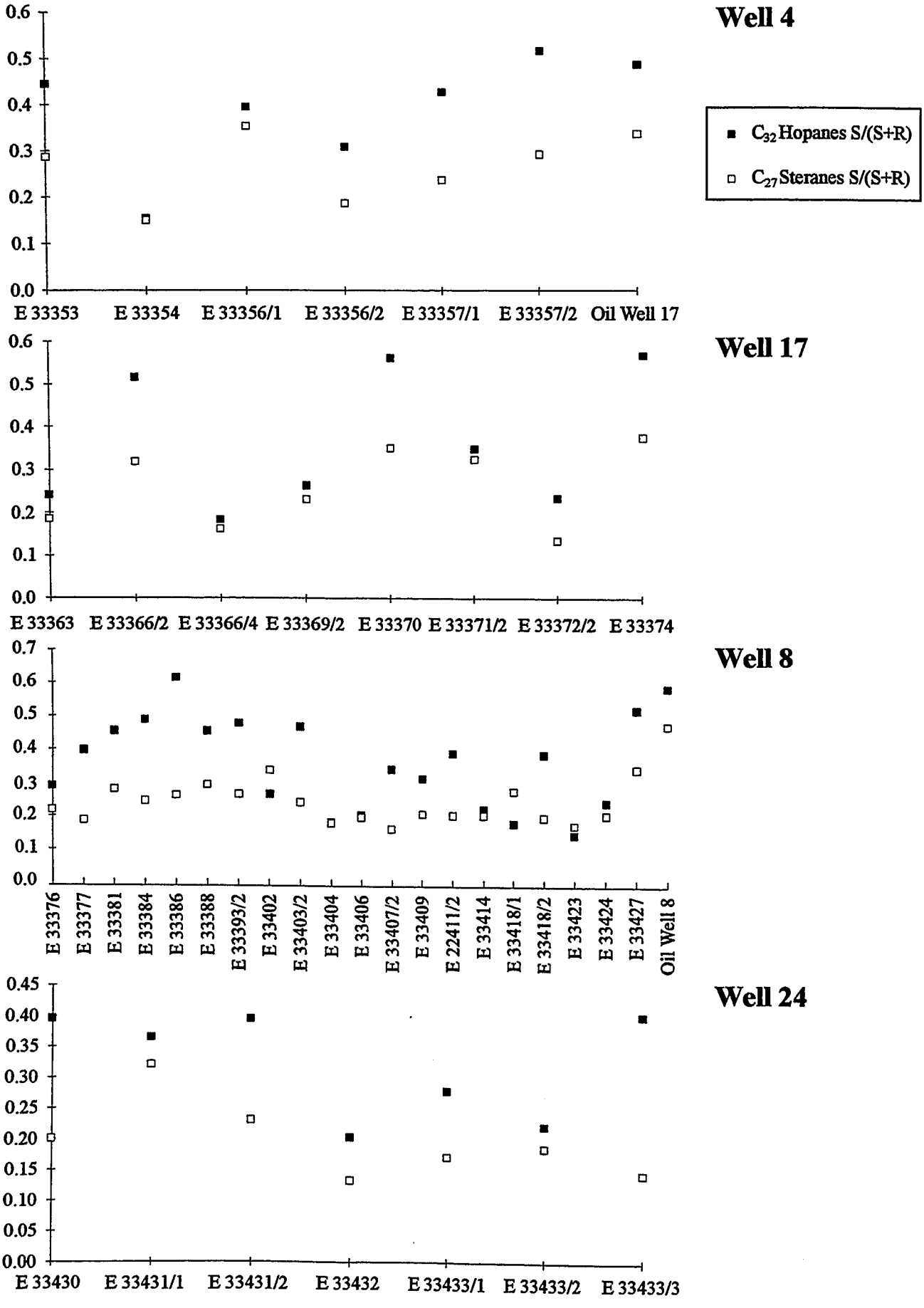

Figure 19: Hopane and sterane maturity determinations for selected samples from all wells and both crude oils. Calculated ratios were C32 hopane 22S/(22S+22R) and C27 sterane 20S/(20S+20R).

organic matter with major contributions from planktonic and/or benthic algae (e.g. Moldowan et al., 1985). Conversely, low amounts of steranes and low sterane/hopane ratios are more indicative of terrigenous and/or microbially reworked organic matter (e.g., Tissot and Welte, 1984, page 426). Based on these observations it can be concluded, that the organic matter in the source rock formation shows signs of both types of organic matter input (Fig. 20, Table 12).

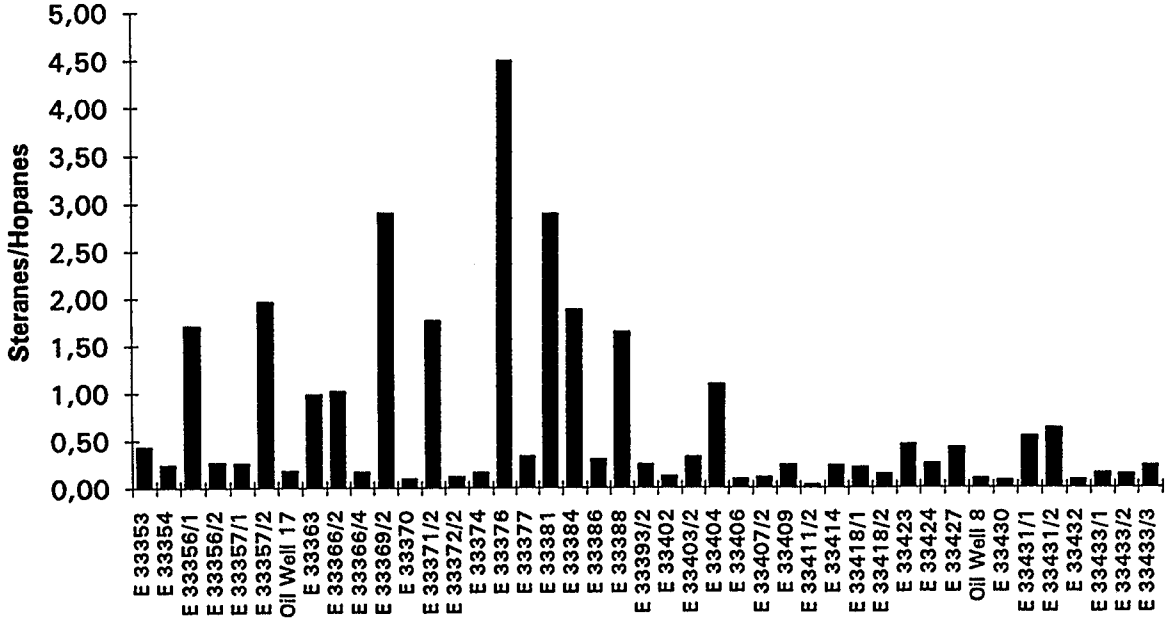

Figure 20: Sterane/hopane ratios of selected samples analysed by GC/MS.

2.1.5.4 Aromatic Hydrocarbons

Regular changes of amounts and distribution patterns of aromatic compounds with increasing maturity observed by different authors (Alexander et al., 1984; 1985; Radke et al., 1982a; 1982b; 1986) have, in the past fifteen years, lead to the general acceptance of aromatic maturity parameters as tools for measuring organic maturation in source rocks and crude oils. In general these maturity indicators rely either on an increase in the degree of alkylation of a given parent compound with maturity or on a change in the isomer distribution of alkyl-aromatic homologues towards thermally more stable isomers (Radke, 1988).

The aromatic fraction of nine selected samples, which were chosen to cover all wells and source lithofacies, were analysed by gas chromatography with coupled FID and HECD detectors. The main goal of this analysis was to achieve a maturity assessment for the four wells analysed. These wells were, due to the lack of suitable vitrinite reflectance data, selected to cover a wide depth range for the source rock unit studied. Due to contamination of the only shale sample in well 17 (E 33360) by a wax coating of the core no kerogen type I was analysed in this well.

Initial GC analysis performed after MPLC revealed a superabundance of monoaromatic sulphur compounds which interfered seriously with the compounds relevant for maturity estimation. A chromatographic separation of the monoaromatic sulphur compounds proved unsuccessful so that the sulphur compounds in the aromatic fraction had to be removed by oxidation and subsequent MPLC separation. High performance liquid chromatography (HPLC, Radke et al., 1984b) allowed the detailed molecular analysis of the different aromatic ring classes.

The following aromatic ratios were calculated: methylnaphthalene ratio (MNR), ethylnaphthalene ratio (ENR), dimethylnaphthalene ratio (DNR), trimethylnaphthalene ratio (TNR), methylphenanthrene ratio (MPR), dimethylphenanthrene ratio (DPR), methyl-phenanthrene index 1 (MPI 1), methylphenanthrene index 2 (MPI 2), methyldibenzothiophene ratio (MDR), methyldibenzothiophene ratio 1 (MDR 1), methyldibenzothiophene ratio 2,3 (MDR 2,3), and the methyldibenzothiophene ratio 4 (MDR 4) (Radke and Welte, 1983; Alexander et al., 1984; 1985; Radke et al., 1986; Radke, 1987; 1988). Only the MPI 1, MPI 2 and MDR 4 ratios show an increase with depth (Fig. 21, Table 13). The increase in MPI 1 and MPI 2 is only noticeable for the samples with a kerogen type II (solution seam and laminite samples), marked in figure 21 according to their corresponding kerogen type. Samples with a kerogen type I (mainly shales) show a reverse trend.

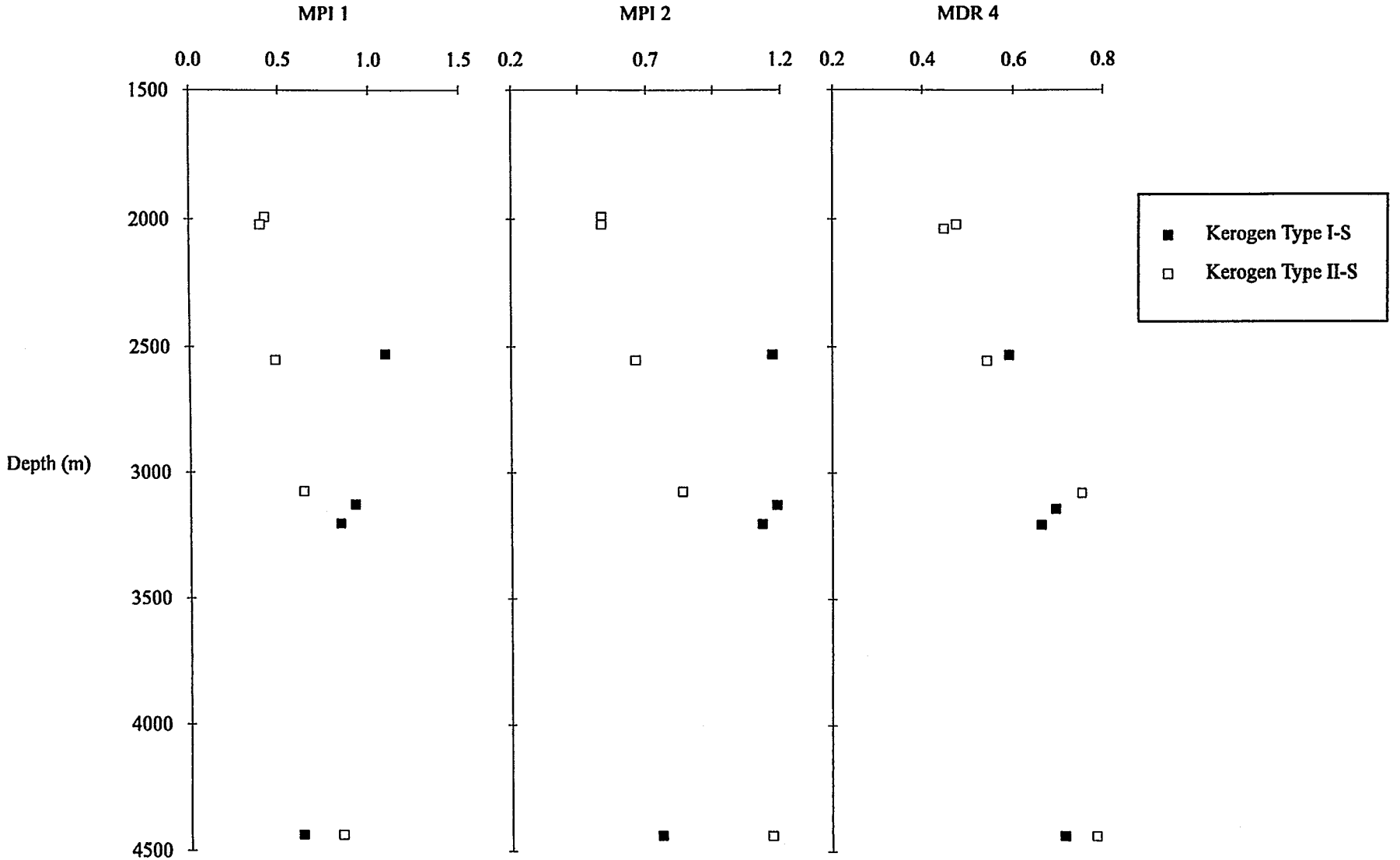

Figure 21: Methylphenanthene-Index (MPI) 1 and 2 and Methyldibenzothiophene Ratio (MDR) 4 of selected samples plotted against sample depth.

2.1.5.5 Characterisation of the asphaltene fractions

One of the characteristics of sulphur-rich source rocks is the high asphaltene content in source rock bitumens and correlated crude oils. Extremely high yields of extractable organic matter rich in high molecular weight, polar material are common for carbonate-evaporite source rocks (Palacas, 1989). Soluble organic matter contents ranging between 10 and 80 percent of the total organic carbon have been reported by Palacas (1984), Palmer and Zumberge (1981), Powell (1984), and Tannenbaum and Aizenshtat (1985) in interbeds of immature carbonate-evaporite facies.

Asphaltenes are classically seen as intermediate products along the pathway leading progressively from kerogen to hydrocarbons (Tannenbaum and Aizenshtat, 1985; Orr, 1986). Their generation at low levels of maturity is attributed to the preferential cleavage of weak carbon-sulphur and sulphur-sulphur bonds in type II-S kerogens (Orr, 1986). However, high soluble organic matter contents are sometimes assumed to be of primary origin, at least in immature source rocks. Powell (1984) stated that the extreme reducing conditions in the depositional environment of sulphur-rich source rocks can cause retardation of the condensation or polymerisation of kerogen precursor molecules, resulting in abnormally high ratios of lipid-like soluble organic matter (predominantly resins and asphaltenes) to insolubles (kerogen). Sinninghe Damsté et al. (1989) proposed that high asphaltene contents in bitumens associated with sulphur-rich kerogens are possibly formed directly, by interaction of hydrogen sulphide with unsaturated and functionalised lipids, rather than through degradation of kerogen.

High asphaltene contents in oils are attributed to their solubilisation by interactions with the high-sulphur aromatic and resin components as originally proposed by Pfeiffer and Saal (1940) and more recently advocated by Tissot (1984).

Independent of where the asphaltenes come from, their importance as sources of geochemical information are undisputed. The pyrolysates of asphaltenes show great similarity to both the associated kerogens (Tannenbaum and Aizenshtat, 1985; Orr, 1986; Sinninghe Damsté et al., 1989; Muscio, 1991) and oils (Rubinstein et al., 1979; Aquino Neto et al., 1981), which makes asphaltene pyrolysis a powerful tool for correlations.

The analysis of asphaltenes by degradation or desulphurisation has lead to interesting insights. In a review article Rullkötter and Michaelis (1990) stated that high-molecular-weight material may contain palaeoenvironmental information which cannot be retrieved from the analysis of the low-molecular-weight constituents of geological samples. Sinninghe Damsté et al. (1990) showed that certain biomarkers may be selectively preserved in high molecular weight sulphur-

rich organic matter, and that the analysis of these materials may provide additional information on their depositional environments.

The presence of very large amounts of resins and asphaltenes in solvent extracts of immature carbonate rocks has important implications for the hydrocarbon generation process during subsequent stages of catagenesis. These substances could act, in addition to the solid kerogens, as major precursors of hydrocarbons (Tissot, 1984), and, according to Palacas (1983), should be transformed under somewhat less intense thermal conditions due to the less condensed structure of these substances. Lewan (1992) stated that, as determined by hydrous pyrolysis, early hydrocarbon generation proceeds in two overall reactions. The first is the generation of bitumen by cleavage of weak non-covalent bonds in the kerogen, and the second as thermal maturation increases, the partial decomposition of bitumen (i.e. high molecular weight soluble organic matter) to a free-flowing liquid oil. In this second stage the amount of kerogen remains constant.

The above stated geochemical properties of high molecular weight soluble organic matter have important implications for petroleum exploration, especially for heavy-oil resources in carbonate or evaporitic regimes. For basin modelling of such carbonate-evaporitic source facies data on the kinetics of hydrocarbon generation from asphaltenes should also be considered since they sometimes comprise an important amount of the total organic matter.

In order to elucidate the geochemical characteristics of the asphaltenes present in the source rock and oil samples of the study area, and to quantify their contribution to petroleum generation, a series of analyses were performed. These included the routine TOC and Rock-Eval analyses, elemental analysis, one-step and multi-step PyGC analyses, MSSV pyrolysis and a series of kinetic evaluations. In this chapter only the TOC, Rock-Eval and elemental analysis data are discussed.

Only four asphaltene samples were analysed because the analytical techniques used are usually applied to rock or kerogen samples where large sample amounts are commonly available. Asphaltenes can only be moved from one sample holder to another in solution. Since the sample holders for TOC and Rock-Eval analysis are porous, several tests had to be made to find out which sample amount is necessary, and which inorganic substrate is best for asphaltene analysis. Therefore large quantities of asphaltenes were necessary and these were only available from the four samples listed below. Only both oil samples (E 33435, Well 8; E 33436, Well 17), one intraformational reservoir sample (E 33427, Well 8) and one source rock sample (E 33366/4, Well 4) contained sufficient amounts of asphaltenes for this type of analysis.

The TOC contents of the four asphaltenes analysed varied between 61 and 65.3 % (Table 14). TOC contents of asphaltenes reported in the literature lie usually around 80 % (Speight and Moschopedis, 1981). The organic carbon content of these asphaltenes is therefore quite low.
The hydrogen index varies from 756 mg HC/g TOC for the oil sample from Well 8 to 1286 mg HC/g TOC for the source rock extract from Well 4. The oxygen index remains in a relatively narrow range of 2 mg CO_2/g TOC (oil Well 8) to 18 mg CO_2/g TOC (source rock extract Well 4). The same two samples also have the highest and lowest Tmax values of the sample suite, namely 436°C for the oil and 409°C for the extract sample (Table 14).
Elemental analysis of the asphaltenes from the reservoir oil sample E 33427 and the two oil samples E 33435 and E 33436 confirmed the results from Rock-Eval analysis although a significant discrepancy was noticed in the organic carbon contents (Table 15). The total organic carbon content of the samples (C %) as measured by elemental analysis was more or less 10 % higher than the values determined by the combustion method routinely applied to source rock samples (LECO). The estimation of asphaltene TOC by LECO seems therefore quite inaccurate. All asphaltene samples showed a very high sulphur content ranging between 9.4 and 10.5 %. The S/C ratio of the asphaltene samples was 0.05 for the three samples and defines them, according to Orr (1993), as derivates of high-sulphur kerogens.
The asphaltene fraction of oil E 33435 (Well 8) had the lowest H/C ratio (1.07), while the reservoir sample and the oil from Well 17 showed identical values of 1.23 for the H/C ratio. The O/C ratios are very low for the three samples analysed (Table 15). Orr (1986) noticed the same effect of reduced O/C ratios in asphaltenes as compared to the source rock kerogens. The low amount of oxygen in the asphaltenes could be an indication that the major part of the oxygen is located in highly condensed aromatic structures which remain part of the kerogen throughout maturation. Thus, during their generation from kerogen in the course of early diagenesis the asphaltenes would observe an oxygen depletion as compared to the corresponding kerogen. The sulphur content would remain, at least during early hydrocarbon generation, more or less constant in both asphaltene and corresponding kerogen. The thermal cracking of a C-S bond may occur in any one of both bonds connecting a sulphur atom to a carbon chain (R-C-S-C-R, where R alkyl or aromatic). Thus the sulphur atom would be either incorporated into the asphaltene or would remain bonded to the kerogen or would be lost from the system by reduction to H_2S. Statistically this would lead to constant sulphur content in asphaltenes and kerogen.

2.1.6 Kerogen Characterisation

Kerogen was the main organic constituent in the source rock formation analysed in this study. The high S2 values determined on unextracted source rock samples and on extracted kerogen concentrates by Rock-Eval demonstrated, that a major portion of the organic matter was still available for the formation of hydrocarbons during further burial and heating (Table 1, 3). The characterisation of the source rock kerogen in terms of thermal lability, type and composition of petroleum it is likely to generate as well as the changes in petroleum gross composition which might occur during kerogen maturation was the main goal in this part of the study.

The classical theory of kerogen formation by biochemical degradation, polycondensation and insolubilisation (Tissot and Welte, 1984) has been modified in the past few years according to new evidence of kerogen composition. Tegelaar et al. (1989) proposed that kerogen is formed at a relatively early stage of diagenesis and that a significant fraction of it is derived from selectively preserved biomacromolecules. Selective preservation is indeed a reasonable proposition as preserved parts of organisms, such as spores, algae or pollen can be recognised in both coal and kerogen. The biomacromolecules preserved in the kerogen have been analysed by different chemical techniques, so that both precursor organic matter and geochemical composition of some of these compounds are relatively well known. Goth et al. (1989) for example, showed that cell wall material of the algae *Tetrahedron* is selectively preserved in the Messel oil shale kerogen. This material, which is rich in aliphatic structures, was termed algenan. Resistant biomacromolecules derived from bacteria, and termed bacterans, were described by Le Berre et al. (1992). Selective preservation has been generally accepted as being a mechanism which leads to kerogen formation, although the amount of material which is incorporated into the kerogen by this path is sometimes assumed to be minor.

Analysis of kerogen by different pyrolysis techniques allows the estimation of hydrocarbon potential, generation characteristics, precursor organisms, main organic compounds classes and bonding characteristics of the kerogen. Various techniques were applied in this study in order to elucidate the composition of the kerogen present in the source rock formation.

2.1.6.1 Kinetics of petroleum generation

The generation of petroleum from kerogen is a process which depends on numerous parallel and/or successive chemical reactions. Many different types of bonds are present in kerogen (e.g. C-C, C-S, C-N, C-O), each having distinct rupture energies. The rupture energy of a given bond type varies according to, for example, neighbouring functional groups or chain length. The ease with which a given kerogen can generate petroleum depends therefore on the type, amount and distribution of bonds in its matrix.

The hydrocarbon generation characteristics of a given kerogen can be described by its distribution of activation energies. Type I kerogens generally contain a large proportion of labile organic matter which is interlinked by mainly carbon-carbon bonds. The predominance of one bond type in the kerogen results in a narrow activation energy distribution, with a characteristically high mean activation energy due to the stable carbon-carbon bonds (Tissot and Welte, 1984). Higher amounts of different bond types in the kerogen imply a wider activation energy distribution, as for example present in type II and III kerogens.

The kinetic description of the hydrocarbon generation characteristics of a given kerogen is commonly used as a tool for modelling its behaviour in geologic time. The onset of petroleum generation can be calculated, using the kinetic parameters activation energy and frequency factor, for different geologic heating rates.

Kinetic analysis of source rock samples from the basin analysed in this study was performed in order to estimate the beginning of hydrocarbon generation, i.e. to produce data concerning the lowest temperature necessary to generate petroleum from the kerogen at different heating rates.

A total of five extracted source rock samples were selected, primarily by their organic carbon content, for programmed-temperature pyrolysis with subsequent kinetic modelling of bulk petroleum generation (E 33360, E 33363, E 33366/4, E 33424, E 33432). Palacas (1983) stated that the presence of very large amounts of resins and asphaltenes in organic extracts of immature carbonate rocks could have important implications for the hydrocarbon generation process during subsequent stages of catagenesis since these substances could act, in addition to the solid kerogens, as major precursors of hydrocarbons under less intense thermal conditions. In order to test this hypothesis five asphaltene fractions (E 33357/2 As, E33366/4 As, E33401 As, E 33406 As, E 33409 As) were precipitated from the total source rock extracts and analysed as indicated above.

The mathematical model has been described by Schaefer et al. (1990) and is based on the kinetic analysis of measured bulk petroleum formation rate (dM/dT) versus temperature (T) curves

$$\frac{dM}{dT} = \sum_{i=1}^{n} M_i \frac{A}{r} \exp\left(- \frac{E}{RT} - \frac{A}{r} J_i \right)$$

$$J_i = \int_0^T \exp\left(- \frac{E}{RT} \right) dT$$

assuming in each case n=25 first-order reactions with activation energies regularly spaced between 46 and 70 kcal/mol and a single pre-exponential factor A. The model furthermore implies the measurement of dM/dT versus T profiles at three heating rates of r = 0.1, 0.7 and 5.0 K/min. These heating rates are low enough as to ensure correct temperature measurements (Burnham et al., 1988) and sufficiently different to derive a reasonable starting value of A from the shift of peak generation rate temperatures (Jüntgen and van Heek, 1968). A total number of 26 parameters, namely 25 initial potentials (partial petroleum yields) M, associated with the 25 activation energies E, and the pre-exponential factor A are optimised by a least-squares iteration method that compares measured and calculated formation rates at 300 (100 per heating rate) temperatures until the corresponding error function (sum of squared differences) shows a well-defined absolute minimum (Schenk et al., 1992).

The petroleum generation curves of the source rock samples measured at heating rates of 0.1, 0.7 and 5.0 K/min are shown in the figures 22a-e. The best fit between experimental (dotted lines) and calculated (solid lines) formation rates were obtained with the activation energy distributions depicted in Figs. 23a-e. The pre-exponential factors ranged between 2.0 E+15 and 5.8 E+17.

Suprisingly all source rock samples show a relatively broad activation energy distribution, independent of the kerogen type as defined by Rock-Eval. The expected narrow activation energy distribution which is characteristic of type I kerogens was not encountered. The two source rock samples, which possess a type I kerogen (E 33366/4 and E 33424), show the lowest main activation energies, the lowest frequency factors and in general a wide distribution of activation energies (Figs. 23c, 23d). These observations are probably due to the high organic sulphur content (10 and 12%, Table 4) of these type I kerogens. It has been shown that the thermal degradation of type II-S kerogens occurs at a very early stage of thermal history of the rocks (Rullkötter et al., 1985; Tannenbaum and Aizenshtat, 1985; Orr, 1986; Sinninghe Damsté et al., 1989; Rullkötter et al., 1990). A type I-S kerogen, as defined by Sinninghe Damsté et al. (1993) seems, according to these findings, also to react in a similar fashion.

The asphaltene samples show very constant activation energy distributions ranging from 46 to 56 kcal/mol and pre-exponential factors between 6.6 E+14 to 2.2 E+15 (Fig. 24a-e, 25a-e).

The adaptation of the laboratory-derived non-isothermal kinetic models to different time-temperature regimes of geological maturation by a simple readjustment of the parameter "heating rate" in the equation above is illustrated in Fig. 26. This extrapolation compares calculated bulk petroleum formation rates for a laboratory heating rate of 0.1 K/min and three geological heating rates of 10^{-12}, 10^{-11} and 10^{-10} K/min (0.53, 5.3 and 53 K/10^6a) using sample

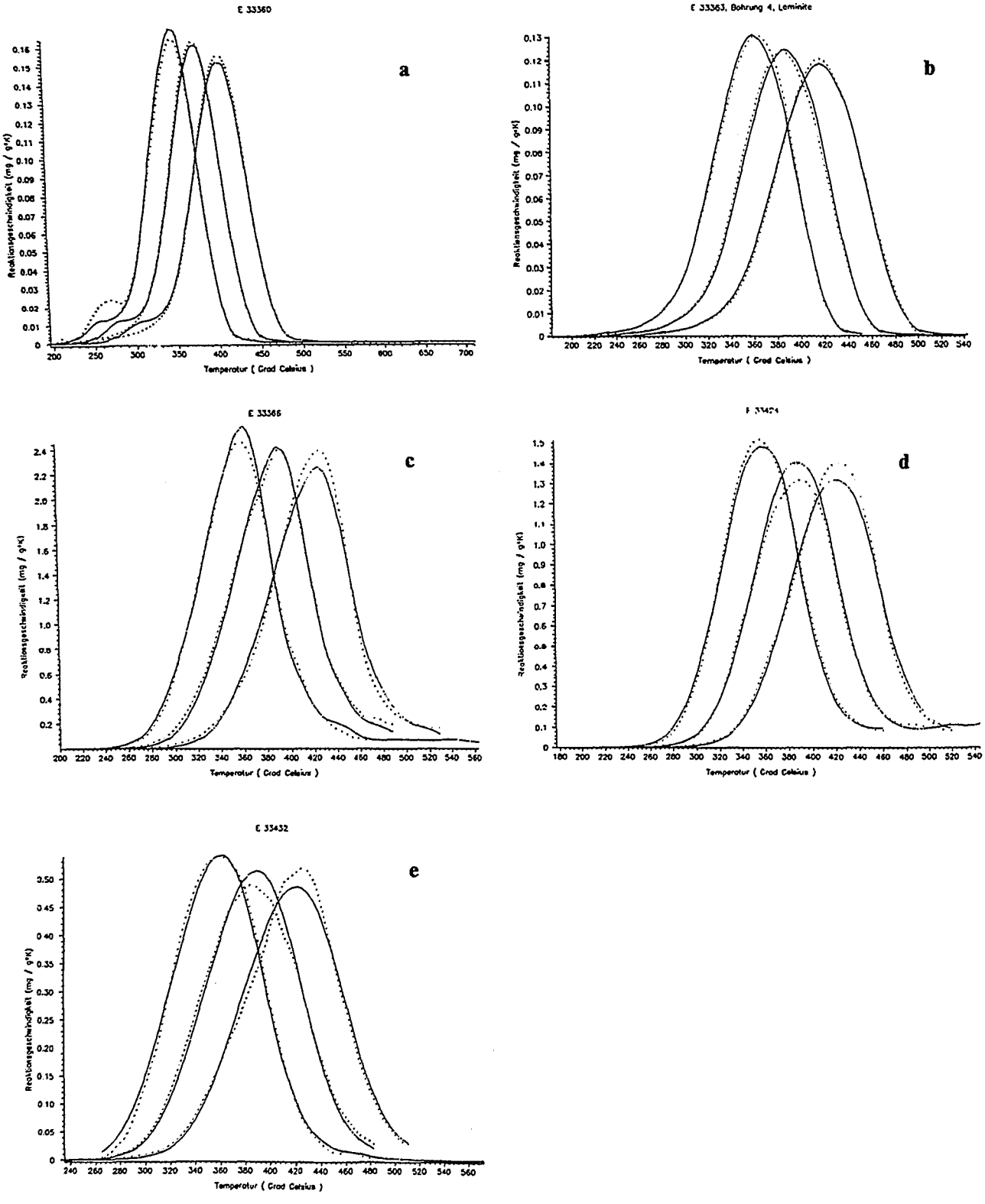

Figure 22: Hydrocarbon generation curves measured at heating rates of 0.1, 0.7 and 5.0 K/min of whole rock samples E 33360 (a), E 33363 (b), E 33366/4 (c), E 33424 (d) and E 33432 (e). Best fit between experimental (dotted lines) and calculated formation rates (solid lines) were obtained with the activation energy distributions shown in Fig. 33.

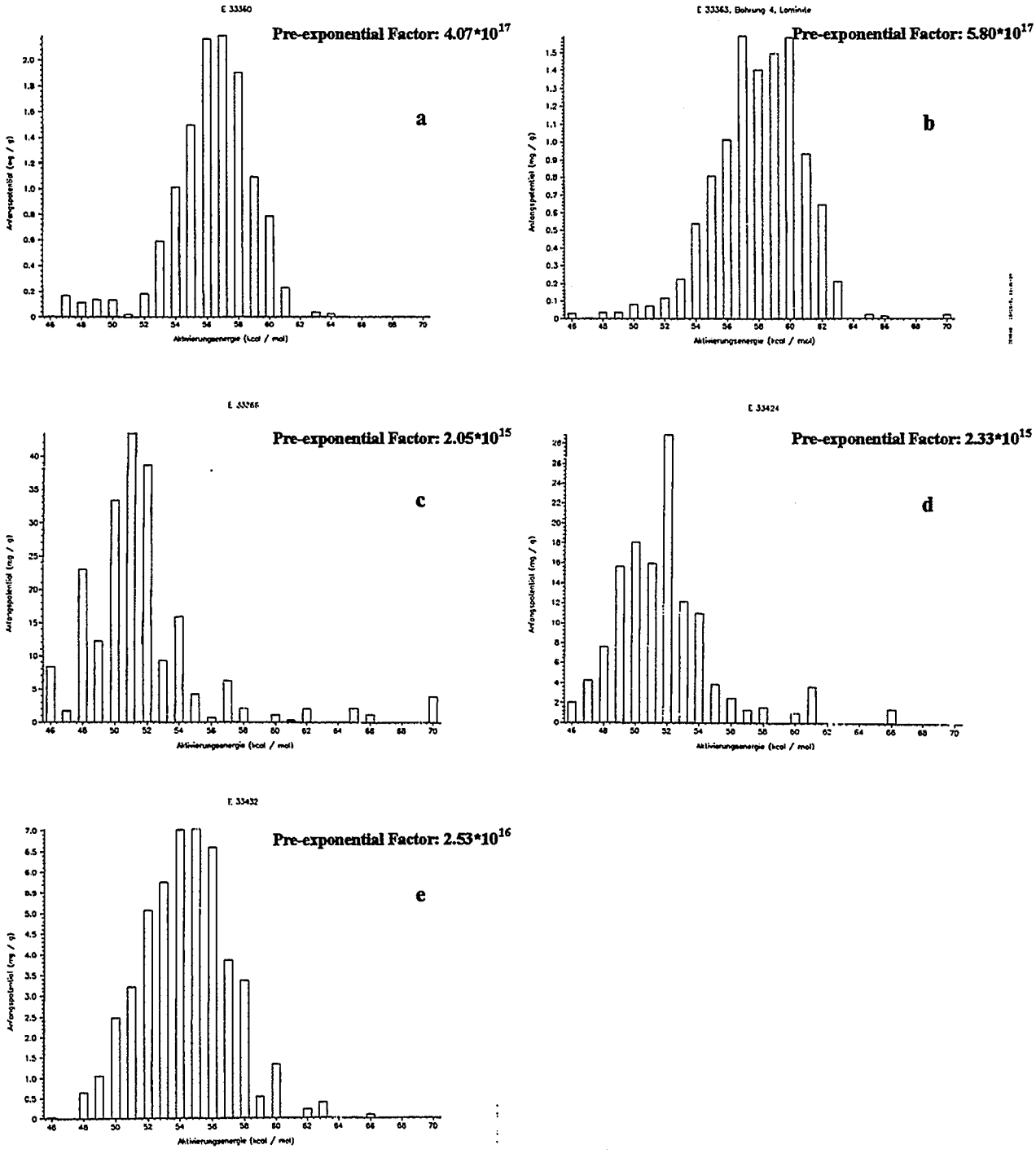

Figure 23: Activation energy distributions calculated for the whole rock sample E 33360 (a), E 33363 (b), E 33366/4 (c), E 33424 (d) and E 33432 (e). Corresponding pre-exponential factors are written in the upper right corner of each figure.

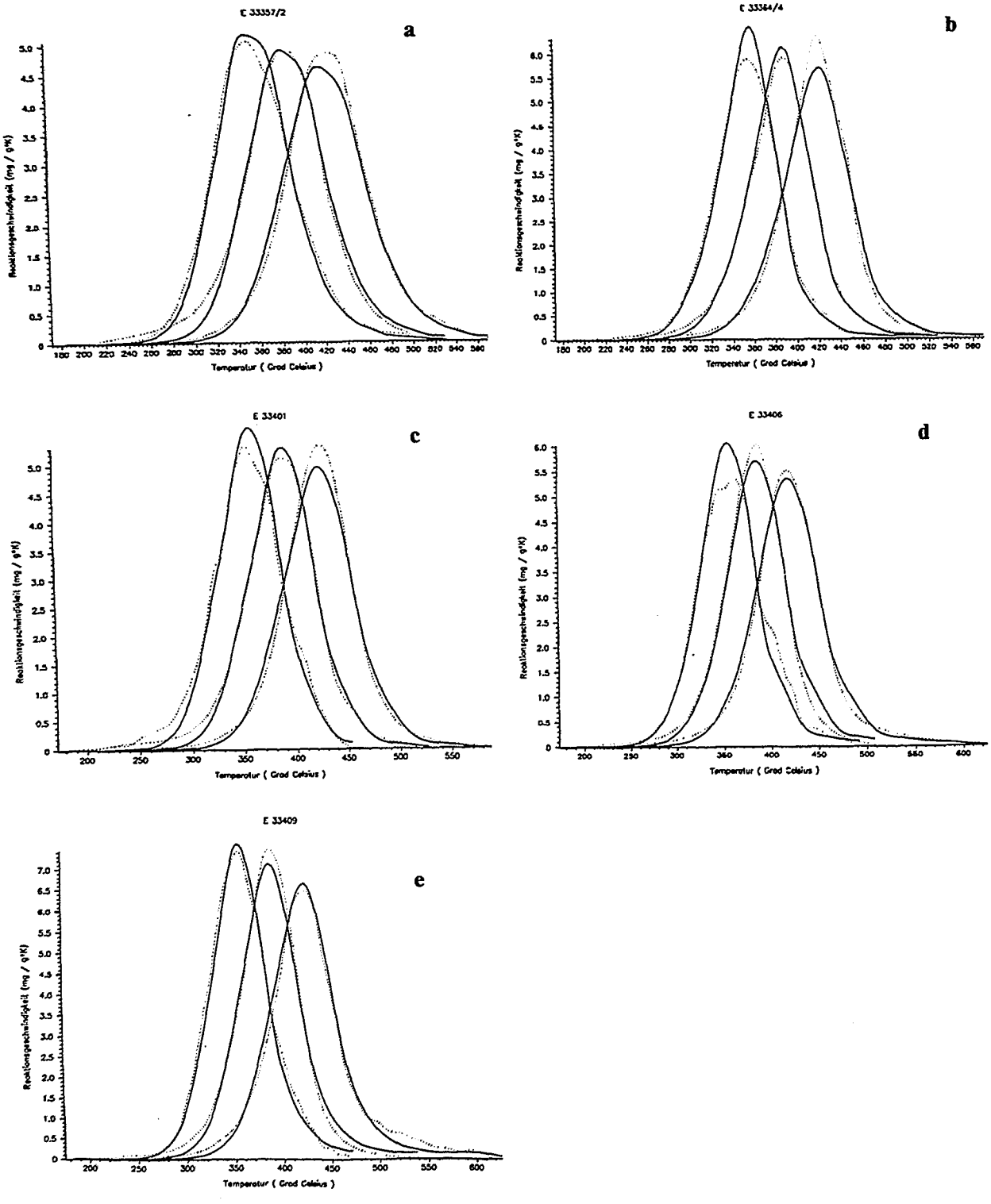

Figure 24: Hydrocarbon generation curves at heating rates of 1.0, 0.7 and 5.0 K/min of whole rock samples E 33357/2 (a), E 33366/4 (b), E 33401 (c), E 33406 (d), and E 33409 (e). The best fit between experimental (dotted lines) and calculated formation rates (solid lines) were obtained with the activation energy distributions shown in Fig. 35.

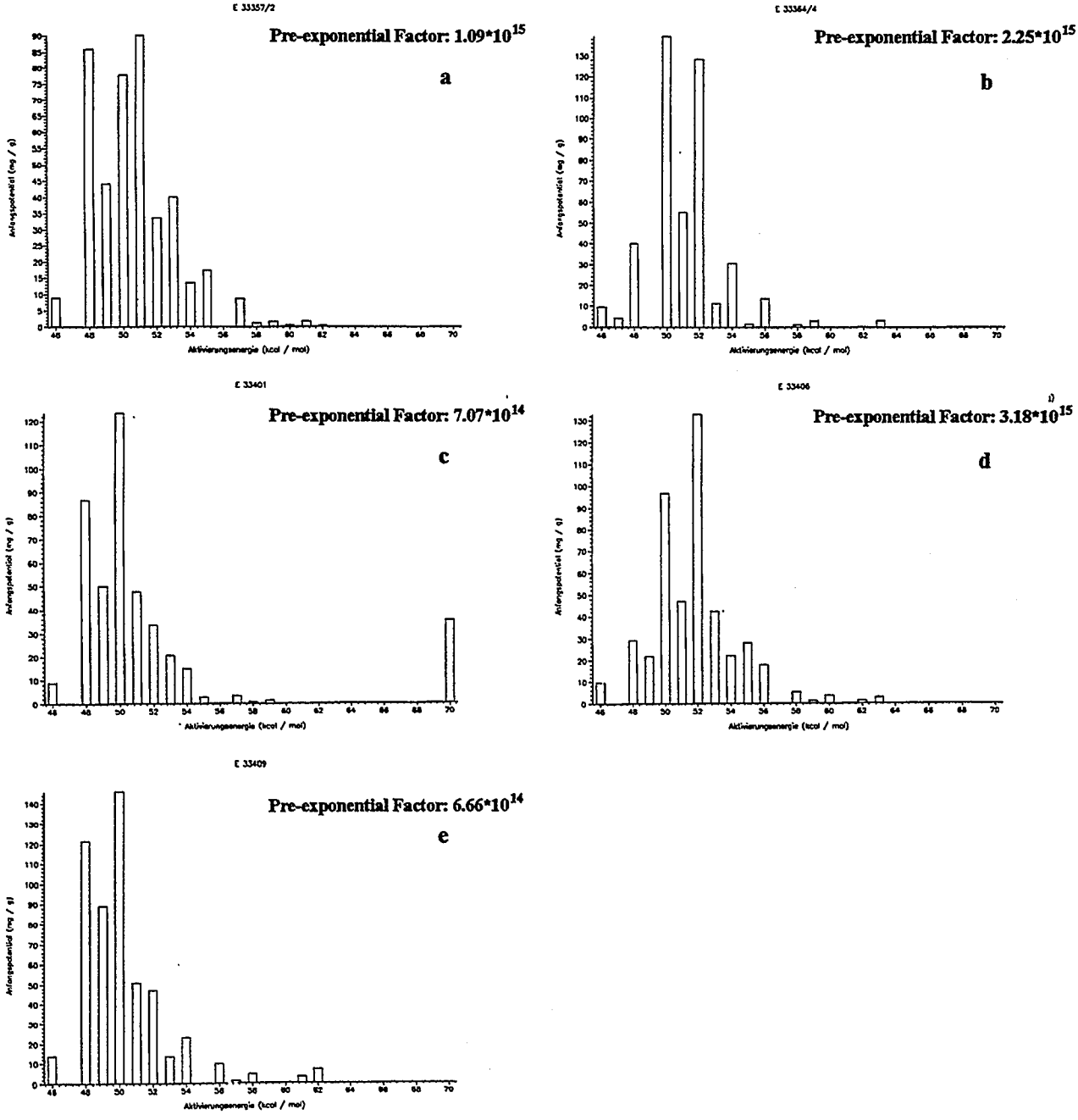

Figure 25: Activation energy distributions calculated for the asphaltene samples E 33357/2 (a), E 33366/4 (b), E 33401 (c), E 33406 (d), and E 33409 (e). Corresponding pre-exonential factors are written in the right corner of each figure.

E 33366 as an example. Geological Tmax values, calculated according to the respective bulk petroleum formation rates at 0.1 K/min, are found between 110 and 165°C for asphaltene and source rock samples. The formalism of non-isothermal kinetics implies that maximum formation rates increase whereas Tmax values and curve widths decrease with decreasing rate of heating (Jüntgen and van Heek, 1968).

The cumulative proportions of total petroleum potential with increasing activation energy of the source rock samples, as shown in Fig 27, point to relatively inhomogeneous organic matter in each of the samples. The more or less gradual increase of each of the depicted curves is due to the comparatively large number of parallel reactions involved in the pyrolytic generation of hydrocarbons which, in turn, is related to the composition of the organic matter. Homogeneous organic matter is normally characterised by an abrupt increase in the cumulative proportions of total petroleum potential, indicating a small number of reactions involved in the generation of hydrocarbons (Schenk et al., 1992). The asphaltene samples show a similar behaviour as depicted in Fig. 28.

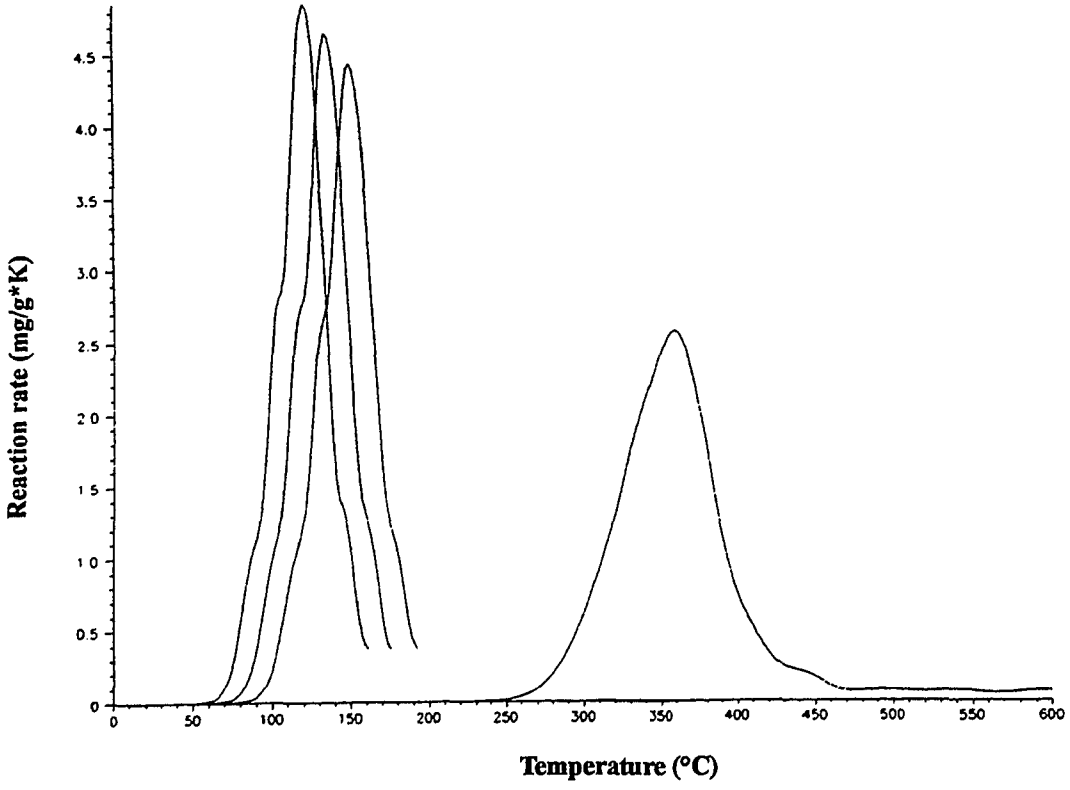

Figure 26: Calculated bulk petroleum formation rates of sample E 33366/4 for a laboratory heating rate of 0.1 K/min and three geological heating rates of 10^{-12}, 10^{-11} and 10^{-10} K/min.

For a single first-order reaction the temperature T_{max} of maximum formation rate ν_{max} can be approximated by

$$T_{max} = E/(\ln A - \ln r + \ln M - \ln \nu_{max}{}^{-1})$$

where M denotes the total potential associated with this reaction. At every rate of heating r the value of T_{max} will mainly be determined by the ratio of the activation energy E and the logarithm of the pre-exponential factor A; this ratio E/lnA may be termed "normalised" activation energy (Schenk et al. 1992). Figs. 29 and 30 show, for all samples, the cumulative proportion of total bulk petroleum potential with increasing "normalised" activation energy (normalised to 1°C/min heating rate). The shape of the curves still displays the inhomogeneous character of the source rock samples (Fig. 29), but in addition, the shift of these curves with increasing E/lnA reflects increasing temperatures of hydrocarbon generation under laboratory conditions. In Fig. 30 the asphaltene samples display a very homogeneous normalised activation energy distribution, which implies a strong chemical similarity between the samples.
In Fig. 29 it is interesting to notice that the sulphur-rich source rock samples E 33366/4 and E 33424, which had the lowest activation energies (Figs. 23c, 23d, 27), now show the highest values for E/lnA. This was due to the influence of the low pre-exponential factors of these samples. In Fig. 29 the influence of the pre-exponential factors on the activation energy is removed so that the "normalised" activation energies depend directly on the temperature. The E/ln A distributions of the asphaltene samples show remarkable similarity to the source rock samples, both in the formation curve form and distribution of E/ln A values (Fig. 30).
For a distributed energy model the simplified quantity E/(lnA-lnr), with E representing the dominant activation energy of the distribution of each sample (Figs. 23a-e, 25a-e), is a good measure of T_{max} at both laboratory and geological heating rates r (Horsfield and Schenk, 1993). This simplified quantity is plotted as a function of ln r for the five source rock samples in Fig. 31. These figures confirm the decrease in T_{max} with decreasing heating rate, specially in going from laboratory to natural conditions. The stronger decrease of the thermal stability of source rock samples with a kerogen type I-S (E 33366/4 and E 33424) as compared to the three others (Fig. 31) is due to the lower pre-exponential factors and the lower dominant activation energies. According to these facts it seems likely that, under geological conditions, kerogens of type I-S generate hydrocarbons at lower levels of thermal stress than typical type II kerogens.

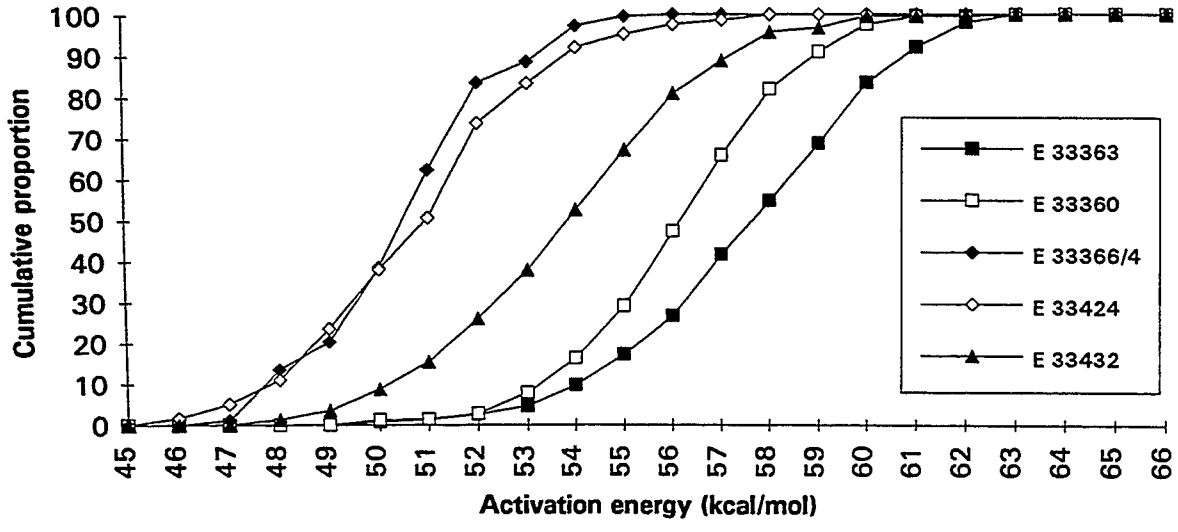

Figure 27: Cumulative proportion of total petroleum potential with increasing activation energy for the source rock samples analysed.

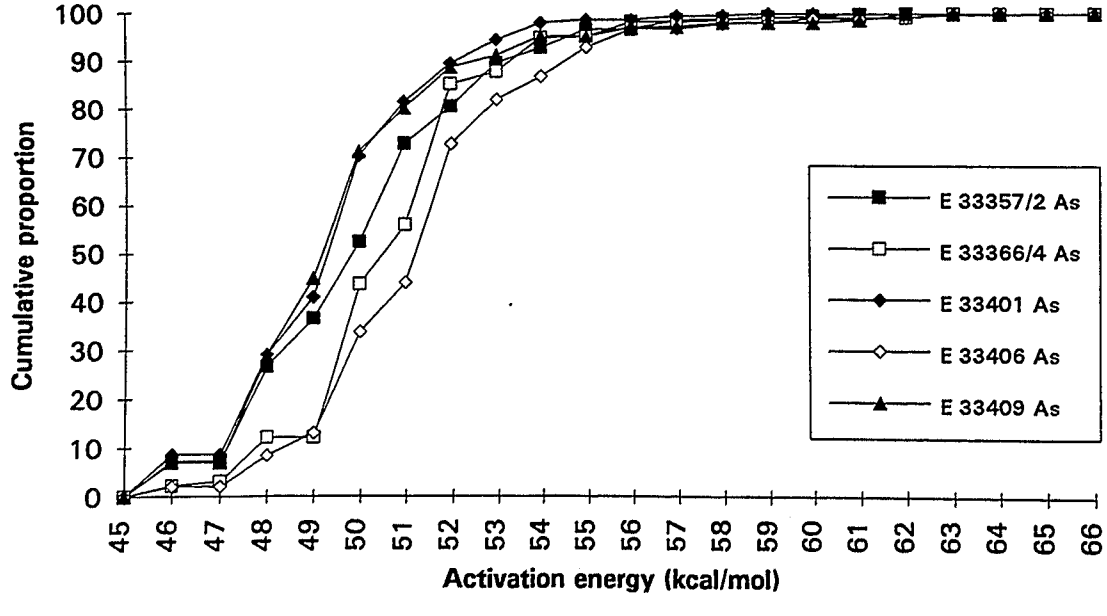

Figure 28: Cumulative proportion of total petroleum potential with increasing activation energy for the asphaltene samples analysed.

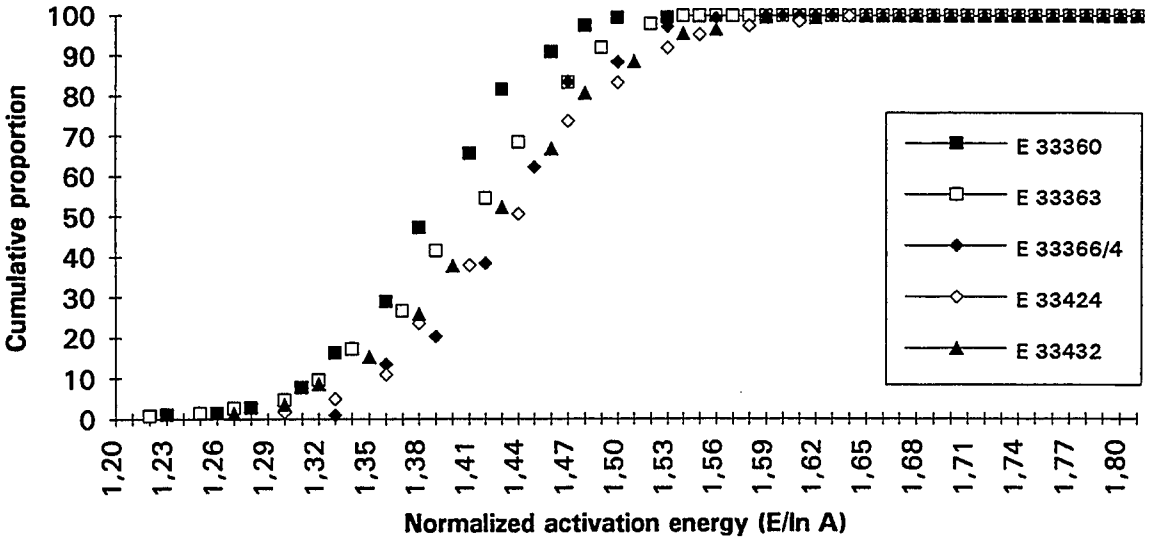

Figure 29: Cumulative proportion of total petroleum potential with increasing normalised activation energy for the whole rock samples analysed.

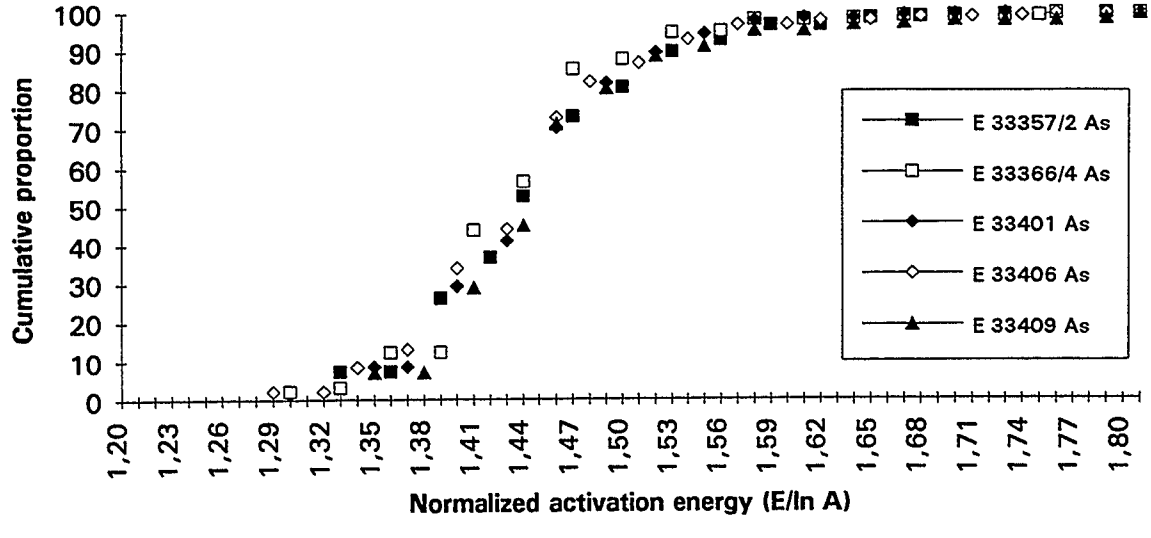

Figure 30: Cumulative proportion of total petroleum potential with increasing normalised activation energy for the asphaltene samples analysed.

The plot of the simplified quantity E/(lnA-lnr) against ln r of the asphaltene samples is almost identical to that of the source rock samples, indicating the same kind of hydrocarbon generation characteristics (Fig. 32).

The dominant activation energies were used to calculate temperatures of peak generation (Tmax) from the different samples at different heating rates. Fig. 33 shows the results for a heating rate of 10^{-12} K/min (0.5 K/ma). The Tmax of the kerogens of type II and I-II were calculated using data from Schaefer et al. (1990) and Schenk et al. (1993). Figure 33 confirms previous data (Tissot, 1981; Baskin & Peters, 1992) that sulphur-rich organic matter is thermally more labile than sulphur-poor OM. It additionally demonstrates that the kerogens of type I-S, present in the shale sequences, as well as the corresponding asphaltenes are least stable, due to the fact that the kinetics of volatile product generation are almost identical. The asphaltenes of the type II-S kerogens also lie in the same range, while the corresponding kerogens, present in the laminites, reach peak generation at slightly higher temperatures (5 to 15°C). The generation of volatile products from the asphaltenes occurs therefore at lower levels of thermal stress than from the kerogen (for type II-S). The highest Tmax were found, as expected, in the type I-II kerogens. Thus the theory that asphaltenes generate hydrocarbons at lower levels of thermal stress than corresponding kerogens as proposed by Palacas (1983) can be corroborated, at least for the samples analysed in this study and using the open system method as described above.

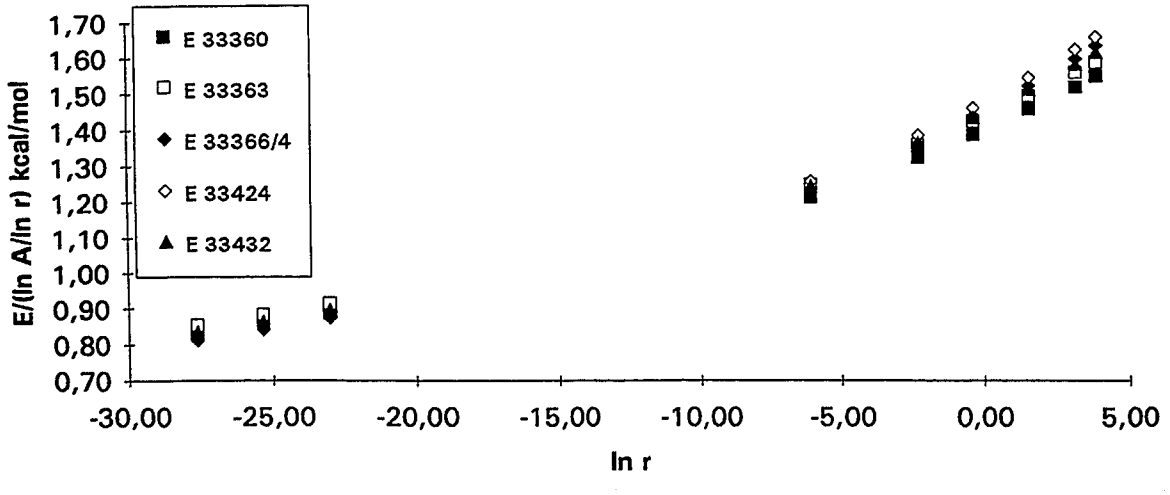

Figure 31: E/(lnA-lnr) versus ln r of the whole rock samples with ln r representing six laboratory and three geological heating rates.

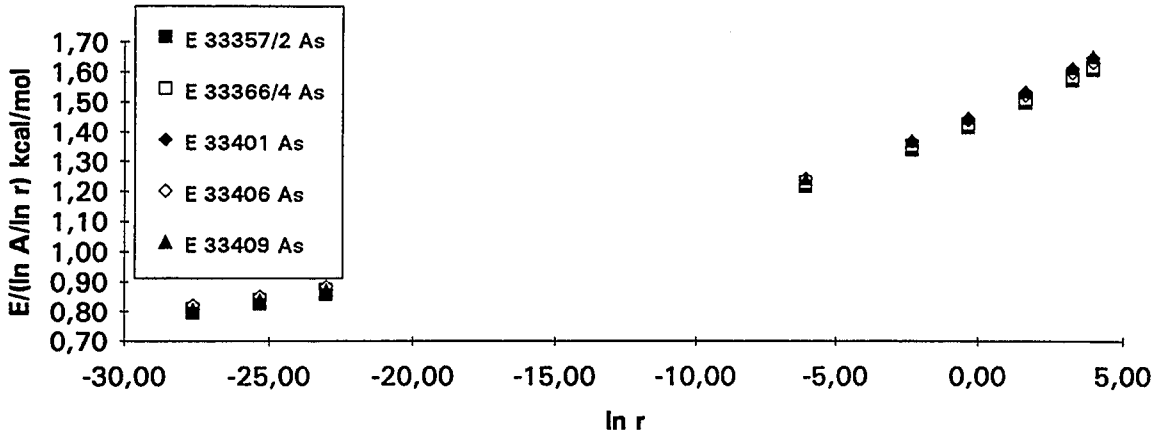

Figure 32: E/(lnA-lnr) versus ln r of the asphaltene samples with ln r representing six laboratory and three geological heating rates.

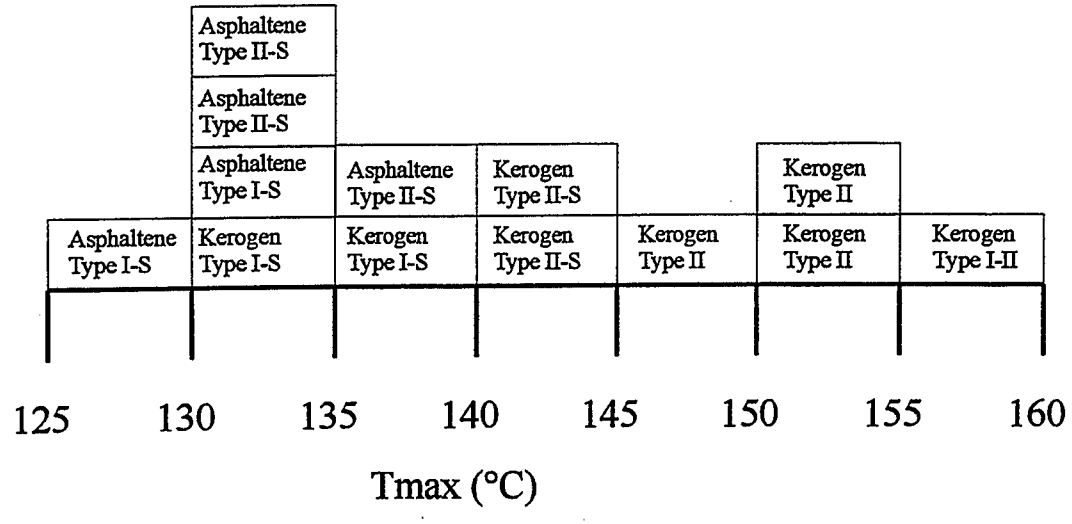

Figure 33: Temperatures of peak petroleum generation at a heating rate of 0.5 K/ma for all samples analysed as well as for two samples from Schaefer et al (1990). Asphaltene types refer to the kerogen type present in the source rock sample from which they were extracted.

2.1.6.2 Characterisation of the kerogen and asphaltenes by pyrolysis studies

The characterisation of kerogen-type based on elemental analysis or Rock-Eval pyrolysis, provides a good basis for the description of gross kerogen composition. The estimation of basic properties of the kerogens or of the petroleums generated therefrom, such as gas-oil ratios (GOR) or wax content must be performed by other methods.

Pyrolysis-gas chromatography (Py-GC) using coupled flame ionisation detection (FID) and sulphur selective Hall® electrolytic conductivity detection (HECD) provides a more detailed insight into kerogen composition.

This technique was selected for the analysis of selected source rock formation kerogens. The samples analysed included kerogens of type I-S and type II-S as well as kerogens which were of intermediate composition.

This Py-GC study focused on four questions. First, what is the difference between the kerogens of Types I-S and II-S? Second, is there a difference between the pyrolysates of kerogens and of the corresponding asphaltenes or between kerogens and the asphaltenes of associated oils? Third, are there differences in the thermal lability of the different kerogens and corresponding asphaltenes? And finally, can sulphur compounds generated during Py-GC be used as maturity or palaeoenvironmental indicators?

In order to answer these questions two Py-GC techniques were used. a) In one-step Py-GC the products released over the temperature range of 300-600°C (40°C/min) are analysed. b) In multi-step Py-GC selected samples were analysed in three pyrolysis stages, whereby three gas chromatograms and, hence, three sets of analytical data were obtained. The first set was for pyrolysate collected between 300-375°C, the second for pyrolysate obtained by heating the residue of the first stage from ambient to 450°C, and the third by heating the residue of the first two stages to 600°C. The concept of multi-step PyGC is that at increasing levels of thermal stress bonds of increasing stability in the analysed substances are cracked. This technique distinguishes in a general way, between products that are associated with immature, mature and overmature kerogens, respectively (Horsfield, 1989). Multi-step pyrolysis was employed because of the limited maturity range of the available samples.

2.1.6.2.1 One-step PyGC

Fifteen kerogen and seven asphaltene samples were analysed by one-step PyGC. The samples selected represented both kerogens of type I and II as defined by Rock-Eval. The samples and results of this analysis are listed in Table 16.

Asphaltenes were available only from the source rock samples E 33366/4 (type I-S kerogen), E 33402 (type I-S kerogen), E 33424 (type I-S kerogen), and E 33431/2 (type I-S/II-S kerogen),

the intraformational reservoir sample E 33427 and the produced oil samples E 33435 (Well 8) and E 33436 (Well 17).

Kerogen samples

n-alkyl and isoprenoid moieties

The C_{5+} pyrolysate compositions of the kerogens analysed in this study are very similar. This is illustrated in Fig. 34 by the chromatograms of two samples which covered a hydrogen index range from 597 mg HC/g TOC (E 33388, Fig. 34a) up to 932 mg HC/g TOC (E 33423, Fig. 34b). All kerogens analysed were dominated by doublets of n-alk-1-enes and n-alkanes extending up to n-C_{30} and by different, mainly thiophenic, sulphur compounds (e.g.: Fig.34, 35a, 36a). Aromatic compounds were of only subordinate importance.

Resolved (C_1-C_5/C_{6+}, resolved GC traces, valley-valley integration) and total (C_1-C_5/C_{6+}, complete GC traces, horizontal baseline) gas/oil ratios (GOR) calculated from PyGC range from 0.39 mg/mg to 0.69 mg/mg and 0.11 mg/mg to 0.22 mg/mg respectively. These results are slightly higher than GOR's calculated for the Posidonia shale (Düppenbecker and Horsfield, 1990; Table 17).

The fact that most of the hydrogen-rich kerogens generate hydrogen-rich compounds during pyrolysis has been known for a long time (e.g. Larter, 1978; van de Meent et al., 1980). Larter and Horsfield (1993) pointed out that neither n-alkyl pyrolysate distribution nor chain lengths are controlled by random chain scission during pyrolysis. Model experiments (Douglas and Larter, 1980; Larter et al., 1983) suggest that alkyl groups in kerogen molecules may produce on pyrolysis alkyl fragments of length and distribution closely related to those of the incorporated parent lipids. The same observation was made by Largeau et al. (1984) in their study of immature torbanites as compared to extant Botryococcus braunii algae. They noticed that the hydrocarbons produced by PyGC of a Botryococcus biopolymer (PRB) showed a very good agreement with the structure of PRB as indicated by IR spectroscopy and ^{13}C NMR analyses.

The occurrence of prist-1-ene in the kerogen pyrolysates indicates the immaturity of the samples analysed here. Prist-1-ene is the principle acyclic isoprenoid found in kerogen pyrolysates (Larter et al., 1979). It is supposed to be derived from tocopherols bound by C-C or C-O bonds in kerogen. Prist-1-ene was shown to decrease in kerogens as pristane is generated in the subsurface (Van Graas et al., 1981; Goosens et al., 1988) or in artificial oils during artificial maturation (Burnham et al., 1982; Eglinton, 1988). The prist-1-ene precursor in flash pyrolysis was demonstrated to be the same as that which produces pristane in the subsurface (Larter and Horsfield, 1993). Phytane precursors in kerogens are less well

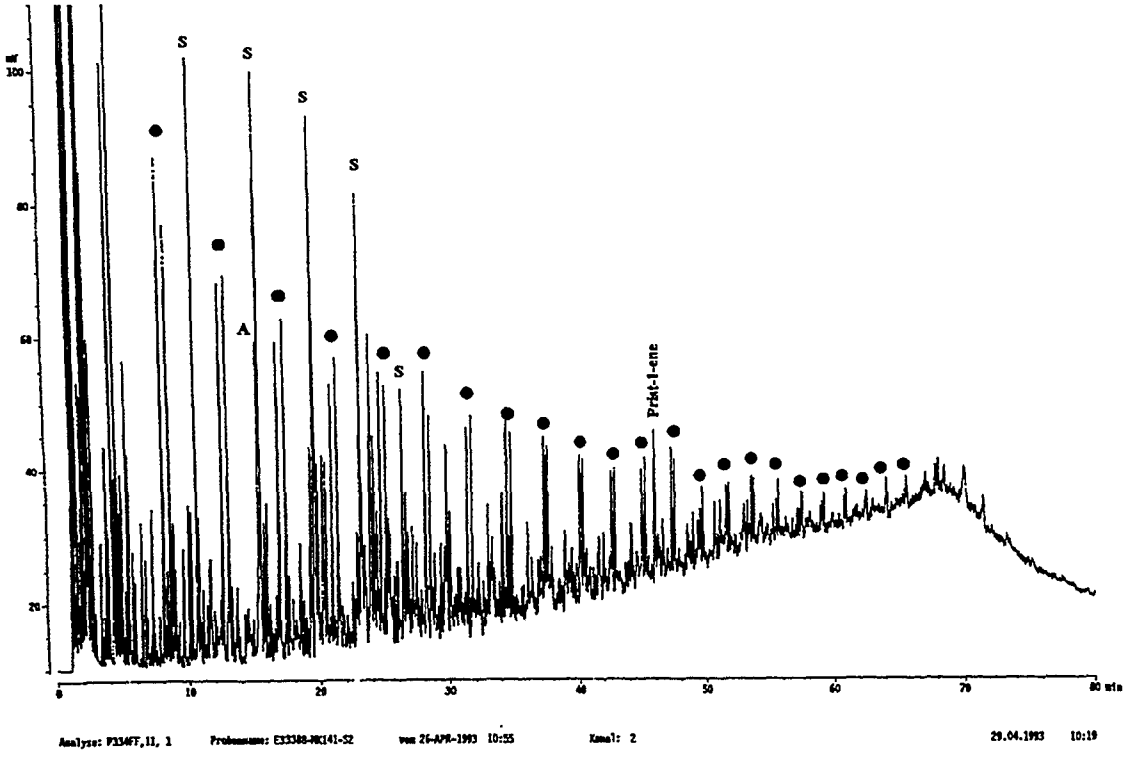

Figure 34a: GC-trace of the pyrolysate generated by mudstone sample E 33388. Alkane-alkene doublets marked by points, sulphur compounds by S and aromatic compounds by A.

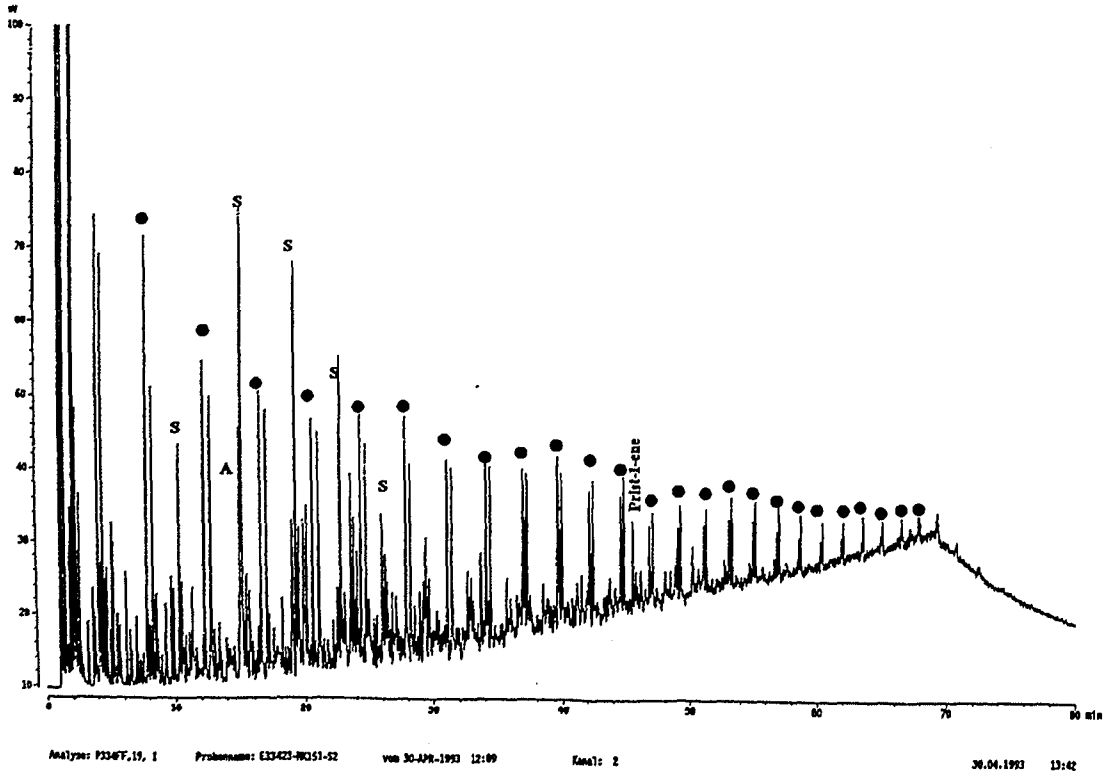

Figure 34b: GC-trace of the pyrolysate generated by shale sample E 33423. Alkane-alkene doublets marked by points, sulphur compounds by S and aromatic compounds by A.

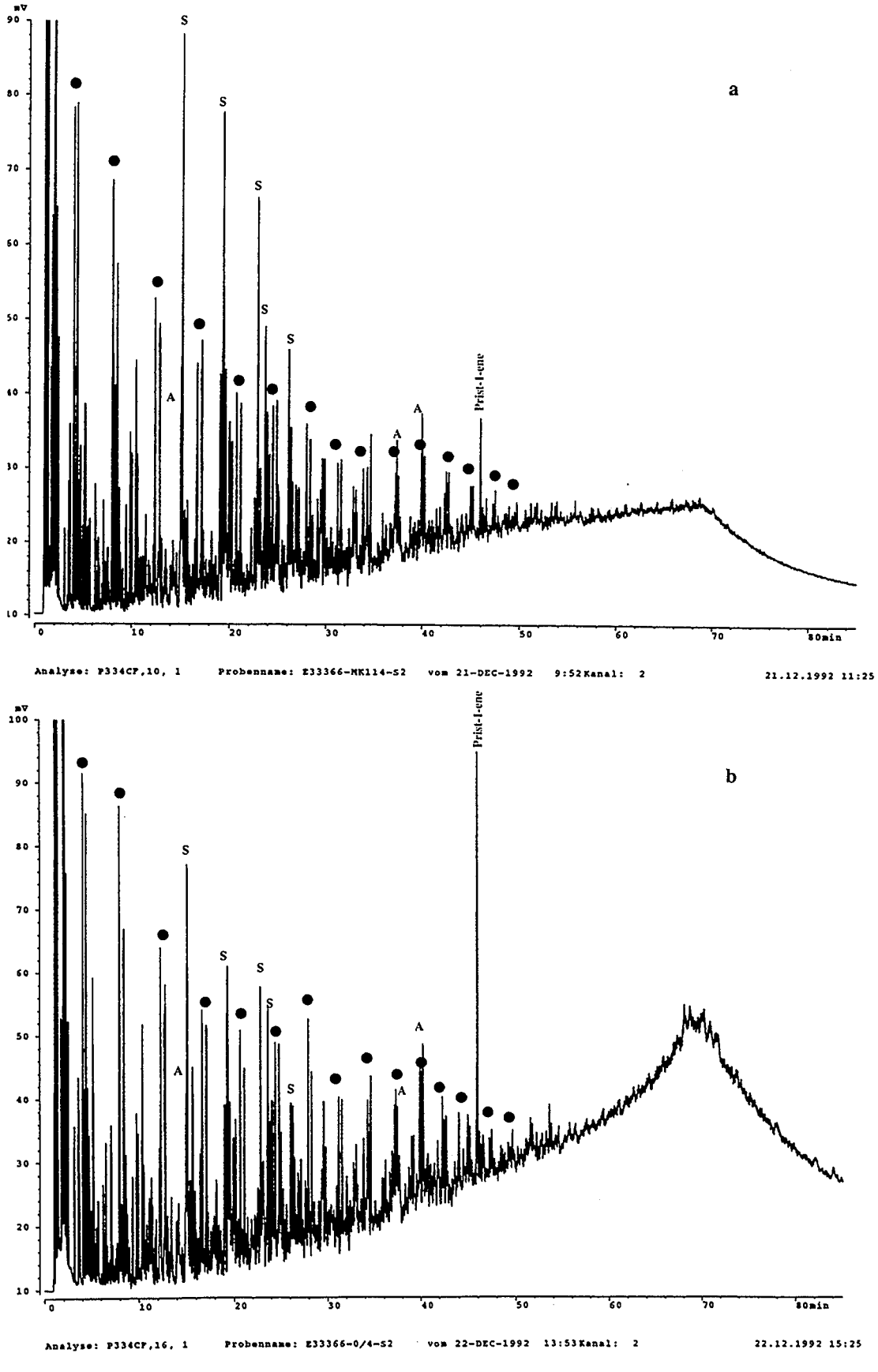

Figure 35: GC-traces of pyrolysates generated from the kerogen (a) and the asphaltenes (b) of shale sample E 33366/4. Alkane/alkene doublets are marked by points, sulphur compounds by S and aromatic compounds by A.

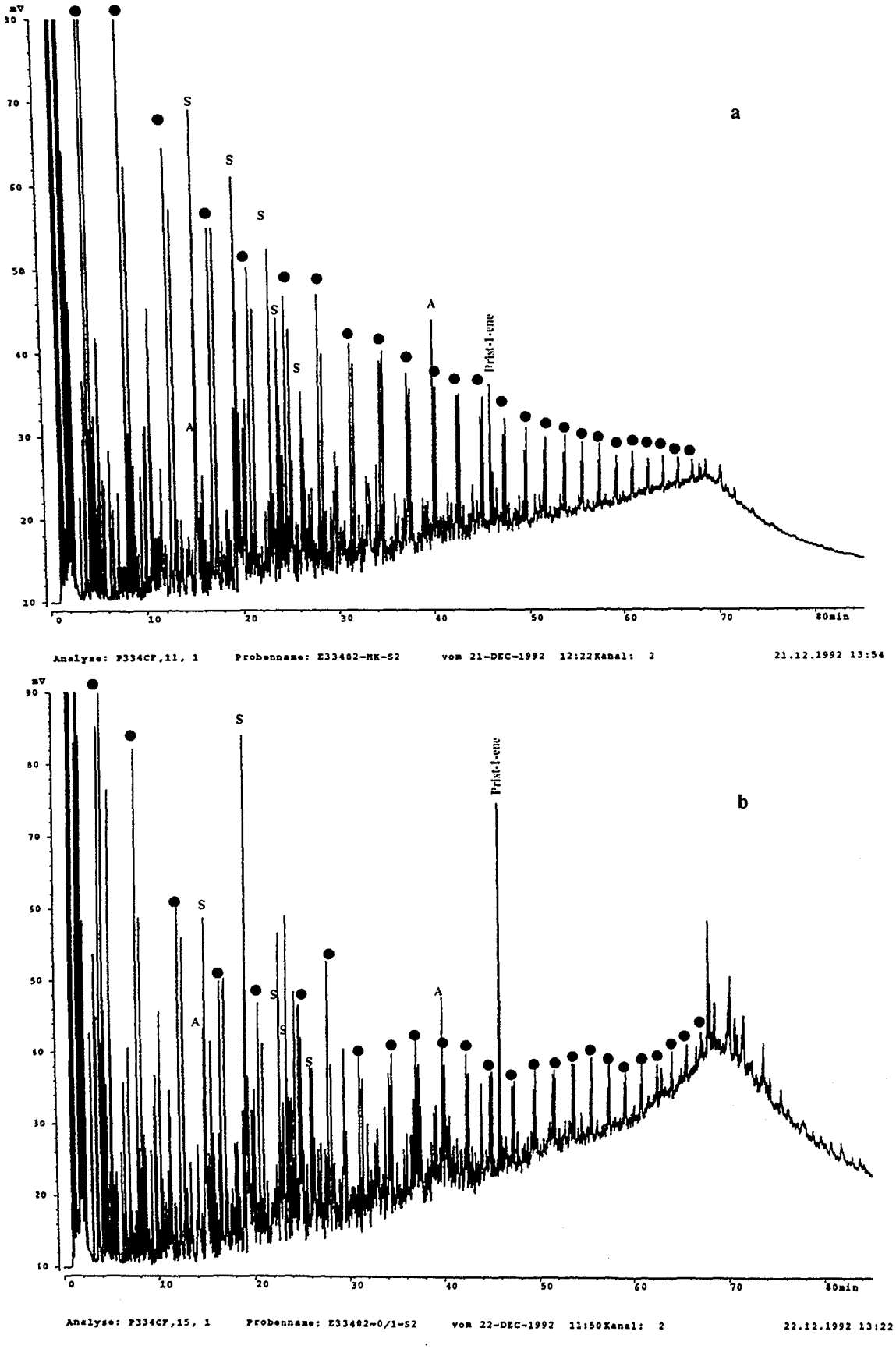

Figure 36: GC-traces of pyrolysates generated from the kerogen (a) and the asphaltenes (b) of shale sample E 33402. Alkane/alkene doublets are marked by points, sulphur compounds by S and aromatic compounds by A.

understood. No major phytenes have as yet been found in high temperature kerogen pyrolysates although some have been identified during hydrous pyrolysis experiments (Eglinton, 1988).

PyGC offers a means of discriminating kerogens according to the gross composition of their pyrolysates and the petroleums they are likely to generate in nature (Larter and Horsfield, 1993). Fig. 37 predicts the cumulative gross composition of petroleum that would be generated from the analysed kerogens, according to PyGC, throughout their entire maturation history. The definition of petroleum type for each field in the small ternary diagram was adapted from the study performed by Horsfield (1989). The apices of Fig. 37 are defined by the proportions of (1) total resolved C_1 to n-C_5 pyrolysate, (2) summed n-alk-1-enes and n-alkanes in the n-C_6 to n-C_{14} range and (3) summed n-alk-1-enes and n-alkanes in the n-C_{15+} range. It is well known that pyrolysis temperature exerts a strong control on the gas content of pyrolysate from a given precursor (Jones and Cramers, 1977). The relatively mild programmed heating conditions used here are, according to Horsfield (1989), thought to favour the preservation of first-formed pyrolysis fragments and, hence, give an optimised assessment of chain length distribution in the volatisable parts of the kerogen. The pyrolysates of the source rock kerogens fall mainly in the paraffinic-naphthenic-aromatic field and range into the gas field in Fig. 37. Thus these sulphur-rich type I/II-S kerogens fall in the same fields as, for example, Toarcian shale and Woodford shale kerogens in the study of Horsfield (1989), who also stated that the dominantly low wax P-N-A composition seemed to typify marine shales containing autochthonous organic matter in abundance.

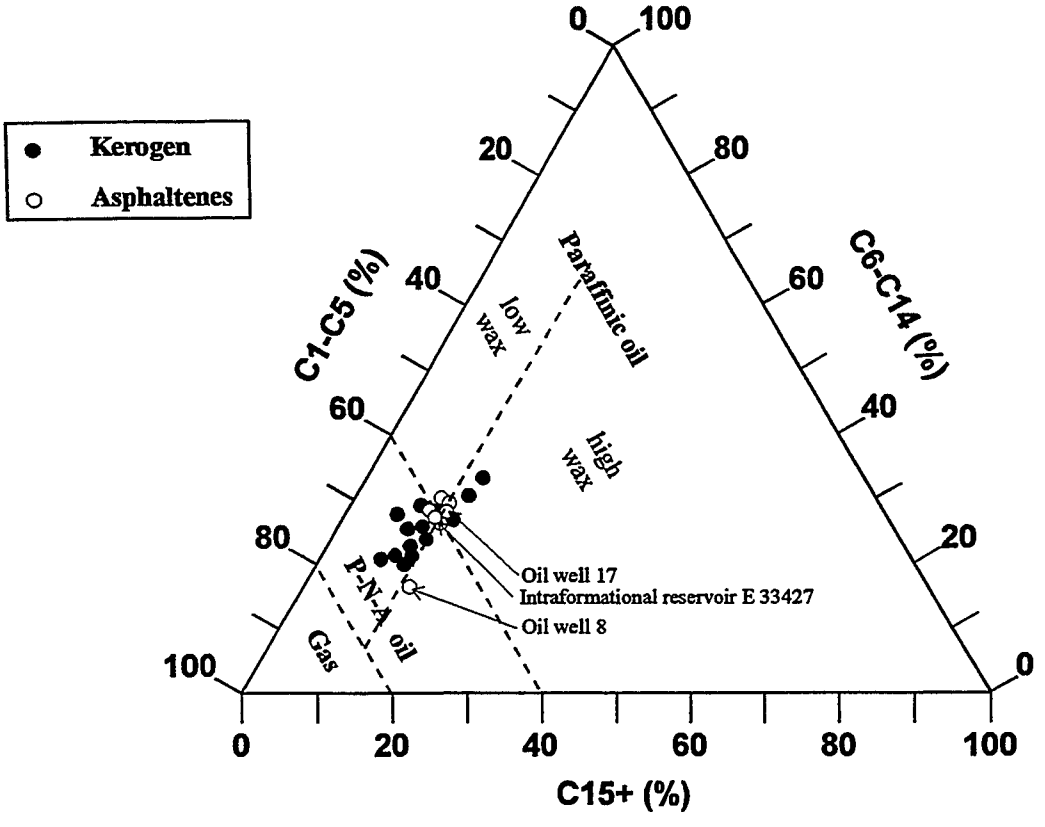

Figure 37: Cumulative gross composition of petroleums generated from the analysed asphaltenes and kerogens calculated according to alkane chainlength distribution.

Sulphur compounds

The main sulphur compounds identified in the kerogen pyrolysates are shown in Fig. 38, where the Hall® trace of sample E 33366/4 between 10 and 30 minutes exemplifies the profusity of sulphur compounds generated by these kerogens. The compounds generated consisted mainly of alkylated thiophenes and minor proportions of alkylated thiolanes. The most prominent compounds in the C_3-alkylated thiophenes were 2-ethyl-5-methyl-thiophene and 2,3,5-trimethylthiophene, while in the C_2-alkylated thiophenes 2,5-dimethylthiophene was dominant.

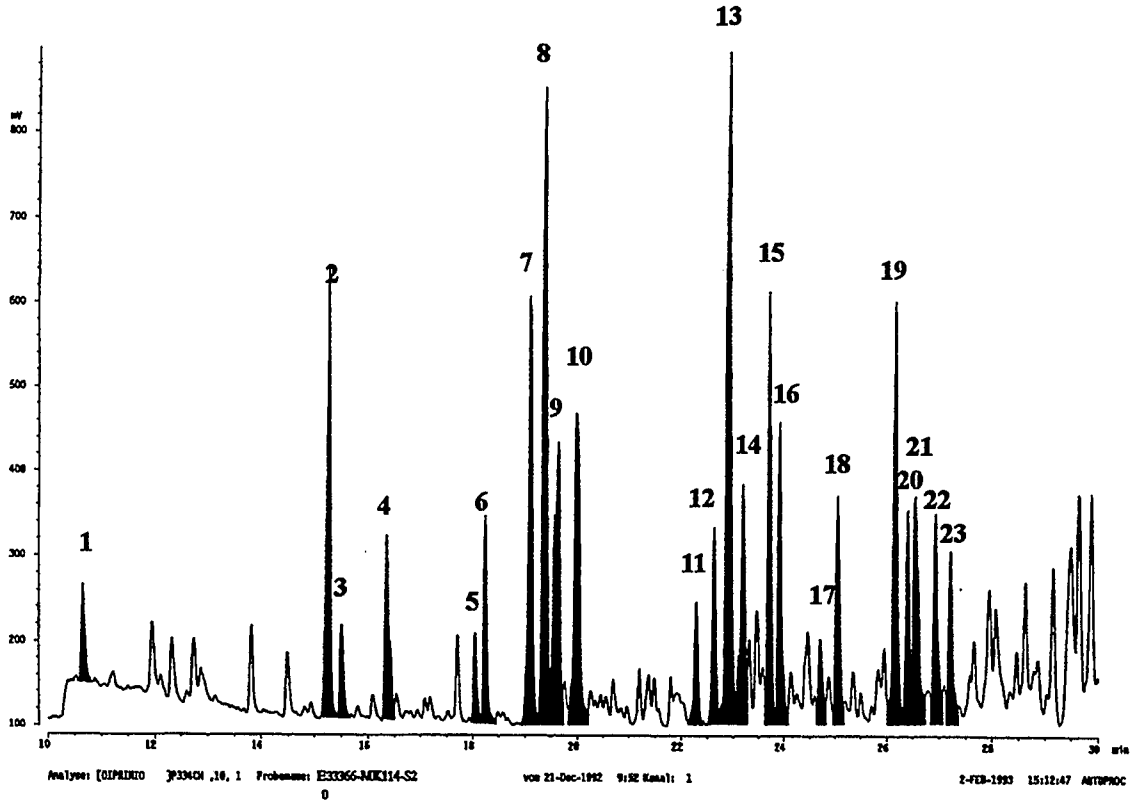

1: Thiophene
2: 2-methyl-thiophene
3: 3-methylthiophene
4: Thiolane
5: Methyl-dihydro-thiophene
6: 2-methyl-thiolane
7: 2-ethyl-thiophene
8: 2,5-dimethyl-thiophene
9: 2,4-dimethyl-thiophene
10: 2,3-dimethyl-thiophene
11: 2-ethyl-thiolane
12: 2-propyl-thiophene
13: 2-ethyl-5-methyl-thiophene
14: 2-ethyl-4-methyl-thiophene
15: 2,3,5-trimethyl-thiophene
16: 2-methyl-5-vinyl-thiophene
17: 2,3,4-trimethyl-thiophene
18: Isopropyl-thiophene+3:1-thiophene
19: 2-methyl-5-propyl-thiophene+ 2,5-diethyl-thiophene
20: 2-butyl-thiophene
21: 2-ethyl-3,5-dimethyl-thiophene+ 3-ethyl-2,5-dimethyl-thiophene
22: 5-ethyl-2,3-dimethyl-thiophene
23: C4:1-thiophene

Figure 38: Hall trace in the time range 10 to 30 min of shale sample E 33366/4. Identified sulphur compounds are shaded and numbered.

Source rock asphaltene samples

n-alkyl and isoprenoid moieties

The source rock asphaltenes produced pyrolysates which certain differences to those of the corresponding kerogens (Fig. 35, 36). In general the asphaltene pyrolysates displayed a molecular signature of highly immature material as shown by the predominance of prist-1-ene (Curry and Simpler, 1988, Larter and Horsfield, 1993) and the large number of, mainly thiophenic, sulphur compounds (Fig. 35b, 36b). The chain length distribution pattern of the n-C_{5+} n-alk-1-ene and n-alkane doublets remained, on the other hand, remarkably similar to that of the kerogen pyrolysates, suggesting that the n-alkyl moieties of the substances compared shared common precursors. This is also supported by the alkane/alkene chain length distribution of the asphaltene samples, as described by the triangular plot of Horsfield (1989), which is almost identical to the distribution of the kerogen pyrolysates (Fig. 37).

Sulphur compounds

The sulphur compounds present in the pyrolysates of the asphaltenes samples were dominated by the same compounds as in the kerogen pyrolysates, namely 2-ethyl-5-methyl-thiophene, 2,3,5-trimethylthiophene and 2,5-dimethylthiophene. The total amount of sulphur compounds as compared to the yield of hydrocarbons was on the other hand always smaller for the asphaltene samples than for the corresponding kerogen. This is demonstrated by the data in Fig 39 where the ratio of resolved sulphur compounds resolved/C5+ yields (alkane/alkenes plus aromatic compounds) is shown for the four samples where kerogen and asphaltenes were available (Table 16).

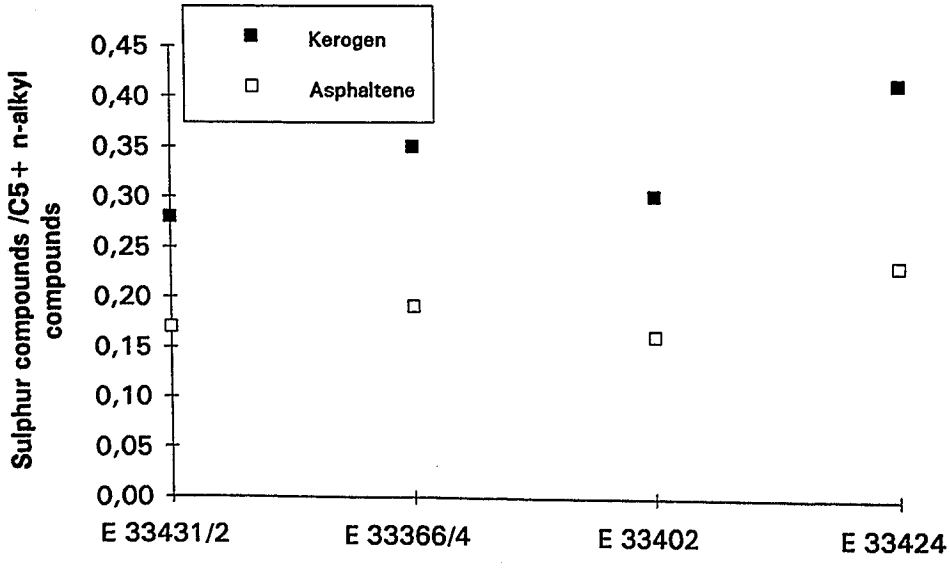

Figure 39: Ratio of resolved sulphur compounds to resolved C5+ n-alkyl compounds of the four samples where PyGC was performed on both kerogen and asphaltenes.

Oil asphaltenes

n-alkyl and isoprenoid moieties

Asphaltenes precipitated from three oil samples were analysed by PyGC. These consisted of asphaltenes from one interlayered reservoir of well 8, sample E 33427, and asphaltenes from the two produced oil samples from wells 17 (E 33436) and 8 (E 33435).

The pyrolysates generated by PyGC from these three samples were dominated by n-alkane/alkene doublets. Prist-1-ene was monitored only in samples E 33427 (interlayered reservoir well 8) and E 33436 (produced oil well 17), whereas it was absent in the pyrolysate of the asphaltenes from the produced oil from well 8 (E 33435, Fig. 40).

The pyrolysates of asphaltenes precipitated from the three oils showed remarkable relationships to the kerogens and asphaltenes from the source rocks (Figs. 34, 35, 36, 40). The asphaltenes from the interlayered reservoir sample from Well 8 (E 33427, 40a) had an almost identical pyrolysate composition as the kerogens from Well 8 (e.g. sample E 33402, Fig. 36a) and also as the asphaltenes from the oil produced in Well 17 (E 33436, Fig. 40c). Figure 37 exemplifies the close similarity of n-alkyl distributions of these samples to the distributions of the kerogen concentrates and source rock asphaltenes described previously. This compositional similarity is consistent with the results reported by Orr (1986) on kerogen/asphaltene relationships in sulphur-rich Monterey oils.

The oil produced from Well 8 (E 33435), on the other hand, showed signs of higher maturity than any of the samples analysed as yet. This is demonstrated by the absence of prist-1-ene.

sulphur compounds

The sulphur compounds present in the pyrolysates of the three oils were dominated by by the same compounds as in the source rock kerogen and asphaltene pyrolysates, namely 2-ethyl-5-methyl-thiophene, 2,3,5-trimethylthiophene and 2,5-dimethylthiophene. The amount of sulphur compounds was, on the other hand, distinctly lower than in the other samples analysed. This can easily be recognised in the GC trace of the pyrolysates (Fig. 40) where the sulphur compound peaks are all smaller than neighbouring n-alkyl compounds. The lower proportion of sulphur compounds in these pyrolysates is also reflected in the very low S/C5+ compound ratios of these samples, which are all below 0.10 (Table 16).

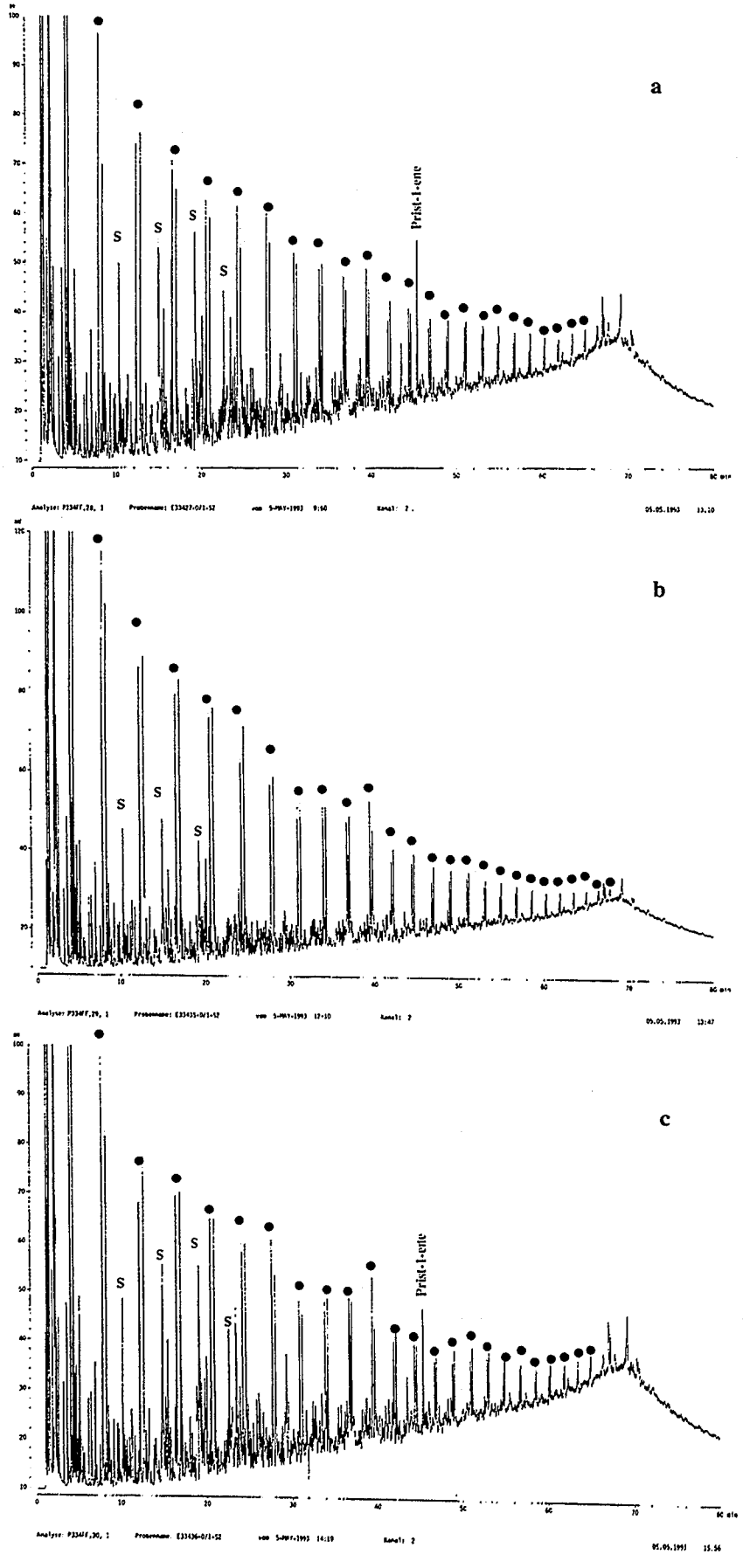

Figure 40: Pyrolysate composition of asphaltene samples from an impregnated, fractured dolostone (interlayered reservoir, sample E 33427, well 8, a) as well as from the crude oil samples from wells 8 (b) and 17 (c). Alkane/alkene doublets are marked by points, sulphur compounds by S and aromatic compounds by A.

Interpretation

The distribution of n-alkyl moieties in all pyrolysates was very similar, as exemplified by Fig. 37. Major differences are only recognised when the proportions of prist-1-ene and sulphur compounds are taken into account. The prist-1-ene content of source rock asphaltenes was always higher than in the corresponding kerogen pyrolysate, whereas in the oil asphaltene pyrolysates the prist-1-ene content was comparable to that of the kerogens (samples E 33427, interlayered reservoir, and E 33436, produced oil well 17), or completely absent (E 33435, produced oil well 8). This observation can in general be assumed to indicate that the reservoired oils are of higher maturity than the source rock, and thus were not generated therein, but rather migrated into their present location from a more mature source rock equivalent situated at greater depth. These observations are backed by the lower proportion of sulphur compounds in the oil asphaltene pyrolysates (Table 16).

The differences between the asphaltene pyrolysate of the reservoired oil and the asphaltenes of the source rock samples may alternatively be due to migration/expulsion effects where possibly a large portion of the polar compounds remain absorbed in the organic matter leading to a relative increase of these compounds in the source rock and a depletion and alteration due to fractionation in the reservoir oil as proposed by Sandvik et al. (1991). Compositional fractionation effects during expulsion have been observed by Leythaeuser et al. (1984, 1988) who concluded that the extent of preferential expulsion from shale source rocks was in the sequence saturated hydrocarbons > aromatic hydrocarbons > NSO compounds. Wilhelms et al. (1990) estimated expulsion efficiencies from a clastic Jurassic source rock in the Norwegion North Sea. They assumed expulsion via bulk flow with "chromatographic modification" that caused saturated and aromatic compounds to migrate more readily than polar and asphaltic compounds.

The similarity between the n-alkyl distributions of the pyrolysate of the asphaltenes from the interlayered reservoir in well 8, from the produced oils from wells 17 and 8 and from virtually all the source rock kerogen and asphaltene samples analysed, as demonstrated by ternary diagram of Horsfield (1989) in figure 37, provides, on the other hand, an excellent oil-source rock correlation. In fact, the very low degree of variation in this diagram is astonishing in view of the large differences in bulk pyrolysate composition. The use of of only one compound class (i.e. n-alkyl moieties) for prediction of petroleum composition seems inadequate for the sulphur-rich organic matter analysed in this study.

An indirect determination of the petroleum type generated, analogous to the triangular plot of Horsfield (1989) based on n-alkane/alkene distributions, was attempted using the relative proportions of individual compounds in the pyrolysates. The abundance of alkylthiophenes in

pyrolysates of kerogens and asphaltenes has been shown to be strongly correlated with the organic sulphur content (Eglinton et al., 1990). Eglinton et al. (1990) proposed a ternary plot of the relative abundance of 2,3 dimethylthiophene (2,3-DMT) in relation to two other hydrocarbon products (1,2-dimethylbenzene and n-C_9:1) for differentiation between sulphur-rich and sulphur-lean organic matter. This plot was modified by exchanging 2,5-dimethylthiophene for 2,3-DMT and toluene for 1,2-dimethylbenzene (these two compounds are much easier to identify on FID chromatograms) and by adding the n-C25 alkene to the n-C9 alkene in order to allow for the distinction of high wax petroleum types.

These compounds were selected because they all have very similar retention times and thus appear close together on a chromatogram. Figure 41 shows a direct comparison of Horsfields triangular plot and the novel ternary plot using the results of the PyGC experiments and results from other source rocks and typical maceral types analysed using the same method. The four fields shown in figure 41a and termed „aromatic", intermediate", „paraffinic" and „high sulphur" describe in a general manner the bulk composition of the pyrolysates which plot therein. The aromatic field contains pyrolysates generated from samples containing terrestrial organic matter, the intermediate field was defined by pyrolysates from marine source rocks, the paraffinic field by lacustrine source rocks and the high sulphur field by the sulphur-rich source rocks of this study.

In the classical petroleum-type prediction triangular diagram of Horsfield (1989) the pyrolysate composition of all the samples analysed in this study plot in a relatively narrow field (Fig. 41b). In the sulphur-saturated-aromatic ternary plot the variation in pyrolysate composition is much clearer. Only the four kerogen and corresponding asphaltene samples as well as the oil asphaltenes are plotted in this figure. The relationships described previously concerning the variations in sulphur compound contents are clearly visible in Figure 41a. The produced oil samples from wells 17 and 8 are characterised by distinctly lower amounts of sulphur, whereas the source rock samples as well as the asphaltenes precipitated from the intraformational reservoir of well 8 (E 33427) all plot in a more or less well defined field in the high sulphur zone.

The novel ternary diagram presented here, thus clearly differentiates the bulk pyrolysate composition of the samples analysed much better than the previous approach of Horsfield (1989). The divergence of the produced oil samples from the general location of the source rock samples in figure 41a is probably due to differences in the maturity of these samples, indicating that this ternary diagram may also be applicable for maturaty evaluations.

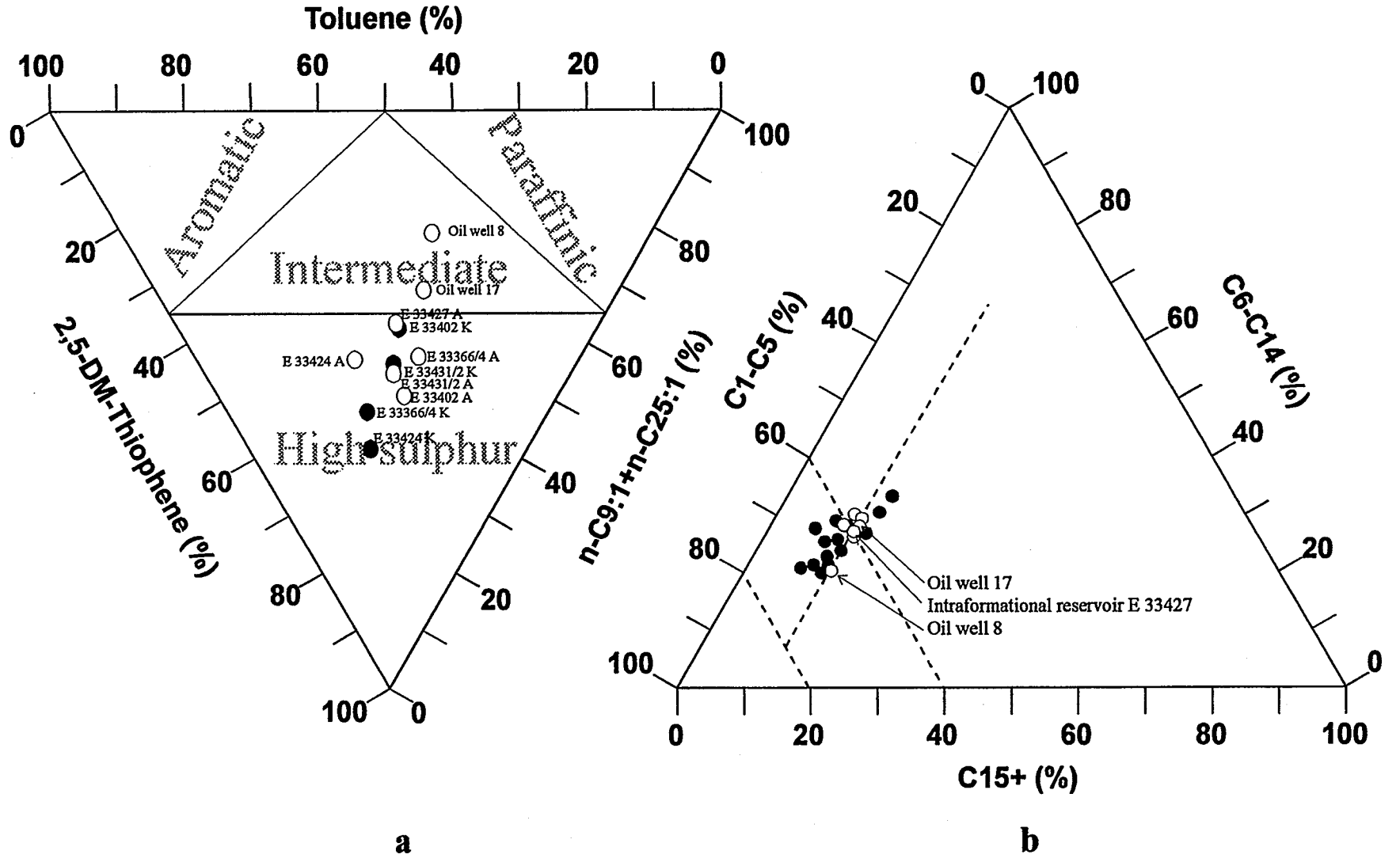

Figure 41: Differentiation of pyrolysate composition using the relative proportions of selected alkyl-, aromatic- and sulphur compounds (a) as compared to corresponding n-alkane chainlength distributions (b). Kerogen samples are marked by solid circles, asphaltenes by open circles.

2.1.6.2.2 Multi-step PyGC

Three kerogen samples (E 33366/4 containing a kerogen type I-S, E 33384 with a kerogen type II-S and E 33431/2 with an intermediate kerogen type I/II-S) and two asphaltene samples (E 33366/4 and E 33431/2) were analysed by multistep PyGC.

Multi-step PyGC is a rapid method to assess kerogen (or asphaltene) maturation characteristics. It provides a crude measure of the "ease" with which specific moieties are released from kerogen or asphaltenes at different temperatures. Results from analyses using this technique published by Horsfield (1989) indicate that (1) compositional characteristics inherited from biological systems are in some kerogens preserved to high levels of thermal stress, (2) a progressive shortening of average n-alkyl chain length with increasing levels of thermal stress does not always occur during the maturation of kerogen, and (3) the thermal lability of n-alkyl moieties in kerogens is very variable.

All kerogens generated a differing molecular fingerprint in each temperature range indicating the heterogeneity of the samples analysed, which is probably due to the incorporation of sulphur into the kerogen during early diagenesis. The sequential degradation of resins, asphaltenes and kerogen of the Monterey formation by Richnow et al. (1991) demonstrated that different compounds were linked via sulphur, oxygen or aromatic entities to the macromolecular structure. They proved that n-alkanes, hopanoids and isoprenoids are attached to the macromolecules by more than one linkage, and furthermore that some compounds, such as hopanoids or n-alkanes are bound simultaneously by sulphur and oxygen bonds. The chemical inhomogeneity of the macromolecular structures described by Richnow et al. (1991) should also be reflected during maturation of the samples, since each bond type should break at different temperatures.

As exemplified by kerogen sample E 33366/4 mainly sulphur compounds are produced in the low heating range (Fig. 42a). In the temperature range from 375-450°C almost 70 % of the total resolved hydrocarbons are released from the kerogen (Fig. 42b, 43). A comparison of this medium temperature analysis to the one-step PyGC of the same sample (Fig. 35a) reveals that both are virtually identical. In the highest temperature range (450-600°C) only minor quantities of *n*-alkyl moieties were recognisable (Fig. 42c). According to Takeda and Asakawa (1988), heating of vitrinite particles to 450°C under standard Rock-Eval conditions raised Ro from 0.4 to about 1.5% Ro. The cut-off between step 2 and step 3, of the multi step pyrolysis approach applied here, is therefore assumed to corresponds to an equivalent natural maturity of about 1.5-1.6% Ro (Larter and Horsfield, 1993). An Ro estimation of the cut-off between step 1 and step 2 is difficult due to the lack of experimental work in this low temperature range, but the

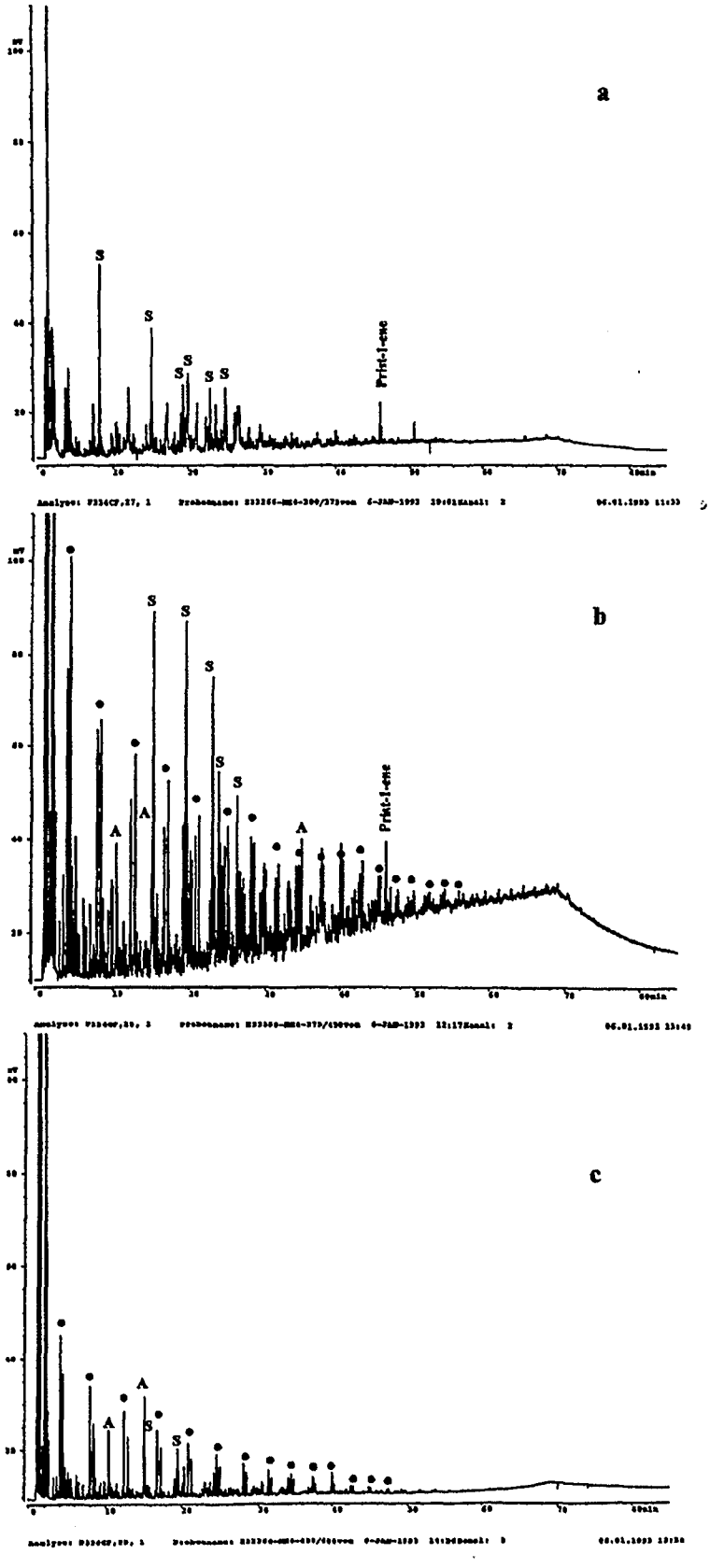

Figure 42: GC-traces of the pyrolysates of kerogen sample E 33366/4 generated in the temperature ranges 300-375°C (a), 375-450°C (b) and 450-600°C (c). Alkane/alkene doublets are marked by points, sulphur compounds by S and aromatic compounds by A.

low proportion of alkyl moieties together with the strong predominance of sulphur compounds points to a Ro of around 0.5%.

The other two kerogen samples analysed reacted in almost the same fashion as sample E 33366/4. Again the pyrolysates of the medium temperature pyrolysis are almost identical to the one-step pyrolysis results of the kerogen samples (Fig. 36a, 44b, 45b). The decrease in sulphur-compound content with increasing thermal stress is demonstrated by Fig. 46 where the ratio of sulphur compounds to hydrocarbons (saturated and aromatic) in the C_7-C_{10} range is plotted versus heating temperature range. With increasing temperature the proportion of sulphur compounds decreases drastically in all samples. The highest proportion of sulphur compounds was generated by the type I-S kerogen (E 33366/4, shale sample) in the lowest heating range. The samples with a kerogen type II-S and I/II-S (E 33384, laminite; E 33431/2, solution seam) show a distinctly lower proportion of sulphur compounds in the first two heating step, whereas at the highest temperature stage the proportion of sulphur compounds is relatively constant for all kerogen samples analysed.

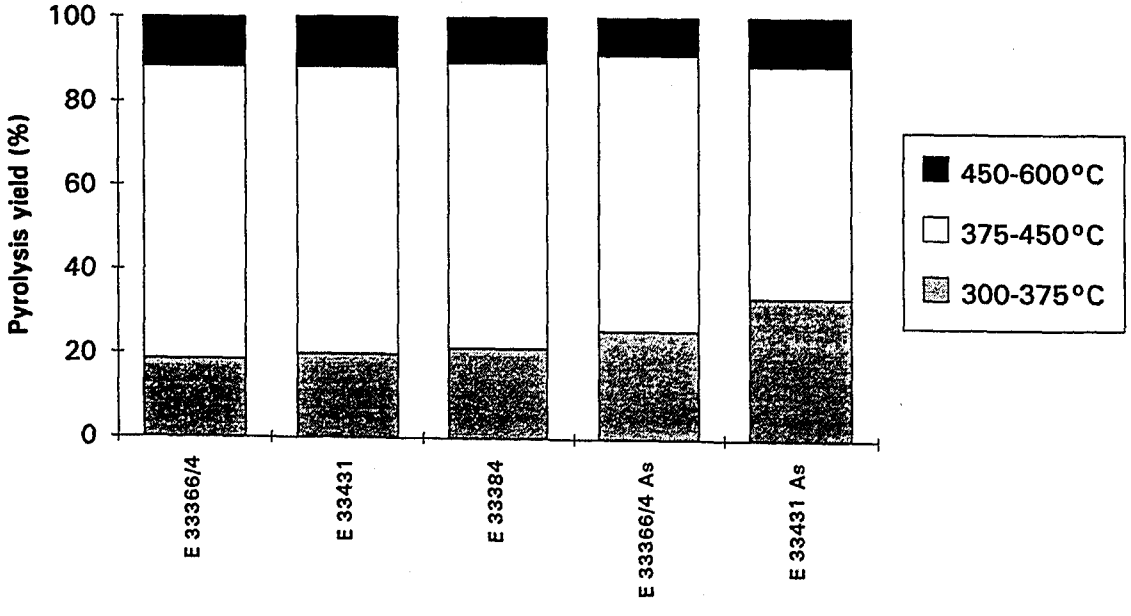

Figure 43: Relative proportion of total pyrolysate generated at each heating step of multistep PyGC.

Due to the large amounts generated in the 375-450°C step (ca. 70% of total pyrolysate) one last multistep experiment was performed using one of the kerogen samples (E 33366/4), where this temperature range was further subdivided into three individual steps (375-400°C, 400-425°C, 425-450°C) in order to achieve better resolution of the hydrocarbon generation characteristics. In this final five-step pyrolysis-GC experiment 25 % of the total pyrolysate was released in the first step (300-375°C), 35% in the second, 25% in the third, 5% in the fourth and 10% in the fifth step. The generation of sulphur compounds reached a maximum in the 375-400°C temperature range and decreased rapidly in the following steps, while peak generation of n-alkyl moieties occurred in the 400-425°C step. Figure 47 shows the GC traces of the five pyrolysates generated throughout this experiment. In the five step pyrolysis experiment the systematic change in pyrolysate composition with increasing temperature is much clearer than in the three step experiments. Fig. 48 shows the ratio of sulphur compounds to hydrocarbons (saturated and aromatic) in the C_7-C_{10} range. The proportion of sulphur compounds decreases constantly with increasing temperature, implying that the generation of these compounds occurs at lower temperatures than for the other hydrocarbons.

In multi-step PyGC of the asphaltene samples (the same three heating steps as for the first kerogens measured) a major difference in hydrocarbon release per heating step, as compared to the corresponding kerogen samples, was noticed (Fig. 43). Between 25 and 33 % of the pyrolysate was generated during the low temperature step. This very high proportion was due to the large unresolved hump of the pyrolysates (Fig. 49a, 50a), which is a characteristic of the asphaltenes pyrolysates analysed here and is due to the volatisation of large, complex molecules from the asphaltenes which can not be resolved by the technique applied. The ratio of sulphur compounds to hydrocarbons (saturated and aromatic) in the C_7-C_{10} range also decreases with temperature in the asphaltene pyrolysates (Fig. 46), whereby the proportion of sulphur compounds generated in the first temperature stage is much lower than that of the kerogen pyrolysates.

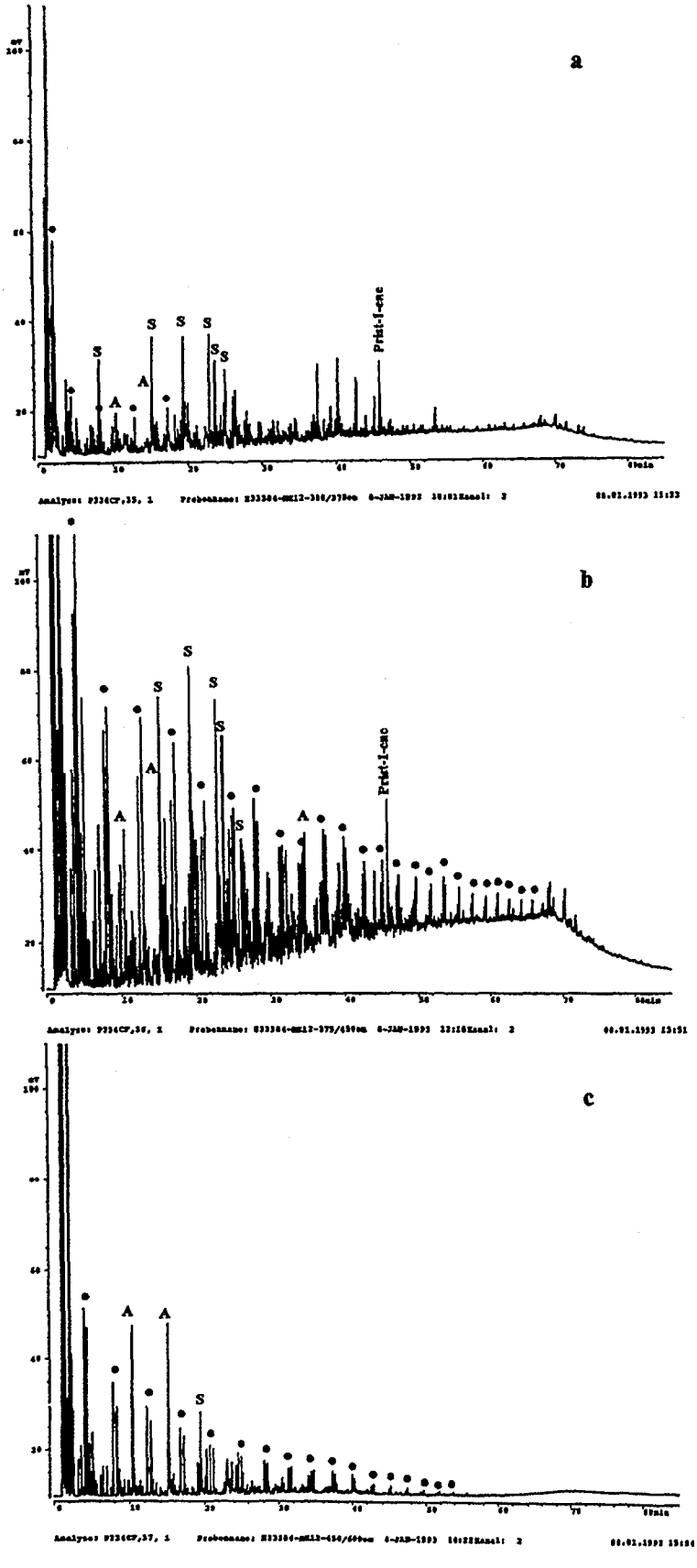

Figure 44: GC-traces of the pyrolysates of kerogen sample E 33384 (laminite, well 8) generated in the temperature ranges 300-375°C (a), 375-450°C (b) and 450-600°C (c). Alkane/alkene doublets are marked by points, sulphur compounds by S and aromatic compounds by A.

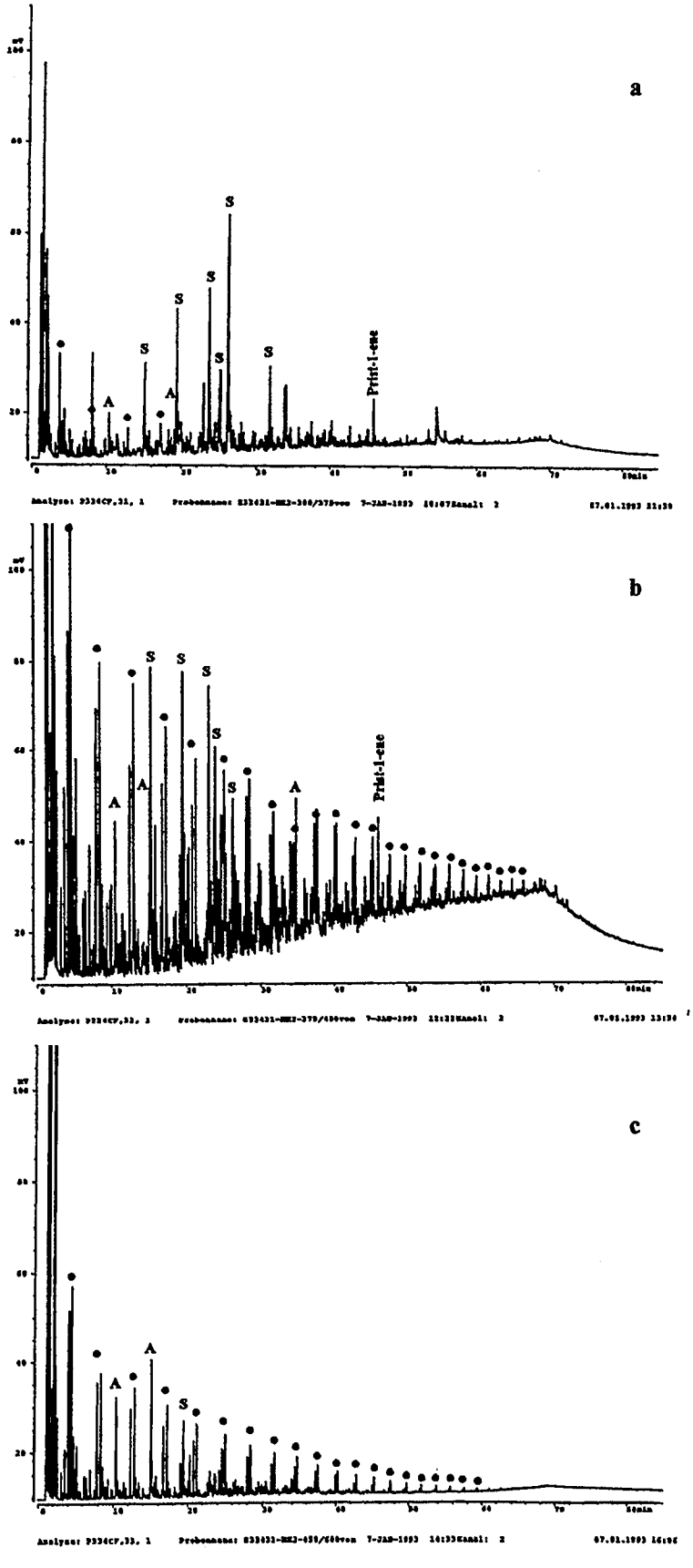

Figure 45: GC-traces of the pyrolysates of kerogen sample E 33431/2 (solution seam, well 24) generated in the temperature ranges 300-375°C (a), 375-450°C (b) and 450-600°C (c). Alkane/alkene doublets are marked by points, sulphur compounds by S and aromatic compounds by A.

The three temperature ranges initially used in this pyrolysis approach were too large to correctly determine relative differences in hydrocarbon generation characteristics of each sample (kerogen or asphaltene). The quantitative analysis applied, on the other hand, allowed a relative determination of the distribution of bond classes in the kerogen. The low temperature generation of mainly sulphur containing moieties, can be taken as a direct indication of carbon-sulphur (C-S) bond cracking. The generation of hydrocarbons with a lower proportion of sulphur compounds and rich in n-alkyl moieties at higher temperature is probably due to the cracking of C-C bonds in the kerogen. The lower proportion of sulphur compounds generated by the asphaltene samples at the low temperature stage indicate that these compounds seem to be depleted in the asphaltenes.

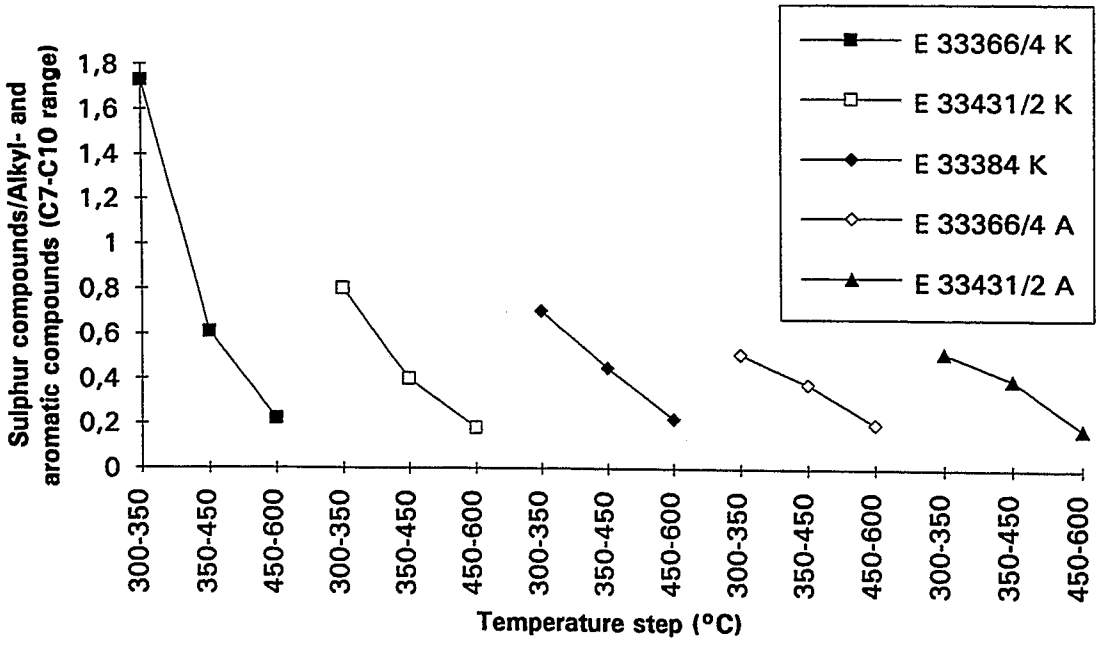

Figure 46: Ratio of sulphur compounds to alkyl- and aromatic compounds in the C7-C10 range plotted versus Multistep PyGC heating stage temperature. Kerogen pyrolysates are marked (K), asphaltene pyrolysates (A).

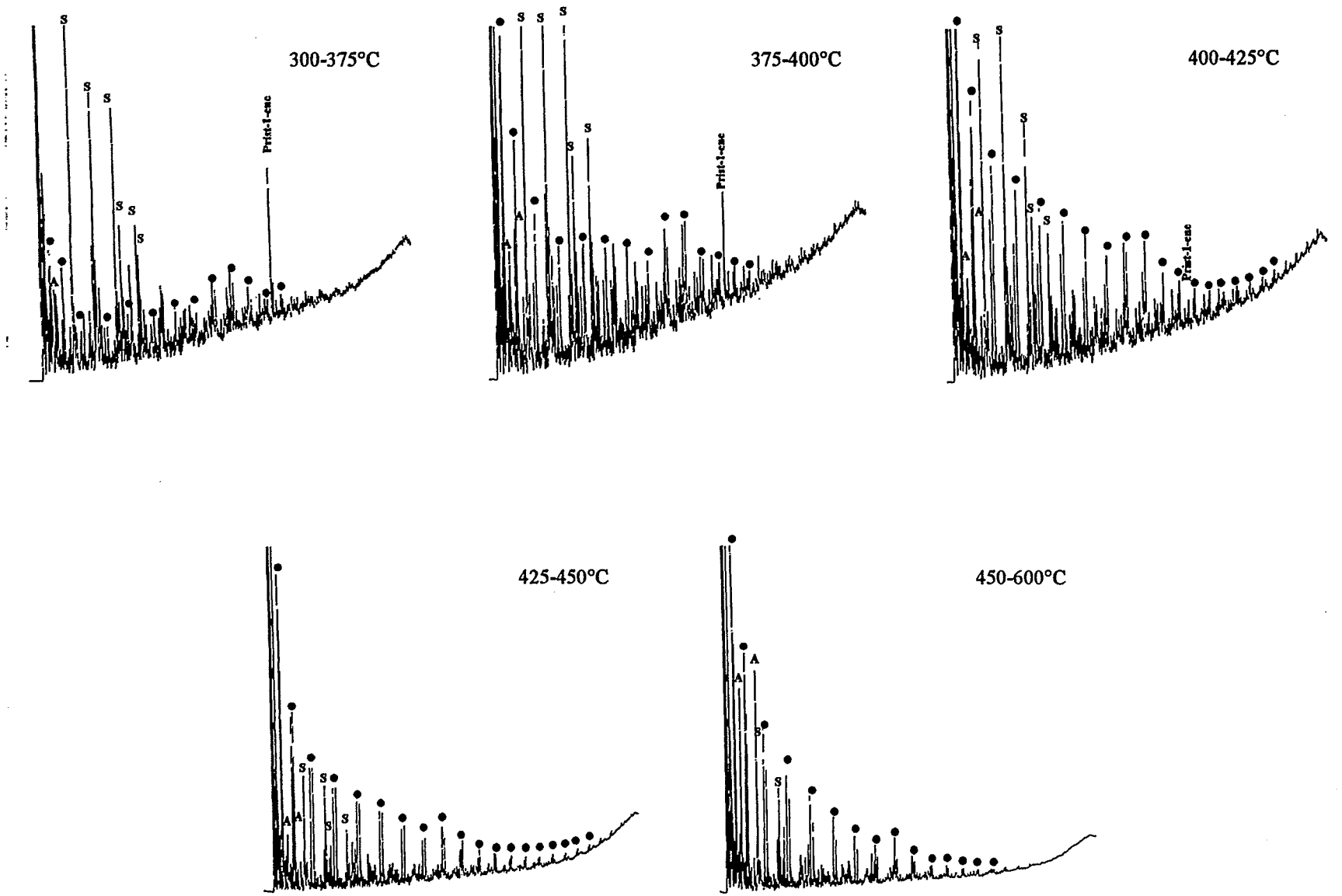

Figure 47: GC-traces of the pyrolysates of kerogen sample E 33366/4 generated in the five temperature ranges depicted. Alkane/alkene doublets are marked by points, sulphur compounds by S and aromatic compounds by A.

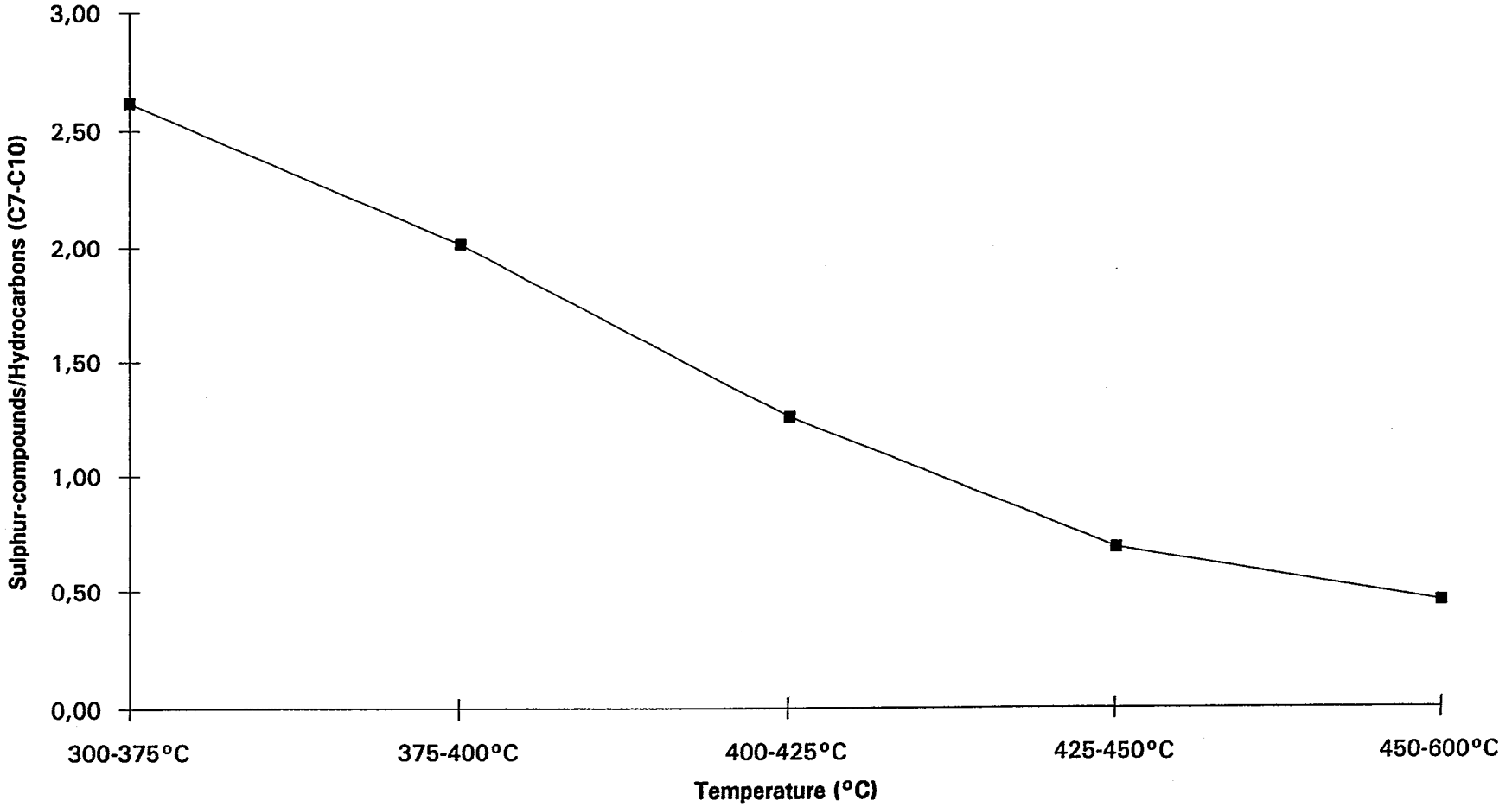

Figure 48: Ratio of sulphur compounds to hydrocarbons in the C7 to C10 range for the different heating steps of the five step multistep PyGC experiment.

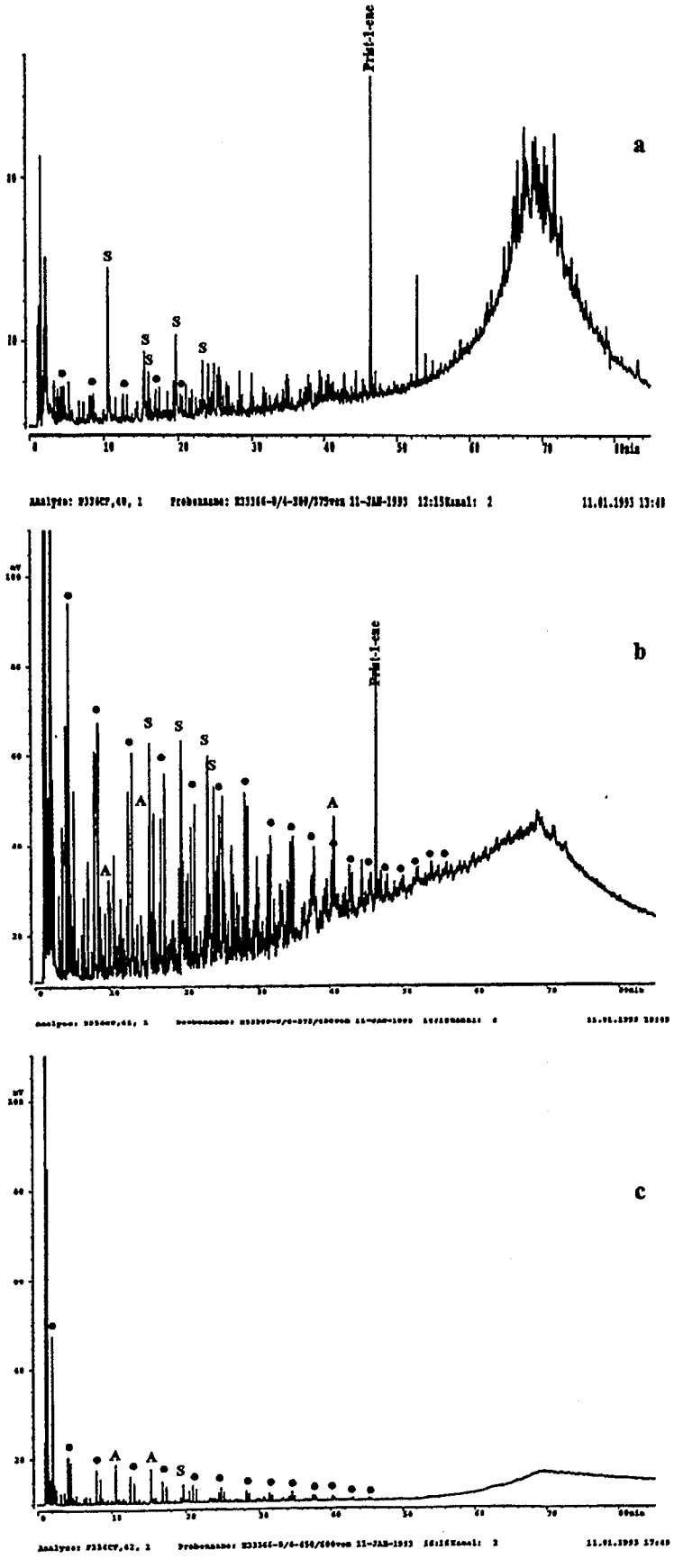

Figure 49: GC-traces of the pyrolysates of asphaltene sample E 33366/4 generated in the temperature ranges 300-375°C (a), 375-450°C (b) and 450-600°C (c). Alkane/alkene doublets are marked by points, sulphur compounds by S and aromatic compounds by A.

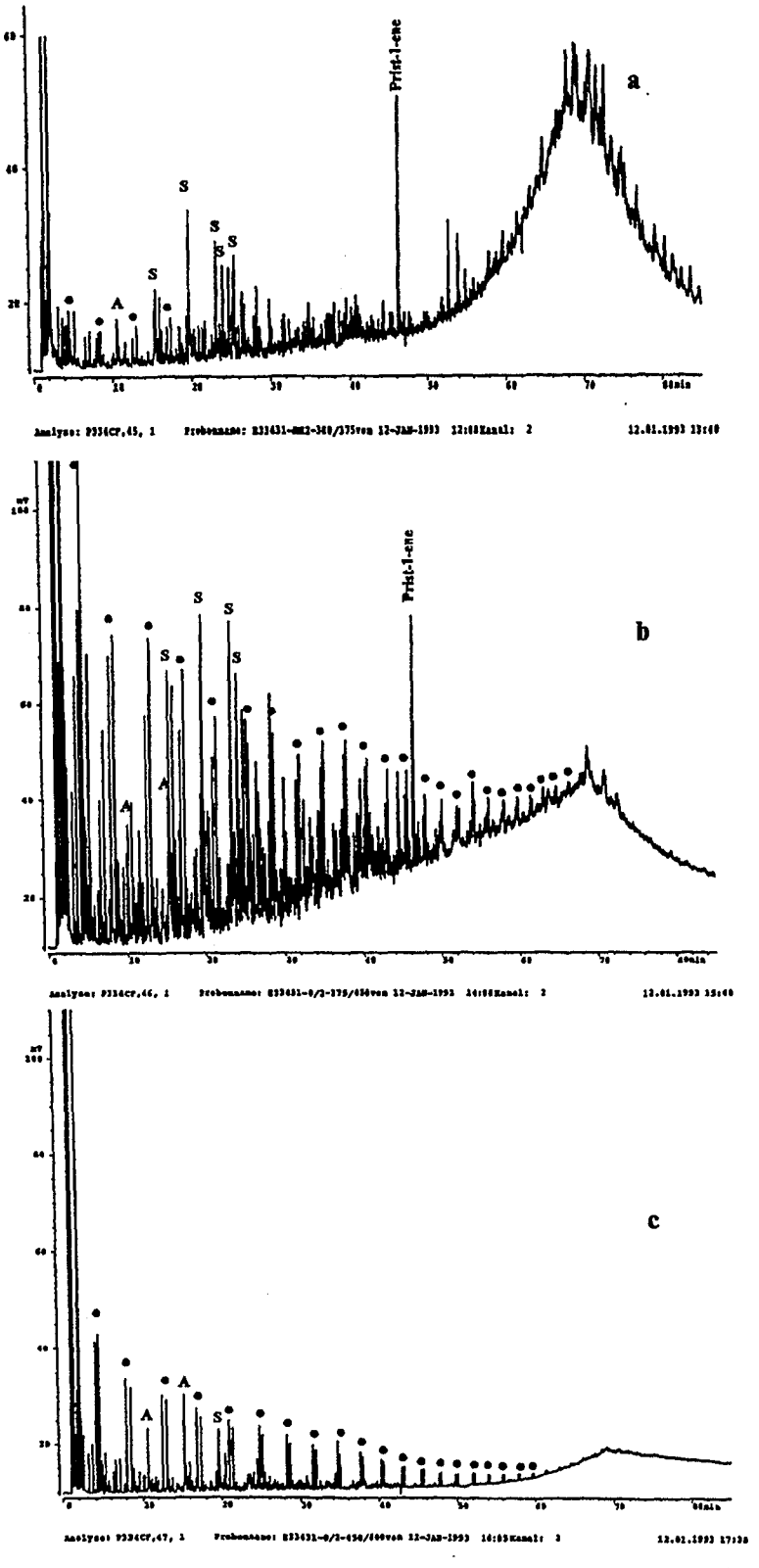

Figure 50: GC-traces of the pyrolysates of asphaltene sample E 33431/2 generated in the temperature ranges 300-375°C (a), 375-450°C (b) and 450-600°C (c). Alkane/alkene doublets are marked by points, sulphur compounds by S and aromatic compounds by A.

2.1.7 Maturity assesment

2.1.7.1 Results of Rock Eval and SOM analyses

The temperature of peak hydrocarbon generation during Rock-Eval pyrolysis (Tmax) is known to increase progressively with maturation (Espitalié et al., 1977; Tissot and Welte, 1984). According to the depth series sampled in this study, an increase of Tmax with depth was expected. There is, however, no indication of a maturity trend with depth (Table 1). A reliable maturity assessment was problematic due to the variations of kerogen types encountered among all samples. However, the uniformly low values can be assumed to indicate an immature to early mature source rock.

The average values for each well, on the other hand, show a slight but systematic increase in Tmax with depth. Well 17 has an average Tmax of 408.8°C, Well 4 of 409.9°C and Well 8 reaches 410.5°C. The highest average Tmax is found in the deepest well with a value of 415.3°C (Well 24). This increase in average Tmax with depth may be interpreted as an indication of maturity increase with depth, although this very small difference in the Tmax values among all wells (6.5°C) as compared to the relatively thick depth interval (2400m) indicates that this modest Tmax increase is probably not the most important factor for the evolution of the source rock analysed.

The determination of maturity is extremely difficult in carbonate source rocks due to the lack of vitrinite particles in the sediment. The sulphur-rich nature of the organic matter in these source rocks further complicates the application of chemical maturity indicators. Before novel maturity indicators can be looked for, at least a relative maturity assessment of the different wells was necessary. Therefore, the conventional maturity parameters, developed and calibrated on siliciclastic source rocks, were evaluated first.

Analysis of the soluble organic matter confirmed the results regarding the immature nature of the source rock formation derived from screening data, microscopy and elemental analysis of the kerogens. The extract composition, the n-alkane distributions, results from biomarker and aromatic maturity ratios indicated that the bitumen present in the source rock is the product of a very initial stage of petroleum generation.

The extract composition compares favourably with the results of work performed by Tannenbaum and Aizenshtat (1984a; 1985), who observed high bitumen contents in immature sulphur-rich source rocks of Israel. The source rocks sampled by these authors in two wells, with bitumen contents of up to 300 mg/g TOC, showed a vitrinite reflectance of 0.3-0.4 % and had, according to burial history reconstruction, been subjected to temperatures of around

40°C (Tannenbaum and Aizenshtat, 1984a). Similar observations were made by Rullkötter et al. (1990) in bituminous sediments of Nördlinger Ries. They observed extract contents of almost 200mg/g TOC, 10-15% of which were saturated compounds, in rocks with elevated sulphur contents which had never been exposed to temperatures above 30°C. High amounts of polar compound-rich bitumen are implied to be typical for sulphur-rich source rocks at early stages of maturity (Orr, 1986; Rullkötter, 1990; Sinninghe Damsté, 1993; Tannenbaum and Aizenshtat, 1985). The amount of polar compounds in the extract of carbonate source rocks can be expected to show an inverse correlation to the maturity, since heteroatomic bonds break earlier during maturation than carbon-carbon bonds.

The hydrocarbon contents of the source rock analysed in this study are more or less 10 % higher than those reported by Tannenbaum and Aizenshtat (1985) or Rullkötter et al. (1990). This fact can probably be explained by a slightly higher degree of maturity of the source rocks analysed in this study. Correspondingly they must have been subjected to higher temperatures, that is at least above 40°C.

The most notable feature of the saturated compounds was the strong odd over even predominance of the n-alkanes in the C_{23} to C_{31} range. The carbon preference index (CPI) is known to reach values around unity with increasing maturation (Tissot and Welte, 1984, page 184). The rate of change depends on the organic matter type and source rock depositional environment as indicated by high and low CPI's alternating in successive beds from the same well (Tissot and Welte, 1984, page 184-185). The reason for such observations is that the n-alkane distribution present in the sediment depends on the original distribution of the n-alkanes and on the dilution by newly generated n-alkanes. The strong odd over even n-alkane preference noticed in almost all samples of this study certainly indicates that the maturity of the source rock was low.

Analysis of the biological marker molecules from the saturated hydrocarbon fraction was expected to help in obtaining a maturity assessment. The extent of isomerisation at C_{22} in 17α (H), 21β(H)-hopanes was measured for the C_{32} hopanes on selected samples from all wells. The results can be translated into a relative maturity range for the source rock according to the scheme by Mackenzie (1984). The hopane isomerisation values were between 30 to 50 % in well 17, 25 and 55 % in well 4, whereby the samples with a high degree of isomerisation were assumed to have been impregnated by an oil of higher maturity, 20 to 60 % in well 8, and 20 to 40 % in well 24. These values translate to maturities between 0.4 and 0.8 % Ro. The highest maturity value is due to the complete isomerisation in some samples of well 8. The average

isomerisation value in well 8 lies around 45 % which would imply a vitrinite reflectance of more or less 0.55 %.

Sterane isomerisation rates of the C_{29} steranes showed a lower variability in the samples of each well as compared to the wide scatter of data from the hopanes. The extent of sterane isomerisation ranged between 20 and 35 % in all wells. This implies maturities between 0.5 and 0.65 % Ro. It should be recognised, however, that the extractable organic matter of the source rock formation studied here represents at best 20 percent of the total organic matter. Furthermore, the biomarker fractions of the solvent extract represent only a small fraction of the total extract. When taking into account that large amounts of labile functionalised lipids present in the sediment upon deposition can be quenched by inorganic sulphur species and incorporated into the high molecular weight organic matter as organic sulphur compounds (OSC) during early diagenesis (Sinninghe Damsté et al., 1989; Schouten et al., 1994), the interpretation of biomarker data with respect to maturity of organic matter should be performed with great caution. The biological precursors of hopanes with more than 30 carbon atoms, for example, are bacterial hopanepolyol derivates with several hydroxyl groups on the side chain (Ourisson et al., 1987; Rohmer et al., 1992). Richnow et al. (1993) observed that deuteration patterns on the side chains of hopanes released from the macromolecular fraction of a sulphur-rich oil by stepwise chemical degradation, indicated that the sulphur functionalities were present in similar positions as the oxygen-containing functionalities in the precursor molecules. Replacement of oxygen by sulphur in the precursor lipid during early stages of diagenesis and subsequent incorporation into a macromolecular matrix was, therefore, deduced to be likely. Steroidal compounds were found to build up preferentially sulphur-linked fragments of the macromolecular structures studied by Richnow et al. (1993), whereby the distribution of individual steranes in the free and degradable fractions were nearly identical.

Rullkötter et al. (1985) noticed in a study of oils and asphalts from carbonate source rocks of Israel, that differences exist between the isomerisation level of polycyclic biological marker hydrocarbons in sulphur-rich carbonate source rocks and shale source rocks at comparable levels of thermal stress. The coincidence of low proportions of hydrocarbons in the extracts of apparently immature samples with an advanced level of isomerisation of the biomarkers illustrated the differences in hydrocarbon formation between carbonates and shales. The higher rate of biomarker isomerisation reactions was attributed to the incorporation of sulphur into the organic matter. The maturity of the carbonate source rock in the wells analysed in this study, as assessed by biomarker isomerisation, can, therefore, be assumed to represent a maximum value. Lower maturities than those expressed above are probably more likely.

Maturity estimation by means of aromatic hydrocarbon maturation parameters, like MPI-1, MPI-2 and MDR 4, was partially successful, at least regarding the recognition of relative maturities. Only the kerogens of type II, with their predominantly autochthonous organic matter, show the expected maturity increase with depth according to the aromatic maturity indicators MPI 1 and MPI 2. Since a reliable calibration of MPI values with vitrinite reflectance does not exist for type II kerogens, the observed MPI increase with depth can only be used as a tool to assess relative maturity levels.

The MDR 4 also shows an increase with depth (Fig. 21), while the MDR indicates immaturity of all samples (Table 13, Radke et al., 1982a; Radke, 1988). The MDR 4 is the only aromatic ratio which exhibits a clear increase with depth independent of variations of kerogen type or lithofacies. The relative maturity of the wells as monitored by MDR 4 increases up to well 8. Well 24 has, according to this ratio, the same maturity as well 8.

Rock-Eval analysis of the asphaltenes of four samples, including two produced oils, showed a clear maturity trend. Fig. 51 shows the location of the data points in the HI vs. OI diagram of Espitalié et al. (1985). The trend indicated by the location of the data points is very similar to the kerogen evolution pathways described by Espitalié et al. (1985). As in the case of kerogens, the asphaltenes analysed show decreasing oxygen contents with decreasing hydrogen contents. This evolution is normally attributed to organic matter maturation.

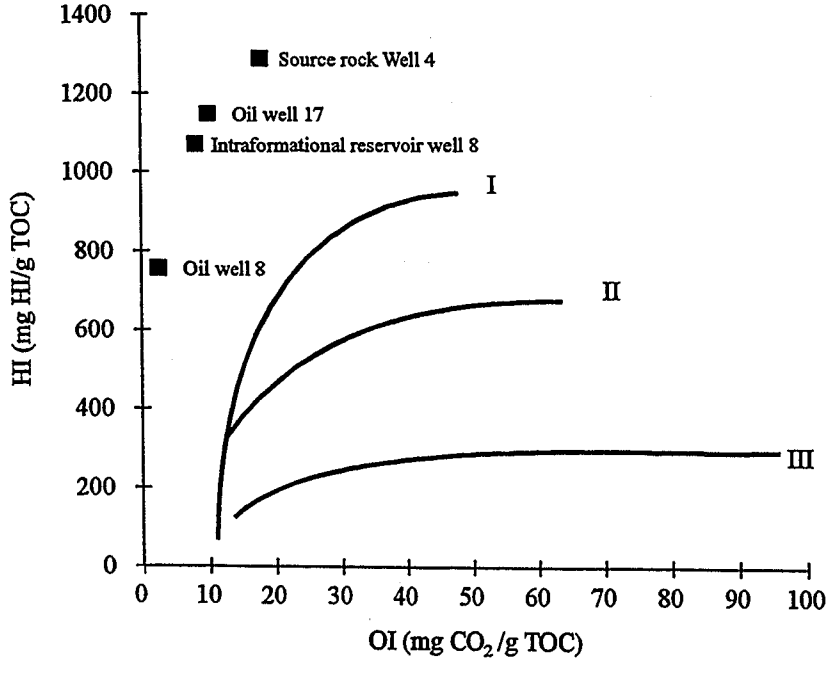

Figure 51: Plot of hydrogen index versus oxygen index showing the location of the four asphaltenes measured. Solid lines indicate maturation pathways of the different kerogen types.

The maturity indicator Tmax is plotted against the hydrogen index of the asphaltene samples in Fig. 52. The trend observed indicates that hydrogen depletion is an effect of increasing maturity (Fig. 52). The same trend was observed by Pelet et al. (1986) in the elemental composition of resins and asphaltenes from increasingly mature samples from the Paris Basin. According to the figures 51 and 52 the asphaltenes from the source rock sample from well 4 are the least mature. The produced oil from well 17 and the intraformational reservoir sample from Well 8 show slightly higher asphaltene maturities, while the asphaltenes from the produced oil from well 8 have the highest maturity. This maturity classification corresponds relatively well with the results from biomarker analysis of source rock extracts from these wells. The non-impregnated samples from Well 4 show a very low maturity according to both hopane and sterane data (Fig. 19). Samples from Well 8 are generally more mature, while the oil from Well 8 has the highest degree of maturity observed.

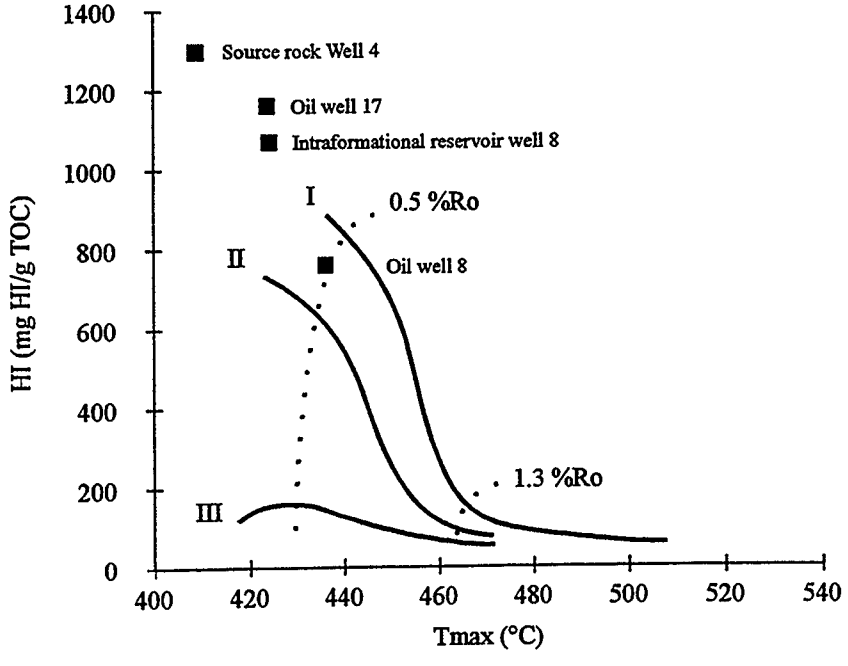

Figure 52: Plot of hydrogen index versus Tmax showing the location of the four asphaltenes measured. Solid lines indicate maturation pathways of the different kerogen types. Dotted lines show Ro values generally used for determination of begining and end of the oil window.

The high hydrogen indices of the asphaltene samples analysed imply that they should, if at all, be mainly comparable to a type I kerogen. If one assumes that Tmax values of the asphaltenes are also comparable to the Tmax values of a type I kerogen, then an aproximation of maturity can be made using the data of Barnard and Cooper (1981). The asphaltenes from well 4 with a Tmax of 409°C would, therefore, represent a vitrinite reflectance of between 0.4 and 0.5%. The intraformational reservoir from well 8 and the oil from well 17 would both be in the maturity range of 0.5 to 0.6 % Ro (425°C Tmax), and the oil produced from well 8 (436°C) should be characteristic of a maturity of around 0.7% Ro (Fig. 53). The relatively high amounts of asphaltenes in the extracts paired with their easy precipitation and analysis makes asphaltene Rock-Eval a tool which should be further developed.

The conversion of aromatic maturity ratios into vitrinite reflectance values was impossible due to the missing calibration of the MPI-1, MPI-2 and MDR-4 ratios to maturities below 0.5% Ro in general and to the sulphur-rich source rock type in particular. The development of new maturation ratios from the available SOM data was also impossible due to the relatively small maturity span between the least mature and the most advanced mature well. At best a very rough estimate of the actual maturity of the organic matter present in the source rock formation can be made by means of the HI vs. Tmax diagram of Espitalié et al. (1985, Fig. 54). In this diagram almost all samples plot below the 0.5% Ro line.

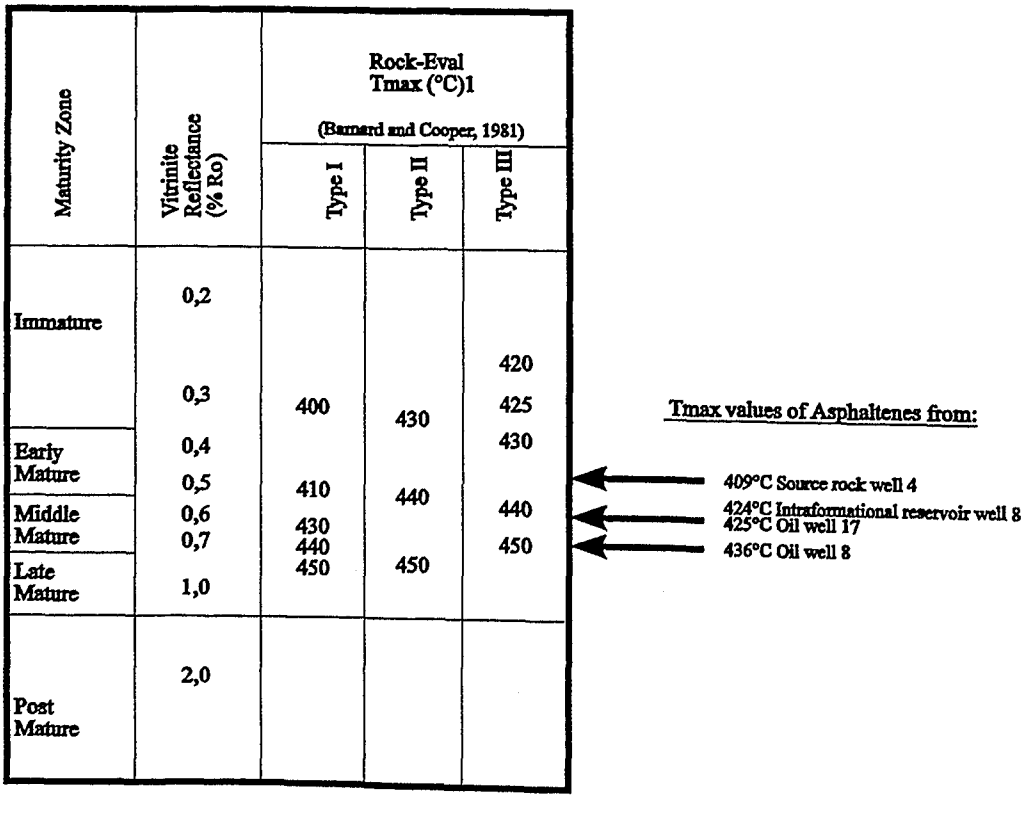

Figure 53: Correlation of vitrinite reflectance and Rock-Eval Tmax maturity parameter according to kerogen types (Barnard and Cooper, 1981). Asphaltene Tmax temperatures are shown by arrows.

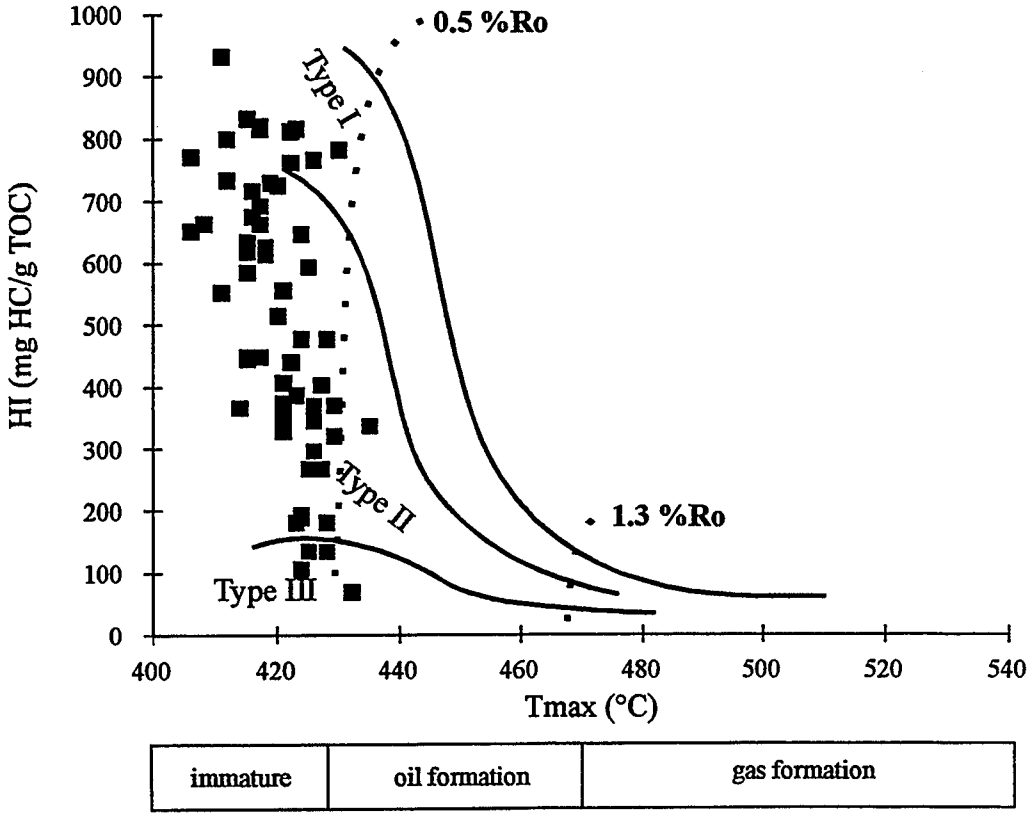

Figure 54: Hydrogen index versus Tmax for maturity estimation according to kerogen type for all samples analysed (Espitalié et al., 1984).

2.1.8 Artificial maturation

Laboratory simulation of in situ hydrocarbon formation from kerogen or source rock samples is an important research topic in petroleum geochemistry. Artificial maturation experiments that simulate natural diagenesis and catagenesis of the organic matter provide: (1) a better understanding of the mechanisms of petroleum formation; (2) data which can normally not be obtained from the analysis of natural samples (e.g. amount and time of gas formation); (3) data required for the estimation of kinetic behaviour of the organic matter and for the migration properties of the generated petroleum (e.g. gas/oil ratios, amount of heterocompounds produced at different temperatures).

Defining experimental conditions for the accurate simulation of natural evolution is a difficult problem. The thermal maturation experiments performed in different laboratories have used one of three techniques: (1) pyrolysis in a medium swept by an inert gas (e.g. Monin et al., 1990); (2) pyrolysis in a sealed tube (usually glass, Horsfield and Düppenbecker, 1991; or gold tubes, Monthioux et al., 1985); (3) pyrolysis in an autoclave (Lewan et al., 1979). The anhydrous open system pyrolysis is characterised by the generation of unsaturated hydrocarbons which makes a direct comparison to naturally generated products difficult. This type of analysis is better used in the characterisation of the total kerogen composition, and not for the simulation of temperature dependant hydrocarbon generation (Monthieoux et al., 1985).

Due to the restricted maturity interval available for analysis, two artificial maturation techniques were employed in order to analyse the hydrocarbon generation characteristics of the source rock formation.

The open system hydrous pyrolysis technique (Krooss, 1993) employed here was selected because it provides a quantitative insight into the different stages of hydrocarbon generation and expulsion. The large sample amounts produced by this technique made it specially interesting for detailed molecular analysis of the generated compounds.

MicroScale-Sealed-Vessel (MSSV) pyrolysis (Horsfield et al., 1989) was employed in order to assess the generation characteristics of whole rock samples, isolated kerogen and corresponding asphaltene fractions. It has the advantage over Py-GC in that it is a simulation technique rather than an analytical tool and hence its pyrolysate composition is likely to be comparable to natural petroleum for a given source rock-petroleum system (Horsfield, 1990).

2.1.8.1 Open system hydrous pyrolysis

Considerable progress has been achieved with respect to elucidation and quantification of hydrocarbon generation and migration processes by hydrous pyrolysis experiments (Eglinton et al., 1988; Baskin and Peters, 1992; Lewan, 1992). Most such experiments reported in the literature were performed as closed-system bulk experiments (simulation of the entire liquid window interval in a single heating step), or in stepwise fashion (aliquots of sample heated at increasingly higher temperatures). In either case, however, the initially generated and expelled pyrolysis products remain during the experiment in the reaction vessel and are hence likely to enter into secondary reactions with those products which are generated and expelled during subsequent heating stages. This aspect appears to be dissimilar from nature, where hydrocarbon products are usually expelled to a high proportion as soon as a minimum oil saturation, roughly 25%, of the available porosity is reached (Leythaeuser et al., 1988a,b; Welte, 1987). In order to better mimic this particular feature of the natural hydrocarbon generation and migration processes, Open System Hydrous Pyrolysis utilising an experimental design reported previously (Krooss, 1993) was performed. By this method the expelled pyrolysis products are, at the end of each heating step, sampled and removed quantitatively from the reaction vessel, without having to reduce the temperature or pressure in the autoclave vessel.

Open System Hydrous Pyrolysis (OSHP) of an unextracted source rock sample (E 33383) from well 8 was carried out using a stepwise isothermal heating program starting at 230° C going up to 350° C at 22 MPa (220 bar). The temperature was increased in steps of 10° C and held constant for 72 hours in each heating step. Sampling of gas and liquid products was performed at the end of each isothermal interval. The products were quantified and grouped into four classes: light (gas + volatile liquids), saturated, aromatic, and polar (NSO + asphaltenes) compounds. Hydrous pyrolysis of rock samples in the form of rock chips or cores provides a better simulation of natural petroleum generation than isolated kerogens or unconsolidated mixtures of kerogen and mineral powders. Organic matter in a rock sample is embedded naturally within its inorganic matrix. According to Lewan (1992) this condition more accurately simulates the natural system than the use of kerogens.

As indicated by the bulk geochemical data shown in Table 18 the sample used in this experiment can be classified as a high quality, immature, oil-prone source rock with a kerogen type I/II-S.

The decrease in TOC, S2 and HI and the increase in Tmax observed after Open System Hydrous Pyrolysis demonstrated the effective conversion of kerogen into petroleum products using this method (Table 18).

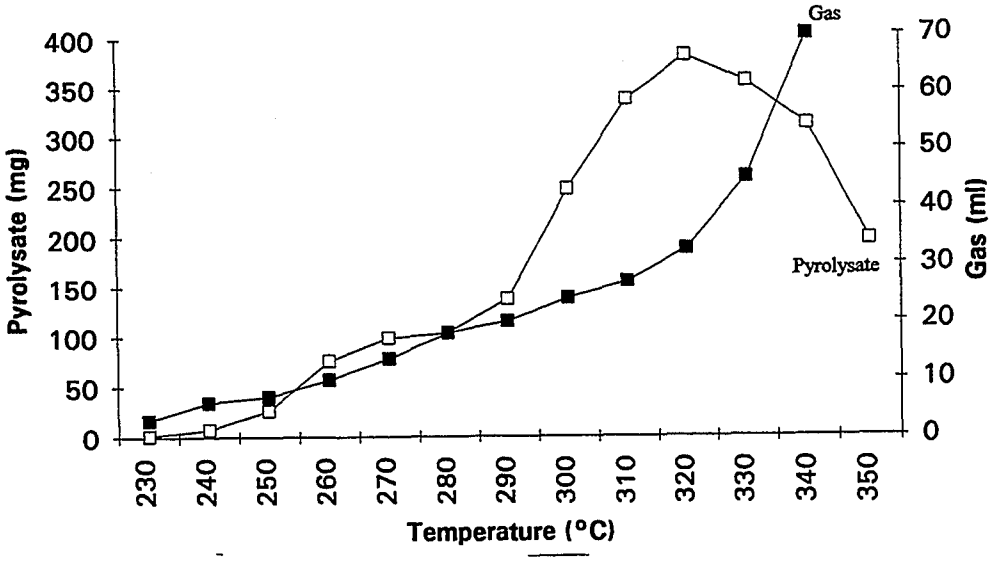

Figure 55: Yields of gas and pyrolysate per heating step of OSHP.

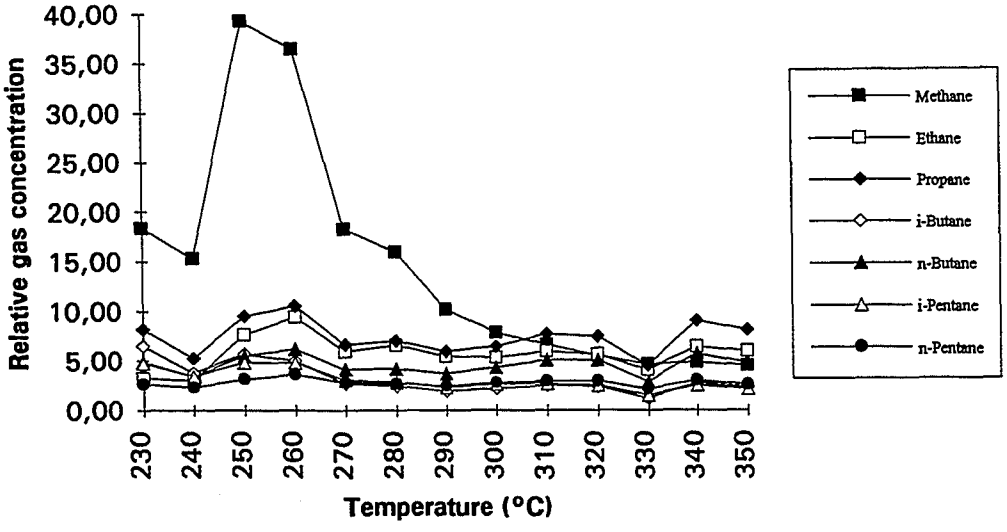

Figure 56: Gas composition generated during each step of OSHP.

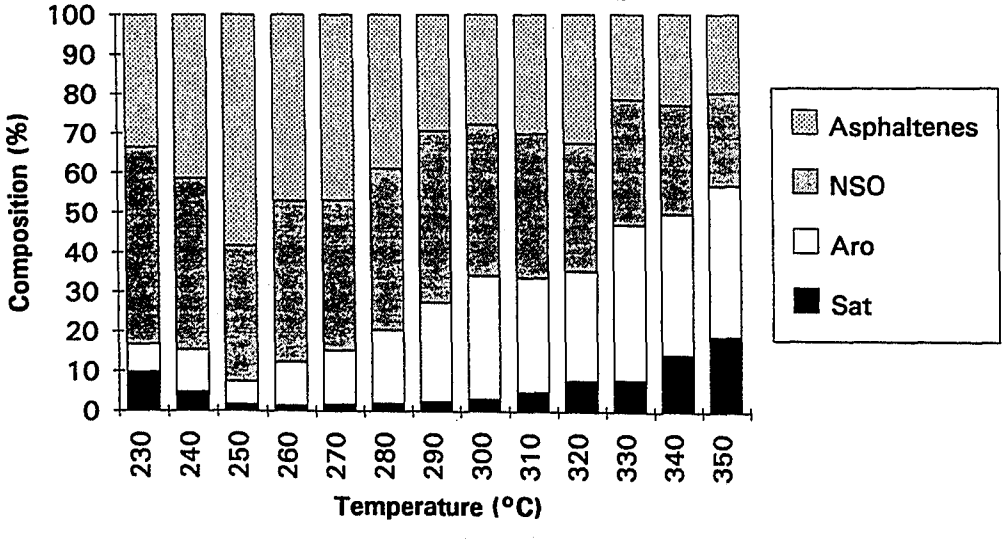

Figure 57: Compound class distribution of the pyrolysates generated per heating step of OSHP.

The volume of gas generated per heating step by this hydrous pyrolysis procedure is shown in Figure 55. The maximum gas volume was produced at a temperature of 350°C, where it exceeded the volume of the sampling vessel making a quantification impossible.

During this experiment the relative proportion of methane in the individual gas mixtures decreased with increasing temperature (Fig. 56). The concentrations of the other gases up to *n*-pentane showed almost no variation with increasing temperature (Fig. 56). On a cumulative basis (sum of generated gas up to a given temperature) methane is clearly the dominant product. The maximum rate of methane generation occurs between 240 and 260°C.

The amount of petroleum-like material generated and expelled per heating step is shown in Figure 55. A first slight increase can be seen up to a temperature of 270°C, after which the generation rate seems to remain constant before it increases dramatically from 300°C to reach a maximum at 320°C. This pyrolysis temperature for peak oil expulsion is 30°C lower than temperatures reported in the literature for similar kerogen types analysed by hydrous pyrolysis (Lewan, 1985; Baskin and Peters, 1992).

The change in compound class composition with temperature is shown in Figure 57. The increase with higher temperature in the relative proportions of saturated and aromatic hydrocarbons of the bulk oil generated and expelled follows the general trend observed in natural systems.

The gas/oil ratios (weight produced gas/weight produced liquids) calculated for all samples show an initial strong decrease up to a temperature of 250°C followed by an increase up to a temperature of 290°C, following which the ratio drops again and then increases continuously up to 340°C (Fig. 58).

The proportion of long chain *n*-alkanes (n-C_{28} - C_{30}) in the produced oils increases with increasing pyrolysis temperature up to a temperature of 350° C. This is demonstrated by the proportion of low-molecular-weight to high-molecular-weight n-alkanes expressed as the ratio Σn-C_{17}-C_{19}/Σn-C_{27}-C_{29} (LHCPI), which reaches a maximum of 34.7 at 310° C and then drops to 4.72 at 350° C (Fig. 59).

The generation and expulsion of pristane and phytane reaches a maximum at temperatures 10° C to 20° C prior the peak generation and expulsion of comparable *n*-alkanes (Fig. 60). Eglinton et al. (1988) also noticed that in the lower temperature range, of a hydrous pyrolysis experiment performed using a Kimmeridge kerogen, the ratio of isoprenoids to n-alkanes increased steadily, indicating the more favourable release of the former from the kerogen in that temperature range.

Biomarker ratios of the pyrolysates show that the C_{27} steranes ($\beta\beta/\alpha\alpha+\beta\beta$, and S/S+R) and the 17$\alpha$(H)-Bishomohopanes (S/S+R) seam to monitor the maturity-progress in this source

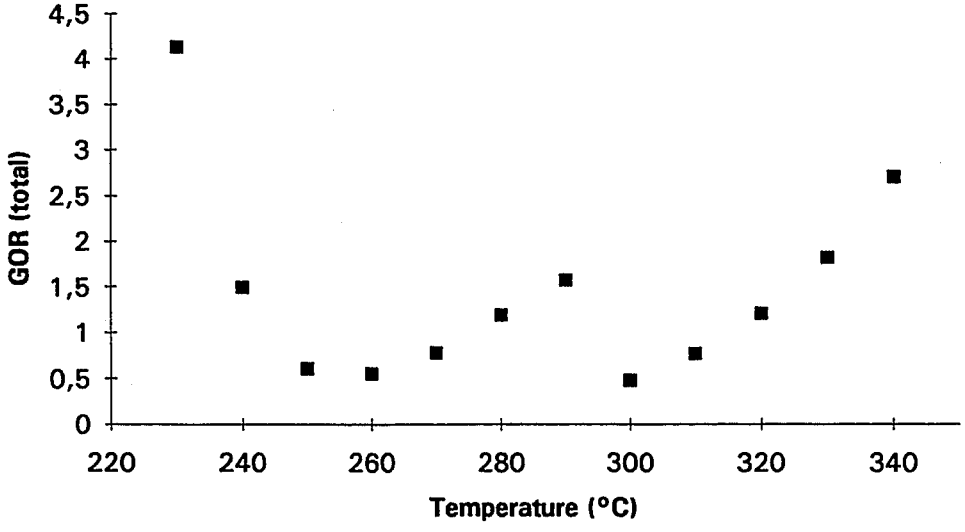

Figure 58: Gas/oil ratio (weight/weight) of the pyrolysates generated per heating step of OSHP.

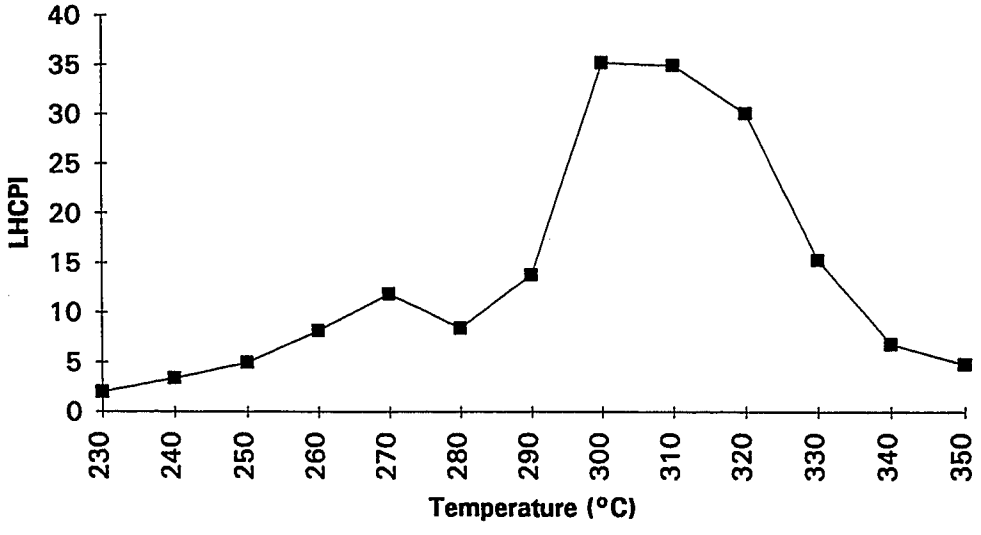

Figure 59: Light hydrocarbon preference index (LHCPI) of the alkanes generated per heating step of OSHP.

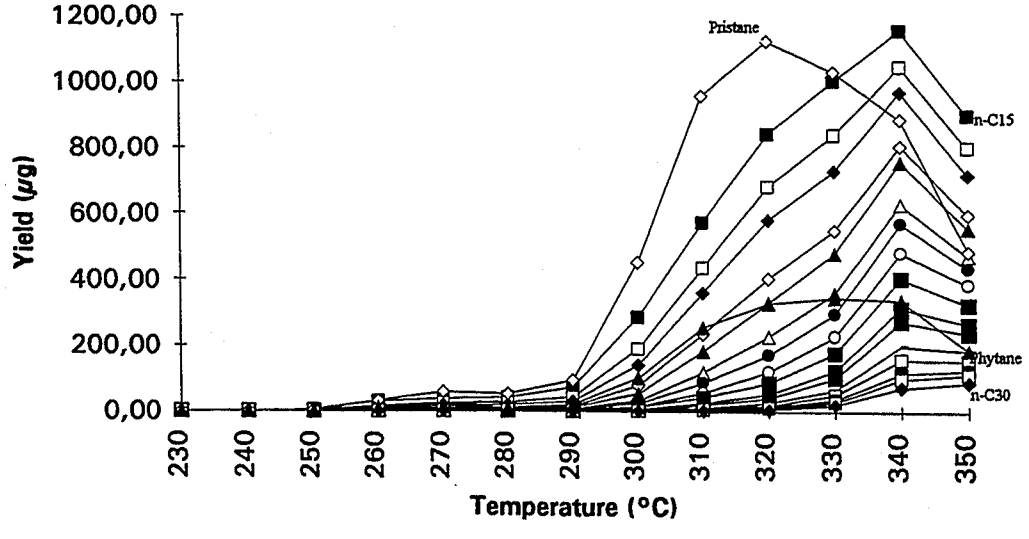

Figure 60: Yields of n-alkanes and selected isoprenoids per heating step of OSHP.

rock most accurately. The sterane and hopane content decreases with increasing temperature (Fig. 61).

Analysis of the aromatic compounds (C10+) showed, as in the natural source rock extracts, a superabundance of monoaromatic sulphur compounds which, due to coelution, occluded the naphthalines and phenanthrenes usually analysed. This predominance of sulphur compounds was specially prominent in the samples taken between 230°C and 290°C.

The yield of sulphur compounds was evaluated semiquantitatively. The absolute concentration of individual sulphur compounds (benzothiophenes) was determined using internal standards. The entire HECD trace was then quantified according to the benzothiophene concentration. The HECD does not respond linearly to the molecular size of individual compounds, it responds to the proportion of sulphur in the molecule. This implies that small molecules with one sulphur atom produce a much stronger signal than larger molecules with one sulphur atom. Thus the total sulphur compound concentration calculated by this procedure underestimated the amount of compounds with a molecular weight higher than benzothiophene and overestimated the amount of compounds with a lower molecular weight. A semiquantitative comparison of the sulphur compound content in each sample is therefore the best which can be achieved by this technique.

The yield of sulphur compounds generated at each heating stage, derived from the semiquantitative method described above, was calculated as a percentage of the total amount of sulphur compounds generated in all heating steps. Fig. 62 shows this data plotted against sample temperature. The generation of sulphur compounds increases drastically up to a maximum at 280°C, at higher temperatures almost no more sulphur aromatics are produced.

Analysis of the aromatic hydrocarbon fraction, after removal of the sulphur compounds by the oxidative method described in chapter 1.4, allowed the calculation of absolute yields for individual molecules at each temperature. The results, which can also be described as generation rates, are summarised in Fig. 63. The main temperature of aromatic compound generation is in the range of 330°C to 350°C, which fits quite well to temperature range stated by Rowland et al. (1985) for the main generation of aromatic compounds from sediments during hydrous pyrolysis (340°C to 360°C).

The generation of hydrocarbons in the course of the OSHP experiment occurs in two distinct phases. The first is characterised by a high proportion of mainly sulphur-containing polar compounds. This first type of pyrolysate is generated between 250° and 290°C. In the second generation phase a different pyrolysate is generated, characterised by higher proportions of hydrocarbons (reaching up to 60%) and lower amounts of polar compounds.

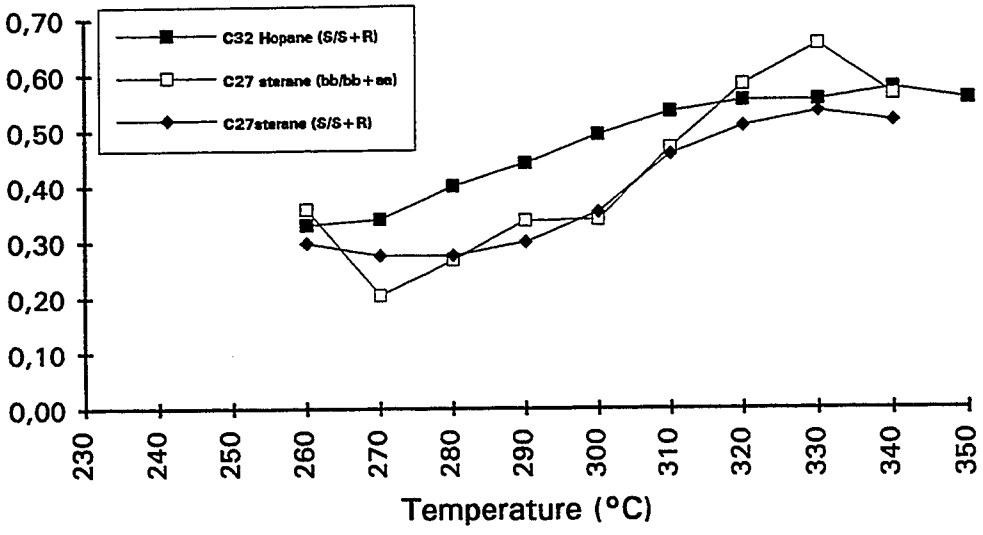

Figure 61: Selected hopane and sterane isomerisation ratios monitored on the samples of OSHP.

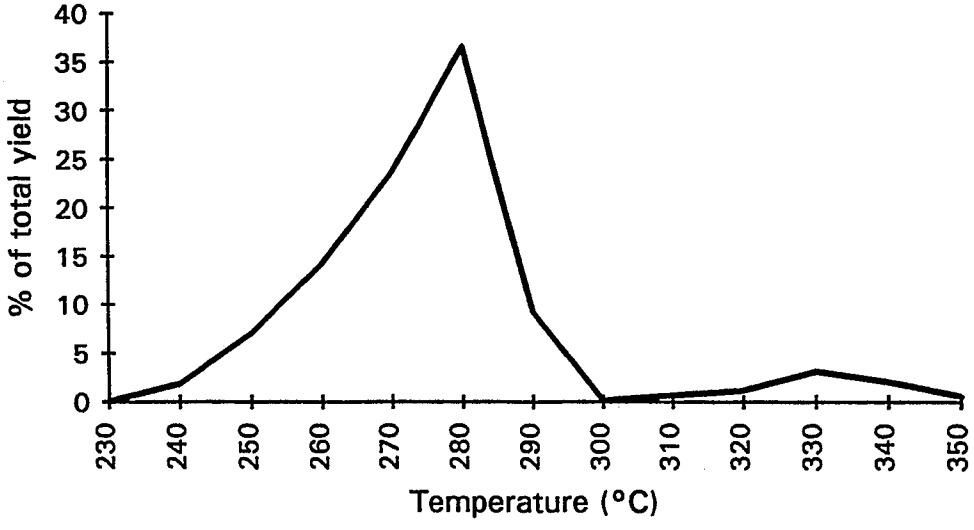

Figure 62: Percentual amount of total sulphur-romatic compounds generated per heating step of OSHP.

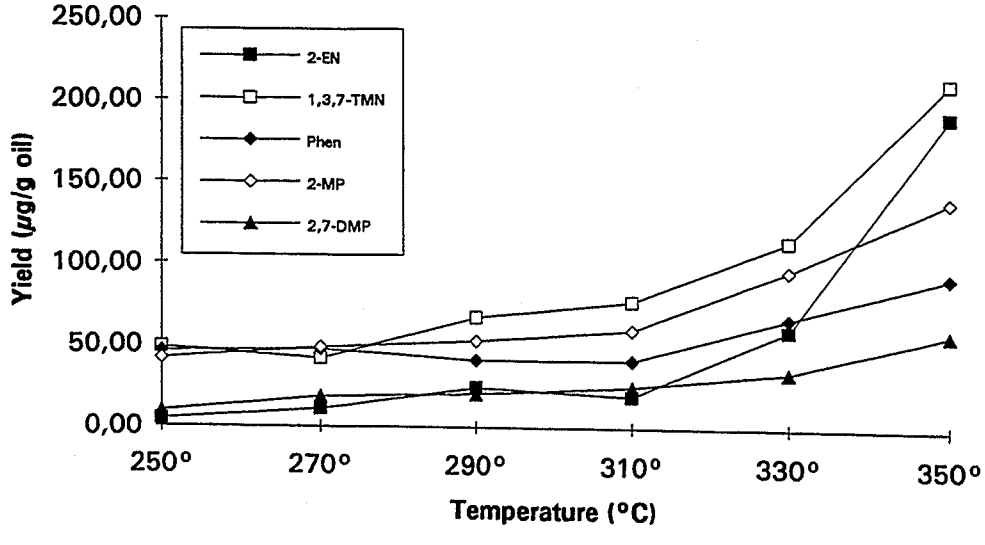

Figure 63: Yields of selected aromatic compounds per heating step of OSHP.

The two generation phases can be recognised in the systematic changes of amounts of compound classes or individual compounds in the course of the experiment. The amount of pyrolysate generated throughout the experiment shows, for example, a bimodal distribution (Fig. 55), with a first mode in the 250°-290°C range and a second peaking at 320°C. The gas/oil ratio also monitors the two phases very well. The first drop in the gas/oil ratio measured between 230°C and 250°C, is probably due to the degassing of the source rock sample, the initial increase in GOR (from 250°C to 290°C) is then due to an increasing gas generation during heating. The drop in GOR between 290°C and 300°C is due to an abrupt increase in the oil generation rate (Fig. 58). At this stage a fundamental change in the hydrocarbon generation reaction occurs.

The amounts of asphaltenes generated per heating step also demonstrates the two main pyrolysate types generated in this experiment. The decrease in asphaltene content in the first heating steps (Fig. 57), together with the relatively uniform asphaltene content of the samples taken at temperatures of more than 300° reflects the early generation of predominantly polar compounds from the kerogen probably by cleavage of weak heteroatomic bonds.

The dominance of sulphur-containing polar compounds in the first pyrolysate generation phase is demonstrated by the percentual amount of sulphur-aromatic compounds generated per heating step (Fig. 62), which reaches a clear maximum at 280°C. Eglinton et al. (1988) observed exactly the same maximum temperature of sulphur compound generation in hydrous pyrolysis experiments using Kimmeridge kerogen. The large amount of sulphur compounds in the low temperature pyrolysates must be taken as an indication that hydrocarbon generation is taking place predominantly due to the cleavage of carbon-sulphur bonds in the kerogen. Eglinton et al. (1990) noticed that the loss of thiophenic species from kerogens requires lower activation energies than does hydrocarbon generation, and suggested that this was due to the cracking of weak carbon-sulphur linkages in the alkyl chains bonding the thiophenes to the kerogen. Comparison of the sulphur compound generation diagram (Fig. 62) to Fig. 58, which shows the evolution of the gas/oil ratio with temperature, indicates that the generation of sulphur compounds, probably by cleavage of C-S bonds (Jones, 1984; Palacas, 1984; Tannenbaum and Aizenshtat, 1985; Lewan, 1985), must be one of the two reactions postulated from the GOR results. The cleavage of C-S bonds is, according to the experimental data, therefore terminated at a temperature of 300°C (drop of GOR, Fig. 58).

The second generation phase is dominated by aromatic compounds and, specially, by the intense generation of alkanes at temperatures above 290°C (Fig. 60). The increase in the proportion of long chained n-alkanes with increasing temperature, as shown by the decreasing LHCPI (Fig. 59), is a notable feature. This increase in the amount of long chain n-alkanes

generated and expelled with higher temperature is contrary to natural trends and contrary to the observations made by Eglinton et al. (1988) on hydrous pyrolysis of a Kimmeridge Clay kerogen, which showed evidence of cracking of long chain to shorter chain n-alkanes. This discrepancy is probably due to the open system method applied in this hydrous pyrolysis experiment, which was expected to reduce the effects of secondary cracking reactions. The generation of long chained n-alkanes at high temperatures ought therefore be due to the generation of n-alkyl moieties from resistant biopolymers (algaenanes, bacteranes) inherited from living organisms and bound in the kerogen and not to artefact effects. In this context Rullkötter and Michaelis (1989) stated, based on the results of Horsfield (1989) and Horsfield et al. (1989), that many kerogens which appear to have formed preferentially via selective preservation of aliphatic biopolymers do not exhibit a shortening of n-alkane chain length in their pyrolysates with increasing level of induced thermal stress.

2.1.8.2 Micro-Scale Sealed Vessel Pyrolysis

Progressive changes in gross petroleum composition which might occur during maturation of a source rock sample can be simulated by MSSV pyrolysis experiments. This method was performed with one source rock sample (E 33383), one kerogen sample (E 33366/4) and its corresponding asphaltene fraction (E33366/4 As) in order to estimate the relative contributions of asphaltenes and kerogen to the generation of hydrocarbons during maturation. The MSSV pyrolysis technique employed here has been described by Horsfield et al. (1989).

The GC traces in Fig 64 (for the 270°, 310° and 350°C experiments of each of the samples analysed) are representative of the compositional variability displayed in the series of experiments.

n-Alkanes, isoprenoid alkanes, alkyl substituted aromatic hydrocarbons, alkyl substituted thiophenes and a complex mixture of largely unresolved components were identified in the MSSV pyrolysates. In all samples analysed both isoprenoid and n-alkanes are generated in progressively larger amounts with increasing temperature. The n-alkanes are most prominent in the 330° and 350°C experiments, whereas thiophenic sulphur compounds dominate the low temperature pyrolysates. For example, up to 310°C 2-methylthiophene and 2-ethyl-5-methylthiophene are the most prominent peaks in the n-C_{6+} range.

The relative amounts of "oil" (C_{6+}) and "gas" (C_1-C_5) generated per heating step by MSSV pyrolysis of each sample are shown in Figure 65. The constant increase in gas with temperature, as observed for the whole rock sample, is a common phenomenon observed during pyrolysis, which is attributed to primary gas generation and secondary cracking reactions of the generated hydrocarbons. An interesting observation is the two-step increase in

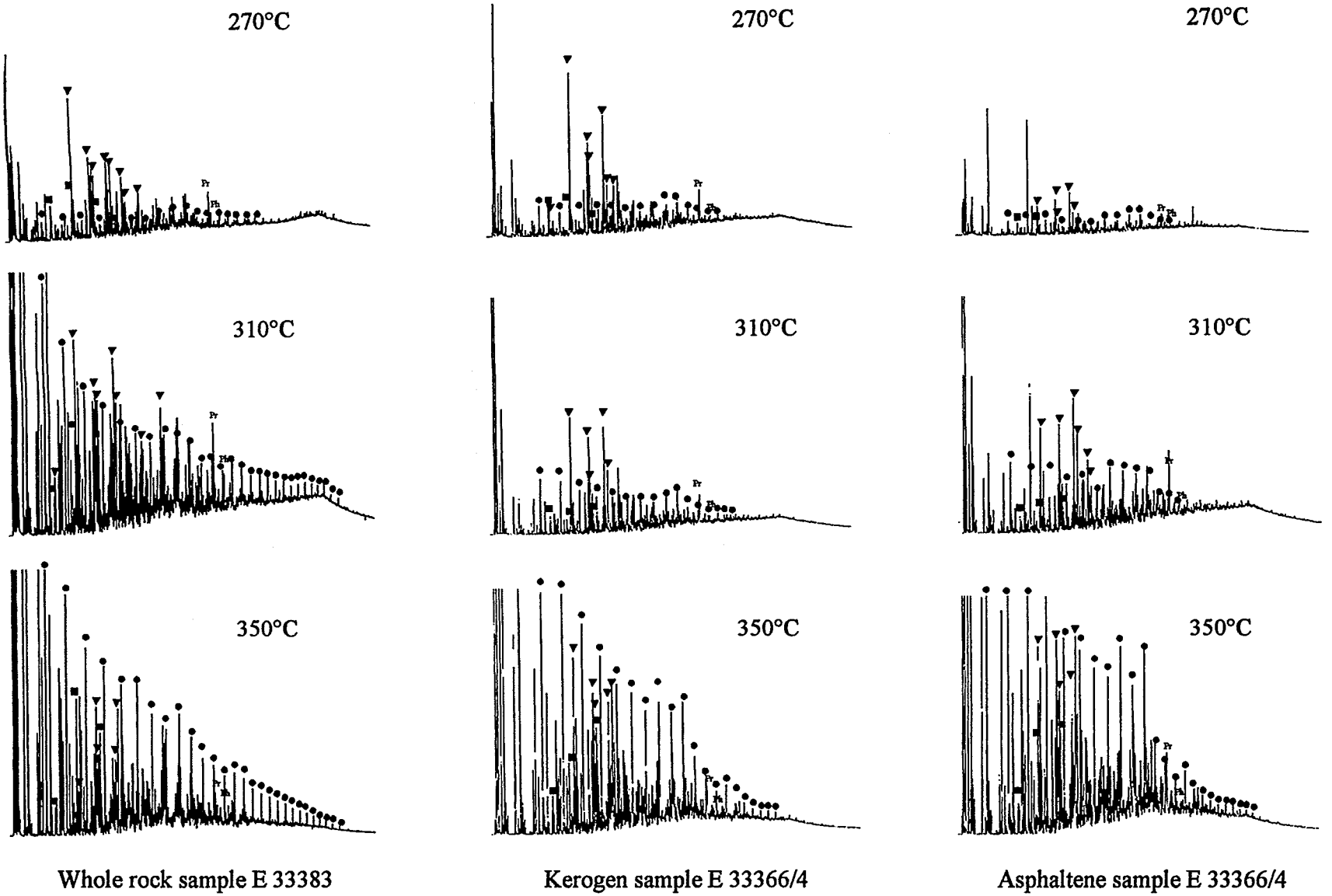

Figure 64: GC traces of whole rock (E33383), kerogen (E 33366/4) and asphaltene (E 33366/4) MSSV pyrolysates for three selected temperatures. Alkanes are marked by points, sulphur compounds by triangles, aromatic compounds by squares and pristane and phytane by Pr and Ph respectively.

oil-like pyrolysate with temperature for the whole rock sample. The first generation stage takes place at 290°C (Fig. 65a). The next temperature stage shows only a slight increase in hydrocarbon generation, while at 330°C the main oil generation stage is reached. At 350°C secondary cracking reactions dominate over hydrocarbon generation, leading to a decrease in oil and an increase in gas in the pyrolysate.

The kerogen sample shows a strong bimodality in both gas and oil generation with temperature (Fig 65b), while the asphaltene sample displays a more regular increase in the yields with temperature. The asphaltenes show the strongest increase in oil yield at 310°C as compared to 330°C for the kerogen sample (Fig 65b, c). Light hydrocarbons (C_1-C_5) make up 5.5% of the total chromatographed 270°C and 290°C pyrolysates, 5.8% of 310°C pyrolysates, 7.7% of the 330°C pyrolysates and 13% of the 350°C pyrolysates of the whole rock and kerogen samples. For the asphaltene sample they represent only 4.6% and 5.0% in the total chromatographed 270° and 290°C pyrolysates respectively, at 310°C the light hydrocarbons make up 5.5%, at 330°C 6.5% and at 350°C 11.2% of the total cromatographed pyrolysates. The gas/oil ratios (GOR) of the individual pyrolysates reach 0.07, 0.07, 0.08, 0.11 and 0.19 kg/kg for the 270°, 290°, 310°, 330° and 350°C experiments of the whole rock and kerogen samples, respectively. For the asphaltene sample the GOR's reach 0.06, 0.07, 0.09, 0.10 and 0.18 kg/kg for the 270°, 290°, 310°, 330° and 350°C experiments, respectively.

The GOR values listed above are very similar to values reported by Horsfield and Düppenbecker (1991) for a Green River Shale kerogen analysed under similar experimental conditions.

Figure 66 shows the relationship between the generation of C_2-C_5 n-alkanes versus C_{6+} n-alkanes for the kerogen and asphaltene samples. Interestingly one single gradient occurs up to the 330°C experiments. At 350°C the data points shown in Fig. 66 below the line extrapolated from the former temperature stages, indicating a lowering in the proportion of the C_2-C_5 yield as compared to the proportion of C_{6+} n-alkanes. This is probably due to hydrocabon cracking reactions and not to generation dependant variations. Changes in GOR with temperature in the temperature range from 270°C to 330°C thus seem to be unrelated to the generation of n-alkanes. This fact was also noticed by Horsfield and Düppenbecker (1991) in Posidonia Shale and Green River Shale kerogens. They deduced from this observation that the essentially fixed chain length distribution of n-alkanes implied a homogeneous and ordered kerogen, the nature of which was more consistent with derivation from a preserved biopolymeric kerogen precursor than with a neoformed hetero-polycondensate.

Figure 67 shows the chain length distribution of normal alkanes of the MSSV pyrolysates analysed in this study in comparison to other selected kerogens. The three samples, asphaltene,

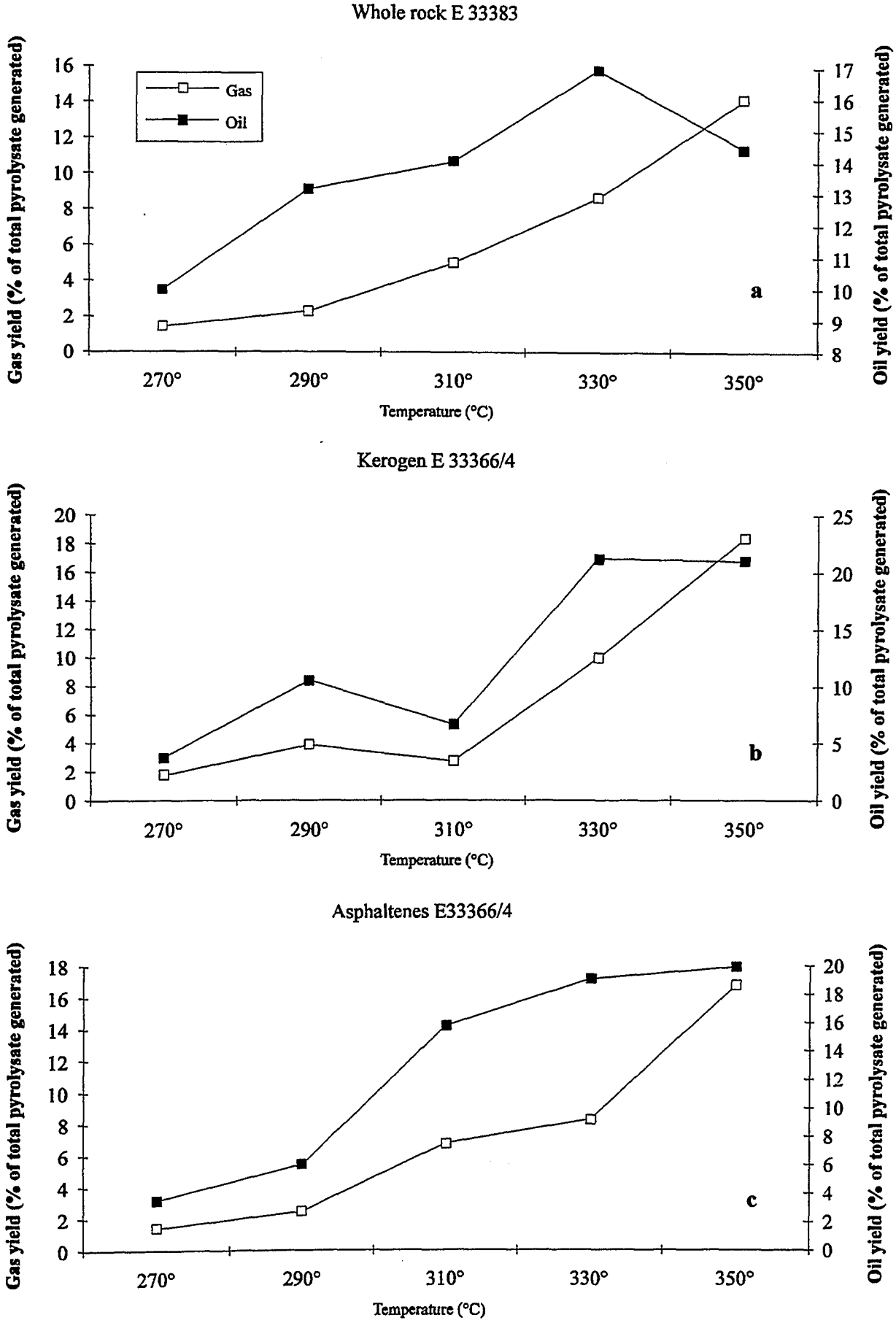

Figure 65: Oil and gas yields generated during MSSV of a whole rock (E 33383, shale, a), a kerogen (E 33366/4, shale, b) and ist corresponding asphaltene fraction (E 33366/4, c). Yields are expressed as a percentage of the total amount (oil and gas) generated.

kerogen and whole rock sample, plot in a very narrow field in the gas-rich part of the diagram, close to the fields in which the Posidonia Shale, a tertiary coal and sporinite plot. It is interesting to notice that while the kerogen and asphaltene sample produced pyrolysates with nearly identical n-alkane composition, the whole rock sample generated pyrolysates with a more or less 5% higher proportion of gas. This may be due either to the occurrence of a slightly different kerogen type in this sample or to mineral matrix effects.

This series of MSSV experiments revealed significant differences in the pyrolysate generation between the samples analysed. This is obvious even on a gross compositional basis, for example in the generation of gas (C_1-C_5) and oil (C_{6+}) as shown in Fig. 65. The bimodal generation of both oil and gas during MSSV pyrolysis of the kerogen sample contrasts strongly with the relatively constant generation of oil and gas from the asphaltenes of the same sample. The whole rock sample showed oil and gas generation characteristics between the two extremes described above, which is easily explained since the unextracted whole rock sample contained both kerogen and asphaltenes. The further discussion centres therefore mainly on the differences in hydrocarbon generation from the kerogen and the asphaltene sample.

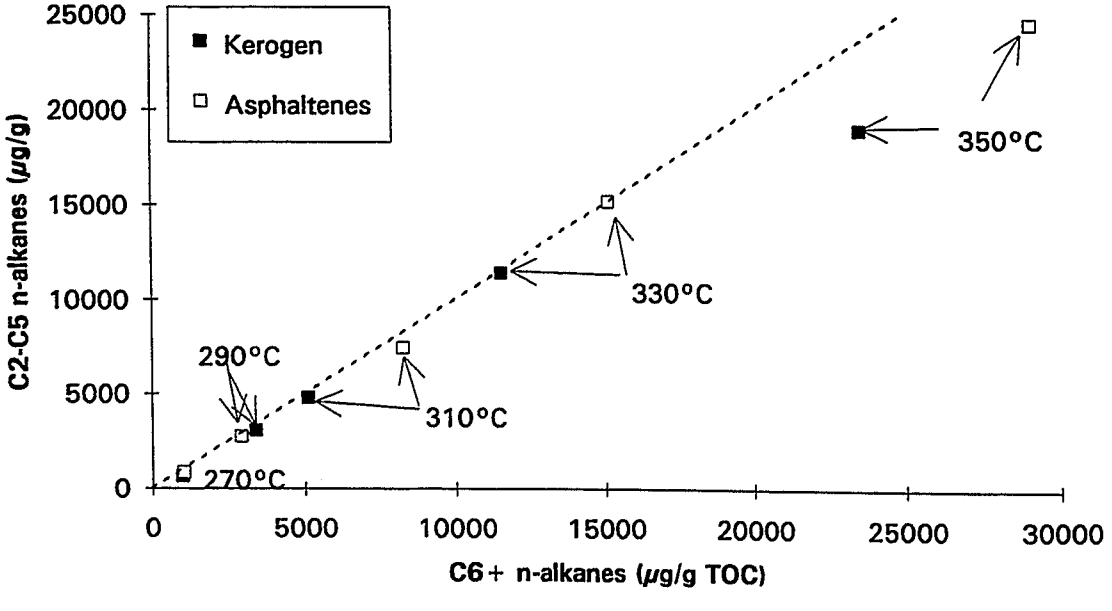

Figure 66: Yield of C2-C5 n-alkanes versus yield of C6+ n-alkanes for the kerogen and corresponding asphaltenes analysed by MSSV (sample E 33366/4).

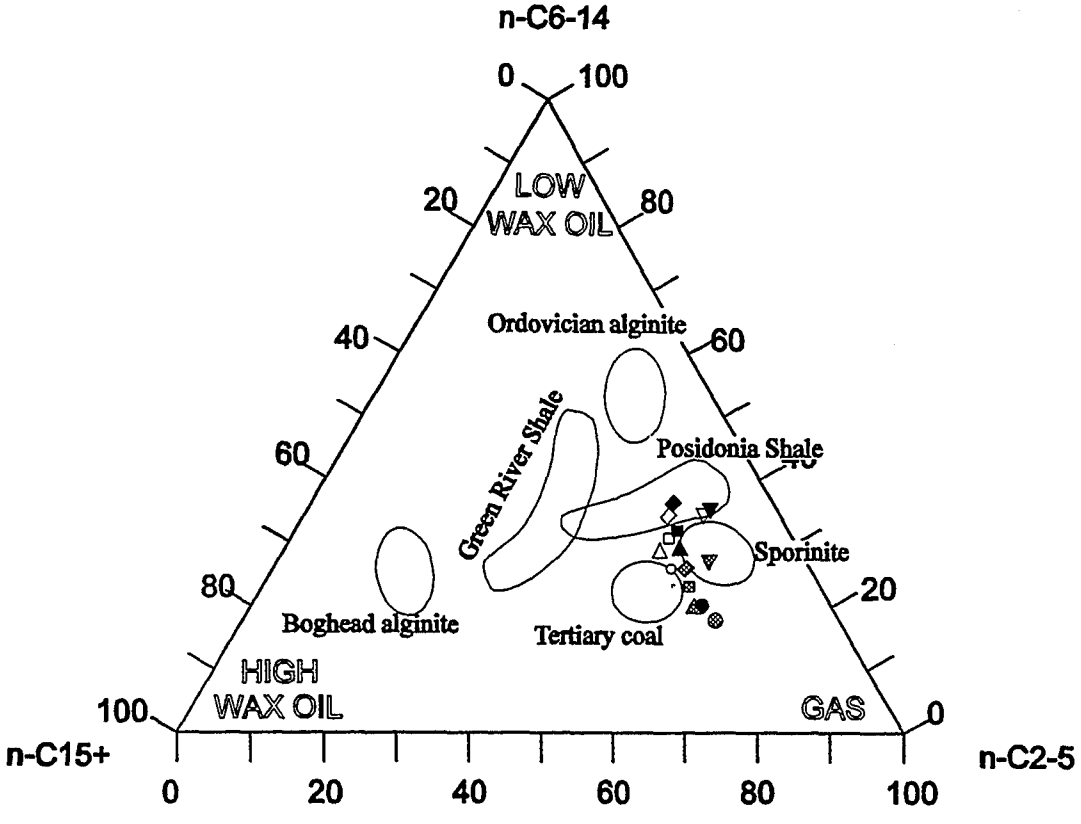

Asphaltenes	Kerogen	Whole Rock	Py. Temperature
○	●	⊗	270°C
△	▲	⊗	290°C
□	■	⊠	310°C
◇	◆	⊗	330°C
▽	▼	⊗	350°C

Figure 67: Chain length distribution of normal alkanes of the MSSV pyrolysates. Fields corresponding to other samples than those reported in this studyare from Düppenbecker (1992).

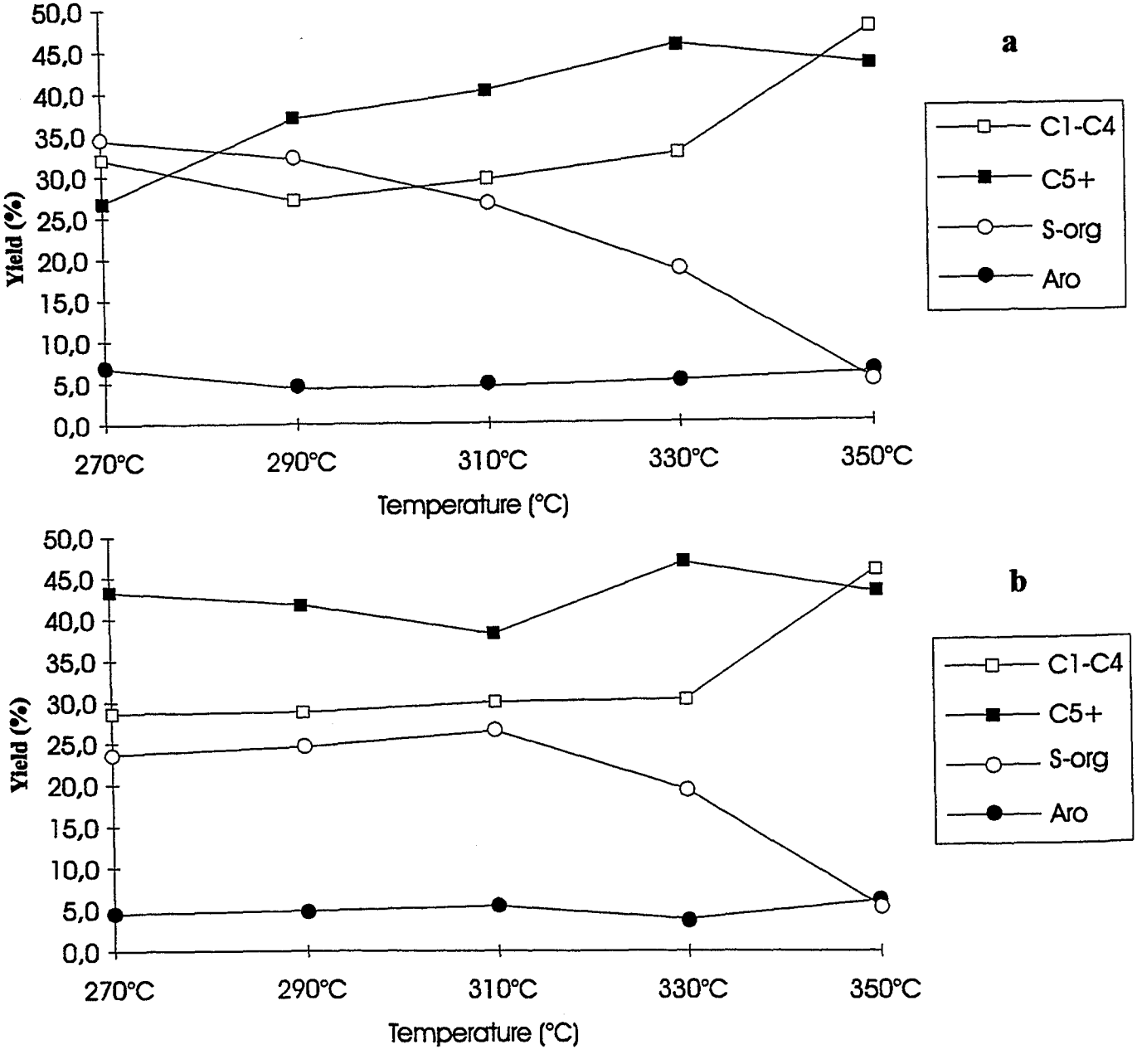

Figure 68: Yields of gas, C5+ saturated compounds, sulphur compounds and aromatic compounds generated per MSSV heating step for the kerogen sample E 33366/4 (a) and the corresponding asphaltene sample E 33366/4 (b) expressed as a percentage of the total amount generated in each step.

The observations made on a gross compositional basis were confirmed by molecular data. Fig. 68 shows the percentual yields of C_1-C_4 (gases), C5+ n-alkanes, resolved sulphur compounds and aromatic compounds generated at each temperature step for the kerogen and asphaltene samples. The main characteristics of the kerogen sample as shown in this figure are 1) a strongly decreasing yield of sulphur compounds with temperature, 2) a vaguely recognisable bimodal increase of the C_{5+} n-alkanes with temperature, 3) a relatively constant increase in gas yield with temperature, and 4) constant yields of aromatic compounds. The asphaltenes showed major differences in the generation characteristics as compared to the kerogen sample. The percentual amount of the different compound classes (gas, n-C_{5+} n-alkanes, resolved aromatic and sulphur compounds, Fig, 68b) remains constant throughout the temperature program. The first slight change is visible at 330°C, due to a decrease in the content of sulphur compounds and an increase in the n-C_{5+} content. At 350°C the highest percentage of gas is being generated due to secondary cracking reactions.

In the course of further molecular analyses the absolute amount of selected compounds (n-C5-n-C15 alkanes, 2-methylthiophen, 2-ethylthiophene, 2,5-dimethylthiophen, 2,4-dimethyl-thiophene, 2,3-dimethylthiophene, 2-ethyl-5-methylthiophene, 2,3,5-trimethylthiophene, benzene, toluene, orthoxylene, naphthalene and 1-methylnaphthalene) generated during MSSV pyrolysis per heating step was calculated (by substracting the amount at lower temperature from the amount at higher temperature). The total amount of each compound generated throughout the experiment was calculated and expressed as 100 %. The absolute amount of each compound generated per heating step was then expressed as a percentage of the total (Δ %).

The percentual amounts of each n-alkane generated from the kerogen sample per heating step are shown in Fig. 69. The Δ% distribution of each compound can be seen as the description of the chemical reactions which produce it. If the generation of any compound occurs from one main source, then a plot of the amount generated per heating step should resemble a unimodal distribution. This is clearly not the case with the n-alkanes of the kerogen sample. They show a bimodal generation trend with temperature increase (Fig. 69). With increasing chainlength the absolute proportion generated at 290°C increases up to n-C_{15}, while the main temperature of generation remains relatively constant at 330°C for n-alkanes from n-C_{12} on and 350°C for n-alkanes in the gas to n-C_{11} range. From n-C_{16} onwards quantification problems due to compound coelution made the data unreliable.

The same kind of calculation was performed on selected sulphur and aromatic compounds. The results are shown in Figs 70 and 71. The bimodal generation of the individual compounds is clearly visible in both cases. Especially in the case of the sulphur compounds (Fig. 70) two

main generation temperatures, 290°C and 330°C, occur. For the aromatic compounds (Fig. 71) this feature was only noticed for toluene, orthoxylene and 1-methylnaphthalene. Naphthalene and benzene showed one dominat temperature of generation at 330°C.

The calculation of Δ% contents of individual compounds per heating step as described above, was also performed for the compounds generated from the asphaltene fraction. Figs. 72-74 show the main results. In almost all cases the generation of the compounds is unimodal. The main generation temperatures range from 310°C for the sulphur compounds and 350°C for the n-alkanes and most aromatics. Only naphthaline and toluol show a bimodal generation. Since both were minor constituents of the total pyrolysate, coelution with unidentified sulphur compounds could not be ruled out.

The bimodal generation characteristics observed in the total pyrolysate of the kerogen (Fig. 68a) were thus reflected on a molecular level. The strong decrease in the yields of sulphur compounds during MSSV pyrolysis of the kerogen sample indicates that the bimodal generation of oil is probably due to the thermal breakdown of first C-S and later, at higher temperatures, carbon-carbon bonds in the kerogen as proposed by different authors (e.g.: Tissot and Welte, 1984; Rullkötter et al., 1985; Tannenbaum and Aizenshtat, 1985; Orr, 1986; Sinninghe Damsté et al., 1989; Rullkötter et al., 1990).

The generation characteristics of the asphaltene fraction indicate that the generation of hydrocarbons is due to one main bond cracking reaction. The main bond type can be assumed to be the carbon-carbon bond due to the high temperature necessary for cracking. S-C bonds seem to play a subordinate role in the asphaltene as compared to the kerogen sample.

The quantitative approach used in this analysis allows the identification of the compounds bound by carbon-sulphur bonds to the kerogen. Nevertheless, it must be kept in mind, that the quantification of individual compound groups or classes (gas, n-alkanes, aromatics, sulphur compounds) is biased by the ease with which these compounds are detected. Complex substance mixtures which can not be resolved by the gas chromatographic technique applied are thus completely ignored in the quantification. The distribution of compound classes shown in Fig. 68 is therefore only a picture of the relative amounts of compounds which were identified.

The trends shown in Fig. 68a allow a relative evaluation of the characteristics of oils generated by the kerogen analysed at different temperatures. If the amount of sulphur compounds in the pyrolysate is assumed to be representative of the proportion of heterocompounds in the respective oils during natural maturation of the sample, one can expect that in an early generation stage the kerogen generates a low API gravity oil rich in polar compounds. With increasing maturity the kerogen generates oils with a higher proportion of aliphatics and gas.

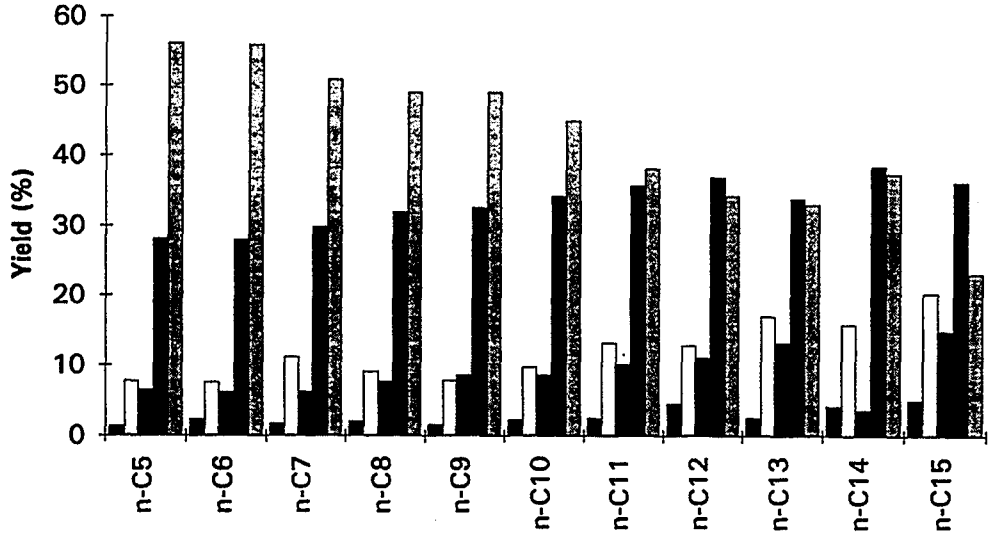

Figure 69: n-alkane yields per MSSV heating step of kerogen sample E 33366/4 expressed as a percentage of the total amount generated. The legend to this figure is shown in Fig. 70.

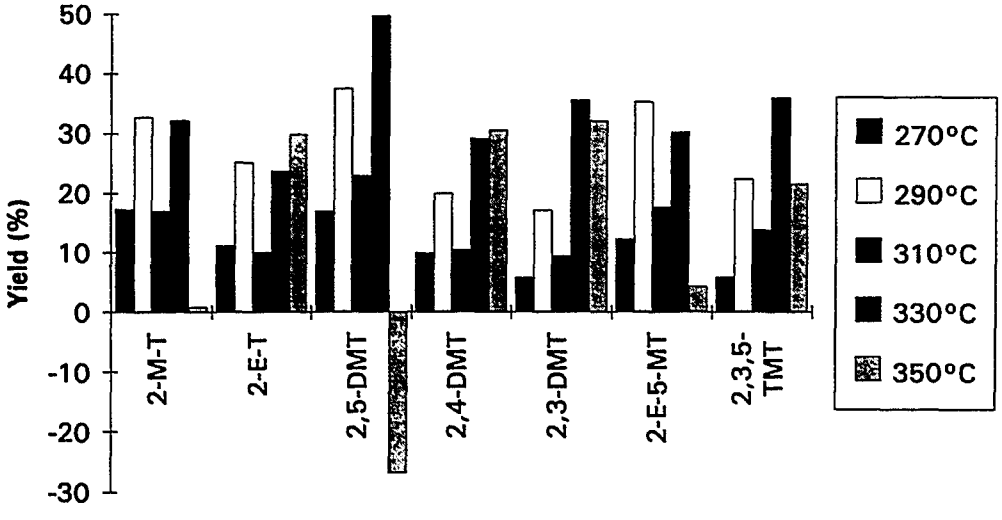

Figure 70: Sulphur compound yields per MSSV heating step of kerogen sample E 33366/4 expressed as a percentage of the total amount generated.

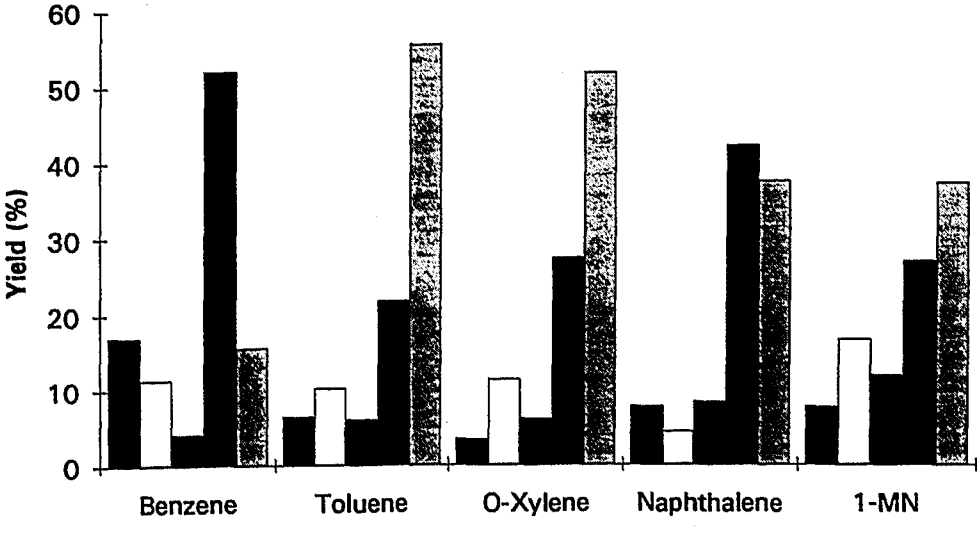

Figure 71: Aromatic compound yields per MSSV heating step of kerogen sample E 33366/4 expressed as a percentage of the total amount generated. The legend to this figure is shown in Fig.70.

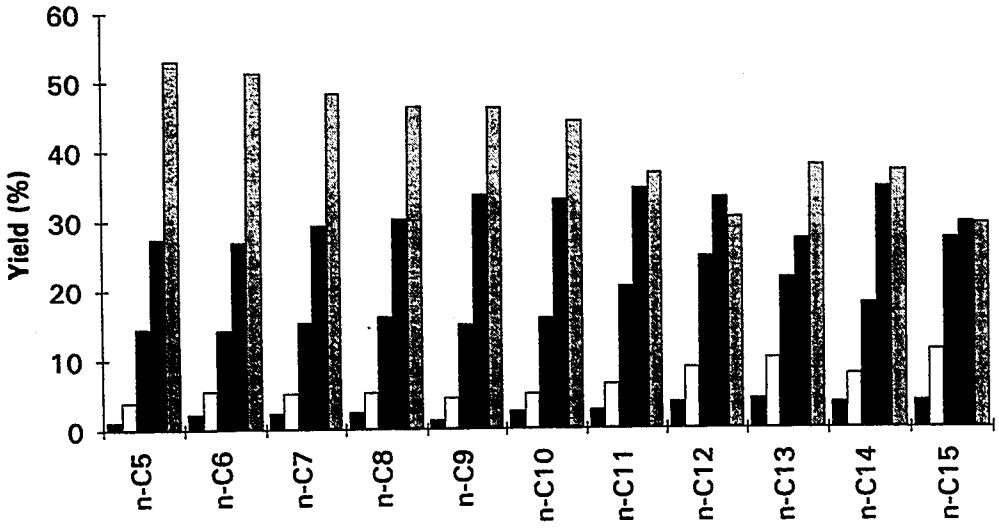

Figure 72: n-alkane yields per MSSV heating step of asphaltene sample E 33366/4 expressed as a percentage of the total amount generated. The legend to this figure is shown in Fig. 70.

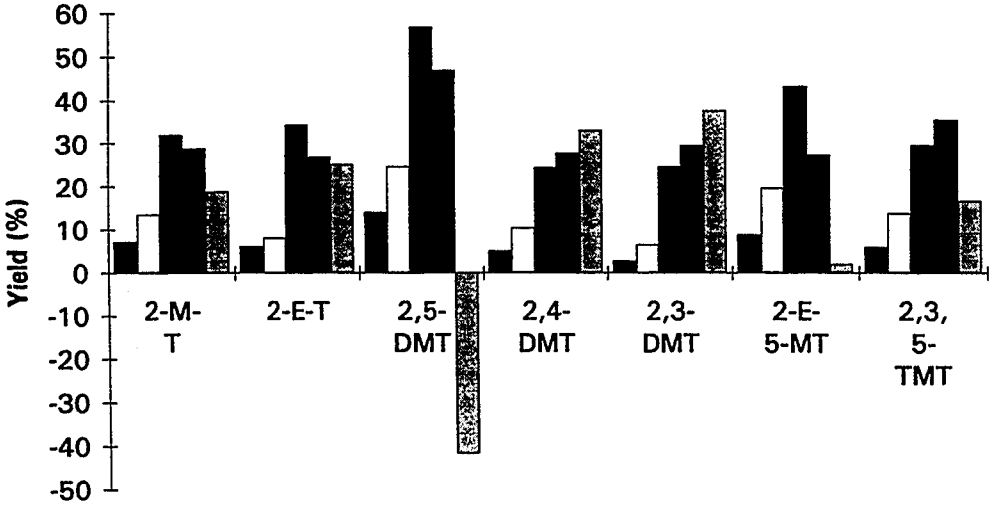

Figure 73: Sulphur compound yields per MSSV heating step of asphaltene sample E 33366/4 expressed as a percentage of the total amount generated. The legend to this figure is shown in Fig. 70.

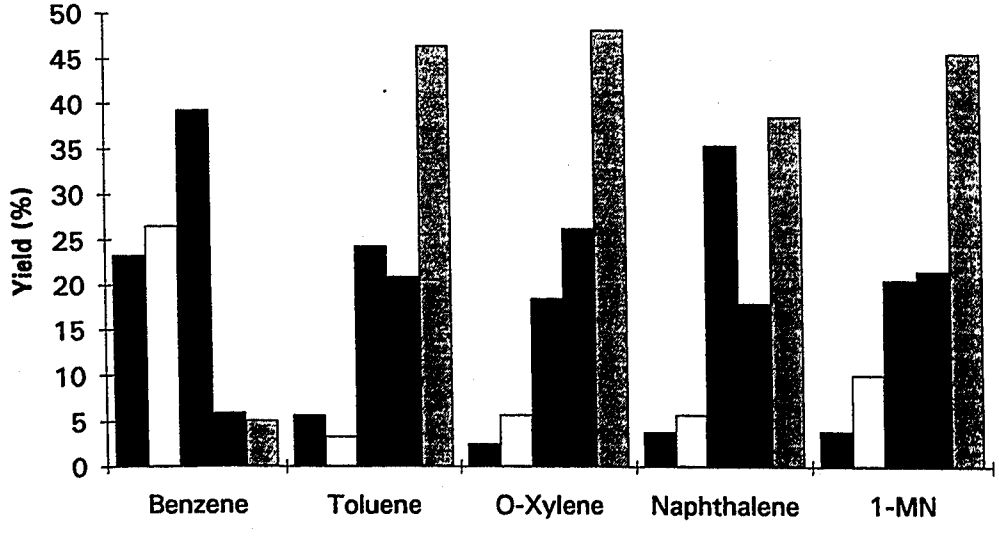

Figure 74: Aromatic compound yields per MSSV heating step of asphaltene sample E 33366/4 expressed as a percentage of the total amount generated. The legend to this figure is shown in Fig. 70.

Exactly the same trend was observed during the OSHP experiment and in the multistep PyGC experiment.

This series of artificial maturation experiments has shown that the early generation of hydrocarbons from the source rock formation analysed in this study is mainly due to the cracking of carbon-sulphur bonds in the kerogen. Due to this reaction sulphur-rich bitumen is generated. Asphaltenes, which are a major constituent of the bitumen, have already lost most of their C-S bonds during the generation process and are therefore almost unreactive at low temperatures.

2.1.9 Experimental simulation of hydrocarbon generation and expulsion using natural source rock samples

The geochemical analysis of source rock and oil samples in this study allowed the recognition of the main source lithologies and characterisation of their depositional environments, the determination of the hydrocarbon generation kinetics, organic matter maturity levels, and of the relative expulsion efficiencies of individual layers. Maturation experiments helped in recognising the characteristics of petroleum products generated at increasing levels of thermal stress and the respective gas/oil ratios allowing an estimation of the properties of the petroleum generated at each temperature stage.

As shown in the previous chapters, within the source rock formation analysed the carbonate-poor lithologies are the main zones of hydrocarbon generation and expulsion. Geochemical analysis of another carbonate source rock formation by di Primio (1990) and Leythaeuser et al. (in press) showed that hydrocarbon generation took place in both the pure micritic limestone layers as well as in the stylolites and solution seams. However, only these pressure solution features were capable of expelling petroleum efficiently. The migration mechanism was assumed to be oil phase migration driven by an increase in fluid pressure within the solution seams and stylolites due to kerogen conversion. There was evidence to suggest that, the overpressured stylolites and solution seams released their hydrocarbon charge in an explosive fashion into tectonically or overpressure-induced fractures.

The driving force of petroleum migration in the source rock formation studied in this thesis is, because of the low degree of kerogen conversion, probably not due to the occurrence of fluid overpressures. Sediment compaction and overburden pressure seems, therefore, to play an important role in the expulsion of petroleum in this case.

Microscopic analysis showed that the pure limestones were recrystallised and had no signs of porosity. Therefore, the carbonate matrix was assumed to be impermeable for hydrocarbons, acting as a seal during migration. Stylolites and solution seams, on the other hand, were expected to be ideal pathways for movement of petroleum in a lateral direction. The same must of course be said for the laminites (alternations of seals and migration pathways) and also for the shales (acting like large-scale solution seams). An interconnection of individual layers of source lithologies by fractures would lead to the formation of a three-dimensional oil-wet network. Microscopic analysis showed that oil-impregnated fractures occur quite commonly in the source rock formation analysed.

2.1.9.1 Permeability measurements

In order to test the above explained assumption concerning the low permeability of mudstone samples permeability experiments were performed using slabs of mudstone-wackestone cored from natural samples in different orientations (parallel and perpendicular to bedding). The experimental procedure has been described by Krooss et al. (1993). The rock cores were sealed laterally by a heat-shrunk teflon tube inside an aluminium tube. The sample was then introduced into a flow cell where a lateral confining pressure of 6 to 10 MPa was applied to the sealing sleeve in order to prevent a bypassing of fluids along the sides of the sample. The permeability measurements of the limestone samples were performed with water according the Darcy law for incompressible media:

$$v = -\frac{k}{\mu} * \frac{(P_2 - P_1)}{L}$$

where:

v = volume flux (m/s)

k = permeability (m^2; 1 Darcy = 10^{-12} m^2)

μ = viscosity of water at room temperature ($1.005*10^{-3}$ Pa s)

L = sample thickness (m)

P1 = entry pressure (Pa)

P2 = outlet pressure (Pa)

Pressure gradient= 4 MPa.

For a series of samples of pure mudstone-wackestone and one mudstone with clay flakes the permeability was analysed by this method. Only the mudstone with clay flakes showed a measurable permeability at room temperature and also at 84.5°C (Table 19). In both cases an average permeability of around 60 nDarcy was calculated. This mudstone sample has thus an average permeability which is comparable to those of compacted shales (Roperts, 1994). The assumption that pure mudstones and wackestones act as seals, and that they do not take part in the expulsion of petroleum seems, therefore, quite realistic.

A final experiment was performed with the mudstone sample that showed signs of permeability. The oil produced from Well 17 was used instead of water in this case and the temperature was held at 84.5°C. The goal of this experiment was to find out if such a viscous fluid could migrate through the low permeability sample, and if it did, to see if the migration pathways were microscopically visible. The pressure gradient applied was 4 MPa. The experiment lasted 60 hours at the end of which no oil had appeared at the other side of the

sample. The mudstone core was removed from the flow cell, cut in half and embedded in epoxy resin.

Fluorescence microscopy revealed that the clay flakes present in this sample were interconnected by a network of microfractures (Plate 3f). Microscopic analysis of a sample aliquot revealed that these fractures were present in the sample prior to the permeability experiments and that the fractures were not fluorescent. The oil, recognisable by its characteristic yellow fluorescence colour (Plate 3f), had impregnated these fractures and the clay flakes themselves during the experiment in nearly 50 percent of the sample volume. The lower half of the sample showed no signs of oil impregnation whatsoever (not shown in Plate 3f). The results of this experiment indicate that permeability in the mudstone and wackestone samples is controlled by the occurrence of fractures, and that even the highly viscous oil produced from Well 17 can migrated through this fracture network at the temperature and pressure applied given enough time.

The permeability experiments described above indicated that the assumption of impermeable mudstone and wackestone layers was correct. In order to verify the previously established results on migration mechanisms and efficiencies (postulated oil phase migration along stylolites and solution seams, laminites and shales), a series of experiments using a triaxial high pressure/high temperature flow cell (Hanebeck, 1995) were performed.

2.1.9.2 High pressure/high temperature experiments

The experimental simulation of primary petroleum migration processes is a relatively new field of study. Experimental petroleum generation, on the other hand, has been performed by a multitude of pyrolysis methods including hydrous pyrolysis (Lewan, 1985; Winters et al., 1983; Rowland et al., 1986; Barth et al., 1989; Baskin and Peters, 1992), open system dry pyrolysis (Larter, 1978; Horsfield et al., 1988), closed system dry pyrolysis (Monthioux et al., 1985; Horsfield et al., 1989; Horsfield and Düppenbecker, 1991) and flash pyrolysis (Eglinton et al., 1990). Winters et al. (1983) were the first to address the problems inherent to most experimental simulation techniques: the main variables in nature (time, low reaction rates, pressure, adsorption effects, catalytic effects, etc.) cannot be reasonably reproduced by hydrous pyrolysis, or in fact by any experimental simulation techniques applied up to date. Some of the results from such experiments are comparable to observations made in the natural system, but all techniques show varying inconsistencies. As a consequence the understanding of geochemical processes based on laboratory simulations is hampered by some doubt concerning the extrapolation of the results from experimental simulations to nature.

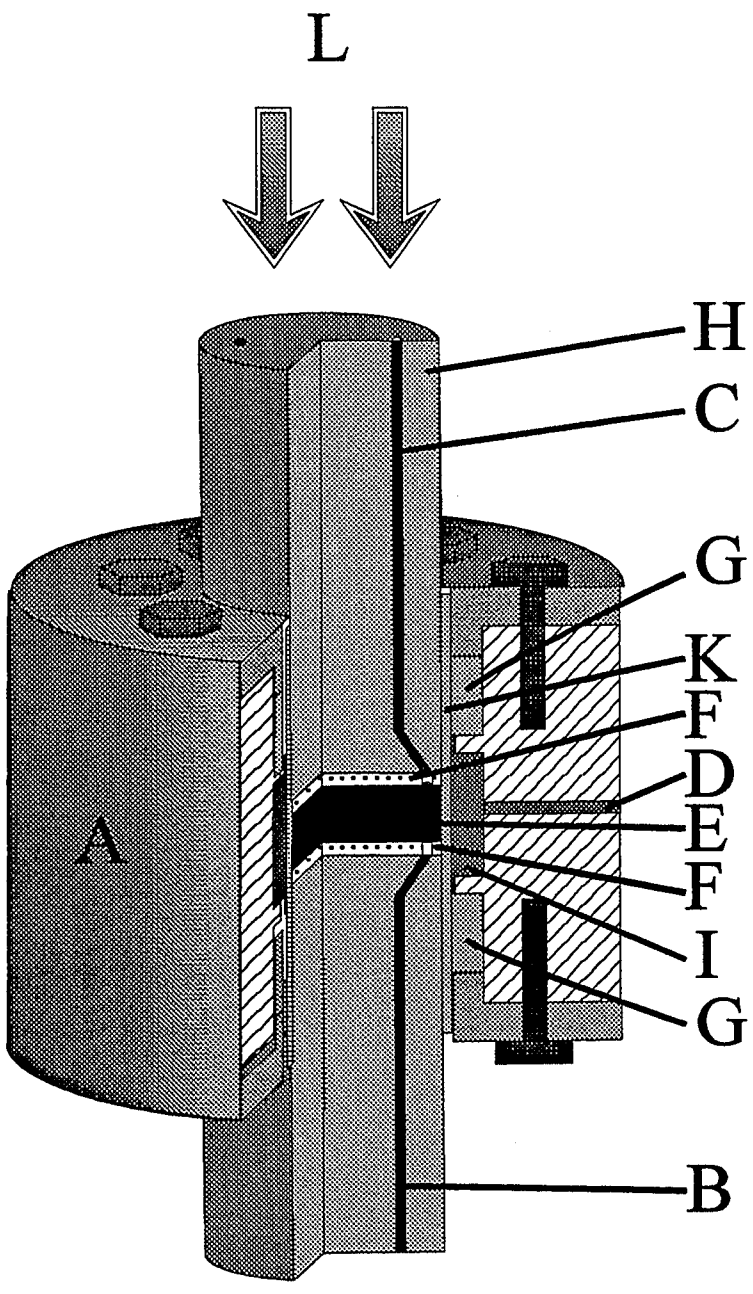

(A) stainless steel body
(B, C) 1/8" conduits
(D) connector for confining pressure
(E) cylindrical rock sample (28.5 mm diameter)
(F) porous stainless steel disks (reservoirs)
(G) graphite packing material
(H) stainless steel pistons
(I) confining pressure compartment
(K) double-layered sleeve
(L) axial load simulating lithostatic stress

Technical specification:

Sample diameter:	28.5 mm	(alternatively: 10 mm)
Sample length:	max. 30 mm	
Axial load:	max 98 kN (10 t)	
Confining pressure:	3 - 50 MPa (30 - 500 bar)	
Pore pressure:	0.1 - 40 MPa (1 - 400 bar)	
Temperature:	320 - 350 °C (depending on sealing material)	

Figure 75: High temperature - high pressure triaxial flow cell (after Hanebeck, 1995)

The most important experimentally irreproducible variable is certainly time. The influence of time has been compensated by temperature, under the assumption that reaction rates increase with temperature whereas the reactions themselves remain the same. The role of pressure, including lithostatic, confining and fluid pressure, has been largely ignored in previous experiments. Especially, for primary migration processes pressure seems to play an important role. The expulsion of generated hydrocarbons from a source rock is probably controlled by both fluid and overburden pressure (Ropertz, 1994 and references therein). Some control of pressure during experimental simulation has recently been achieved by Takeda et al. (1990) and Lafargue et al. (1989). In both cases source rock samples were pyrolysed in a closed system under controlled pressure conditions. While Lafargue et al. (1989, 1994) used dry samples and controlled only the confining pressure during the experiment, Takeda et al. (1990) were able to control both fluid and overburden pressure during their experiments.

The most recent progress in designing migration experiments has been achieved by Hanebeck (1995). In his high temperature - high pressure triaxial flow cell (HPHT-cell) core samples of a source rock can be pyrolysed under controlled lithostatic, confining and fluid pressures. Vertical changes in sample thickness during the experiments can be monitored with an accuracy of 1/100 mm. A detailed description of the apparatus is given by Hanebeck (1995) and a summary is provided by Fig. 75.

The HPHT-cell is at present the most adequate technique for simulating hydrocarbon generation and expulsion, since it allows the best simulation of natural temperature and pressure conditions. This experimental approach was, therefore, used for simulating petroleum generation and expulsion from the carbonate source rocks analysed in this study.

Sample selection

The best type of sample for the experimental simulation of hydrocarbon generation and migration would of course have been a kerogen-rich shale because this sample type showed the highest organic matter contents and quality, but shale lithologies were found to be completely inadequate because they fell apart during plug drilling. Thick solution seams were the next best possibility. Solution seams surrounded by carbonate matrix proved to be highly stable and thus perfect for drilling small scale plugs.

Two plugs were drilled from sample E 33422 with a solution seam oriented parallel to the vertical axis of the plugs. One long plug of a series of solution seams grading into a shale layer was drilled from sample E 33434. This plug was cut in half, thus providing one plug with solution seams oriented perpendicular to the vertical axis of the plug but interconnected by a swarm of vertical fractures, and one plug which consisted of an almost pure shale adjacent to a

coarse grained grainstone layer. One plug with a thick stylolite oriented parallel to the vertical axis was drilled from sample E 33365.

Experimental procedure

In order to analyse the effect of overburden pressure on the expulsion efficiency of hydrocarbons a series of experiments under constant temperature and different pressure conditions had to be performed. Reservoirs consisting of porous steel plates were placed either in direct contact to the source layer or in contact to a fracture which lead to the source layer of each plug. After the experiment the steel plates were removed from the plug sample and ultrasonically extracted using dichloromethane as a solvent. Hydrocarbons which visibly coated the upper and lower surfaces of the plugs in contact with the reservoirs were washed off with dichloromethane and added to the reservoir extract. The plugs were then cut in half. One half was soxhlet extracted (24 hours, dichloromethane as solvent), the other was embedded in epoxy resin and studied microscopically. Thin sections were made out of the extracted halves of the cores.

The individual samples were analysed under the following conditions:

Experiment # 1 Sample E 33365 (Stylolite-bearing mudstone, Well 4, 2540 m)

Temperature:	320°C		
Confining pressure:	300 bar	Fluid pressure:	150 bar
Lithostatic pressure:	300 bar	Time:	72 hours

Experiment # 2 Sample E 33422/3 (Solution seam-bearing mudstone, Well 8, 3194 m)

Temperature:	320°C		
Confining pressure:	150 bar	Fluid pressure:	100 bar
Lithostatic pressure:	150 bar	Time:	72 hours

Experiment # 3 Sample E 33422/4 (Solution seam-bearing mudstone, Well 8, 3194 m)

Temperature:	320°C		
Confining pressure:	500 bar	Fluid pressure:	350 bar
Lithostatic pressure:	500 bar	Time:	72 hours

Experiment # 4 Sample E 33434/1 (Solution seam-bearing wackestone, Well 24, 4440 m)

Temperature:	320°C		
Confining pressure:	300 bar	Fluid pressure:	250 bar
Lithostatic pressure:	300 bar	Time:	72 hours

Experiment # 5 Sample E 33434/2 (Grainstone-shale sample, Well 24, 4440 m)

Temperature:	320°C		
Confining pressure:	300 bar	Fluid pressure:	250 bar
Lithostatic pressure:	300 bar	Time:	72 hours

Fluid pressures were hydrostatic. The lithostatic pressures applied of 150, 300 and 500 bars correspond roughly to burial depths of 1, 2 and 3 km respectively.

Time and temperature were maintained constant for all experiments in order to reduce the amount of variables and to ensure that all effects noticed were only due to differences in pressure. The fluid pressure was maintained below confining or lithostatic pressure in all experiments in order to ensure a tight sealing of the core samples. The extract yields obtained from the pyrolysed plug and from the reservoir plates were quantified and the amount expelled (into the reservoir) expressed as a percentage of the total amount generated. Thus the expulsion efficiencies shown in Table 20 are absolute values.

Results

Experiment #1 was performed as a test of apparatus and approach. The hydrocarbons generated and expelled were, therefore, only analysed by whole oil gas chromatography. The GC traces are depicted in Fig. 76 and show a very close resemblance in the n-alkane distribution between the oil which remained in the core and the oil which was expelled into the stainless steel plate reservoir. The extract yields and expulsion efficiencies are shown in Table 20. The expulsion efficiency for experiment # 1 reached a value of over 30 %.

Experiment # 2 was conducted using the lowest pressures of all experiments. After 72 hours the HPHT-cell was allowed to cool and the sample removed. The reservoir plates showed no visible hydrocarbon staining or impregnation, although both the source rock plug and the plates had a strong oil smell. Extraction of both core and plates, as described above, showed that a small amount of hydrocarbons had actually been expelled. The expulsion efficiency reached only 1.6 % (Table 20). Gas chromatography of the saturated fractions allowed the determination of absolute expulsion efficiencies of the individual n-alkanes and selected isoprenoids. Figure 77 shows the result of this calculation. The expulsion efficiency of n-

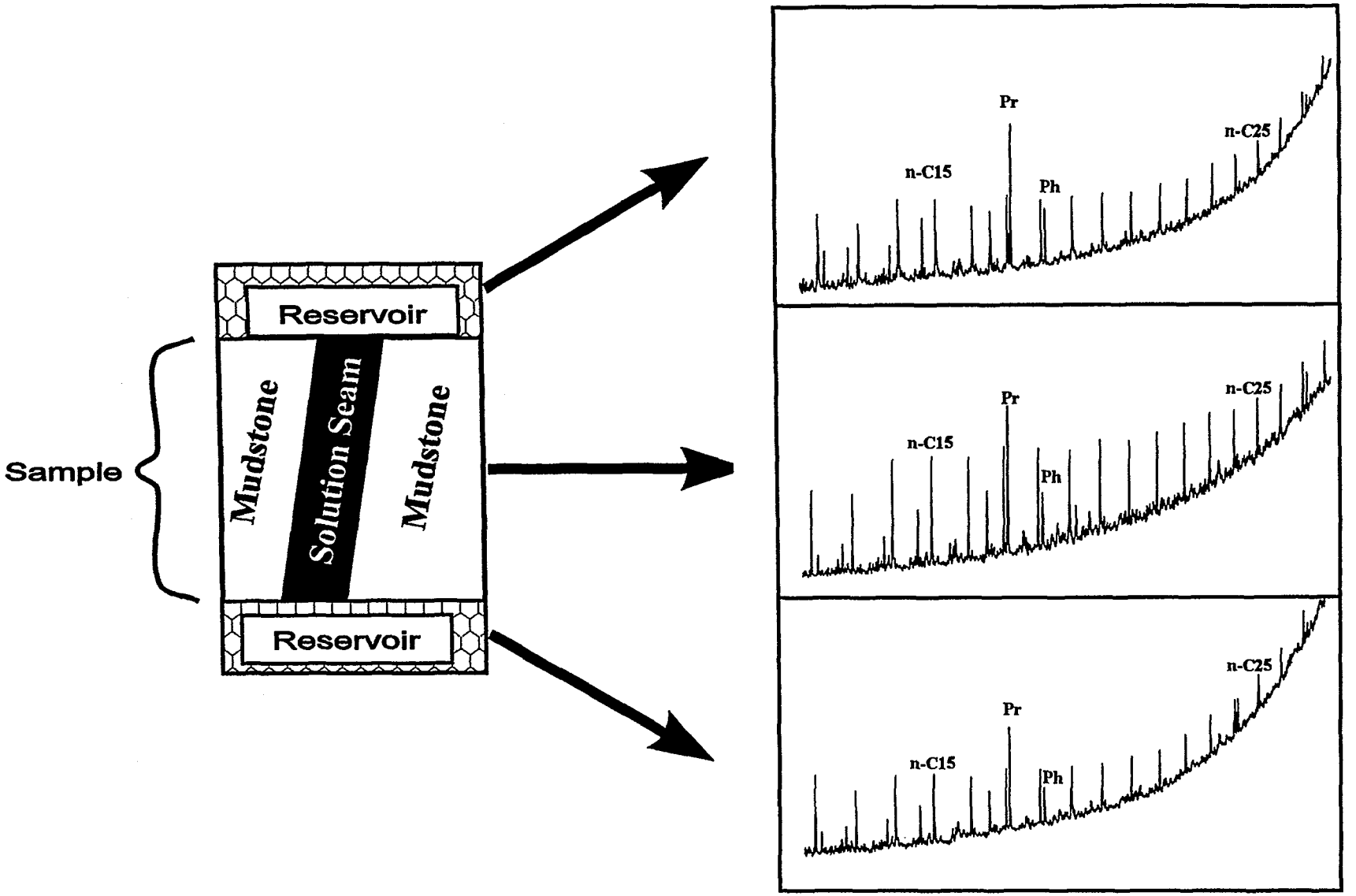

Figure 76: **Scheme of sample and reservoir orientation in experiment #1 and GC-traces of the extracted pyrolysates.**

alkanes and selected isoprenoids remains rather uniform for all compounds analysed independent of the chain length. The average expulsion efficiency of less than 10 % for the n-alkanes is quite low, although the expulsion efficiency calculated for the extract is even lower. The reason for this discrepancy could possibly be found in the compound class distribution of the extracts separated by MPLC (Fig. 78). The soxhlet extract of the core sample has an asphaltene content of over 40% while virtually no asphaltenes are present in the reservoir extracts. Thus the lower expulsion efficiency calculated for the total extracts could be due to the higher molecular weight of the asphaltene fraction which was retained exclusively in the source rock plug during the experiment.

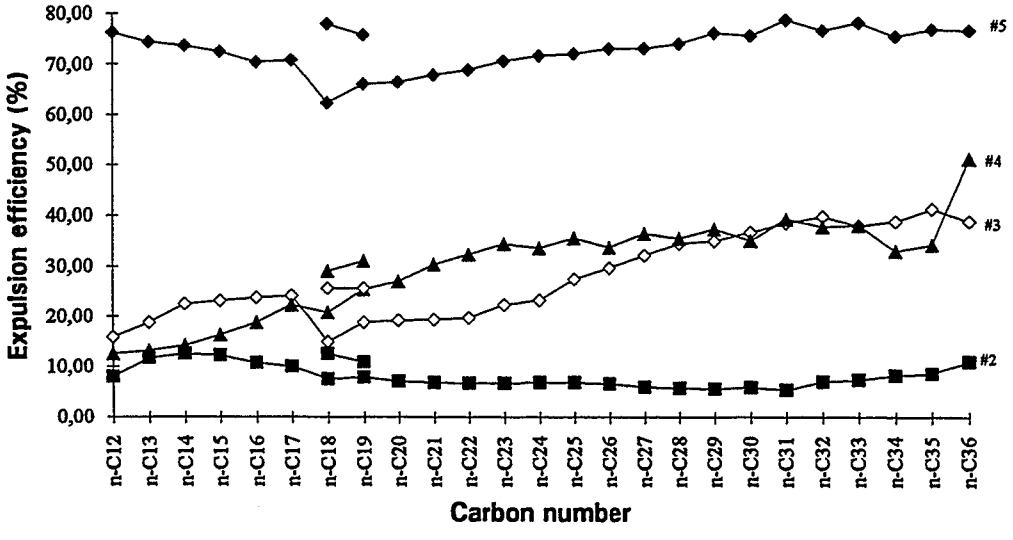

Figure 77: Calculated expulsion efficiencies of n-alkanes and selected isoprenoids in experiments #2, 3, 4 and 5.

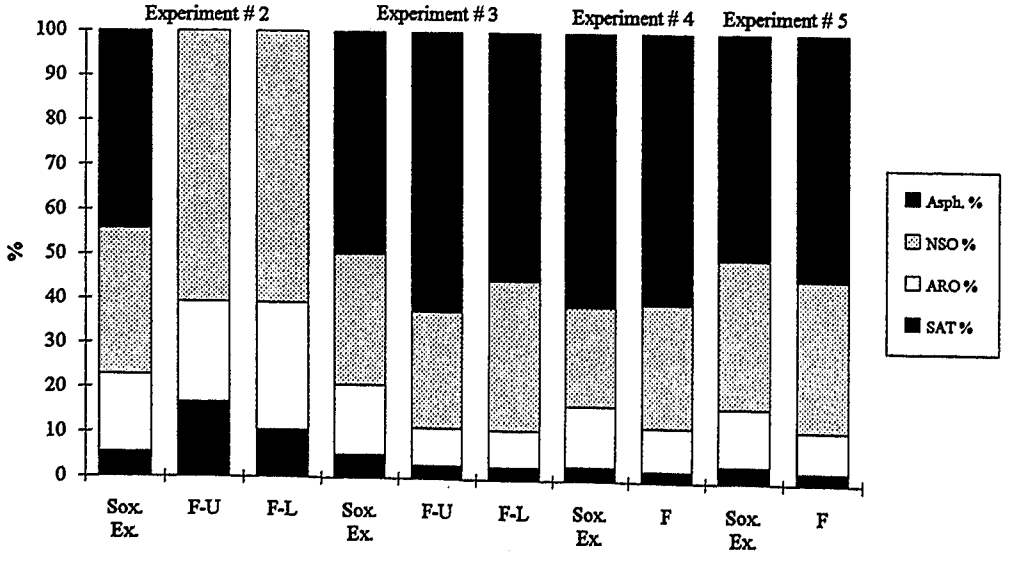

Figure 78: Compound class distribution of the pyrolysates of experiments #2, 3, 4 and 5.

Experiment # 3 was conducted using a plug from the same sample as experiment # 2. The homogeneity of the solution seam in sample E 33422 allowed the coring of nearly identical subsamples, thus making a direct comparison of the results of these experiments under different pressures possible, without having to worry about variations of organic content or organic matter type. The results of this 500 bar experiment are shown in figs. 77, 78 and table 20. The total extract expulsion efficiency reached almost 28 %, the expulsion efficiency of the individual n-alkanes and isoprenoids reached a maximum of around 35 %. An interesting feature of the n-alkane expulsion efficiency is the decrease in expulsion efficiency with decreasing chain length. This observation was also made in other experiments and will be discussed in detail below. The compound class distribution of the individual samples is shown in fig. 78. In contrast to the low pressure experiment (# 2) all samples of experiment # 3 show more or less similar compound class distributions. The quantity of pyrolysate generated during this experiment was 66 % lower than the amount generated during the low pressure experiment (Table 20). Since organic matter content and type can be considered identical in both samples, and since the temperature and duration of the experiments were identical, the observed difference in the amount of pyrolysate generated must be due to the pressure difference between these experiments. These results compare favorably to the results of the experiments by Price and Wenger (1992) who analysed the influence of fluid pressure on the generation of hydrocarbons by hydrous pyrolysis. They concluded that increasing pressure significantly retards all aspects of organic matter metamorphism, including hydrocarbon generation, maturation and thermal destruction.

Microscopic analysis of the source rock samples of the experiments # 2 and # 3 after pyrolysis revealed that almost no fluorescent organic matter remained in the cores. The original untreated sample showed that the few liptodetrinite particles which were visible under fluorescence were concentrated in the intergranular space. The main organic component was bituminous groundmass. In the sample submitted to pyrolysis at 150 bar no liptodetrinite particles could be found. Bitumen was seen to fill open vugs, fractures and in some cases was recognised in the intergranular porosity (Plate 4a). The sample submitted to 500 bar during pyrolysis showed a similar picture. In one portion of the solution seam a former organic rich layer was found, which had retained fluorescence at the boundary to the reservoir plate while in the centre of the rock no fluorescence at all remained (Plate 4b, 4c). The boundary zone showed several fractures oriented mainly parallel to bedding (Plate 4b). The lack of figurated liptinites after pyrolysis as well as the impregnation of vugs with bitumen indicate that kerogen conversion seems to have been very effective in both experiments.

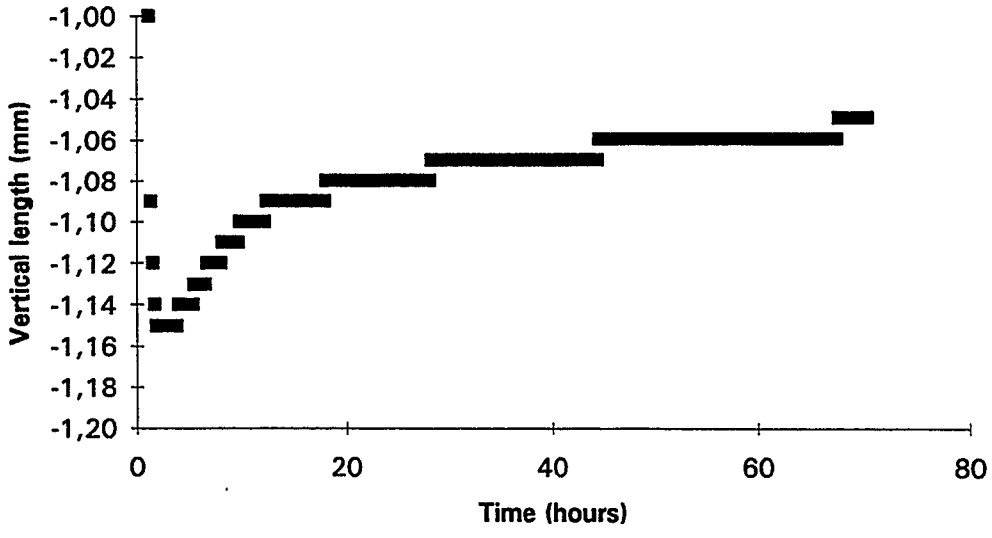

Figure 79: Variation in the vertical thickness of the sample in experiment #4 with time.

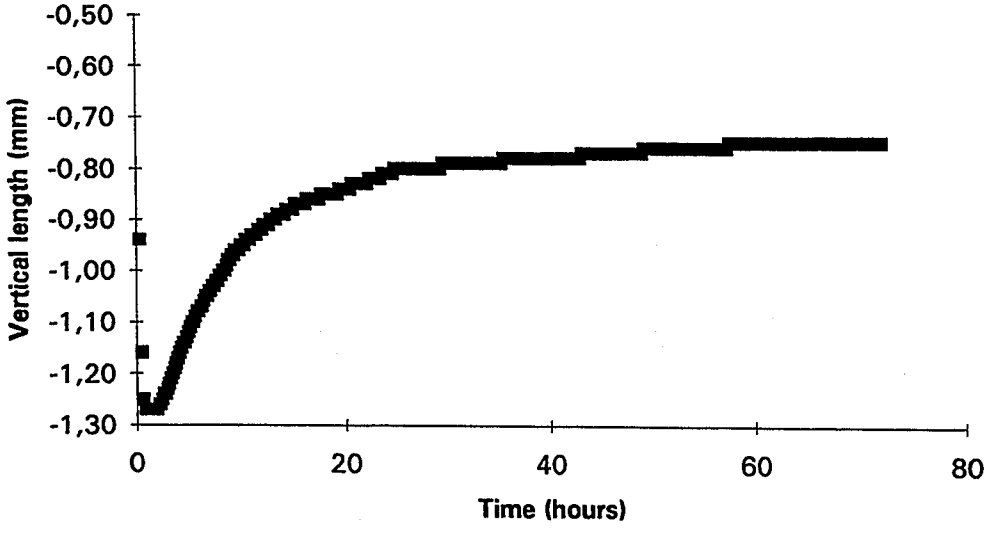

Figure 80: Variation in the vertical thickness of the sample in experiment #5 with time.

Experiment # 4 was performed at a pressure of 300 bar (lithostatic and confining) with a sample which contained numerous parallel solution seams and stylolites which were interconnected by a series of vertical fractures. The upper part of the core consisted of a limestone layer of 5 mm thickness which, according to the permeability measurements, was assumed to be impermeable. In this experiment the porous steel plate was set in direct contact to the fractures (which cut through the carbonate layer) while the other side of the sample was sealed by an impermeable copper plate. Thus all products generated during heating could only escape from the source rock along the fracture into the reservoir. The amount of extract generated and expelled during this experiment is shown in Table 20. The expulsion efficiency of the total extract reached almost 14 %, that is expulsion along this fracture system was proved to be feasible. The compound class distribution of the expelled pyrolysate was almost identical to that of the residual pyrolysate in the source rock sample (Fig. 78). The expulsion efficiency of individual n-alkanes and isoprenoids parallels that of experiment # 3, and thus shows the same decreasing expulsion efficiency with decreasing chain length as observed in experiment # 3 which is discussed below (Fig. 77). Microscopical analysis of the sample after pyrolysis showed that all fractures in the source rock were completely impregnated with oil (Plate 4d), clearly indicating the migration pathway. The lack of liptinite particles in the sample after pyrolysis showed that, as in the former experiments, kerogen conversion had taken place.
Experiment # 4 was the first in which a vertical volume changes were monitored. Directly after the sample and apparatus had terminated the usual thermal expansion during heating up to 320°C the length of the sample started to shrink losing almost 1/10 mm in length in total (Fig. 79). The compaction observed during this experiment is discussed below.
Experiment # 5 was performed under the same experimental conditions as experiment # 4. The sample used showed a clean separation of solution seam and carbonate grainstone. Microscopic analysis of the sample before and after the experiment showed that while fluorescing liptinites were the dominant macerals before heating (Plate 4e), no such macerals were visible after the experiment (Plate 4f). Kerogen conversion can therefore assumed to have been very effective. Expulsion efficiency of the total extract and of the n-alkanes and selected isoprenoids reached almost 70 % (Fig. 77, Table 20). The compound class distribution of the extracts were almost identical (Fig. 78). This sample showed also the highest rate of compaction during the experiment (Fig. 80). The vertical volume reduction monitored during this experiment reached 0.5 mm. The original sample had a thickness of 13.5 mm of which the solution seam comprised 7 mm. If we assume that the compaction was restrained to the clay-rich zone then the solution seam was compacted by over 7 %.

The expulsion of hydrocarbons from this sample took place through the carbonate grainstone. Microscopic analysis revealed that the only fracture in this sample showed no signs of oil staining. The carbonate grainstone, on the other hand, showed a very coarse grained appearance and had a strong yellow fluorescence after the experiment. This feature can assumed to be due to a hydrocarbon impregnation of the limestone, thus indicating the migration pathway.

3 Discussion

3.1 Depositional environment

3.1.1 Characterisation of the depositional environment

The integration of sedimentological, bulk and molecular organic geochemical data allows the reconstruction of the palaeodepositional environment of the source rock formation analysed in this study. The result is a model which describes and explains the observed variations in organic matter quality and quantity.

The sedimentologic and petrographic analysis of the source rock formation lead to the recognition of four main lithofacies, termed carbonate mudstone/wackestone (which in some cases included pressure solution generated layers such as stylolites and solution seams which were sampled separately), laminites, shales and dolomitic breccias (interlayered reservoirs). The depositional environments of these lithofacies ranged from shallow marine subtidal carbonate (micritic limestones) to supratidal carbonate environments (dolomitic breccias). Signs of enhanced salinity during deposition of these sediments were found during sedimentological analyses by AGIP. Pseudomorphosed evaporite crystals, gypsum and anhydrite present in laminites are indicative of hypersaline conditions.

A general sequence of the lithofacies recognised in the macroscopic analysis of the cores of the source rock can be described as follows:

Organic lean mudstones/wackestones, which sometimes contained sparse fossils or clay flakes and were generally characterised by the occurrence of stylolites and solution seams as well as carbonate laminites, ranged into argillaceous laminites which showed a marked increase in organic content. These laminites were then seen to lead into shale sequences, which were the source rock portions with the highest organic content. Dolomites and dolomitic breccias occured either between mudstone/wackestone series or following the shale intervals.

This sequence of sediments fits very well to the offlap sequence based on recent Persian Gulf examples described by Shinn (1983) and shown in Figures 81 and 82. The mudstone/wackestones were, according to this interpretation, deposited in the oxygenated subtidal zone. Mudstones with clay flakes can be assumed to indicate shallow turbiditic deposits, whereas the carbonate laminites indicate a deeper water, anoxic environment as demonstrated by the undisturbed lamination. In closer proximity to the shoreline and entering the intertidal zone of Shinn (1983) pure mudstone dominate (burrowed intertidal, Fig. 82), which grade into laminated sediments. The upper intertidal zone is characterised by the occurrence of extense algal laminations with high organic contents. Dolomites are

characteristic of the supratidal zone, but may also indicate subaerially exposed barriers which formerly separated a lagoon from the open sea (Fig. 82). A complete sequence as shown in Fig. 81, is unlikely in the geological record, due to the possibility of subaerial erosion or transgression. Shales were, for example, often seen to grade back into laminites and mudstones indicating the occurrence of a rapid transgression which drowned the cyanobacterial mat environment. During periods of stable conditions the microbial mats would then recolonize the intertidal zone. These transgressions are probably one of the key factors in explaining the excellent preservation of the organic matter. Rapid burial under a fine grained mud would largely facilitate organic matter preservation by providing an anoxic pore water environment, due to rapid the deplenishment of oxygen in the system.

The kerogen types encountered in the source rock formation ranged from type II, type II-S to type I-S without a clear correspondence of a certain kerogen type to a distinct lithofacies. The general trend was that the carbonate dominated samples possessed kerogen of type II-S while the kerogen of the shales ranged into type I-S.
Sulphur-rich kerogens can only form where special conditions in the depositional environment of the sediment occur, i.e., where sulfate is abundant, for example in sea water; where anoxic conditions prevail at the sediment/water interface; where the amount of reactive iron is insufficient to remove all the microbially generated hydrogen sulfide (Orr, 1986). These conditions result in a surplus of free H_2S, which reacts with the organic matter, leading to the formation of kerogens rich in organic sulphur compounds.

The organic matter of the individual lithologies, as observed under the microscope, consisted of mainly amorphous groundmass, alginites, liptodetrinites and a very minor contribution of vitrinites and inertinites. Amorphous organic matter was the main organic constituent of the shale samples, followed by alginites and liptodetrinite. The laminites were also dominated by amorphous organic matter although the proportion of alginitic OM was higher than in the shales. The carbonate dominated sediments were almost barren of organic matter.
The occurrence of amorphous organic matter in a microbial mat environment is a common feature. Largeau et al. (1990) noticed that fossil cyanobacterial organic matter is generally amorphous even at TEM scale.

The characterisation of the depositional environment and organic input of the shale lithofacies was the most intriguing problem. Organic matter-rich shales are usually deposited in anoxic, low energy environments (Littke, 1993). The sedimentologists from AGIP had, therefore, also

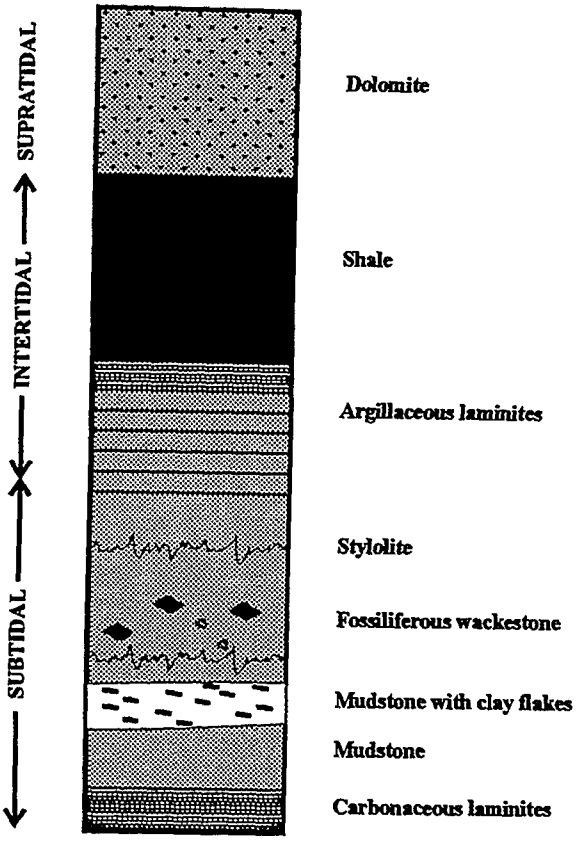

Figure 81: Idealized sedimentary sequence showing the different lithofacies of the source rock formation as related to the depositional environment.

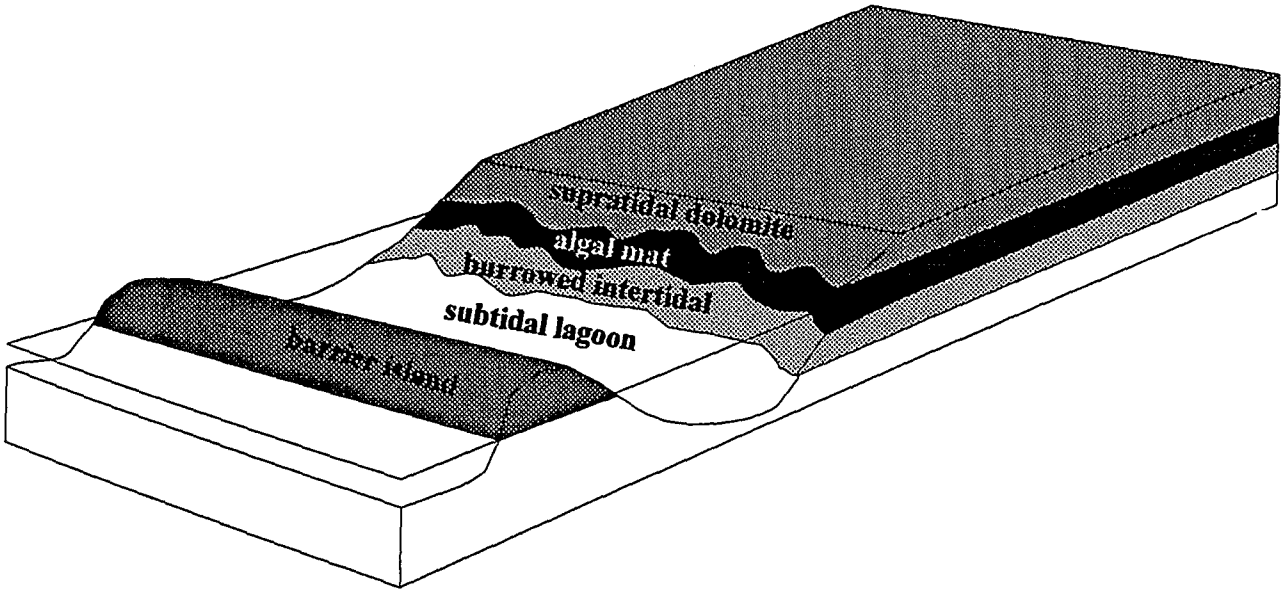

Figure 82: Block diagram schematically showing the depositional environment of the source rock formation. The barrier island and the supratidal zone are characterised by dolomites and dolomitic brecias, the algal mat zone by shales and argillaceous laminites, in the burrowed intertidal and subtidal zones mainly mudstones and wackestones are deposited, whereas carbonate laminites are restricted to the deeper subtidal zone (after Shinn, 1983).

assumed that the shales present in the source rock analysed in this study were the product of such an environment (AGIP internal report). This assumption was underlined by the concentration and excellent preservation of the organic matter (occurrence of chlorophyllinite) and the observed microlamination.

Detailed organic petrologic analyses of the organic material, on the other hand, revealed that microbial mat structures were very common in this lithofacies. Microbial mats are also commonly referred to as "cyanobacterial mats" or "algal mats" (Burne and Moore, 1987).

Microbial mats are generally formed by a sequence of different bacterial colonies (cyanobacteria, filamentous bacteria, sulphur purple bacteria). These organisms form a massive organic fabric, which is periodically covered by detrital sediments due to storms or exposure to the atmosphere (Kenig et al, 1989; Shinn, 1983). The detritus is subsequently recolonised by bacteria. This repetitive process leads to a stack of organic matter rich layers interlaminated with thin detrital sediment layers. The preservation of microbial mats in this environment is, of course, also due to the absence of grazing and recycling organisms.

The scarcity of carbonate minerals in the shale samples analysed in this study could be assumed to be contraindicative of a carbonate depositional environment. Shinn (1983) described recent microbial mats in the Persian Gulf, in which the main mineralogical components are eolian sediments from continental regions. He observed in numerous occasions that microbial mats act as sticky flypaper to trap windblown dust. He concluded that supratidal microbial laminations along the coasts of arid areas can result both from alternating flooding and deposition of marine sediment and microbial mat growth or alternating eolian deposition and microbial mat growth.

From a morphological point of view the photomicrographs of microbial mats of the Messel oil shale published by Hagedorn-Götz (1983) show a remarkable resemblance to the photomicrographs of microbial mats from this study (Plate 2a). The filamentous structures in plate 2e and 2f are also very similar to recent cyanobacterial sheaths described by Grimalt et al. (1992).

The results of organic geochemical screening analyses and elemental analysis of recent microbial mats of Abu Dhabi by Kenig et al. (1989) and Kenig and Huc (1990) showed a high degree of similarity to the data measured in the shales of this study. The TOC, H/C and O/C data, and sulphur contents all correlate very well with data derived from shales in this study. For example Kenig and Huc (1990) analysed isolated kerogens of modern microbial mats sampled in a sabkha channel in Abu Dhabi. They measured H/C and O/C ratios of around 1.3 and 0.28 respectively. The organic sulphur content of the microbial mats measured by Kenig et

al. (1989) ranged from 1.72 to 5.96 % and was attributed to bacterial sulphate reduction probably active in microbial mats immediately below the living mat. In comparison the H/C and O/C ratios measured for the kerogens from the shale samples of this study ranged from 1.41 to 1.84 and 0.12 to 0.29 respectively. Organic sulphur contents ranged from 2.04 to over 12 %. These observations corroborate the assumption that the shale layers are mainly composed of the remains of microbial mats. The second largest contributor to the organic matter in the shales are liptodetrinites. In some cases the liptodetrinites were seen to merge into a bituminous groundmass of the same fluorescence colour.

Analysis of the soluble organic matter on a molecular level allowed a better determination of palaeoenvironment and organic facies. Many carbonate source rocks are characterised by an even carbon number predominance of the n-alkanes (Palacas, 1983, 1989; Tissot, 1981; Tissot and Welte, 1984). Odd over even preference is indicative of higher land plant input since several authors noticed this feature in recent and ancient detrital sediments with important contribution of continental runoff (Bray and Evans, 1961; Meinschein, 1961; Kvenvolden, 1962). The odd numbered hydrocarbons are normally derived from cuticular waxes of continental higher plants (Tissot and Welte, 1984). Even carbon number predominance of the n-alkane is supposed to result from the reduction of even fatty acids or alcohols in strongly reducing environments, typical of carbonate-evaporitic series (Tissot, 1981).
The observed odd over even n-alkane predominance in the C_{23+}-range, which generally peaks in n-C_{29} or n-C_{31} would therefore usually be attributed to land plant waxes. For the marine carbonate sequence analysed in this study the occurrence of land plant waxes in the soluble organic matter would indicate terrigenous influence in the depositional environment. The almost total lack of macerals derived from land plants observed in the samples analysed by microscopy indicate, on the contrary, a very low contribution of land-derived organic matter.
There are two alternative explanations for an odd over even long-chain n-alkane predominance. The first is based on observations made by Gelpi et al. (1968), and Metzger et al. (1985, 1986). They noticed a predominance of the odd-numbered n-alkadienes and trienes dominated by the C_{27} and C_{29} members in the hydrocarbon fraction of the algae *Botryococcus braunii*. These compounds lead upon early diagenesis to an odd over even carbon number preference of the n-alkanes in the chain length range of C_{27} to C_{31}. However, the fresh water algae *Botryococcus* is probably not responsible for the n-alkane fingerprint due to the marine to hypersaline depositional environment inferred for the source rock studied. The second source for the odd over even long chain n-alkane predominance could be derived from the cell walls of microbial mats. Kenig et al. (1989) analysed both recent and burried microbial mats

from a sabkha setting in Abu Dhabi. The saturated hydrocarbon fraction of these microbial mats all show an odd over even n-alkane predominance peaking in n-C_{29} or n-C_{31}, exactly as observed in this study. Concerning the organic input in the modern sabkha environment Kenig et al. (1989) state that "transport of organic matter does not seem to be important in this modern sedimentary system" and that "the geochemical signature of each of the organic facies is specific". They concluded that the organic matter produced by the microbial mat is incorporated directly *in situ* into the sediment. The geochemical signature observed for the modern microbial mat (i.e. the n-alkane distribution) should therefore be due to the chemical composition of the mat itself and not due to input of terrestrial organic matter.

Several other studies have been performed on the geochemistry of microbial mats. Chalansonet et al. (1988), for example, analysed recent cyanobacteria regarding their resistance to chemical treatment. They noticed that several cyanobacterial species posses resistant biopolymers, which are located in the cell envelopes. These biopolymers showed a large degree of similarity to resistant biopolymers isolated from *Botryococcus braunii*, the major difference being that the saturated hydrocarbon chains in cyanobacterial biopolymers are shorter than in *B. braunii* biopolymers.

Boon et al. (1983) analysed recent to subrecent cyanobacterial mats in detail. The most prominent hydrocarbons of the mats were in the range n-C_{15} to n-C_{21}, with a maximum at either n-C_{15} or n-C_{17}. Squalane was also identified and assumed to be the precursor for steroids and triterpenoids in these organisms. Cell walls were seen to be the most resistant structures of cyanobacteria, which remain behind after bacterial degradation of the cell contents, and are thus relatively enriched in the sediment. Analysis of burried cyanobacterial mats showed that sheath material (i.e. cell walls) was the dominant organic material. Py-MS and Py-GC analyses by Boon et al. (1983) demonstrated that furans, phenols and toluene are the dominant compounds of these structures. They also found phytadienes in the Py-GC trace which indicates the survival of chlorophyll or pheophytins.

Cardoso et al. (1978) analysed the lipid classes extracted from recent cyanobacterial mats from Abu Dhabi. They recognised a minor contribution of n-alkanes ranging from n-C_{17} to n-C_{31} with an odd over even predominance.

Of the authors listed above only Kenig et al. (1989) and Cardoso et al. (1978) showed an n-alkane signature with an odd over even predominance in the n-C_{27} to n-C_{31} range. Although not directly referred to in the text, Kenig et al (1989) offered an explanation of this preference by the statement that „all organic matter is directly incorporated into the sediment and represents the biological signature of the main organic precursor". On the other hand, Boon et al. (1983) described halophytes which lived directly adjacent to the saline lake where the

cyanobacterial mats were sampled. Leaf waxes from such plants could be responsible for the n-alkane signature recognised in this study.

The predominance of phytane over pristane in virtually all samples analysed is generally assumed to indicate marine-derived source material deposited under reducing conditions (Tissot and Welte, 1984; Killops and Killops, 1993). Pristane/phytane values of less than 0,6 are taken to be an indicator of anoxic, high-salinity depositional conditions (Peters and Moldowan, 1993). Pristane/phytane values below 0.6 were observed in the saturated compounds of the shale samples. Pristane/phytane values of below 0.1, which ten Haven et al. (1988) state are indicative of hypersaline depositional conditions, were not encountered.

Analysis of the early diagenesis of phytyl esters in a recent sediment by Johns et al. (1980) showed that the dominance of phytane in anoxic sediments may be due to the fact that chlorophylls have reached the sediment without being degraded. When hydrolysis then liberates phytol from the chlorophyll molecule in the anoxic zone only reduction to phytane is likely. Chlorophyll-residues were shown to be present in the samples analysed in this study (presence of chlorophyllinites, Plate 2a-d) so that the mechanism proposed by Johns et al. (1980) may have played an important role in the predominance of phytane over pristane.

Kaplan and Baedecker (1970) and Nissenbaum et al. (1972) suggested in their studies of the Dead Sea that phytane might be derived from phosphatidyl glycerophosphate, a phospholipid with ether linked in alkyl side chains which is found in halophilic bacteria. The natural breakdown of the isoprenoid glycerol ether lipid during diagenesis would increase the phytane concentration thus explaining the low pristane/phytane ratio of ancient sediments from saline environments (ten Haven et al., 1985).

Bacterial degradation plays a major role in homogenising the organic matter during burial of microbial mats. The bituminous groundmass, which was the dominant organic matter type observed under the microscope, is assumed to be the product of bacterial reworking (Rullkötter et al., 1988, 1990; Sinninghe Damsté et al., 1993). Bacterial reworking of the microbial organic matter was observed by Kenig et al. (1989) directly underneath living microbial mats, and by Boon et al. (1983) in burried cyanobacterial mats. High levels of hopanes in organic extracts are believed to result from pronounced bacterial reworking of organic matter (Killops and Killops; 1993). The abundance of triterpanes in almost all samples can therefore be taken as an indication of the amount of bacterial reworking which took place in the sediment.

The relatively large amount of C_{29} steranes could normally be explained by a contribution of land plant organic matter. Matsumoto et al. (1982) and Fowler and Douglas (1987) recognised

however, that C_{29} steranes could also be derived from cyanobacteria. The assumption that microbial mats are one of the main contributors to the organic matter of the source rock formation receives thus further backing.

Calculation of aromatic maturity ratios indirectly helped in recognising paleo-environmental effects. MPI-1 and MPI-2 ratios for the shale samples analysed showed seemingly decreasing maturity with depth. This observation can be attributed to an import of allochthonous overmature organic matter from terrestrial sources. Radke et al. (1991) demonstrated that the influence of reworked organic matter rich in fusinites on maturity estimations in source rocks of the Upper Rhine Graben lead to much too high maturities. The predominance of parent compounds (e.g. phenanthrene) over the alkyl homologues (e.g. methylphenanthrenes) in immature samples is typical of pyrolysis- and combustion-derived polycyclic aromatic hydrocarbons (PAH) and suggests natural fires as a possible source (Radke et al. 1991). Thus, the decreasing maturity with depth noticed for type I kerogens present in the shales could be taken as an indication of the proximity of these wells to a land mass. If it is true, that well 17 was closest to shore and well 24 farthest away, the influence of combustion derived PAH (which lead to too high maturities) would decrease from well 17 to well 24, thus respective maturities monitored by MPI would also decrease.
The observations of Shinn (1983) concerning the dominantly eolian input of minerals to microbial mat environments could help to clarify the observed anomalous maturity trend as monitored by the MPI-ratios. Combustion derived PAH in fusinites were possibly introduced into the microbial mat sediments during subaerial exposure. The degree of exposure would then also define the amount of fusinite input. Thus the regions closer to the shore, which were exposed more frequently, would show the highest contribution of eolian transported fusinites. The inverse MPI-maturity trend with depth, observed in the analysed shale samples, may therefore be more strongly influenced by the depositional environment than by maturity. The occurrence of fusinites and semifusinites in the shale samples (Plate 2g-h) together with observations by Shinn (1983) on the properties of exposed microbial mats thus helped in explaining the maturity anomaly and corroborating the assumption of a microbial mat environment.

The shales therefore seem to be the product of alternations of microbial mat growth and sedimentation with minor algal input. The characteristics of the kerogens of these shales (high H/C, O/C and S/C ratios) were also noticed in kerogen concentrates of other lithofacies

(laminites, stylolites and solution seams) indicating that microbial mats and their degradation products are the main organic constituent of the sediments analysed.

While kerogens of type II-S and the normal type II are supposed to be deposited in marine to hypersaline environments kerogens of type I are normally assumed to be typical for lacustrine source rocks (Talbot, 1988), classical examples being the Green River Formation in USA, the Messel shale in Germany, Autun Boghead in France as well as Tasmanites, Coorongites and Torbanites from various geographical locations (Tissot and Welte, 1984, page 151-153). Most oils generated from lacustrine source rocks are extremely paraffinic and waxy (Powell, 1986). This feature is explained by the fact that many common lacustrine algal species (*Botryococcus Braunii, Tetraedron Minimum*) contain cell walls comprised of highly aliphatic biomacromolecules (algenans, de Leeuw and Largeau, 1993) which could be selectively preserved in the fossil record. Thus the kerogens which are comprised of these algenans are highly aliphatic and yield waxy oils upon thermal stress (Sinninghe Damsté et al., 1993). The occurrence of a partly oxygen-rich type I-S kerogen in marine hypersaline microbial-mat environment, as present during deposition of the source rock analysed in this study, is unprecedented.

3.1.2 Characterisation of the depositional environment using organic sulphur compounds

Organic sulphur compounds (OSC) have received a great deal of attention in the last few years, especially since Sinninghe Damsté et al. (1989) showed that many OSC can be interpreted as products of sulphur incorporation reactions into specific precursors (*n*-alkanes, isoprenoids, steranes, terpanes). The occurrence of some reactive sulphur species (*e.g.*, H_2S, HS^-, polysulfides) in the original environment of deposition is a prerequisite for the formation of these kinds of OSC. In the anoxic environmental setting of the source rock formation H_2S produced by sulphate-reducing bacteria exceeded the input of reactive iron minerals leading to a surplus of free H_2S which reacted with the organic matter. The application of OSC as indicators for depositional settings or diagenetic environments is still being analysed. First palaeosalinity indicators based on the relative abundance of precursors as identified by the carbon skeletons of OSC have been published already by de Leeuw and Sinninghe Damsté (1990). The so called isoprenoid thiophene ratio (ITR; de Leeuw and Sinninghe Damsté, 1990), based on the distribution patterns of C_{20} isoprenoid thiophenes, is particularly interesting (Fig. 83). The isoprenoid thiophenes used for calculating the ITR were identified by GCMS of the low molecular weight aromatic fraction of either oil samples or source rock bitumens.

All kerogen samples analysed by pyrolysis-gas chromatography were characterised by large amounts of organic sulphur compounds (OSC), consisting mainly of thiophenes and thiolanes. The thiophenes and thiolanes encountered in PyGC have, due to the high temperatures used, lost major parts of their sidechains. A tentative identification of the carbon skeleton of the precursor is nevertheless possible. Sinninghe Damsté et al. (1990) have proposed three models to explain the generation of alkylthiophenes by pyrolysis depending on the type of bond between alkylthiophene unit and kerogen:

- The first model assumes that thiophenic sulphur compounds are bound via a carbon-carbon bond to the kerogen. The thiophene produced upon flash pyrolysis would be the same as that produced during natural maturation, since cleavage of the bond β to the thiophene unit is most likely. By this method mainly low molecular weight thiophenes would be generated both in the laboratory and in nature, but this type of bond cleavage reaction would not explain the preferential elimination of akylthiophene and alkane units from sulphur-rich kerogens upon maturation as reported by Egglinton et al. (1990).
- The second model assumes that alkylthiophene units are linked to the kerogen by a single C-S bond. Cleavage of this bond type would, according to Sinninghe Damsté et al. (1990) lead to he generation of the entire alkylthiophene unit both in nature and in the laboratory. This model would not explain the large amounts of low molecular weight alkylthiophenes in kerogen pyrolysates.
- If the alkylthiophene unit is linked to the kerogen by multiple acyclic C-S bonds (Fig, 84, from Sinninghe Damsté et. al., 1990) then the product on pyrolysis bears only minor resemblance to the product of natural maturation of the kerogen. The C-C bond β to the thiophene unit would probably break under the high temperature - short reaction times of flash pyrolysis before the multiple C-S bonds are cracked resulting in the formation of low molecular weight alkylthiophenes. Under natural conditions the C-S bonds would be preferentially cracked resulting in the formation of longer-chain alkylthiophenes.

By assuming that the multiple C-S bonds are the common bond type in sulphur rich kerogens, as postulated by Sinninghe Damsté et al. (1990), the ITR from oils and bitumens may be adapted to alkylthiophene distributions in pyrolysates. Under this assumption the individual alkylthiophenes I to VII of de Leeuw and Sinninghe Damsté (1990), linked by multiple acyclic C-S bonds to the kerogen, would by β cleavage produce low molecular weight alkylthiophenes upon pyrolysis. The isoprenoid thiophenes VI and VII (Fig. 83) would, when linked by multiple C-S bonds to the kerogen, yield upon pyrolysis mainly 3-methylthiophene and 2,3-dimethylthiophene (Fig. 85) by β cleavage. The isoprenoid thiophenes I to V would yield

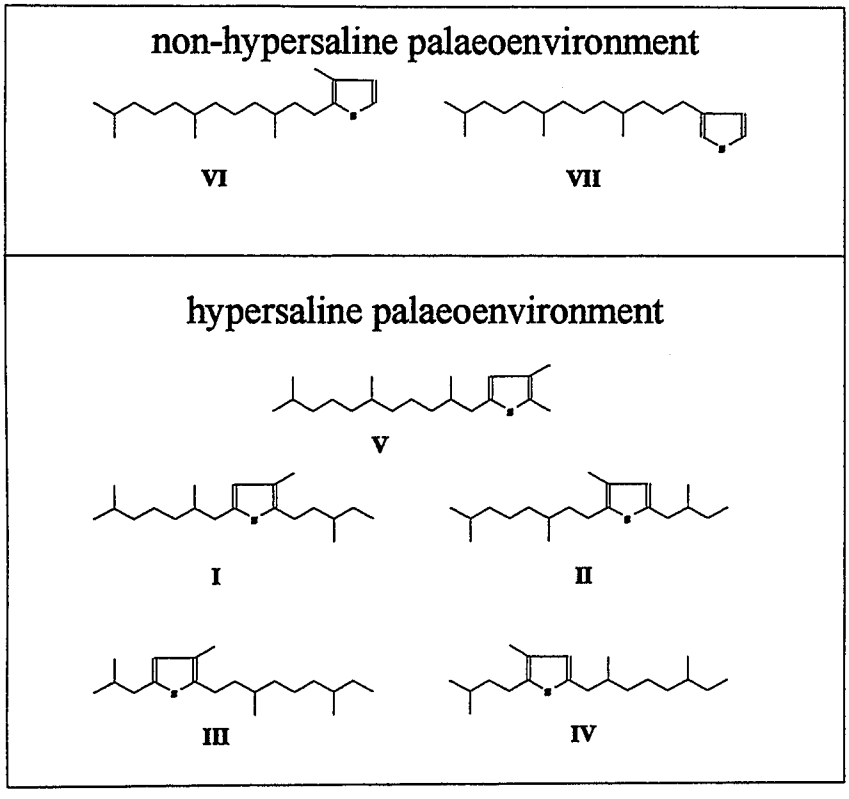

$$\text{Isoprenoid Thiophene Ratio} = \frac{\text{VI} + \text{VII}}{\text{I} + \text{II} + \text{III} + \text{IV} + \text{V}}$$

Figure 83: Description of ITR after de Leeuw and Sinninghe Damsté (1990)

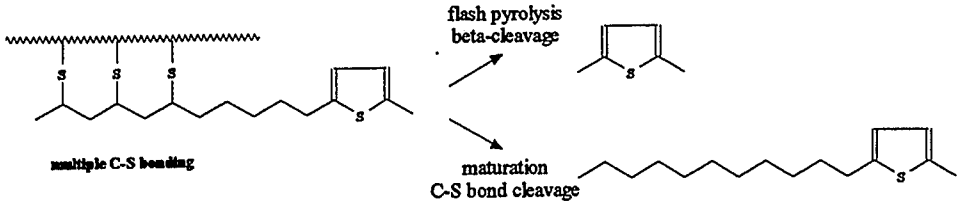

Figure 84: Proposed dominant bonding form of alkylthiophenes in kerogen and their presumed pyrolysis products (after Sinninghe Damsté et al., 1990).

mainly 2,3,5-trimethylthiophene, and probably also 2-ethyl-3,5-dimethylthiophene and 5-ethyl-2,3-dimethylthiophene (Fig. 83, 85). The ratio of 2,3-dimethylthiophene to 2,3,5-trimethylthiophene (2,3/2,3,5 ratio) could therefore be a palaeosalinity (or ecosystem) indicator.

Figure 86 shows the 2,3/2,3,5 ratio of the kerogens analysed. The shale samples generally have 2,3/2,3,5 ratio of over 0.65 while the laminites, solution seems and mudstone/wackestone samples lie below 0.65. The 2,3/2,3,5 ratio therefore seams to reflect the depositional environment. Whether the 2,3/2,3,5 ratio of a given sample is subject to changes during maturation shall be discussed later.

Content and distribution of organic sulphur compounds can, as stated above, reflect the content and distribution of precursor molecules, and hence of the biological input itself. Thiophenes with linear carbon skeletons are probably derived from, e.g., normal fatty acids, isoprenoid skeletons from isoprenoid alcohols, and steroidal carbon skeletons from steroids. In this context the OSC with a steroidal carbon skeleton are of particular interest. Sterols are found in most higher plants and algae but are rare or absent in prokaryotic organisms (Waples & Machihara, 1991). As stated before Matsumoto et al. (1982) and Fowler and Douglas (1987) suggested that steranes may also be derived from cyanobacteria, which are major participants in the formation of microbial mats. Therefore the amount of OSC with steroidal carbon skeletons should be a direct indication of the algal and cyanobacterial input. Linear carbon skeletons are found in both algae and bacteria and should thus be of relatively low variability in the depositional system analysed.

The ratio of linear skeleton OSC to steroidal skeleton OSC (L/S ratio) of five selected samples, in which the HALL trace was quantified, is plotted against the hydrogen index from Rock-Eval of each sample in Fig. 87. The larger L/S ratio of the shale samples E 33366/4, E 33402 and E 33424 indicate either a decrease in OSC with steroidal carbon skeletons or an increase in OSC with linear carbon skeletons. The observed correlation of HI and L/S ratio indicates that the proportion of algal and cyanobacterial biomass decreases in these samples while the proportion of a hydrogen-rich biomass of non algal origin increases with increasing HI. This shift in L/S ratio with increasing HI can be due to either an alteration of the originally deposited organic matter or to a change in the type of organic matter in the samples.

The bulk of the organic matter was proved to be quite homogeneous as indicated by very similar pyrolysate fingerprints of samples with vastly different hydrogen indeces (Fig. 34). The OSC, which are products of sulphur incorporation into the organic matter during early diagenesis, showed differences between samples of different hydrogen indeces. These differences are therefore surely due to different diagenetic evolutions of the organic matter of

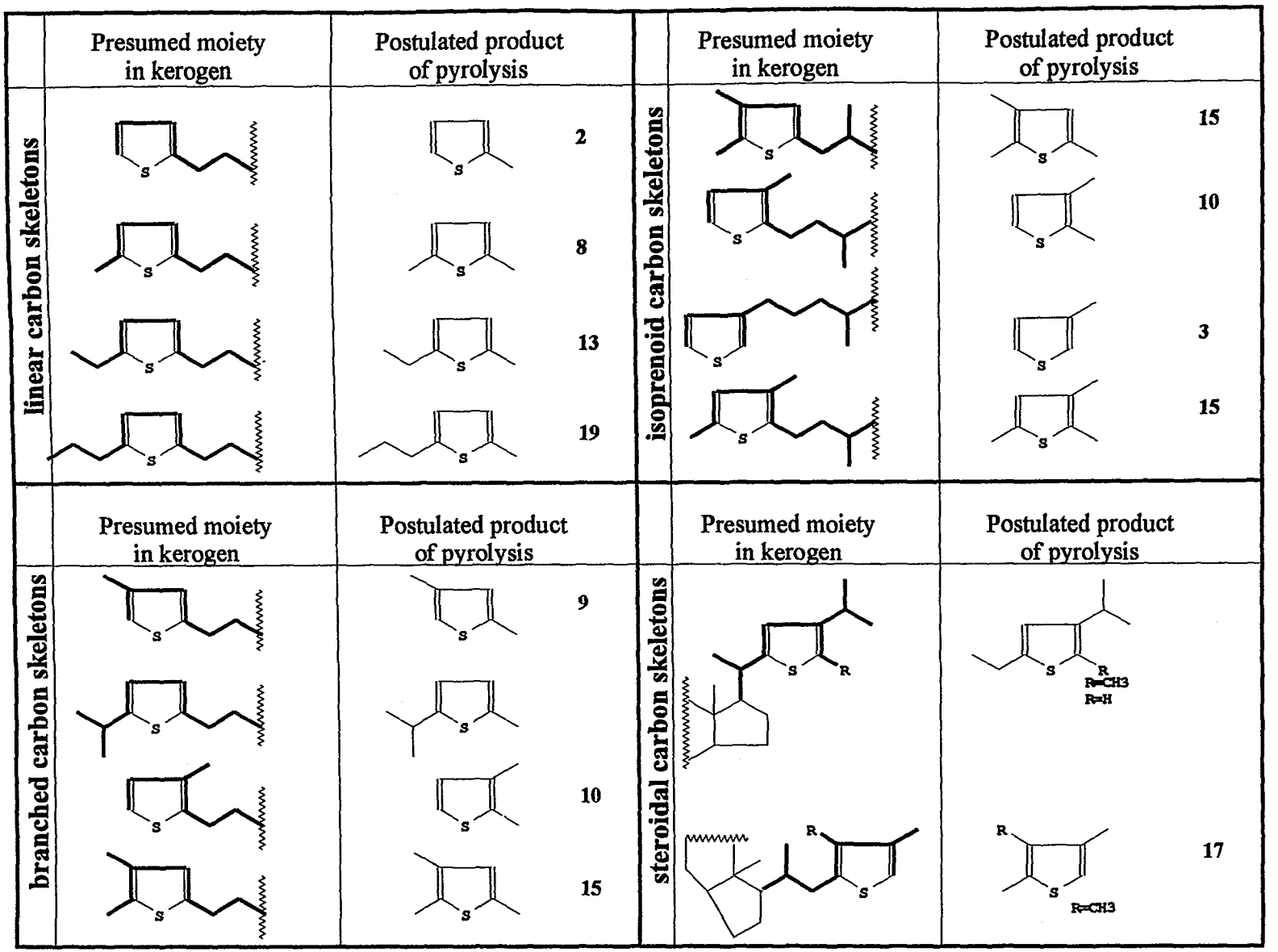

Figure 85: Postulated products of sulphur-containing moieties in kerogen generated upon flash pyrolysis by beta cleavage (after Sinninghe Damsté et al., 1989). Compounds are identified by numbers which are the same as listed in Figure 38.

the samples and not to different input. The observed increase in L/S ratio with increasing HI is therefore interpreted as direct proof of bacterial reworking of the organic matter indicating that this reworking led to an increase in the quality of the organic matter which ultimately resulted in the formation of a type I-S kerogen.

A detailed analysis of the organic sulphur compounds generated during MSSV pyrolysis was only performed on the whole rock sample (E 33383) due to difficulties with the HALL detector. Analysis of the sulphur compounds generated by MSSV pyrolysis showed a strong variability of different compound concentrations with temperature increase. A variety of ratios of sulphur compounds, selected according to their carbon skeletons, were plotted against temperature in order to find ratios that changed parallel to maturity. In the selection of ratios care was taken to compare the ratios from MSSV to those of the thermally untreated kerogens (from PyGC) in order to separate possible facies indicators from maturity indicators. For example a facies indicator should remain relatively unchanged during maturation and a maturity indicator should be unbiased by organic facies. A good example for a facies indicator was found in the already mentioned 2,3-dimethylthiophene/2,3,5-trimethylthiophene ratio which also shows a larger variation between different facies than during maturation (Fig. 88) as demonstrated by the MSSV experiment.

A maturity indicator which may be worthwhile to analyse in more detail was found in the ratio of 2,3,4-trimethylthiophene/isopropyl-methylthiophene+3:1-thiophene (these peaks coelute). The 2,3,4-TMT/Isop-MT+3:1-T ratio (peaks 17 and 18 of figure 38) showed a strong increase with maturity during MSSV pyrolysis and no variation in untreated kerogen pyrolysis (Fig. 89), thus demonstrating its independence of facies. The increase of the 2,3,4-TMT/Isop-MT+3:1-T ratio with maturity implies a relative decrease in the amount of Isop-MT+3:1-T generated with increasing temperature as compared to 2,3,4-TMT. This reaction is probably controlled by the stability of the individual compounds. 2,3,4-TMT can be assumed to be of higher stability than Isopropyl-methylthiophene with its longer sidechain.

Naturally matured kerogens can be expected to show the same behaviour of the ratio with maturity upon pyrolysis. This observation indicates that pyrolysis-GC of sulphur-rich kerogens may allow a maturity estimation of the source rock.

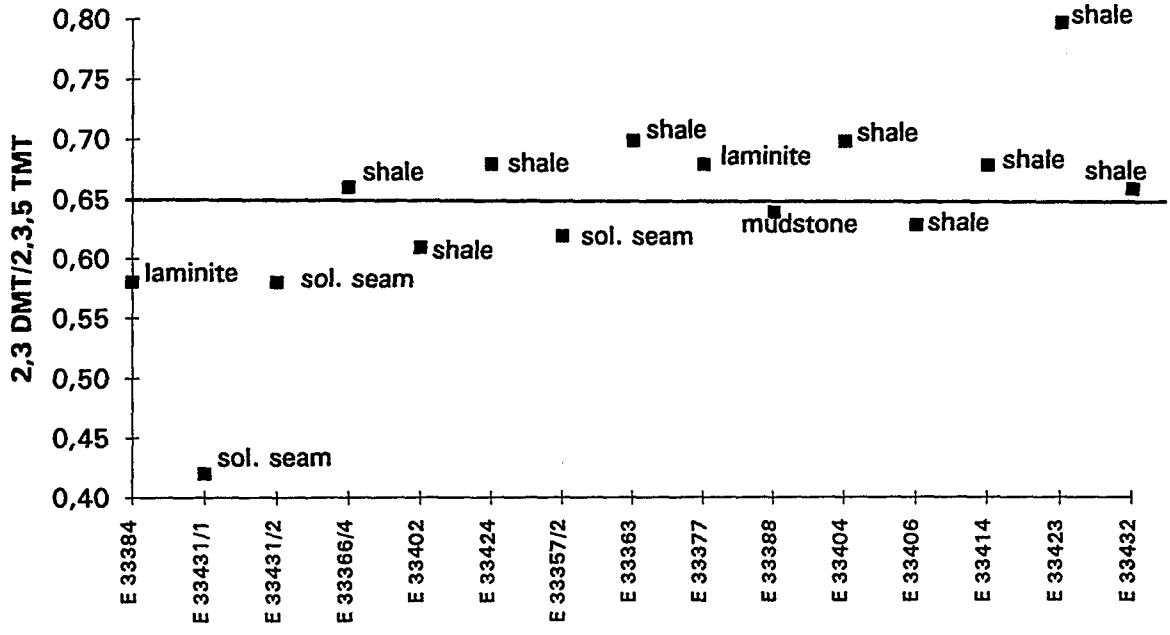

Figure 86: 2,3-dimethyl-thiophene/2,3,5-trimethyl-thiophene ratio of selected samples.

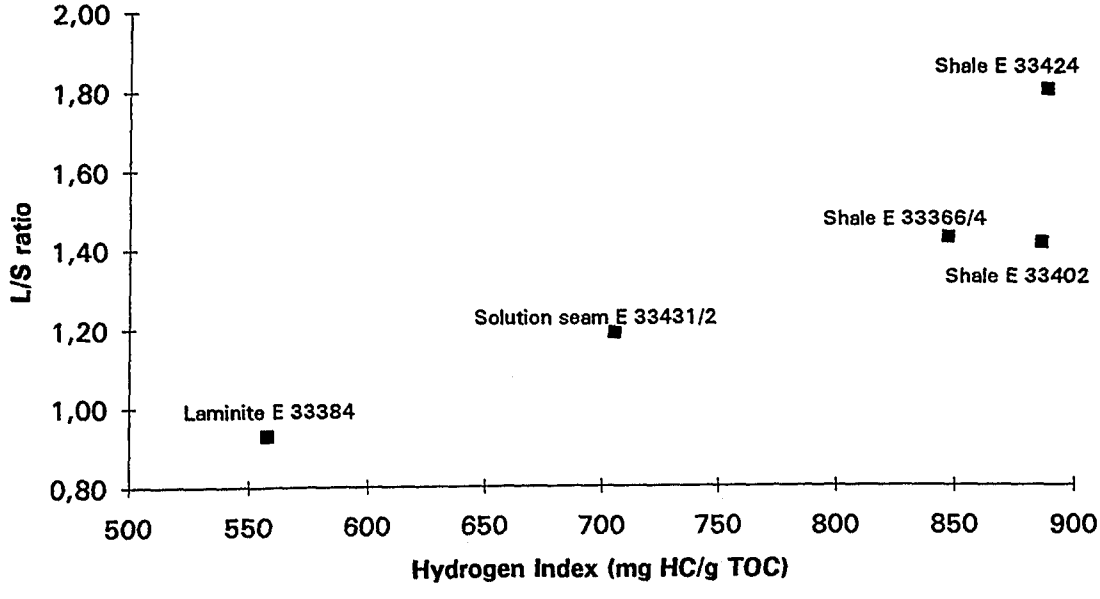

Figure 87: Ratio of alkylthiophenes with a linear carbon skeleton to alkylthiophenes with a steroidal carbon skeleton (L/S Ratio) of five selected samples versus hydrogen index.

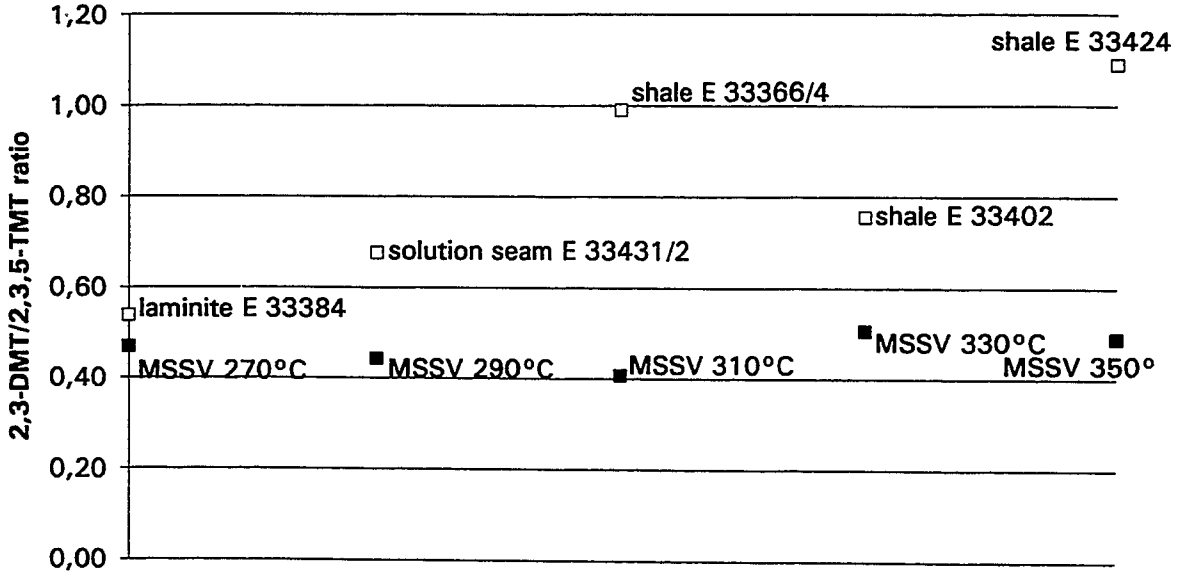

Figure 88: Comparison of 2,3-Dimethyl-thiophene/2,3,5-trimethyl-thiophene ratios of MSSV pyrolysates of the whole rock sample (E 33383) at increasing temperatures to results from PyGC of selected samples.

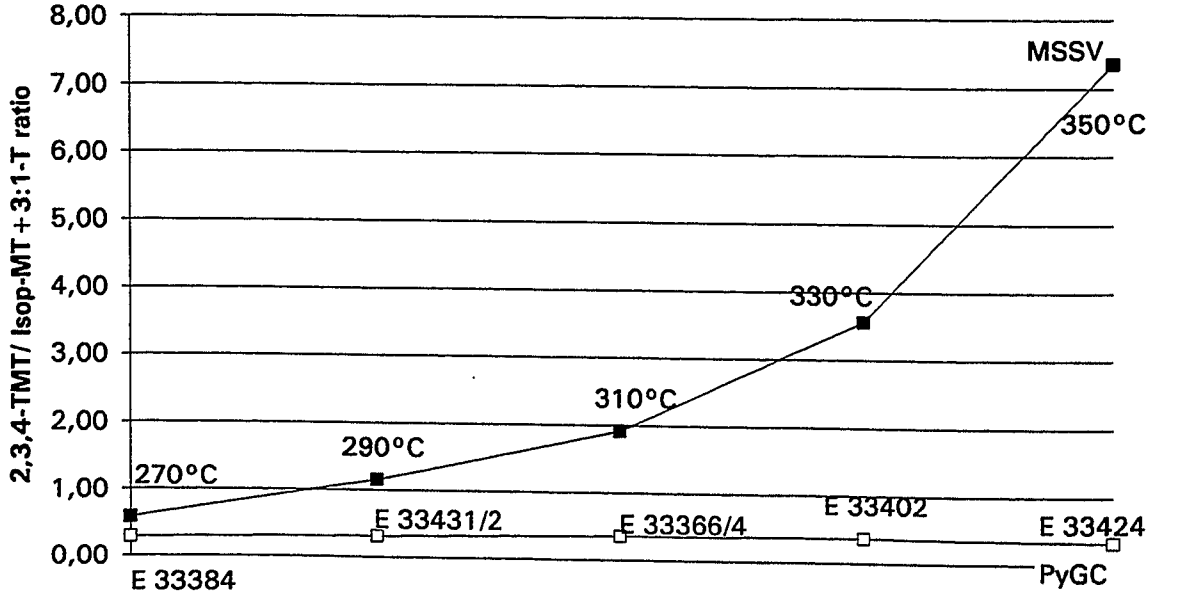

Figure 89: Comparison of the 2,3,4-Trimethylthiophene/Isoprpyl-methyl-thiophene+3:1-thiophene ratios of the MSSV pyrolysates of the whole rock sample (E 33383) at increasing temperatures to results from PyGC of selected samples.

3.1.3 Summary

The main conclusions concerning the type of organic input to the source rocks as well as the observations which lead to these conclusions are summarised below:

Microbial mats	- microscopic observations (Plate 2a-f)
	- n-C_{15} and n-C_{17} predominance
	- elevated O/C ratios
	- MPI 1 and MPI 2 anomaly of the shales
	- C29 steranes
Algae	- microscopic identification of alginites and liptodetrinites (Plate 2a-d)
	- presence of steranes (Moldowan et al., 1985)
	- predominance of n-C_{15} and n-C_{17}
Bacteria	- microscopic identification of bituminous groundmass (Plate 2a-d)
	- L/S ratio of PyGC
	- abundance of hopanes
	- elevated H/C ratio accompanied by the bituminous groundmass
Land plants waxes	- odd over even preference of n-alkanes in the chain length range of n-C_{23} to n-C_{31}

In most cases the identification of the main precursors was made on the basis of a combination of indicators and analytical techniques (i.e. elemental analysis, microscopy and saturated GC). The input of terrestrial plant waxes was inferred only from the odd over even n-alkane predominance and must, therefore, be treated as tentative.

3.2 Hydrocarbon generation

3.2.1 Characterisation of hydrocarbon generation by analysis of the soluble organic matter

Soluble organic matter yields are reported to reach maximum values as high as 180 mgSOM/gTOC during peak generation from siliciclastic type II source rocks (Tissot and Welte, 1984, page 174). The values monitored for the source rock formation could therefore be assumed to indicate a relatively advanced stage of hydrocarbon generation. On the other hand, high extract yields have also been found in low maturity carbonate source rocks by many authors (i.e.: Palacas, 1983; Powell, 1984; Tannenbaum and Aizenshtat, 1985; Sinninghe Damsté et al., 1989; Rullkötter et al., 1990). This abundance of SOM in the source rock alone would normally be enough to demonstrate that the source rock is in the stage of petroleum generation, but the high proportion of polar compounds in the bitumen together with the sulphur-rich nature of the source kerogen allow an alternative interpretation. Powell (1984) and Sinninghe Damsté et al. (1989) proposed that the extremely reducing conditions in carbonate-evaporite environments can retard the formation of kerogen leading to high amounts of primary SOM which is not a product of thermal kerogen degradation. Thus, two explanations of the high amounts of bitumen observed in the source rock exist. The first is based on the early cracking of sulphur-carbon bonds leading to high amounts of polar compounds at initial stages of hydrocarbon generation. The second assumes that the observed high amounts of polar compounds are of a primary nature and not the products of kerogen degradation.

3.2.2 Hydrocarbon generation characteristics as deduced from pyrolysis experiments

Open system pyrolysis plays a major role in predicting petroleum types and occurrence depending on the kerogen characteristics. Bulk flow pyrolysis methods using different heating rates are used for kinetic predictions (Schaefer et al., 1990), while pyrolysis-GC methods can be applied for oil type prediction (Horsfield, 1989). Both techniques have in common that they are based on the analysis of mobile/volatile products.

Carbonate/evaporite sourced oils are characterised by high viscosities, low API gravities, have low proportions of gasoline-range compounds and generally low amounts of hydrocarbons as compared to resins and asphaltenes. These aromatic-asphaltic oils are stated to originate from hydrogen- and sulphur-rich organic matter. The source kerogens of Types I-S and II-S (Orr, 1986; Sinninghe Damsté et. al, 1993) have been shown to generate petroleum rich in resins asphaltenes at low stages of thermal maturity (Tissot et al., 1987; Baskin and Peters, 1992), although primary asphaltenes, formed as per Powell (1984) or Sinninghe Damsté et al. (1989), may also be present in the sediment.

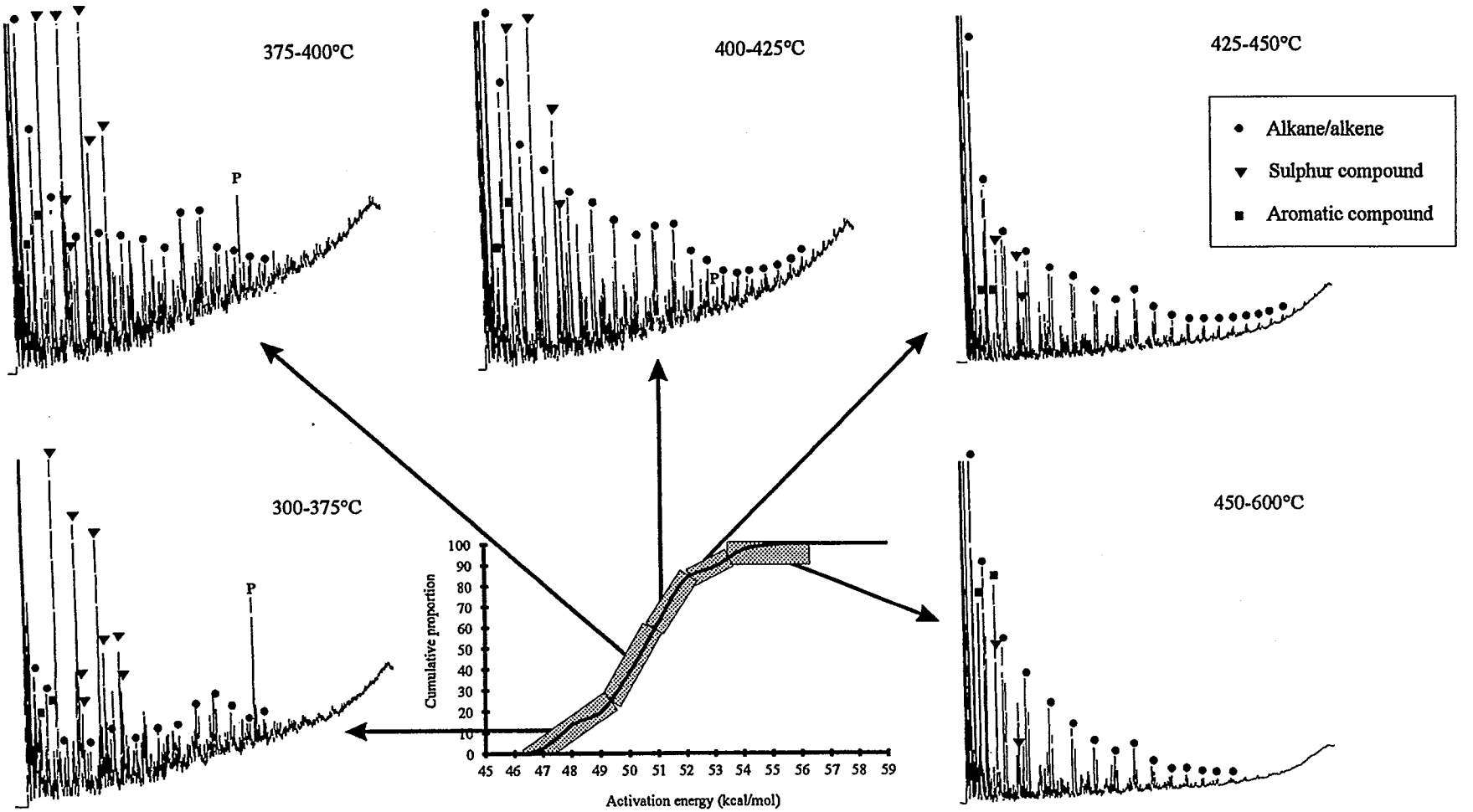

Figure 90: Combination of the results from the five-step PyGC experiment and the hydrocarbon generation kinetics of kerogen sample E 33366/4.

The analysis of organic matter which generates large proportions of high molecular weight material by methods which mainly recognise mobile/volatile products can be assumed to be very inaccurate. Specially the prediction of petroleum type and the determination of kinetic parameters for the generation of oils rich in involatile compounds using pyrolysis methods which cannot detect these species is questionable.

Tmax from kinetic predictions is mainly ascribed as the main hydrocarbon generation stage. The results of the pyrolysis experiments imply that, for carbonate evaporitic environments, a stronger differentiation between early and late maturity products is necessary. In this source facies the lower energies, which may be attributed to S-C bond cleavage reactions, are empirically of greater importance, especially in view of the fact that they may represent the main generation stage under natural conditions.

Figure 90 shows the combination of the results from the five step PyGC experiment and the hydrocarbon generation kinetics of the same sample, based on the degree of conversion achieved in each step of the multistep experiment as compared to the cumulative degree of conversion corresponding to each activation energy of the bulk-pyrolysis results. Figure 90 exemplifies that at low energies (49 to 51 Kcal/mol) sulphur-rich products (mainly thiophenes) dominate in the pyrolysates. This fact can be attributed to the preferential cleavage of S-C bonds, although the presence of the thiophenes indicates that much of the sulphur is present in stable rings as well as in labile S-C bonds. These first pyrolysates indicate that, in nature, sulphur-rich petroleum is generated at this stage. The molecular composition of these oils surely differs from that of the pyrolysis products, since the major proportion of high molecular weight compounds of aromatic/asphaltic oils are thermally involatile and therefore cracked to secondary products during pyrolysis. High yields of low molecular weight alkylthiophenes signify only that the kerogen is rich in sulphur, and it is left to known correlations to infer bulk oil composition. At higher energies, in which the dominant activation energy is included, the pyrolysates contain higher proportions of n-alkanes/alkenes with a fixed chain length distribution and lower sulphur contents, which in nature would be manifested as higher API oils.

An indirect determination of the petroleum type generated during 5-step PyGC, analogous to the triangular plot of Horsfield (1989) based on n-alkane/alkene distributions, was attempted using the relative proportions of individual compounds in the pyrolysates as described in chapter 2.1.6.2. Figure 91 shows a direct comparison of Horsfields (1989) triangular plot and the novel ternary plot using the results of the 5-step PyGC experiment as well as one-step PyGC results from this study and from other source rocks and maceral types analysed using the same method.

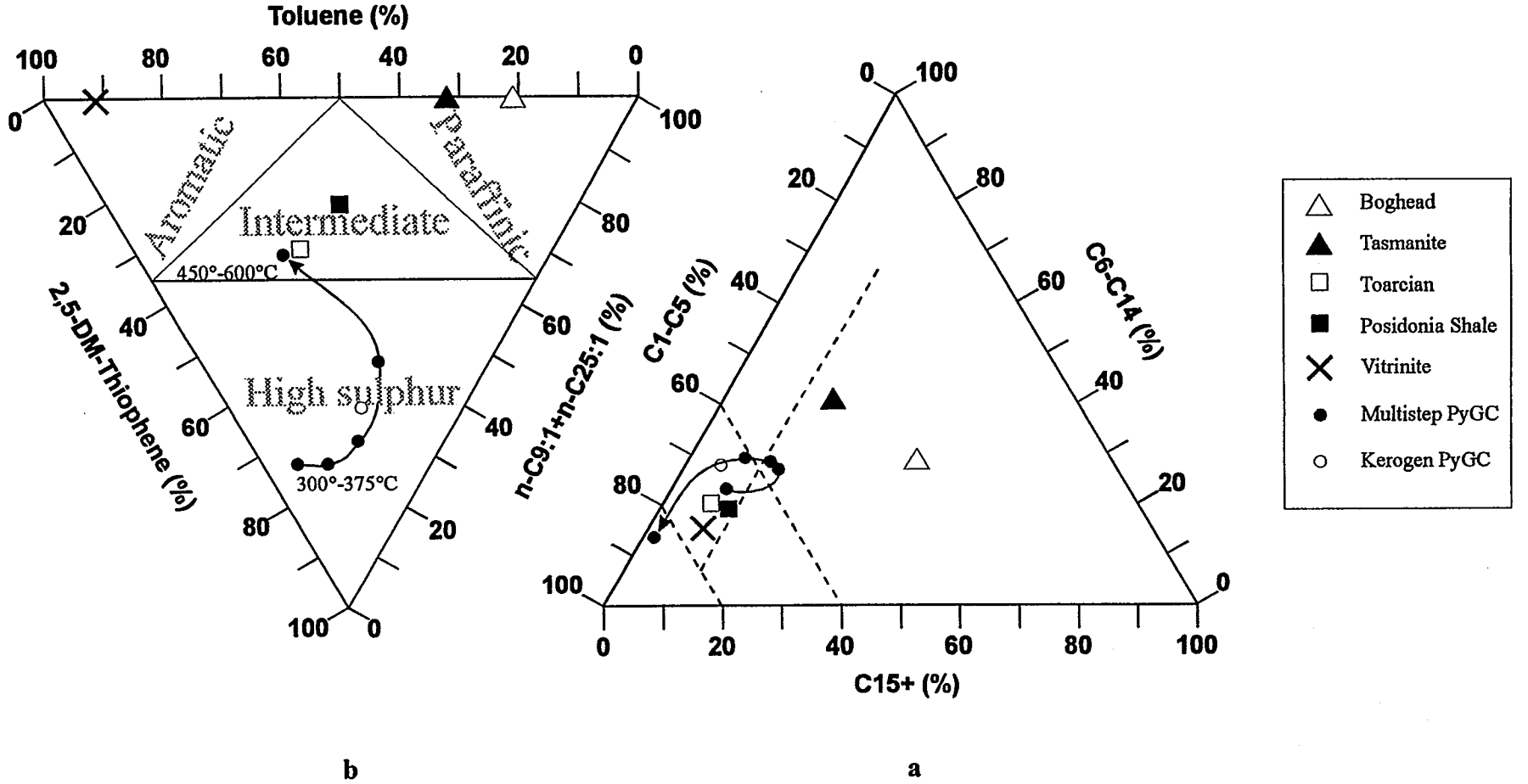

Figure 91: Differentiation of pyrolysate composition using n-alkane chainlength distributions (a) as well as relative proportions of selected alkyl-, aromatic- and sulphur compounds (b). Boghead Coal, Tasmanite, Toarcian Shale (Paris Basin) andPosidonia Shale (Hillsmulde) sample data were taken from Horsfield (1989) and Düppenbecker (1992).

In the classical petroleum-type prediction triangular diagram of Horsfield (1989) the first four steps of the 5-step PyGC experiment plot in a relatively narrow field (Fig. 91a), whereas the last step is clearly shifted towards the gas region of the diagram. The alkane/alkene distribution of the one-step PyGC experiment of the same sample plots on the path extrapolated for the five step experiment, between the final two steps.

In the sulphur-saturated-aromatic ternary plot the variation in pyrolysate composition is much clearer. The first three steps of the 5-step experiment are characterised by very high amounts of 2,5-dimethylthiophene, the fourth step shows an increase in alkyl compounds whereas in the final step the proportion of toluene is dominant. If it is assumed that the proportion of 2,5-dimethylthiophene is proportional to the amount of organic sulphur in the petroleum generated in nature, then the pyrolysate evolution curve shown in fig. 91b describes the generation of heavy, sulphur-rich oils at low levels of thermal stress. With increasing maturity the kerogen analysed successively generates higher proportions of alkyl moieties and aromatic compounds which in nature would be manifested as higher API oils. The pyrolysate generated during the final step of the 5-step PyGC experiment resembles in its composition the pyrolysate of an immature Toarcian kerogen of the Paris Basin.

An answer to the question of whether the bitumen present in the source rock is of a primary nature or not was sought in the detailed molecular analysis of asphaltenes. This high molecular weight organic matter showed a large degree of similarity to the corresponding kerogens as analysed by PyGC. Asphaltenes are generally seen as intermediate products along the pathway leading progressively from kerogen to hydrocarbons (Orr, 1986; Tannenbaum and Aizenshtat, 1985) and a compositional similarity between both would therefore not be surprising. On the other hand, if asphaltenes are products which are formed at the same time as, but not included in kerogen due to extremely reducing conditions (Powell, 1984; Sinninghe Damsté et al., 1989) the same degree of similarity could be expected.

The incorporation of sulphur into organic matter is a process which takes place during earliest diagenesis (for a review see de Leeuw and Sinninghe Damsté, 1990). Therefore condensation and polymerisation processes, although retarded by an extremely reducing environment, should incorporate sulphur into the asphaltene or kerogen matrix in comparable proportions if we assume that the theory of Powell (1984) and Sinninghe Damsté (1989) is correct. Thus, primary asphaltenes should possess the same types and amounts of bonds as kerogen, only in a less well condensed structure. An example of the asphaltene structure according to the theory of Powell (1984) and Sinninghe Damsté et al. (1989) is shown in Fig. 92a, based on the

structural representation proposed by Pelet et al. (1986) and Behar and Vandenbroucke (1986).

If the asphaltenes present in the sediment extract are a product of early hydrocarbon generation by preferential cleavage of S-C and S-S bonds in the kerogen (secondary asphaltenes), then the asphaltenes should show comparable sulphur contents in general, but a lower proportion of sulphide bonds. The resulting asphaltene structure is shown in Fig. 92b, and is characterised by the general lack of sulphide links in the asphaltene molecule. Sulphur contents are thus lower than in the primary asphaltene shown in Fig. 92a, but nevertheless still comparable to those of the corresponding kerogen, since the kerogen can also be assumed to have lost sulphur during C-S bond cleavage.

MSSV pyrolysis of a kerogen and corresponding asphaltene fraction was performed to determine the generation characteristics of both high molecular weight fractions. The analysis on a molecular level of the compounds generated per heating step (Δ values, Figs 69-74) revealed that in the low temperature range, attributed to the cleavage of sulphur-carbon bonds, only the kerogen generated appreciable amounts of pyrolysate. This result was taken as an indication that C-S bonds were significantly depleted in the asphaltenes as compared to the kerogens. The depletion of C-S bonds in asphaltenes was also noted in the multistep PyGC experiments, where the S/C ratios of the asphaltene pyrolysates in the 300°-375°C heating step were much lower than those of the kerogen samples (Fig. 46).

The sulphur content of three asphaltenes precipitated from the produced oils and from an intraformational reservoir, as determined by elemental analysis, was comparable to that of the kerogens (Table 15), but the fact that the amount of S-C or S-S bonds was much lower (MSSV results) implies that asphaltenes are early generation products of the kerogen, which are released by the preferential cleavage of S-C or S-S bonds. Thus the sulphur contents *per se* are high in asphaltenes, but the contribution of S-C or S-S cleavage products is low due to the lack of these bond types in the organic matrix. In consequence the asphaltenes of the source rock formation are only the product of, and not involved in, the early generation of heavy oils by C-S bond cleavage.

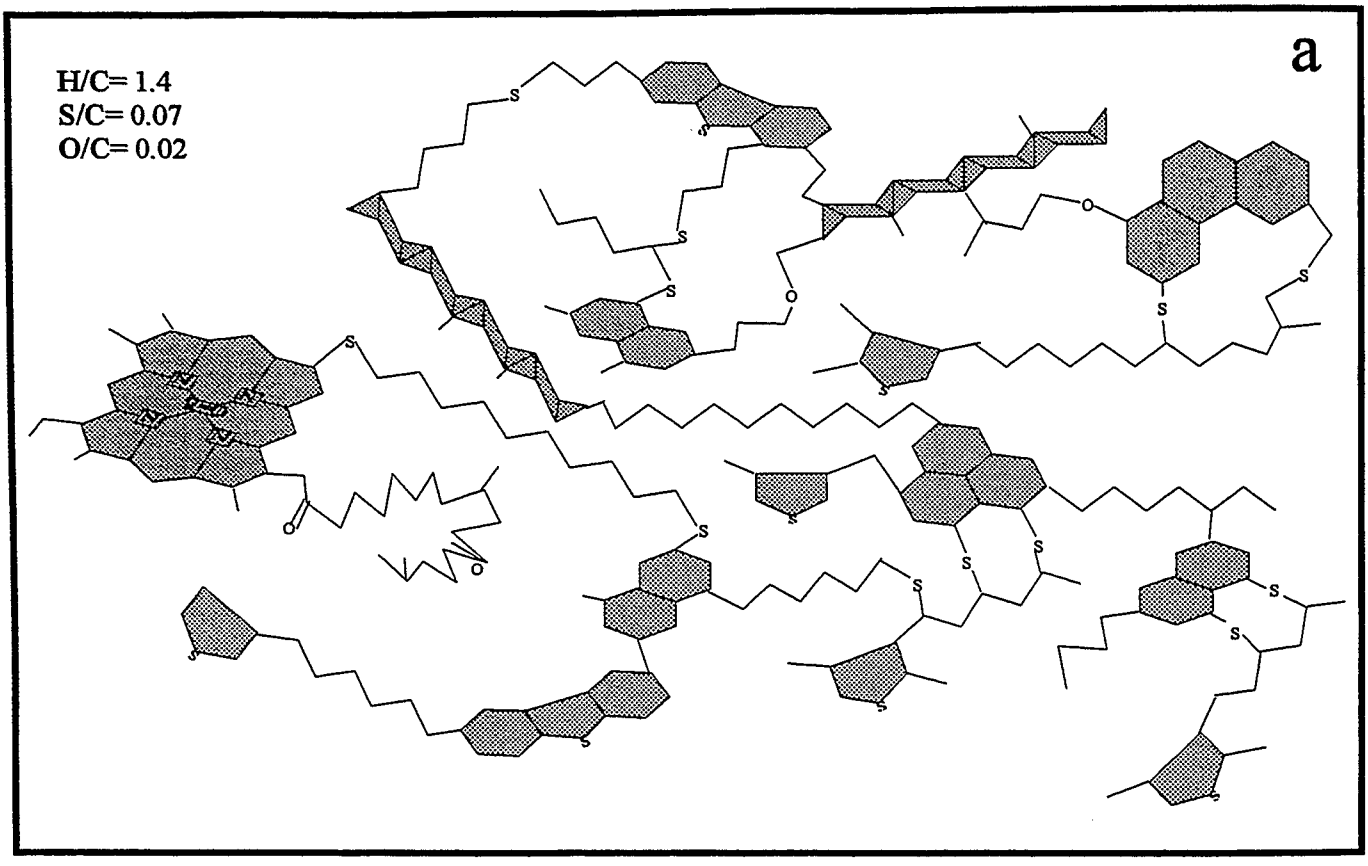

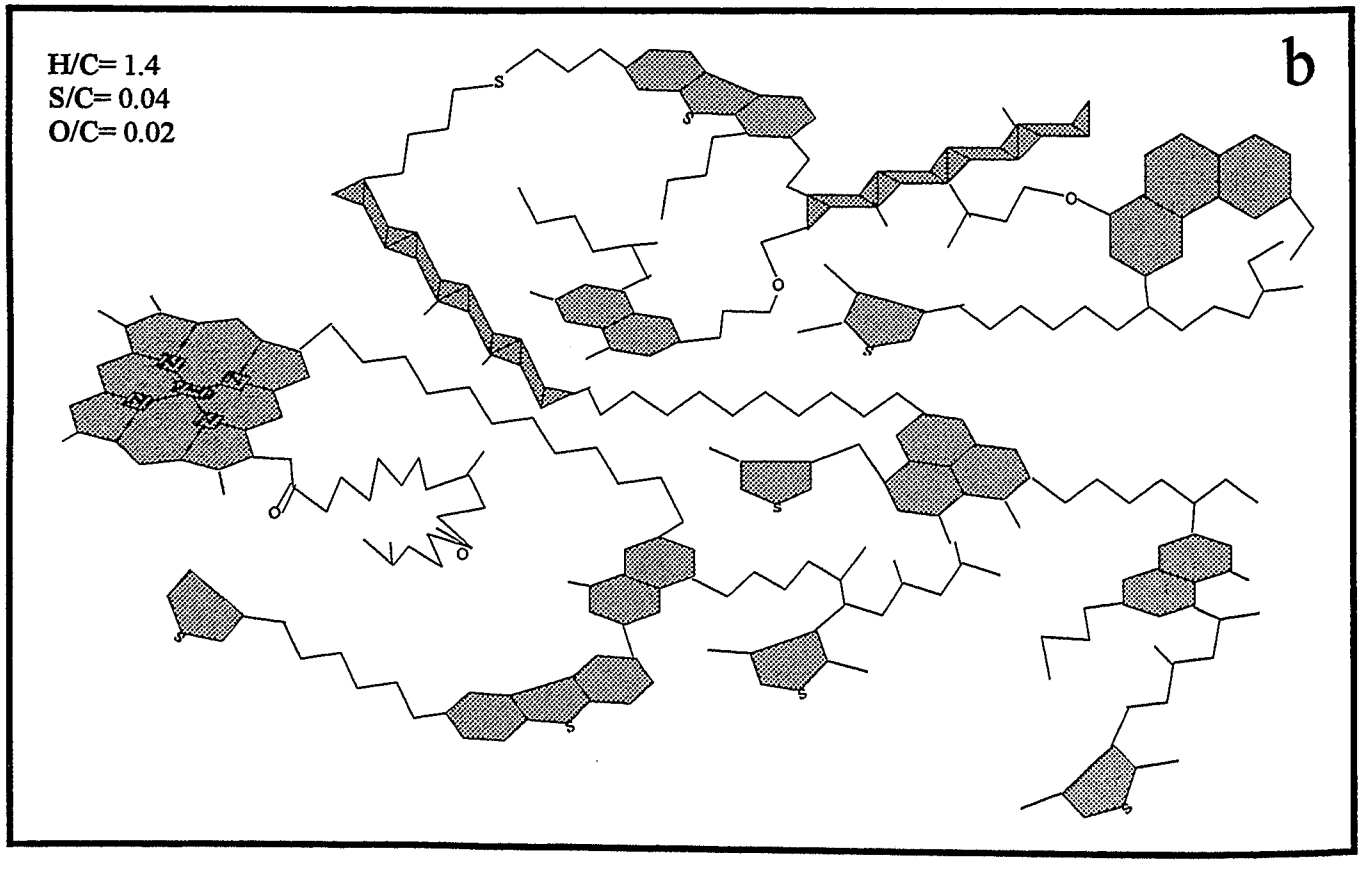

Figure 92: Highly schematic structural models of (a) primary and (b) secondary asphaltenes based on the structural models of Pelet et al. (1986) and Behar and Vandenbroucke (1986).

3.2.3 Heavy oil generation

The results of OSHP and MSSV indicated that the generation of hydrocarbons from the source rock analysed is mainly controlled by two bond cleavage reactions as demonstrated by the bimodal HC-generation curves of Figs. 55 and 65. At low temperatures C-S bonds in the kerogen are broken, leading to the generation of sulphur compound- and asphaltene-rich pyrolysates. At higher temperatures consequently lighter oils are produced by mainly C-C bond cleavage. Relatively high asphaltene contents in oils are attributed to their solubilisation by interactions with the high-sulphur aromatic and resin components (Pfeifer and Saal, 1940; Tissot, 1981; Orr, 1986). According to this concept each petroleum as generated from the kerogen is able to carry out of the source rock a quantity of asphaltenes in proportion to the available concentrations of resins and aromatics. This system of solubilisation by an "atmosphere" of resins and aromatics is sufficiently stable that loss of asphaltenes during migration may be minimal (Orr, 1986).

A kinetic evaluation of both proposed cleavage reactions was performed using the mathematical model described in the kinetics chapter. The best fit between the pyrolysate generation curve from Fig. 55 and the calculated formation rate was obtained with the activation energy distribution depicted in Fig. 93. The pre-exponential factor was 3.03E+18.

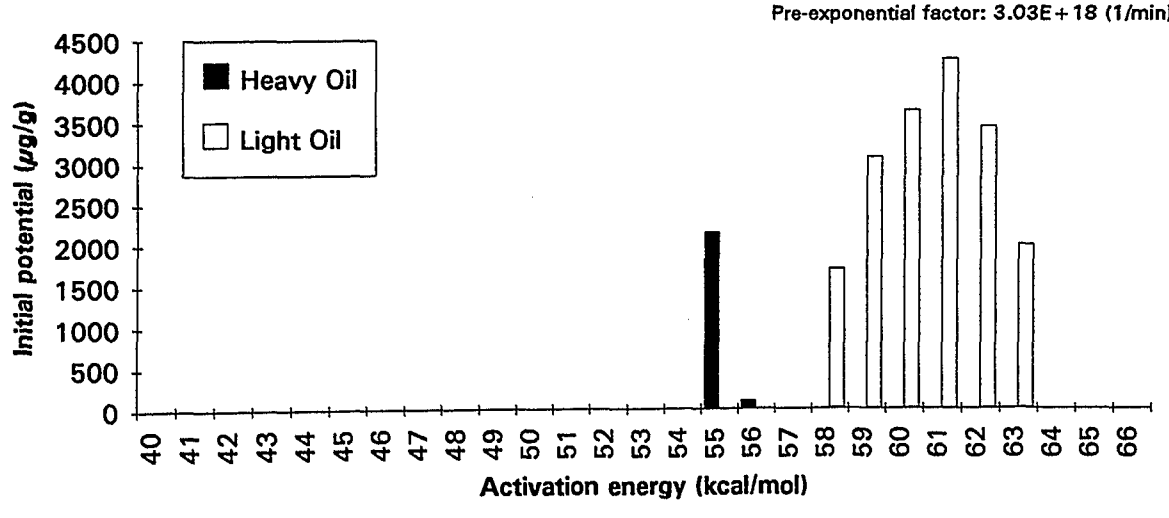

Figure 93: Activation energy distribution calculated using the petroleum generation curve of Fig. 55. The pre-exponential factor is shown in the upper right corner.

The two main reactions of C-S (generation of "heavy oil") and C-C bond cleavage (generation of "light oil") can thus be described by two sets of activation energy distributions, whereby the activation energy distribution for "heavy oil" generation was 6 to 7 kilocalories/mol lower than the main "light oil" generation.

The cumulative proportions of total petroleum potential with increasing activation energy are shown in Fig 94. The abrupt increase of the „heavy oil" curve (i.e. C-S bond cleavage) is due to the comparatively low number of parallel reactions involved in the pyrolytic generation of hydrocarbons in this case which, in turn, is related to the composition of the organic matter. Homogeneous organic matter is normally characterised by an abrupt increase in the cumulative proportions of total petroleum potential, indicating a small number of reactions involved in the generation of hydrocarbons (Schenk et al., 1992). The differentiation of the two reactions, achieved by kinetic evaluation of the OSHP results, indicates that the kerogen consists of two relatively distinct portions.

The kinetic analysis of hydrocarbon generation using the open system pyrolysis FID method was unable to distinguish between the two reactions due to the influence of degradation products from neo-formed high-molecular-weight (HMW) organic matter during the experiment. In the OSHP experiment neo-formed HMW organic matter was expelled together with the low molecular weight compounds in one petroleum phase, removing thus all products from the reacting system.

Fig. 95 shows for both reactions the cumulative proportion of total bulk petroleum potential with increasing "normalised" activation energy (see chapter 2.1.6.1). The shift of these curves with increasing E/lnA reflects increasing temperatures of hydrocarbon generation under laboratory conditions.

The simplified quantity E/(lnA-lnr) is plotted as a function of ln r for the two reactions in Fig. 96. This figure confirms the decrease in T_{max} with decreasing heating rate, specially in going from laboratory to natural conditions. The stronger decrease of the thermal stability of the "heavy oil" generation as compared to the "light oil" generation is due to the lower dominant activation energy. These facts point out, as expected, that under geological conditions "heavy oils" are generated at lower levels of thermal stress than "light oils". As compared to the estimation of peak hydrocarbon generation using the dominant activation energy from the kerogen kinetics data the "heavy oil" generation occurs at lower levels of thermal stress. This is of course due to the method used for kinetic assessment as discussed above. An open system pyrolysis device coupled directly to an FID can only detect those compounds which are in the gas phase at each temperature. The generation of asphaltenes by C-S bond cleavage, that is the generation of heavy oils, must therefore remain largely undetected by this method, since the

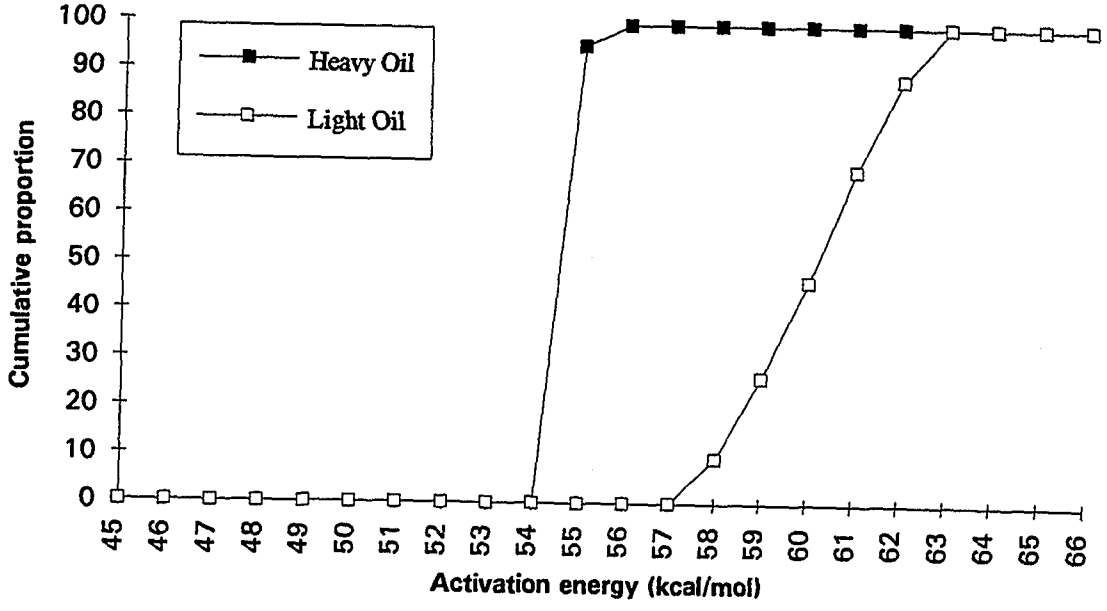

Figure 94: Cumulative proportion of total petroleum potential with increasing activation energy describing the generation of heavy and light oils.

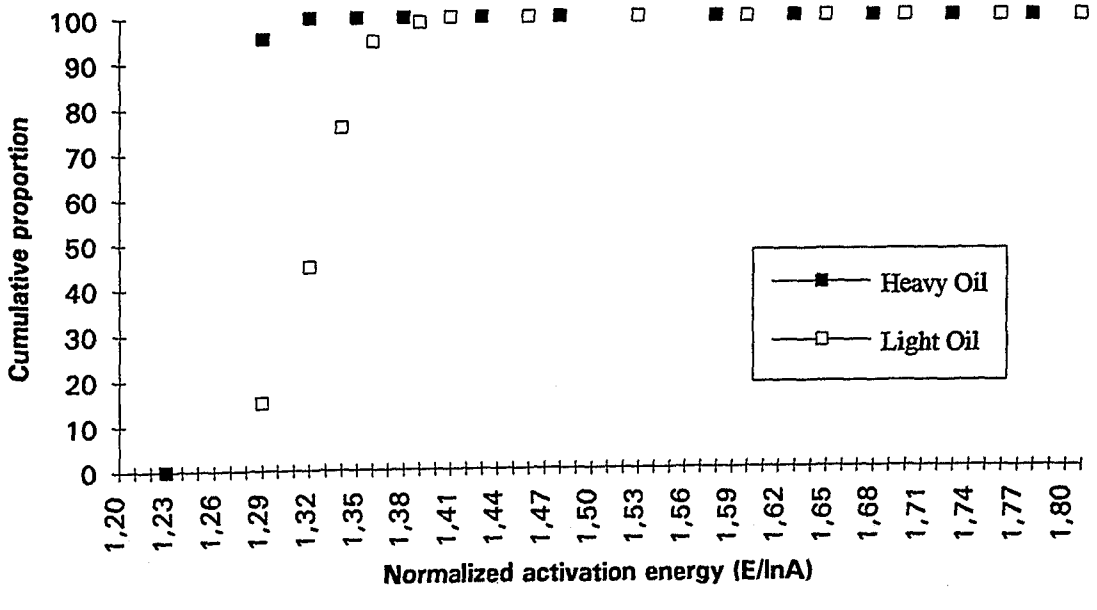

Figure 95: Cumulative proportion of total petroleum potential with increasing normalised activation energy of the heavy and light oil generation reactions.

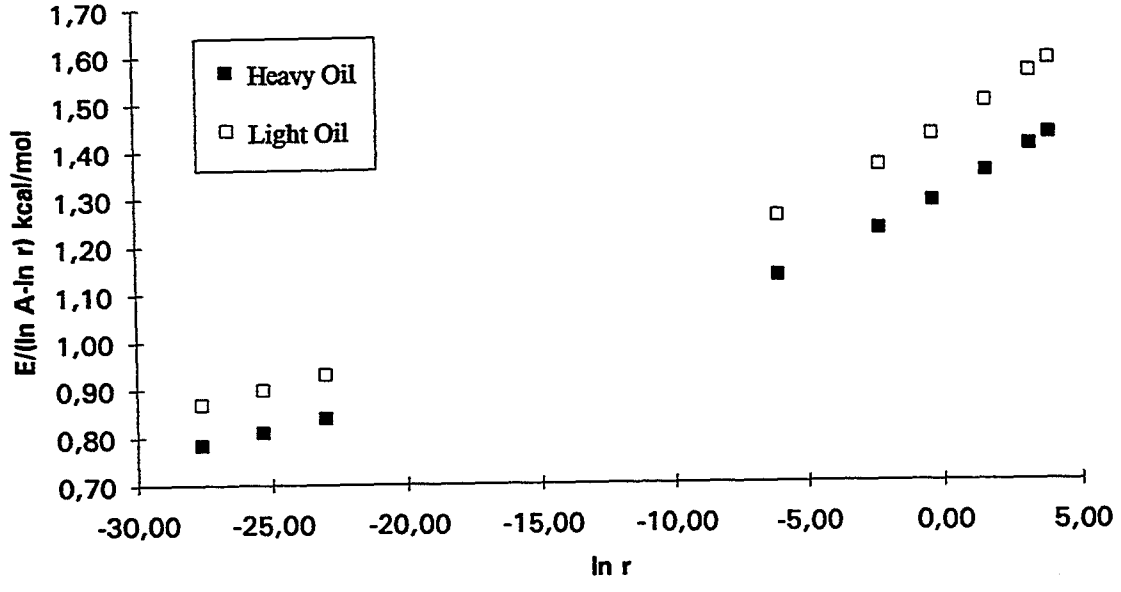

Figure 96: E/(lnA-lnr) versus ln r of the heavy and light oil generastion reactions with ln r representing six laboratory and three geological heating rates.

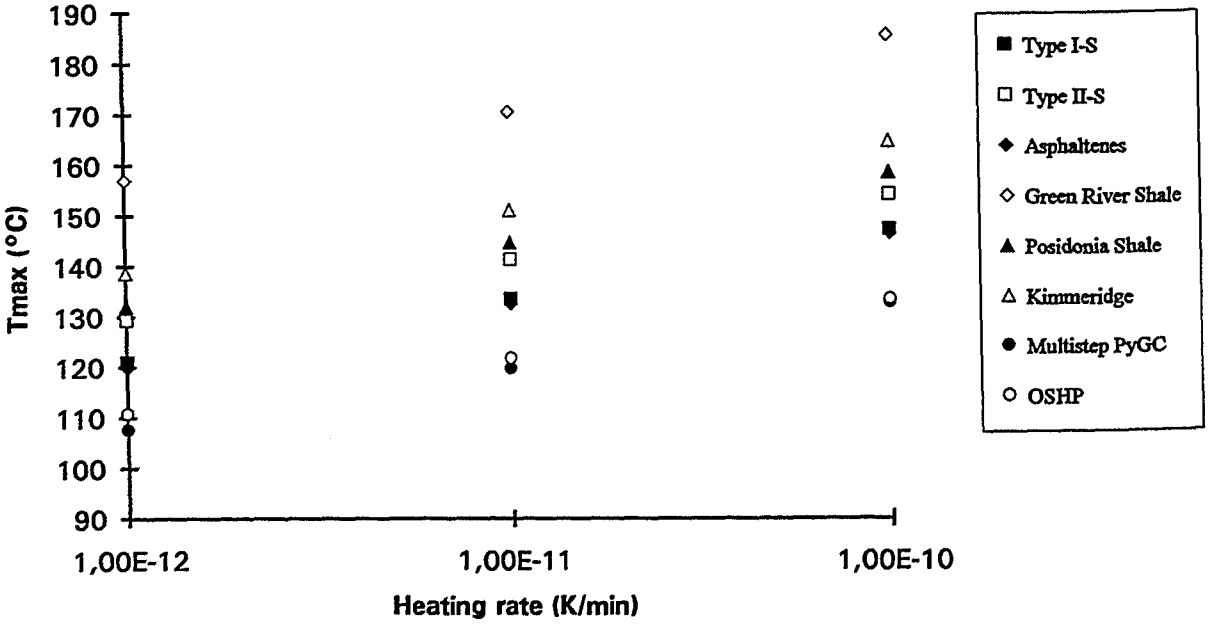

Figure 97: Tmax of petroleum generation versus ln r of kerogens Type I-S, II-S, asphaltenes and selected samples from the literature calculated using the dominant activation energy of the distribution as compared to the temperatures calculated for heavy oil generation from the results of Multistep-PyGC and OSHP.

asphaltenes remain to a large extent in a non-volatile state. Open System Hydrous Pyrolysis offered the possibility of assessing and quantifying the gaseous and liquid products generated throughout the temperature program, thus allowing a kinetic approach to the entire generation process.

The quantity E/(ln A-ln r) shows a linear relationship to the temperatures of maximum pyrolysate generation (Schenk, pers. com.). Tmax values can therefore be calculated from the corresponding E/(ln A-ln r) data for any heating rate. Fig. 97 shows a comparison of Tmax vs. geological heating rate data for different source rocks to the different kerogen types and asphaltene samples evaluated in this study. The data from the Green River Shale was taken from Schenk et al. (1993), while the Kimmeridge and Posidonia Shale kinetic parameters were published in Schaefer et al. (1990). The type I-S kerogen is sample E 33366/4, the type II-S is sample E 33360, and the asphaltene is sample E 33401 As. The "heavy oil" data was calculated from the activation energy distribution for the first reaction recognised in OSHP. The Multistep PyGC data was calculated using 49 kcal/mol as the dominant activation energy representing sulphur-carbon bond cracking as discussed in chapter 3.4.1. Tmax values calculated from both OSHP and multistep PyGC results show a high degree of concordance.

As shown in Fig. 97 the maximum generation of heavy oil from a sulphur-rich source rock is reached 22 to 28°C (depending on the heating rate) before the maximum generation from a typical type II source rock (Posidonia Shale) is reached. As compared to a type I/II source rock (Green River Shale sample) it occurs more or less 40°C earlier.

3.3 Hydrocarbon expulsion

3.3.1 Oil-source rock correlation

A pre-requisite for a migration study is certainty concerning the genetic relationship between the source rock analysed and petroleum found both in intraformational reservoirs of the source formation and in separate reservoir zones.

Oil - source rock correlation was attempted by comparing the distribution patterns of individual compound classes of the different source lithofacies to those of the two oils produced from the Formation A (Fig. 1) underlying the source rock formation in wells 17 and 8.

A comparison of the hopane fingerprint of different lithofacies occurring in the source rock formation in well 8 with the oil produced from Formation A in well 8 shows only a vague similarity. The most notable feature is the higher maturity of the produced oil as compared to the source rock samples (Figs. 17b, 98). Both oils showed a relatively high amount of C_{35} - homohopanes which, as stated above, are indicative of a carbonate depositional environment of the source rock.

The correlation between source rock bitumen and produced oil in Well 17 was slightly better. The oil from Well 17 is, as stated above, of lower maturity than the oil from well 8 and therefore fits better to the low maturity of the source rock (Fig. 99). The hopane fingerprint of the oil from Well 17 also fits quite well to the hopane distribution of certain source rock samples from Well 8. A comparison of the hopanes from a source rock sample and from the oil from Well 17 can be drawn from Figs. 17a and 99a.

The triterpane and sterane distribution patterns of laminites and solution seam/stylolite samples of wells 17 and 8, therefore, showed a high degree of similarity to the distributions found in the oil produced from the Formation A underlying well 17. The n-alkane distributions, CPI's and pristane/phytane ratios were also very similar. The total extract composition showed a higher amount of asphaltenes in the oils as compared to the bitumens from the source lithofacies. Except for the variation in the asphaltene content the source lithofacies of wells 4 and 8 compared very favourably to the oil produced from well 17.

The oil produced from the underlying reservoir strata in well 8 showed signs of higher maturity than the source rock. The n-alkane distribution of the oil was dominated by short chained hydrocarbons as compared to the more heavy-end dominated source rock extracts. Maturity estimations using biomarkers confirmed the assumed higher maturity, thus proving that the oil was generated at a higher maturity than present in the source rock of well 8. The predominance of C_{35} hopane indicated, however, that the oil was the product of a carbonate

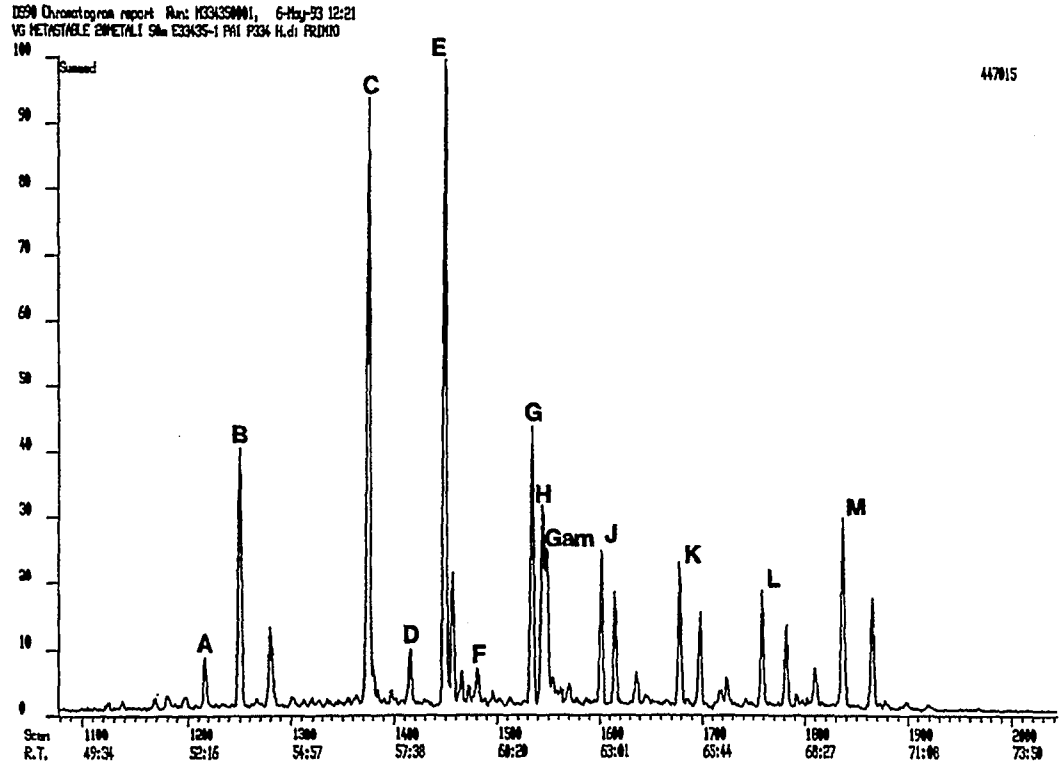

Figure 98a: Hopane distribution of the crude oil sample from well 8 E 33435. See appendix 1 for peak identification.

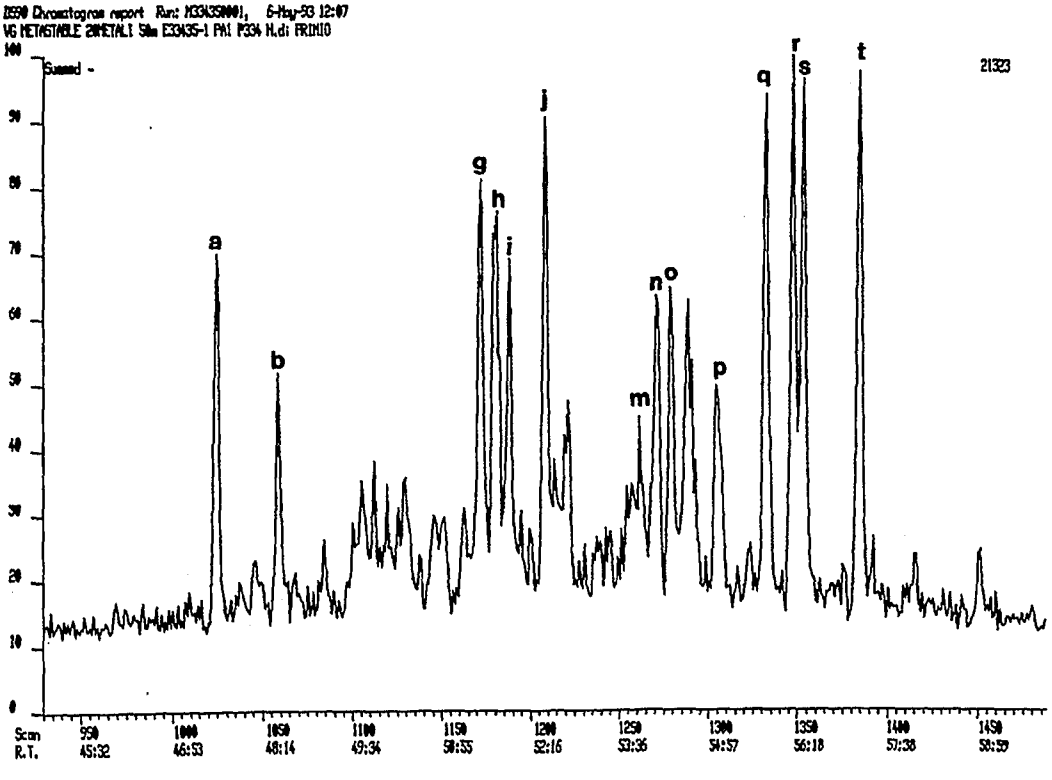

Figure 98b: Sterane distribution pattern of the crude oil sample from well 8 E 33435. See appendix 1 for peak identification.

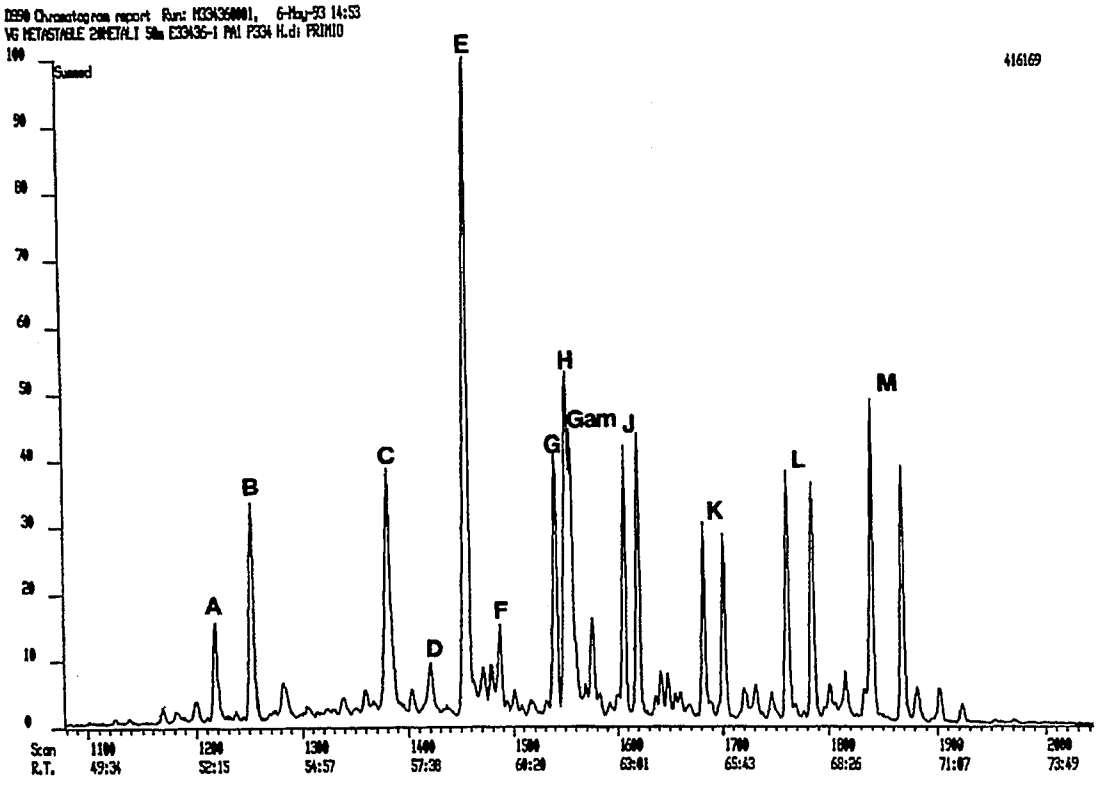

Figure 99a: Hopane distribution pattern of the crude oil sample from well 17 E 33456. See appendix 1 for peak identification.

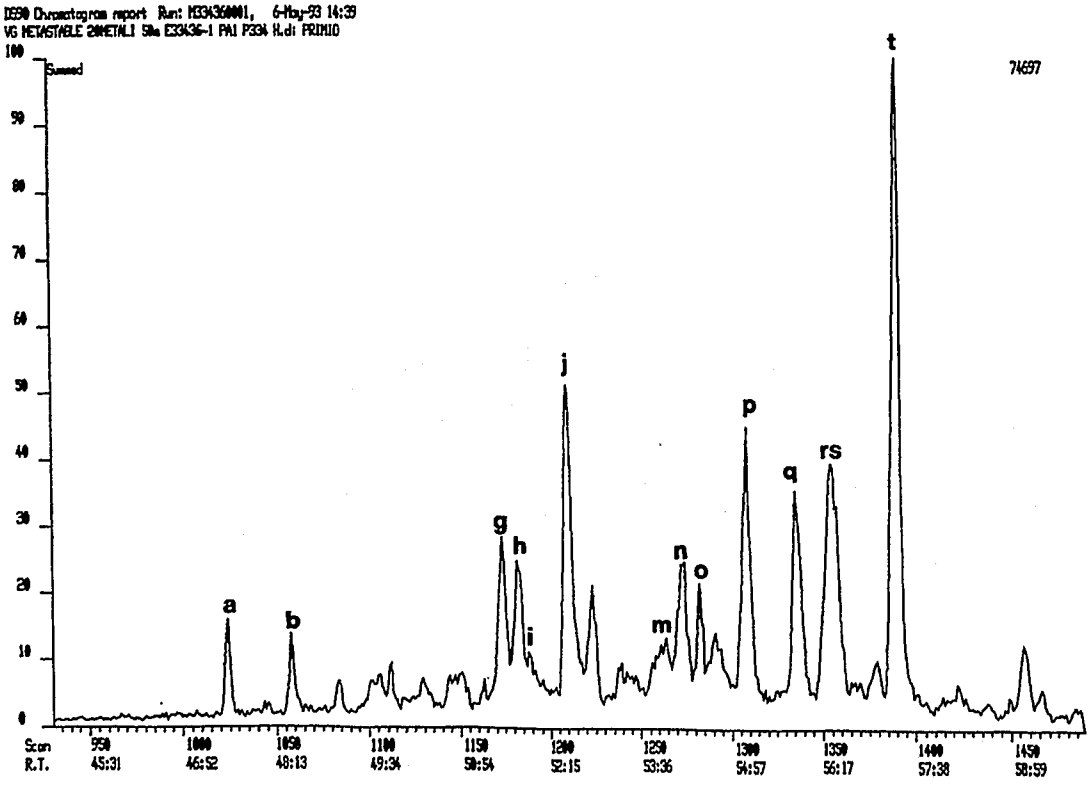

Figure 99b: Sterane distribution pattern of the crude oil sample from well 17 E 33456. See appendix 1 for peak identification.

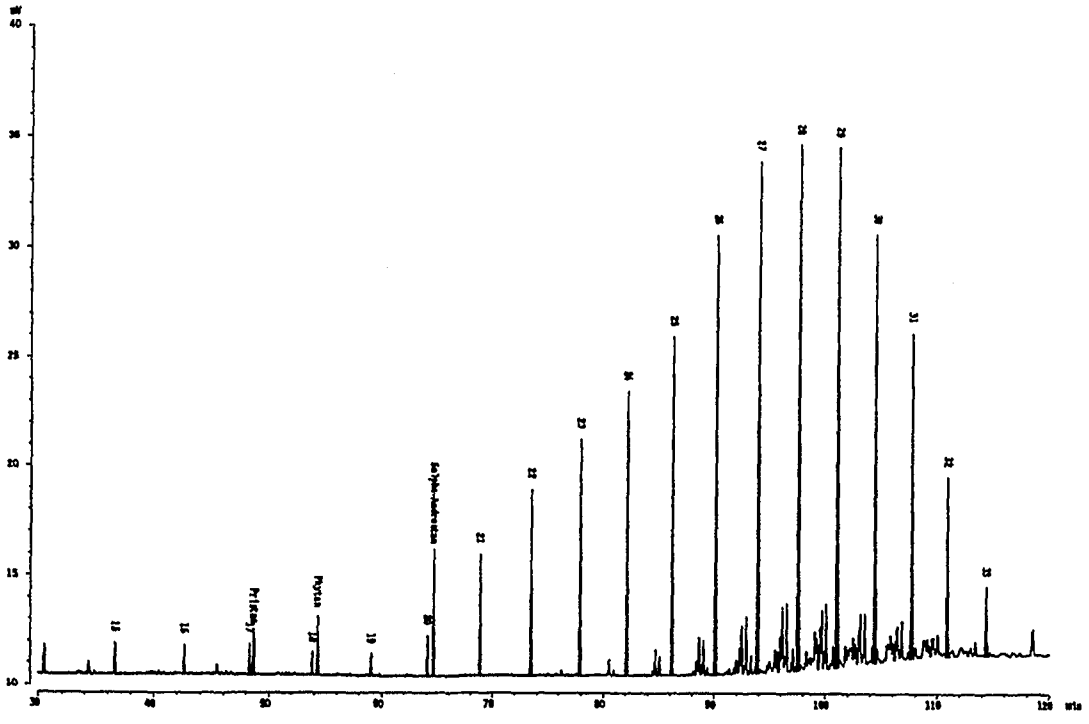

Figure 100: GC-trace of the saturated hydrocarbons of laminite sample E 33354, well 17, 1994 m. 5a-Androstane was added as an internal standard.

source rock. The source rock formation studied seems, therefore, to be present at a more advanced stage of hydrocarbon generation in deeper parts of the basin analysed in this study.
An excellent oil-source rock correlation was provided by kerogen and asphaltene PyGC of source rock and produced oil samples. The nearly identical n-alkyl distributions, especially of the produced oil from well 17 and the source rock kerogens and asphaltenes (Fig. 37), indicates the occurence of common precursors in the asphaltenes analysed.

3.3.2 Quantification of hydrocarbon expulsion from the source rock formation

The comparison of n-alkane contents of adjacent mudstone/wackestone and stylolite/solution seam samples can give insight into the type and efficiency of primary migration from pressure solution influenced layers (Leythaeuser et al., in press). The calculation of relative expulsion efficiencies (REE) for individual n-alkanes from the solution seam or stylolite portions can be performed if it is assumed that: a) the n-alkanes of the adjacent mudtone or wackestone, due to its impermeable nature, have experienced little or no expulsion, and b) the kerogen in matrix and solution seam or stylolite is of the same nature i.e. has generated identical amounts and distributions of compounds. Results of PyGC analyses corroborated this assumption. Pyrolysates generated from kerogen concentrates of mudstone and solution seam samples showed a large degree of bulk compositional similarity (e.g. Fig. 34, 37).

Leythaeuser et al. (1984a,b) showed that uniform n-alkane expulsion efficiencies with chain length are indicative of an oil phase migration mechanism, while decreasing n-alkane expulsion efficiencies with chain length point to migration by gaseous solution. REE calculations were performed for all mudstone or wackestone/solution seam (or stylolite) pairs. A contamination by wax was noticed in laminites and solution seams of well 17 by very high concentration of n-alkanes in the n-C_{20} to n-C_{33} range (Fig. 100). A wax coating seems to have been applied to fragile core segments in order to prevent disintegration. These samples were disregarded for SOM characterisations. Some samples from well 4 showed signs of impregnation by an oil of higher maturity. This was recognised by the calculation of hopane and sterane maturity parameters (see above).

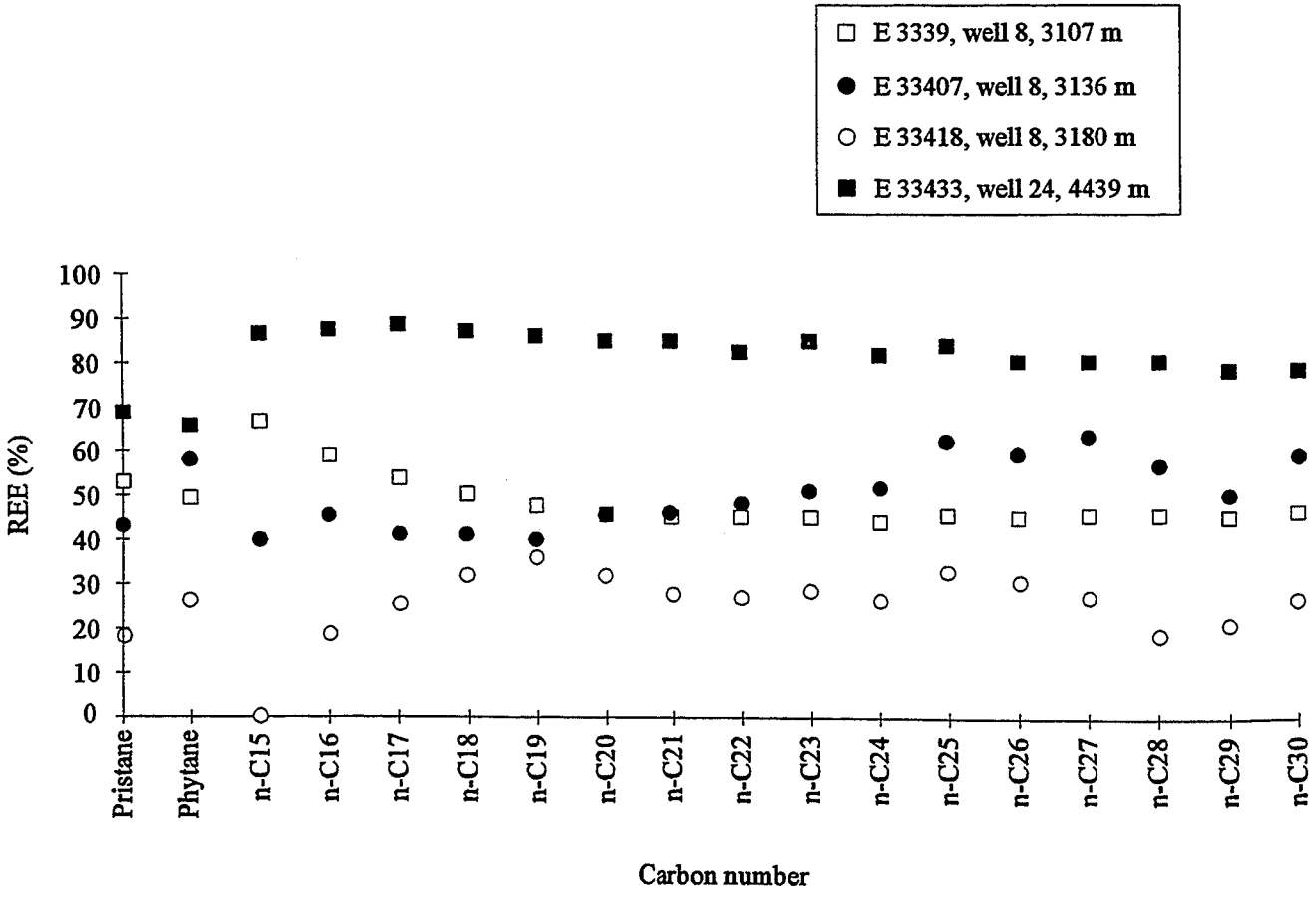

Figure 101: Relative expulsion efficiencies of individual n-alkanes and selected isoprenoids calculated for stylolite or solution seam samples from wells 8and 24.

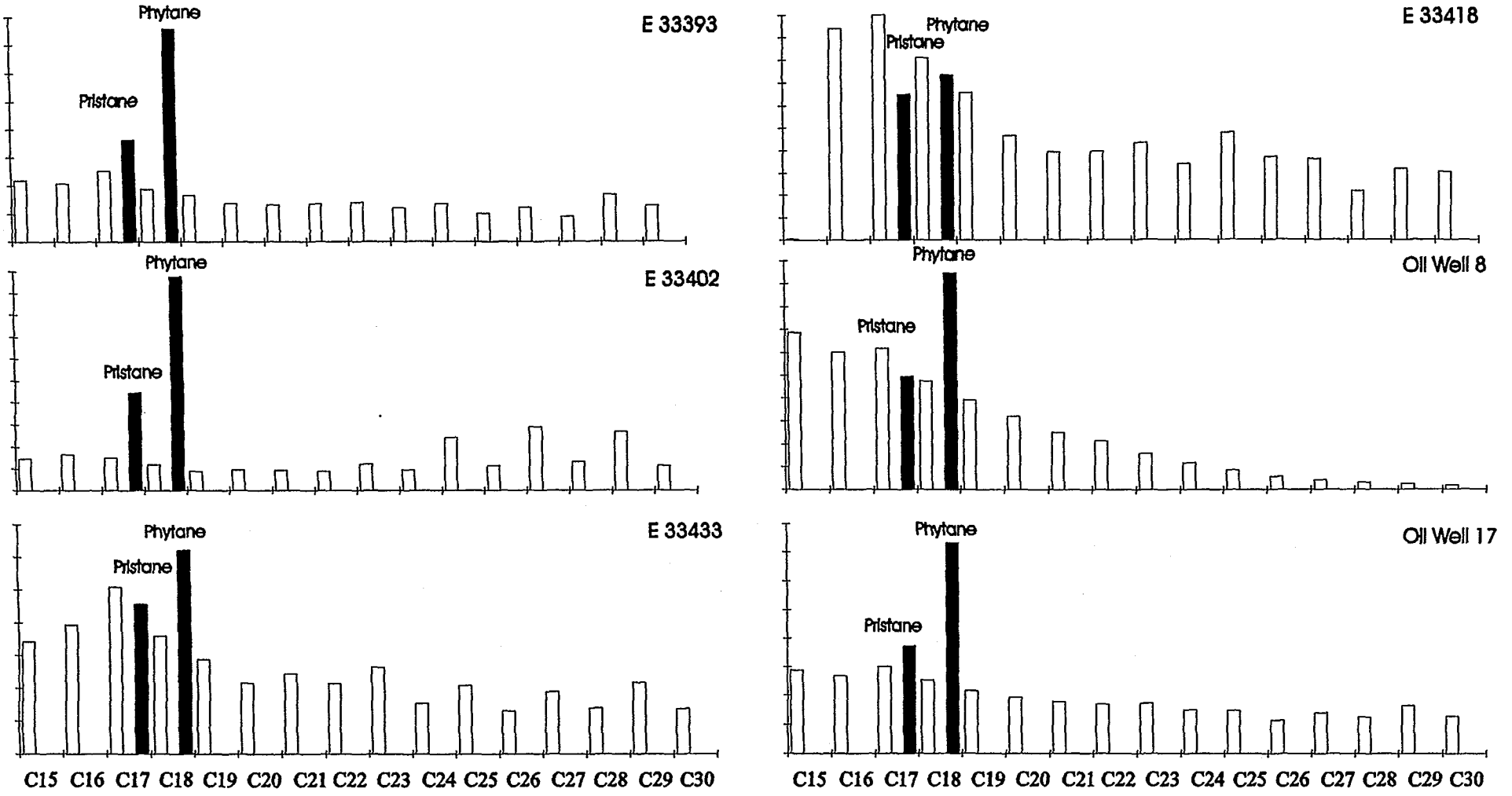

Figure 102: Composition of expelled oil calculated from REE data for selected stylolites and solution seams as compared to measured crude oil compositions.

Because of these problems only the matrix/solution seam sample pairs from wells 8 and 24 were used for REE calculation. These calculations lead to interesting observations: all sample pairs from well 8 showed more or less uniform REE values between 30 and 50 % for the n-alkanes (Fig. 101). Only one sample from well 24 was available for REE calculation, sample pair E 33431/1 (wackestone) and E 33431/2 (stylolite) was not taken into account since a clean separation of the wackestone from impregnated fractures occurring in the sample was impossible. The REE calculated for the samples E 33433 (mudstone and solution seam) revealed constant expulsion efficiencies of over 80 % for the n-alkanes and around 60 % for pristane and phytane (Fig. 101). The increase in expulsion efficiency from values around 40 % in well 8 (3150 m depth) to values over 80 % in well 24 (4500 m depth) is interpreted to be the direct consequence of the increase in burial (i.e. lithostatic pressure). The relatively constant REE values independent of chain length indicate oil phase migration.

The composition of the oil expelled from the stylolite or solution seam can be calculated by multiplying the individual compound content of the reference sample (the matrix sample) with the relative expulsion efficiency of the compound divided by one hundred. The calculated oil composition for each sample pair is shown in Fig. 102, in comparison with the measured compound distribution of the two oils analysed. Carbon preference values (CPI) as well as selected isoprenoid/alkane ratios and pristane/phytane ratios (ISO data) of the calculated oils is listed in Table 21. The calculated composition of the oils expelled from samples E 33393 and E 33402 shows a high degree of similarity to the oil produced from Well 17. The n-alkane and isoprenoid distributions are nearly identical (Fig. 102, Table 21). Calculated oils expelled from samples E 33418 and E 33433 have lower isoprenoid contents and are therefore, at least in this respect, more similar to the oil produced in Well 8 (Fig. 102). This latter oil has CPI values near unity indicating no carbon number preference (Table 21), while all calculated oils as well as the oil from Well 17 show an odd over even predominance. In this respect all calculated oil compositions from Wells 8 and 24 compare better to the relatively immature oil from Well 17 as compared to the petroleum produced from Well 8.

The high degree of similarity between the calculated oil composition (according to REE) and the composition of the produced oil from Well 17 demonstrate oil generation and expulsion has occurred from solution seams and stylolites of the wells analysed.

The restriction to the mudstones/wackestones and corresponding pressure solution features for expulsion efficiency calculation was dictated by the comparability of the organic matter. It was assumed in this case that pressure solution had lead to an enrichment of the same organic matter which is present in the mudstones and wackestones in solution seams and stylolites. The calculation of relative expulsion efficiencies for laminites and shales using carbonate matrix

samples as reference was also performed, but the results may be biased by different types of kerogen with different hydrocarbon generation characteristics. The REE values of laminites and shales exceed in all wells 95%, independent of carbon number. Therefore, if the laminites and shales have the same type of organic matter as the matrix samples, then they are the zones of the source rock which have experienced the most effective expulsion.

The average amounts of extract per gram TOC of all source lithofacies can also give an indication of the extent of petroleum expulsion. Lithologies which did not expel hydrocarbon can be expected to have higher extract contents. Carbonate mudstones and wackestones and laminite samples have the highest SOM contents while stylolites, solution seams and shales have the lowest contents (Table 6). The amount of extract present in the sample seems, therefore, to depend on the amount of carbonate of the lithofacies, i.e. carbonate poor sections have probably expelled hydrocarbons to a higher degree. This interpretation is indirectly consistent with the observation of increasing relative expulsion efficiency with depth. Intervals of the source rock which are capable of compaction are more liable to be able to expel hydrocarbons than intervals where the carbonate minerals create a supporting structure which impedes compaction.

These results indicate that at the stage of maturity and burial of the source rock studied here only stylolites, solution seams and shales have experienced significant hydrocarbon expulsion. The efficiency can be assumed to lie between 30 and 80 % for the n-alkanes depending on the sample depth. Relative expulsion efficiencies for the shales, calculated using the average extract content of the matrix samples as reference and the average extract content of the shales for the depleted sample, gave values around 70 %.

3.3.3 Mechanism and efficiency of petroleum expulsion as derived from experimental simulation

The results from experiments # 1, # 3, # 4 and # 5 indicate that the expulsion of petroleum occurs mainly due to the compaction of the source rock. Kerogen can be assumed to show a plastic behaviour under high pressures, in the same way as coal does (van Krevelen, 1961; Gretener, 1979) and can be supposed to undergo deformation under lithostatic stress (Ungerer et al., 1983). The lithostatic stress is transmitted to the mobile bitumen generated upon kerogen conversion and causes its expulsion (Du Rouchet, 1981) along the pore system or through microfractures. Ropertz (1994) describes the mechanism of petroleum expulsion in the natural system in a similar manner. He states that the pore system of a kerogen-rich source rock is a dynamic system which actively changes during catagenesis due to kerogen conversion and bitumen generation. Thus, the vertical volume reduction observed in experiments # 4 and #

5 can be assumed to be an effect of kerogen conversion and petroleum expulsion accompanied by a reduction of porosity driven by lithostatic pressure. The same effect was probably responsible for hydrocarbon expulsion in experiment # 1 and # 3. In this case the source rock compaction could not be monitored because it occurred parallel to the vertical axis of the core, where core length measurements were not possible.

The main factor impeding petroleum expulsion is the rigidity of the rock. Solution seams with a relatively high proportion of carbonate are not as effective expulsion pathways as carbonate poor shales as was shown by the experiments # 3 and # 5. The carbonate grains build a framework in the source rock which seems to be capable of withstanding the lithostatic pressure, thus impeding compaction and porosity reduction.

High pressure was seen to inhibit kerogen conversion in experiment # 3 as compared to experiment # 2. In this respect Cecil et al. (1977) noted that, because hydrocarbon generation reactions are volume expansion reactions, according to the Le Chateliers principle, pressure increases should retard hydrocarbon generation. Price and Wenger (1992) concluded, based on a series of hydrous pyrolysis experiments, that increasing static fluid pressure greatly retarded all aspects of organic metamorphism, including hydrocarbon generation, maturation and thermal destruction. Dominé and Enguehard (1992) stated that an increase in fluid pressure causes a shift towards higher activation energies for the hydrocarbon-thermal-destruction reactions.

The very similar compound class distributions of source rock extract and reservoir oil in experiments # 3, # 4, and # 5 indicate that under the conditions applied oil phase migration without any recognisable fractionation effects had taken place. The migration of sulphur-rich asphaltic petroleums is commonly assumed to be hindered by the high viscosity of the liquid phase (Tissot and Welte, 1984; England et al., 1987). The permeability experiment with the oil from well 17 indicated however, that migration of heavy oil through low permeability carbonate rocks is feasible.

The fact that overburden pressure is the driving force for petroleum expulsion from clay-rich source rocks was demonstrated by experiment # 5. During this process fluid pressure in the source rock must increase and in some cases possibly even almost reach lithostatic pressure. Thus, fluid overpressures must occur during compaction-driven primary petroleum migration.

The increasing expulsion efficiency with increasing carbon chain length noticed for the n-alkanes in experiments # 3, # 4, and # 5 (Fig. 77) are difficult to explain. Especially, the observation that expulsion efficiencies increase again below n-C_{17} in experiments # 2, # 3, and # 5 presents an interesting question. Since a preferential expulsion of long chain compounds (in the case of experiment # 4) or mainly long chain and certain short chain compounds (in

experiments # 2, # 3, and # 5) is chemically unsustainable, other reasons must be found to explain the observations.

The n-alkane distribution of oils generated at increasing temperature steps was seen to change systematically in the open-system-hydrous-pyrolysis experiment (OSHP) performed in this study. The absolute amounts of n-alkanes generated at each temperature also showed a temperature dependence (Chapter 2.1.8.1). These observations can be used to explain the expulsion behaviour observed in the experimental simulations discussed above.

In the experimental set-up described above a source rock sample was put into direct contact to an empty reservoir. During pyrolysis a petroleum phase was generated, which at a certain point, was expelled into the reservoir. This expulsion is never complete, i.e. a certain amount of the generated compounds remains in the source rock. The expulsion of petroleum is supposed to begin when the pore space of the source rock is saturated with oil to a certain degree. The amount of saturation is still a topic of discussion, but a threshold value of 25% seems to be widely accepted (Ropertz, 1994 and references therein). As stated above, the composition of the generated petroleum changes with maturity. Therefore, petroleum which is expelled from the source rock at a later maturity stage will have a different composition as compared to the products generated at an earlier stage.

This evolution of the composition of petroleums generated at increasing temperature increments is responsible for the expulsion efficiency variations with n-alkane chain length noticed in the experiments # 3, # 4, and # 5. In detail, the following evolution of events is considered:

a) The initial step assumes that the products generated at an early maturity stage are expelled in an oil phase (i.e. without fractionation) with an efficiency of 50 %. This expulsion efficiency value is arbitrary and will be maintained throughout the following calculations. The n-alkane distribution of the oil generated and expelled at a temperature of 230°C (with a relatively high content of long chain n-alkanes) in the OSHP experiment (see chapter 2.1.8.1) is assumed to be representative for an early generated petroleum. In this first stage of expulsion the n-alkanes remaining in the source rock and expelled into the reservoir are exactly identical.

b) At higher temperatures a new petroleum phase is produced in the source rock. This phase will probably have a slightly different composition, with higher proportions of short chain n-alkanes, similar to that of the oil produced at the temperature of 240°C or 250°C during the OSHP experiment. This newly generated oil mixes with the residual oil in the source rock and a part of this mixture (50%) is then expelled. The oil of the second expulsion stage mixes with the oil present in the reservoir. The oil in the reservoir now begins to reveal differences in its n-alkane distribution as compared to the residual oil in the source rock.

c) Due to the mixing of residual and newly generated oil in the source rock and to the partial expulsion of this mixture a certain portion of the first residual oil is also expelled from the source rock. The reservoir oil contains thus a higher amount of the first generated oil (with a higher proportion of long chain n-alkanes) than the source rock. This leads to a relative enrichment of long chain n-alkanes in the reservoir. The calculation of expulsion efficiencies using n-alkane concentrations after expulsion then confirms this effect.

The expulsion model explained above was used to calculate expulsion efficiencies for 13 generation stages using the n-alkane data from the OSHP experiment. An overview of the change in n-alkane composition with increasing temperature is shown in figure 103, where the n-alkane distributions of every second heating step of OSHP are presented. The fact must be emphasised that absolute n-alkane concentrations were used for this calculation, that is, the effect of the temperature dependant variation of hydrocarbon generation rates was also taken into account. The calculated expulsion efficiency distributions of the individual n-alkanes using a mean expulsion efficiency of 50% in each step (that is: half of the products present in the source rock are expelled) are shown in Fig. 104.

In Fig. 104 the first generation/expulsion cycle (230°C distribution) leads to a homogeneous distribution of n-alkanes in both reservoir and source rock. In the second cycle the effect of mixing and expulsion leads to the calculated expulsion efficiency shown in the 240°C distribution. At increasing temperature steps ever greater amounts of short chain n-alkanes are generated and expelled so that the relative difference in amounts of n-alkanes in reservoir and source rock decreases due to dilution of the first petroleums generated and expelled. The calculated expulsion efficiencies are therefore more homogeneously distributed (330°C-350°C distributions). The relative increase in short chain n-alkane expulsion efficiency at 340°C and 350°C is due to the generation of long chain n-alkanes at this temperature (decrease of LHCPI shown in OSHP chapter, Fig. 59).

A similar scheme for the evolution of fractionation effects between expelled and residual hydrocarbon mixtures was presented by Leythaeuser et al. (1984a). The model presented here is, however, based on measured n-alkane concentrations which provide a more reliable basis. The results of the present model indicate also that the assumptions from which the scheme of Leythaeuser et al. (1984a) was derived were correct.

One can of course argue that this "preferential expulsion of long chain n-alkanes" is only an artefact due to the arbitrary assumption that 50% of the products present in the source rock are expelled. It is well known that the expulsion efficiency increases with increasing generation rates, so this effect should also be included into the calculation.

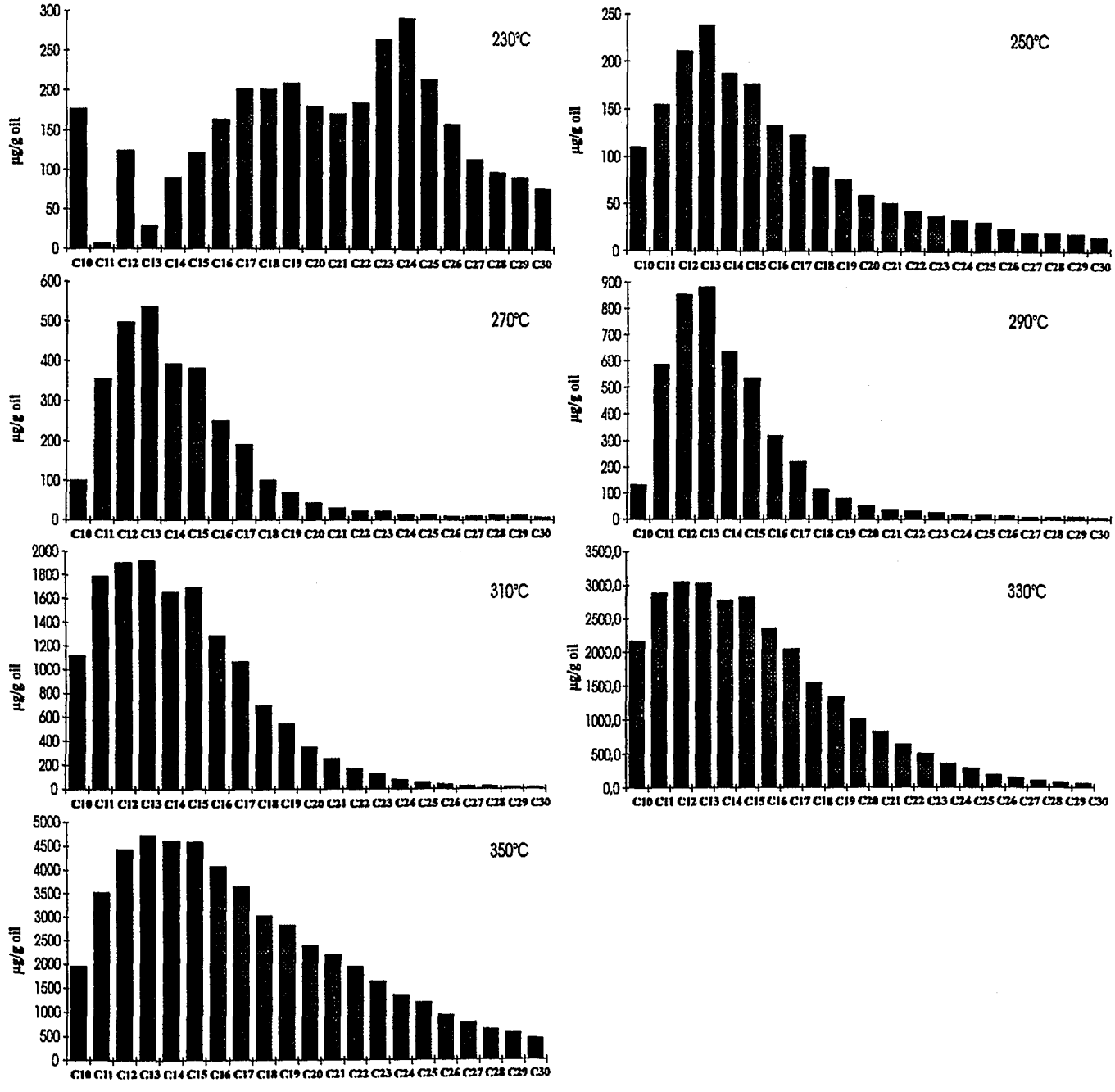

Figure 103: Distribution of n-alkanes in the pyrolysates generated during OSHP. Every second temperature step is shown in this figure.

An increase in the proportion of products expelled with increasing hydrocarbon generation rate was modelled using the same data as above. The calculation started with the assumption that in the first generation/expulsion cycle half of the products present in the source rock were expelled. In the second cycle 2/3 were expelled, in the third cycle 3/4, in the fourth 4/5 and so on up to the ninth cycle where 9/10 were expelled (i.e. 90% expulsion efficiency). The following cycles were also calculated with 90% expulsion efficiency. The results of this calculation are shown in Fig. 105. Here again the enhanced expulsion efficiencies of long chain n-alkanes for the low temperature distributions are clearly visible. The effect of maturity and increasing expulsion efficiency leads, in this case, much faster to a dilution and homogenisation of the calculated n-alkane expulsion efficiencies at higher temperatures. Thus the observed variation in calculated expulsion efficiency with chain length is a feature which seems to be typical of early hydrocarbon expulsion. Nevertheless, the model simulates in great detail some of the effects observed during the experimental simulation of petroleum generation and expulsion using natural source rock cores.

The enhanced expulsion efficiencies of short chain n-alkanes in experiments # 2, # 3, and # 5 cannot be explained by the model described above. Enhanced expulsion efficiencies with decreasing chain length were already observed by Leythaeuser et al. (1984a,b) and attributed to migration by gaseous solution. In the experiments presented here gaseous solution is probably not a key factor of migration since the maximum temperature of the experiments was well below the main temperature of gas generation as monitored by OSHP.

The compaction curves monitored during experiments # 4 and # 5 may help in explaining the anomalous expulsion efficiencies of the source rocks. The main phase of compaction starts immediately after the thermal expansion of the core and lasts approximately 20 hours (Fig. 79, 80). During the following 52 hours the source rock samples continue to compact but at a much lower rate. As stated above, the source rock compaction is directly linked to hydrocarbon expulsion, so it can be assumed that the main phase of expulsion also occurs during these initial 20 hour period. A certain balance between the expelled products and those retained in the porosity of the source rock is then reached. The decrease in compaction rate can be attributed to two processes. The first is that the available pore space has been almost completely destroyed and thus compaction stops. The second is that the fluid pressure in the system increases, due to hydrocarbon generation and porosity reduction due to compaction, until it equals the lithostatic pressure and inhibits further compaction. The second explanation seems more probable since relatively large amounts of pyrolysate were extracted from the compacted sample, indicating the existence of sufficient porosity in the rock after compaction.

If a pressure equilibrium is reached between lithostatic and fluid pressure, oil phase movement must come to an end due to the lack of pressure gradients in the system. This stage can be assumed to be reached after more or less 20 hours in the experiments performed in this study. During the remaining 52 hours molecular diffusion could possibly lead to the enhanced expulsion efficiencies observed for short chain n-alkanes in experiments # 2, # 3, and # 5. The model for calculating expulsion efficiencies described above showed that at low maturities large differences exist between the residual oil remaining in the source rock and the oil in the reservoir. The model calculated that the oil in the source rock contained higher amounts of short chain n-alkanes as compared to the reservoir oil. Molecular diffusion could possibly lead to a homogenisation of the more mobile short chain n-alkane contents in the source rock-reservoir system. The more mobile short chain molecules would thus show enhanced expulsion efficiencies as compared to the lesser mobile compounds.

The final step in the experimental simulation of hydrocarbon generation and expulsion experiments must always be the comparison of the expelled pyrolysate to an oil from the natural system. Figure 106 shows this comparison for the n-alkane distributions of the pyrolysate generated and expelled in experiment #3 and the oil produced from the reservoir strata underlying well 17. The agreement between both n-alkane distribution patterns is amazing, the only slight discrepancy is noticeable in the chain length range of n-C_{25} to n-C_{30}. The experimental approach used in this study seems, therefore, to be adequate for simulating the generation and expulsion of petroleum from this source rock.

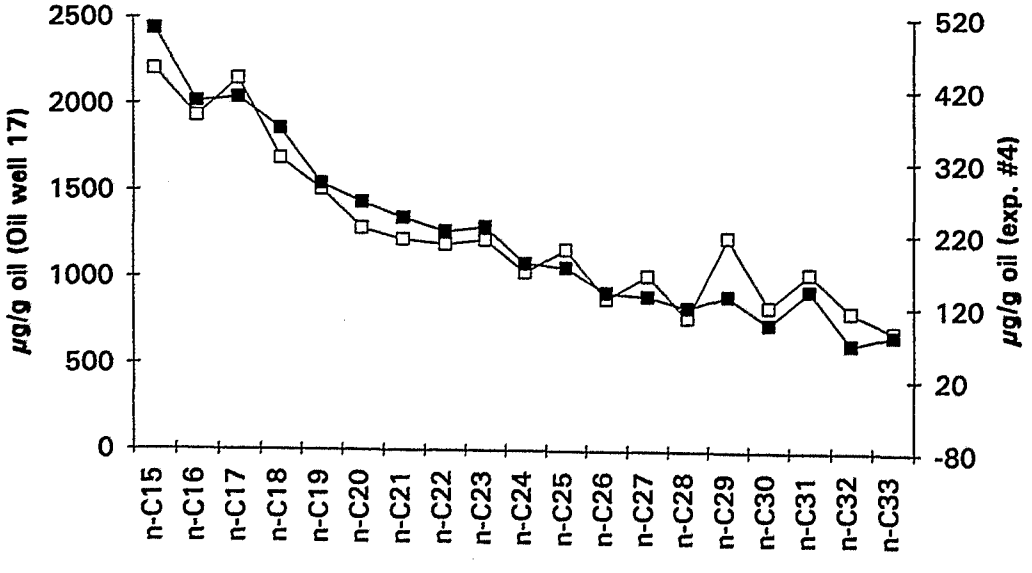

Figure 106: Comparison of the n-alkane distribution of the expelled pyrolysate of experiment #4 to the n-alkane distribution of the crude oil from well 17.

The results of this series of experiments indicate that, for the source rock formation studied here, hydrocarbon expulsion efficiency depends on overburden pressure and the degree to which the sediment can be mechanically compacted. Shale-rich layers are thus the zones where the largest amount of expulsion must have taken place. Petroleum expulsion occurs in oil phase without any fractionation effects. Differences in the n-alkane distribution of expelled and retained oils were demonstrated to be due to the mixing of oils of different maturity. Hydrocarbon generation is hindered by increasing fluid pressures, which themselves occur only in closed systems (such as the source rock - reservoir system of the experiments).

3.4 Mass balance of early petroleum generation and expulsion of the source rock formation

The temperature of maximum petroleum generation of the heavy oil, as estimated from OSHP, can not be directly used for modelling the onset of generation (in this context "generation" means HC-generation by S-C bond cracking) in the basin analysed in this study. As stated before, the shale samples (and stylolite/solution seam samples) can be assumed to have suffered hydrocarbon expulsion (Chapter 3.3.2). The sample analysed by OSHP was a shale sample, therefore the organic matter present in it must have already generated and expelled a certain amount of compounds. Schaefer et al. (1990) demonstrated, in a kinetic study of Posidonia Shale samples of increasing maturity, that the activation energy distribution of samples of increasing maturity is shifted towards higher mean activation energies and lower hydrocarbon potential. The kinetic data derived from the OSHP sample represents therefore only the residual potential present in the remaining organic matter after initial hydrocarbon generation and expulsion.

The surface area under the first reaction in the hydrocarbon generation curve of OSHP (Fig. 55) was quantified as 15 % of the total area. At this point the reliability of the data presented as a hydrocarbon generation curve in the OSHP chapter must be discussed. The products which were sampled during OSHP represented that portion of the generated pyrolysate which had also been expelled from the source rock. Generation and expulsion can be expected to be synchronous processes (Lewan, 1992), that is once petroleum expulsion has started it will continue as a function of the generation rate. This description of hydrocarbon generation and expulsion is in concordance with the models and theories of Cooles et al. (1986), Mackenzie and Quigley (1988), Ungerer et al. (1992), and Ropertz (1994), which are all based on the assumption that a certain amount of the pore space available in the source rock must be saturated by oil or gas before expulsion can take place. Once this threshold value is reached the amount of compounds expelled depends only on the amount generated. Therefore the amounts of pyrolysate expelled (and sampled) during OSHP must reflect the generation rate of the source rock during heating. Thus the data calculated from the "generation curve" of OSHP is assumed to be directly comparable to the true hydrocarbon generation characteristics of the source kerogen.

The value of 15 % for the S-C bond cracking reaction was calculated as a proportion of the total pyrolysate generated. If it is assumed that the conversion rate of the kerogen throughout maturation is 70 % (data of Schenk et al., 1990, for an alginite). The total amount of pyrolysate generated amounts roughly to 70 % of the TOC. Relative to the total organic carbon the S-C bond cracking reaction comprises therefore around 10 %.

This value of 10 % represents the residual potential present in the source rock at the present stage of maturity. An estimation of the initial potential is performed in the following by a series of assumptions and calculations, which are not expected to deliver an exact value, but rather an aproximation of the original kerogen composition.

The degree of hydrocarbon expulsion had been stated to lie between 30 and 80 % for the n-alkanes depending on the burial depth of the sample analysed. Total extract data indicated, on the other hand, that an average of 70 % of the bitumen generated in the shale samples had been expelled (chapter 3.3.2). For this mass balance calculation an intermediate expulsion efficiency value of 50% is assumed for the sample from well 8 analysed by OSHP which delivered the data for the entire calculation.

Since the amount of petroleum expelled was not part of the organic matter when TOC was measured, the proportion expelled (50%) must be added to the bitumen yield of the shales in order to calculate the original yield generated. Based on the average SOM yields of shale samples (roughly 100 mg/gTOC, Table 7) the original SOM content should have been around 200 mg/g TOC. The original extract amount before expulsion thus reaches roughly 20 % of the TOC. It must be kept in mind that TOC wt. % and bitumen weights are not directly comparable due to differences in density, but for reasons of simplification this fact is disregarded in this calculation.

More or less 20 % of the original TOC of the sample were therefore generated prior to OSHP. The residual potential was calculated as being 10 %. Calculation of the total potential of the original TOC of the sample (total potential=100/(residual potential+expelled proportion+ residual TOC)*(expelled proportion+residual potential), that is =100/(10+20+90)*(20+10)) leads to a value of 25 %. Approximately one quarter of the original kerogen may therefore be converted at a relatively low thermal stress.

According to this calculation (based on a series of assumptions and simplifications) almost two thirds of this reaction seem to already have taken place in the source rock analysed in this study, therefore the activation energies calculated from the degradation of the residual organic matter are surely too high. In the maturation study performed by Schaefer et al. (1990) the difference in main activation energy between an immature sample (Wenzen, 0.48 %Ro) and that of a sample which represented the maturity stage of peak oil generation (Harderode, 0.88 %Ro) was 4 kcal. A comparable shift of the main activation energy (i.e. 4 kcal/mol lower activation energy than derived from OSHP) probably did not occur between the original organic matter and the residual portion present in the source rock at date, because the reduction in hydrocarbon potential between the Wenzen and Harderode samples (Schaefer et

al., 1990) was much larger than between the original and residual portion of the sample analysed here.

If it is assumed that two thirds of the reaction have already taken place, and that the residual potential is representative of one third, then the distribution of the missing potential in the form of a gaussian distribution including the present potential leads to a lowering of the main activation energy of the total heavy oil generation reaction by 1 kcal/mol as compared to the residual potential. Thus, by using an activation energy of 53 kcal/mol and the pre-exponential factor of $3.03*10^{18}$ (1/min) the temperature of maximum heavy oil generation is calculated to lie between 99°C and 118°C for the three geological heating rates depicted in Fig. 107. These temperatures are more or less 30-40°C lower than those calculated by Schaefer et al. (1990) for Posidonia Shale samples. Fig. 107 also shows the geological temperatures of maximum petroleum generation calculated from the dominant activation energy of kerogens and asphaltenes analysed in this study together with other well known source rocks, as well as the temperature of maximum heavy oil generation as estimated by multistep PyGC and OSHP.

The homogenisation temperatures measured on aqueous fluid inclusions on the other hand, indicated that the source rock formation has been subjected to much lower maximum temperatures of 75°C as compared to the temperatures calculated from kinetic data. The tectonic history of the region, especially the overthrusting of the source rock in the locations of wells 8 and 24, may have caused the fluid inclusion decrepitation. In this case the leakage of the inclusions would not have been due to an increase in the internal fluid pressure because of temperature increase, and therefore the temperatures monitored by fluid inclusion homogenisation temperatures would be erroneously low.

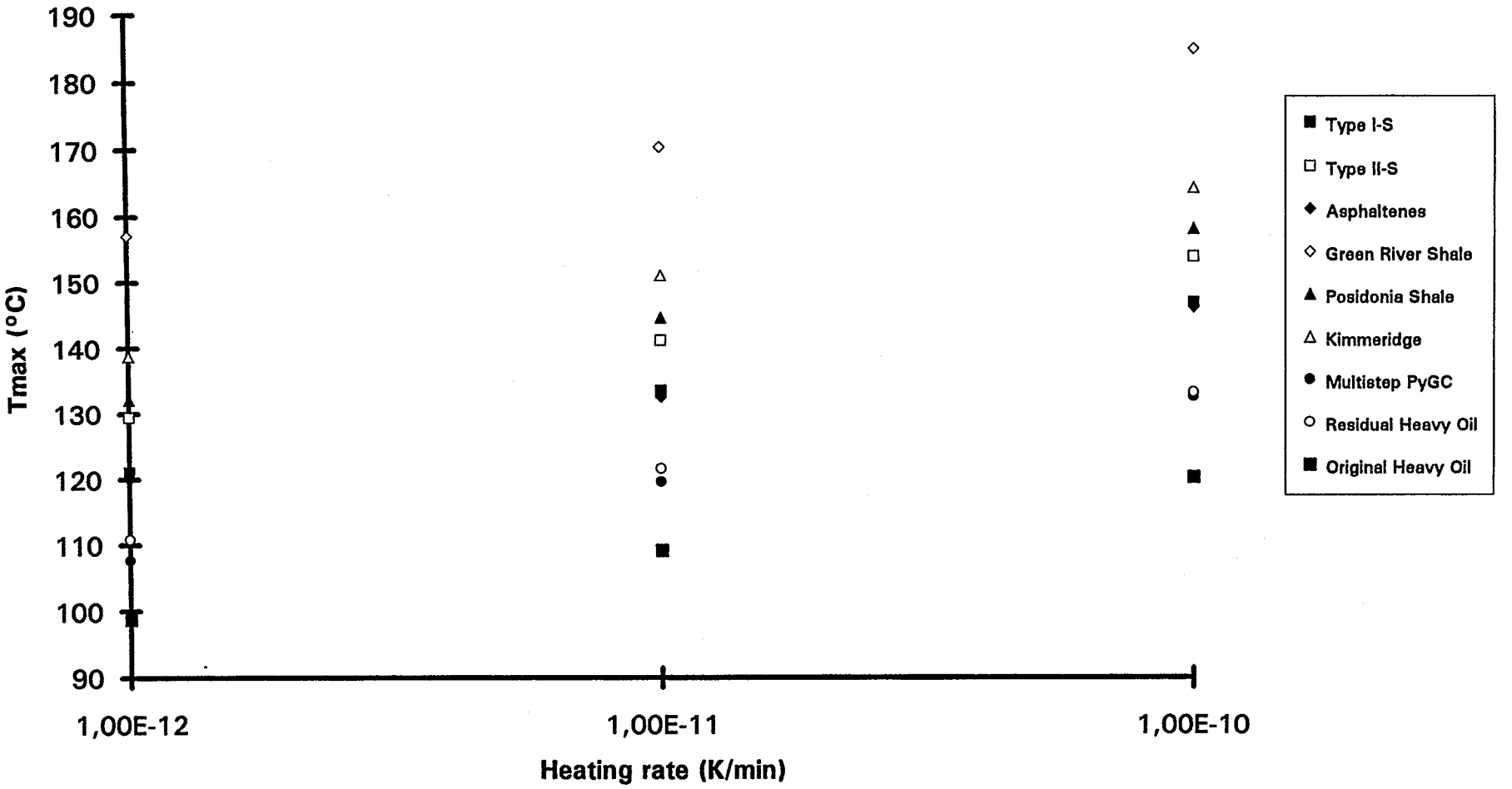

Figure 107: Temperatures of peak hydrocarbon generation versus geological heating rates for kerogens Type I-S, II-S, asphaltenes, MS-PyGC, OSHP and literature data.

4 Conclusions

The source rock formation studied was deposited in a tidal flat environment. The four main lithofacies are carbonate mudstones and wackestones (sometimes containing stylolites and solution seams, and including carbonate laminites), laminites (argillaceous laminites), shales and dolomites (dolostones and dolomitic breccias). The mudstones and wackestones were deposited in a subtidal, oxic (limestones) to anoxic (carbonate laminites) environment. Argillaceous laminites and shales were deposited in the intertidal zone, whereas dolomites are characteristic of the supratidal zone.

The organic matter present in the source rock formation is of a sulphur-rich and hydrogen-rich nature (kerogen types II-S to I-S). The main sources of organic matter were cyanobacterial mats and, subordinately, algae and liptodetrinites. Bacterial degradation of the original organic matter led to the formation of a kerogen type I-S in most of the shale samples.

The source rock formation is of comparable, low maturity in all wells analysed. The maturity of the source rock formation did not exceed 0.5 % Ro in any of the wells analysed. A slight increase of maturity with depth was recognised from well 17 to well 4 (6.5°C increase in the average Tmax, increase in the MDR 4 ratio).

Despite the low maturity hydrocarbon generation has already occured in the source rock formation analysed. Approximately 20% of the available organic matter of the source rock formation has been converted to petroleum at this low maturity.

This generation of hydrocarbons at low maturity is due to the cleavage of carbon-sulphur bonds at low levels of thermal stress. The proportion of the kerogen interlinked by sulphide bonds, and thus liable to be cracked at relatively low levels of thermal stress, was calculated to be approximately 25%. The mean activation energy for the C-S bond cleavage reaction was determined as 53 kcal/mol and a pre-exponential factor of $3*10^{18}$ (1/min). The temperature of maximum hydrocarbon generation by this cleavage reaction lies around 110°C for a heating rate of 0.53 °C/Ma.

The asphaltenes present in the soluble organic matter of the source rock formation are the product of early petroleum generation by C-S bond cleavage. Asphaltenes of primary nature,

according to Powell (1984) and Sinninghe Damsté et al. (1989), were not encountered in the source rock formation.

The source rock studied was correlated by GCMS and PyGC to the oils produced from the reservoirs in Formation A, underlying the source rock in wells 17 and 8. Especially the petroleum produced in well 8 was of higher maturity than the source rock, so that a higher maturity equivalent must be postulated at greater depth.

Stylolites, solution seams and shales were recognised to be the main portions of the source rock which have expelled hydrocarbons. The relatively small proportion of stylolites and solution seams in the source rock as compared to the shale lithofacies indicates that the shales are the main source lithology in the formation analysed.

Oil expulsion occured as an oil phase without fractionation effects, along stylolites, solution seams and shales and into fractures. Oil expulsion was driven by the overburden pressure and reached relative expulsion efficiencies of 30 to 80 % for the n-alkanes in stylolites and solution seams as a function of burial depth. Shales showed average expuslion efficiencies of 70 % for the SOM.

The results of experimental simulation of hydrocarbon generation and expulsion indicated that hydrocarbon expulsion efficiency depends on the overburden pressure and on the degree to which the sediment can be mechanically compacted. Shale layers are thus the zones where the largest amount of expulsion must have taken place.

Hydrocarbon generation was noticed to be hindered by increasing fluid pressures in the closed system of the experimental simulation.

Differences in the n-alkane distribution of expelled oils and oils remaining in the source rock were modelled and demonstrated to be due to the mixing of oils of different composition generated at increasing maturities.

Analysis of organic sulphur compounds (OSC) generated by PyGC and MSSV led to interesting insights. The ratio of 2,3-DMT/2,3,5-TMT, for example, measured by PyGC and MSSV may prove to be an indicator of palaeosalinity, since it is sensitive to changes in the depositional setting and remains fairly constant throughout artificial maturation. The ratio of

OSC with linear carbon skeletons to OSC with steroidal carbon skeletons may be used as a measure of the degree of bacterial reworking of the originally deposited organic matter. The ratio of Isoprpyl-methylthiophene to 2,3,4-TMT may be applicable for maturity estimation by pyrolysis-GC since it shows a strong increase with increasing artificial maturation whereas it is uninfluenced by facies.

5 References

Alexander, R., Kagi, R.I., and Sheppard, P., 1984, 1,8-dimethylnaphthalene as an indicator of petroleum maturity, Nature, v. 308, p. 442-443.

Alexander, R., Kagi, R.I., Rowland, S.J., Sheppard, P.N., and Chirila, T.V., 1985, The effects of thermal maturity on distributions of dimethylnaphthalenes and trimethylnaphthalenes in some ancient sediments and petroleums, Geochimica et Cosmochimica Acta, V. 49, p. 385-395.

Aquino Neto, F.R., Trendel, J.M., Rstle, A., Connan, J., Albrecht, P.A., 1981, Occurence and formation of tricyclic and tetracyclic terpanes in sediments and petroleums; Advances in Organic Geochemistry 1981, p. 659-667, John Wiley & Sons Limited, 1983.

Barnard, P.C. and Cooper, B.S., 1981, Generation of hydrocarbons - time, temperature and source rock quality, in: 5th International Palynological Conference, Cambridge.

Barth, T., Borgund, A.E., and Hopland, A.E., 1989, Generation of organic compounds by hydrous pyrolysis of Kimmeridge oil shale - Bulk results and activation energy calculations, Organic Geochemistry, Vol. 14, No. 1, p.69-76.

Baskin, D.K., and Peters, K.E., 1992, Early generation characteristics of a sulphur-rich Monterey kerogen, American Association of Petroleum Geologists Bulletin, V. 76, No. 1, p. 1-13.

Boon, J.J., Hines, H., and Burlingame, A.L., 1983, Organic geochemical studies of Solar Lake laminated cyanobacterial mats, Advances in Organic Geochemistry 1981, John Wiley & Sons Limited, 1983, p. 207-227.

Bostick, N.H., Cashman, S.M., McCulloch, T.H., and Wadell, C.T., 1978, Gradients of vitrinite reflectance and present temperature in the Los Angeles and Ventura basins, California, in: D.Oltz (Ed.) Low temperature metamorphism of kerogen and clay minerals: SEPM Symposium in Geochemistry, p. 65-96.

Bray, E.E. and Evans, E.D., 1961, Distribution of n-paraffins as a clue to recognition of source beds, Geochimica et Cosmochimica Acta, V. 22, p. 693-696.

Brosse, E., Riva, A., Santucci, S., Bernon, M., Loreau, J.P., Frixa, A. and Laggoun-Défarge, F., 1989, Some sedimentological and geochemical characters of the late Triassic Noto formation, source rock in the Ragusa Basin (Sicily), Organic Geochemistry, Vol. 16, Nos. 4-6, p. 715-734.

Burne, R.V. and Moore, L.S., 1987, Microbialites: Organosedimentary deposits of benthic microbial communities, SEPM Publication, Palaios, v. 2, p. 241-254.

Burnham, A.K., Clarkson, J.E., Singleton, M.F., Wong, C.M., and Crawford, R.W., 1982, Biological markers from Green River Shale kerogen decomposition, Geochimica et Cosmochimica Acta, Vol. 46, p. 1243-1251.

Burnham, A.K., R.L. Braun, and A.M. Samoun, 1988, Further comparison of methods for measuring kerogen pyrolysis rates and fitting kinetic parameters: *in* L. Mattavelli and L. Novelli, eds., Advances in Organic Geochemistry 1987: Oxford, Pergamon Press, Org. Geochem., v. 13, p. 839-845.

Burrus, R.C., 1987, Diagenetic paleotemperature from aqueous fluid inclusions: re-equilibration of inclusions in carbonate cements by burial heating, Mineralogical Magazine, V. 51, p. 477-481.

Carmalt, S.W., and St. John, B., 1986, Giant oil and gas fields, in: Halbouty, M.T., ed., Future Petroleum Provinces of the World: AAPG Memoir 40, p. 11-53.

Cecil, B., Stanton, R., and Robbins, E., 1977, Geologic factors controlling coalification and hydrocarbon maturation, The American Association of Petroleum Geologists Bulletin, v. 61, p. 775.

Chalansonet, S., Largeau, C., Casadevall, E., Berkaloff, C., Peniguel, G., and Couderc, R., 1988, Cyanobacterial resistant biopolymers. Geochemical implications of the properties of *Schizothrix* sp. resistant material, Advances in Organic Geochemistry 1987, Organic Geochemistry, v. 13, Nos. 4-6, p. 1003-1010.

Cooles G.P., A.S. Mackenzie, and T.M. Quigley, 1986, Calculation of petroleum masses generated and expelled from source rocks: *in* D. Leythaeuser and J. Rullkötter, eds., Advances in Organic Geochemistry 1985: Oxford, Pergamon Press, p. 235-245.

Curry, D.J. and Simpler, T.K., 1988, Isoprenoid constituents in kerogens as a function of depositional environment and catagenesis, Organic Geochemistry, Vol. 13, Nos. 1-3, p. 995-1001.

de Leeuw, J.W and Largeau, C., 1993, A review of macromolecular organic compounds that comprise living organisms and their role in kerogen, coal, and petroleum formation, In. M.H. Engel and S. Macko (eds.) Organic Geochemistry.

de Leeuw, J.W., and Sinninghe Damsté, J.S., 1990, Organic sulphur compounds and other biomarkers as indicators of palaeosalinity: in: Geochemistry of Sulphur in Fossil Fuels, Wilson L. Orr and Curt M. White (Eds.), American Chemical Society, Washington DC 1990.

Dewey, J.F., Pitman, W.C., Ryan, W.B.F., and Bonnin, J., 1973, Plate tectonics and the evolution of the Alpine system. Bulletin of the Geological Society of America, V. 84, p. 3137-3180.

di Primio, R., 1990, Organisch-geochemische und mikroskopische Untersuchungen zur Kohlenwasserstoffgenese und primären Migration in karbonatischen Muttergesteinen der Trias Italiens: unpublished mastertheses, RWTH Aachen, 83 p.

Didyck, B.M., Simoneit, B.R.T., Brassell, S.C., Eglinton, G., 1978, Organic geochemical indicators of palaeoenvironmental conditions of sedimentation, Nature, Vol. 272, p. 216-222.

Dominé, F. and Enguehard, F., 1992, Kinetics of hexane pyrolysis at very high pressures 3. Application to geochemical modelling, Organic Geochemistry, v. 18, p. 41-49.

Du Rouchet, J., 1981, Stress fields, a key to oil migration, AAPG Bulletin, Vol. 65, p. 74-85.

Dubreuil, C., Derenne, S., Largeau, C., Berkaloff, C., and Rousseau, B., 1989, Mechanism of formation and chemical structure of Coorongite-I. Role of the resistant biopolymer and of the hydrocarbons of *Botryococcus Braunii*. Ultrastructure of Coorongite and its relationship with Torbanite, Organic Geochemistry, Vol. 14, No. 5, p. 543-553.

Düppenbecker, S.J., and B. Horsfield, 1990, Compositional information for kinetic modelling and petroleum type prediction, in B. Durand, and F. Behar, eds., Advances in Organic Geochemistry 1989: Org. Geochem. Vol. 16, Nos 1-3, pp. 259-266.

Eglinton, T.I., 1988, An investigation of kerogens using pyrolysis methods, Ph.D. thesis, University of Newcastle Upon Tyne, U.K.

Eglinton, T.I., and Douglas, A.G., 1988, Quantitative study of biomarker hydrocarbons released from kerogens during hydrous pyrolysis, Energy & Fuels, V. 2, p. 81-88.

Eglinton, T.I., Douglas, A.G., and Rowland, S.J., 1988, Release of aliphatic, aromatic and sulphur compounds from Kimmeridge kerogen by hydrous pyrolysis: A quantitative study, Organic Geochemistry, Vol. 13, Nos. 4-6, p. 655-663.

Eglinton, T.I., Sinninghe Damsté, J.S., Kohnen, M.E.L., de Leeuw, J.W., Larter, S.R., and Patience, R.L., 1990, Analysis of maturity-related changes in the organic sulphur composition of kerogens by flash pyrolysis-gas chromatography: in: Geochemistry of Sulphur in Fossil Fuels, Wilson L. Orr and Curt M. White (Eds.), American Chemical Society, Washington DC 1990.

England, W.A., Mackenzie, A.S., Mann, D.M., and Quigley, T.M., 1987, The movement and entrapment of petroleum fluids in the subsurface, Journal of the Geological Society, London, Vol. 144, p. 327-347.

Ensminger, A., Albrecht, P., Ourisson, G., and Tissot, B., 1977, Evolution of polycyclic alkanes under the effect of burial (early Toarcian shales, Paris Basin), in: R. Campos and J. Goni (eds.), Advances in Organic Geochemistry 1975, Enadimsa, Madrid, p. 45-52.

Espitalié, J., Deroo, G., and Marquis, F., 1985, La pyrolyse Rock-Eval et ses applications, Revue de l'Institut Francais du Pétrole, v. 40, p. 563-579 and 755-784.

Espitalié, J., J.L. Laporte, M. Madec, P. Leplat, J. Paulet, J., and A. Boutefeu, 1977, Méthode rapide de charactérisation des roches méres de leur potential pétrolier et de leur degré d'évolution: Rev. Inst. Fr. Pétr., v. 32, p. 23-42.

Espitalié, J., K. Sengo Makadi, and J. Trichet, 1984, Role of mineral matrix during kerogen pyrolysis: Organic Geochem., v. 6, p. 365-382.

Fowler, M.G. and Douglas, A.G., 1987, Saturated hydrocarbon biomarkers in oils of Late Precambrian age from Eastern Siberia, Organic Geochemistry, Vol. 11, p. 201-213.

Fu Jia Mo, Dai Yong Ding, Liu De Han, and Jia Rong Fen, 1984, Distribution and origin of hydrocarbons in carbonate rocks (Precambrian to Triassic) in China, in: J.G. Palacas (ed), Petroleum Geochemistry and Source Rock Potential of Carbonate Rocks, AAPG Studies in Geology, v. 18, p. 1-12.

Gelpi, E., Oro, J., Schneider, H.J., and Bennet, E.O., 1968, Olefins of high molecular weight in two microscopic algae, Science, Vol. 161, p. 700-701.

Goosens, H., de Leeuw, J.W, Schenk, P.A., and Brassell, S.C., 1988, The pristane formation index, a molecular maturity parameter. Confirmation in samples from the Paris Basin, Geochimica et Cosmochimica Acta, Vol. 52, p. 2439-2444.

Goth, K., de Leeuw, J.W., Püttmann, W., and Tegelaar, E.W., 1989, Origin of Messel oil-shale, Nature, v. 336, p. 759-761.

Grabowski, G.J. Jr., 1984, Generation and migration of hydrocarbons in Upper Cretaceous Austin Chalk, South-Central Texas, *in* J.G. Palacas, ed., Petroleum Geochemistry and Source Rock Potential of Carbonate Rocks, AAPG Studies in Geology, v. 18, p. 97-116

Granch, J.A. and Posthuma, J., 1974, On the origin of sulfur in crudes, in: B. Tissot and F. Bienner (Eds.) Advances in Organic Geochemistry 1973: Paris, Editions Technip, p. 727-739.

Gretener, P.E., 1979, Pore pressure, AAPG Continuing education course note series No. 4, 131 p.

Grimalt, J.O., de Wit, R., Teixidor, P., and Albaiges, J., 1992, Lipid biogeochemistry of Phormidium and Microcoleus mats, Organic Geochemistry, Vol. 19, P. 509-530.

Hagedorn-Götz, I., 1983, Organisch-geochemische und organisch-petrographische Untersuchungen an Bohrproben des Messeler Ölschiefers, Diplomarbeit RWTH Aachen.

Hanebeck, D., 1994, Experimentelle Simulation und Untersuchung der Genese und Expulsion von Erdölen aus Muttergesteinen, PhD Thesis, RWTH Aachen.

Hofmann, P., Huc, A.Y., Carpentier, B., Schaeffer, P., Keely, B., Maxwell, J.R., Sinninghe Damsté, J.S., de Leeuw, J.W. and Leythaeuser, D., 1993, Organic matter of the Mulhouse Basin, France: a synthesis, Organic Geochemistry, Vol. 20, No. 8, p. 1105-1123.

Horsfield, B. and Schenk, H.J., 1993, Simulating the cracking of oil to gas in reservoirs using laboratory heating experiments. Phase II: Crude oils from the Conoco 6507/7-3, Saga 34/7-10 and Norsk Hydro 30/9-10 wells, offshore Norway, KFA/ICG-4 Internal Report No. 500493.

Horsfield, B., 1989, Practical criteria for classifying kerogens: Some observations from pyrolysis-gas chromatography, Geochimica et Cosmochimica Acta, Vol. 53, No. 4, p. 891-901.

Horsfield, B., 1990, Evaluating kerogen type according to source quality, compositional heterogeneity and thermal lability, Review of Palaeobotany and Palynology, V. 65, p. 357-365.

Horsfield, B., and Düppenbecker, S.J., 1991, The decomposition of Posidonia Shale and Green River Shale kerogens using microscale sealed vessel (MSSV) pyrolysis, Journal of Analytical and Applied Pyrolysis, Vol. 20, p. 107-123.

Horsfield, B., Disko, U., and Leistner, F., 1989, The micro-scale simulation of maturation: outline of a new technique and its potential applications, Geologische Rundschau, Vol. 78, No. 1, p. 361-374.

Horsfield, B., Yordy, K.L., and Crelling, J.C., 1988, Determining the petroleum-generating potential of coal using organic geochemistry and organic petrology, Organic Geochemistry, Vol. 13, Nos. 1-3, p. 121-129.

Huang, W.-Y. and Meinschein, W.G., 1979, Sterols as ecological indicators, Geochimica et Cosmochimica Acta, Vol. 43, p. 739-745.

Hunt, J.M., 1967, The origin of petroleum in carbonate rocks, in: G.V. Chilingar, H.J. Bissel, and R.W. Fairbridge (eds.), Carbonate Rocks, New York, Elsevier, p. 225-251.

Hunt, J.M., Lewan, M.D. and Hennet, R.J-C., 1991, Modelling oil generation with time-temperature index graphs based on the Arrhenius equation, AAPG Bulletin, Vol. 75, p, 795-807.

Javor, B., 1989, Hypersaline Environments: Microbiology and Biogeochemistry, Springer, Berlin.

Johns, R.B., Gillan, F.T., and Volkman, J.K., 1980, Early diagenesis of phytyl esters in a contemporary temperate intertidal sediment, Geochimica et Cosmochimica Acta, v. 44, p. 183-188.

Jones, C.E.R. and Cramer, C.A., 1977, Analytical Pyrolysis, Elsevier, Amsterdam.

Jones, R.W., 1978, Some mass balance and geologic constraints on migration mechanisms, in: Physical and Chemical Constraints on Petroleum Migration, AAPG Continuing Education Course Note Series #8, AAPG Department of Educational Activities.

Jones, R.W., 1984, Comparison of carbonate and shale source rocks: *in* J.G. Palacas, ed., Petroleum Geochemistry and Source Rock Potential of Carbonate Rocks: AAPG Studies in Geology 18, p. 163-180.

Jüntgen, H. and van Heek, K.H., 1968, Gas release from coal as a function of the rate of heating, Fuel, 47, pp. 103-117

Kenig, F., and Huc, A.Y., 1990, Incorporation of sulphur into recent organic matter in a carbonate environment (Abu Dhabi, United Arab Emirates), in: *Geochemistry of Sulphur in Fossil Fuels,* ACS-Symposium Series 429, p. 170-185.

Kenig, F., Huc, A.Y., Purser, B.H., and Oudin, J.L., 1989, Sedimentation, distribution and diagenesis of organic matter in a recent carbonate environment, Abh Dhabi, U.A.E., Organic Geochemistry, Vol. 16, Nos. 4-6, p. 735-747.

Killops, S.D. and Killops, V.J., 1993, An Introduction to Organic Geochemistry, Longman Scientific and Technical, Longman Group UK Ltd., 265 pages.

Kroos, B.M., 1993, Open system hydrous pyrolysis: a new tool for the investigation of petroleum generation and expulsion, 203 ACS National Meeting, Abstract Volume, Abstract No. 95.

Krooss, B.M., Hanebeck, D. and Leythaeuser, D., 1994, Experimental measurement of the molecular migration of light hydrocarbons in source rocks at elevated temperatures, in: A.G. Doré et al. (Eds.) Basin Modelling: Advances and Applications, NPF Süecial Publication 3, p. 277-291, Elsevier, Amsterdam.

Kvenvolden, K.A., 1962, Normal paraffin hydrocarbonsin sediments from San Fransisco Bay, California, American Association of Petroleum Geologists Bulletin, v. 46, p. 1643-1652.

Lafargue, E., Espitalie, J., Broks, T.M., Nyland, B., 1994, Experimental simulation of primary migration, Organic Geochemistry, Vol. 22, Nos. 3-5, p. 575-586.

Lafargue, E., Espitalié, J., Jacobsen, T., and Eggen, S., 1990, Advances in Organic Geochemistry 1989, Organic Geochemistry, v. 16, Nos. 1-3, p. 121-131.

Langford, F.F. and Blanc-Valleron, M.-M., 1990, Interpreting Rock-Eval pyrolysis data using graphs of pyrolyzable hydrocarbons vs. total organic carbon, The American Association of Petroleum Geologists Bulletin, v. 74, No. 6, p.799-804.

Largeau, C., Casadeval, E, Kadouri, A, Metzger, P., 1984, Formation of Botryococcus-derived kerogens: comparative study of immature torbanites and of the extant alga Botryococcus braunii, Organic Geochemistry, Vol. 6, p. 327-332.

Larter, S.R. and Douglas, A.G., 1980, A pyrolysis-gas chromatographic method for kerogen typing, in: Advances in Organic Geochemistry 1979, (Eds.: A.G. Douglas and J.R. Maxwell), Physics and Chemistry of the Earth 12, p. 579-584, Pergamon Press.

Larter, S.R., 1978, A Geochemical study of kerogens and related material, Ph.D. Thesis, University of Newcastle Upon Tyne (unpublished).

Larter, S.R., and Horsfield, B., 1993, Determination of structural components of kerogens using analytical pyrolysis methods, in: Organic Geochemistry, Chapter 16. Eds: M. Engel and S. Macko.

Larter, S.R., Solli, H., and Douglas, A.G., 1983, Phytol containing melanoidins and their bearing on the fate of isoprenoid structures in sediments, in: (Eds.: M.Bjoroy et al.) Advances in Organic Geochemistry 1981, p. 513-521, John Wiley, Chichester.

Larter, S.R., Solli, H., Douglas, A.G., De Lange, F., and de Leeuw, J.W., 1979, The occurence and significance of prist-1-ene in kerogen pyrolysates, Nature, Vol. 279, p. 405-408.

Le Berre, F., Derenne, S., Largeau, C., Connan, J. and Berkaloff, C., 1992, Ocurrence of non-hydrolysable, macromolecular, wall constituents in bacteria. Geochemical implications, In: Organic Geochemistry, Advances and Applications in Energy and the Natural Environment, 15th Meeting of the European Association of Organic Geochemists, Poster Abstracts, p. 428-431.

Leischner, K., 1994, Kalibration simulierter Temperaturgeschichten von Sedimentgesteinen, PhD Thesis, Rur-Universität Bochum.

Lewan, M.D., 1985, Evaluation of petroleum generation by hydrous pyrolysis experimentation, Phil. Trans. R. Soc. Lond., A 315, p. 123-134.

Lewan, M.D., 1992, Laboratory simulation of petroleum formation: Hydrous Pyrolysis, in: M.H. Engel and S.A. Macko (eds), Organic Geochemistry, Plenum Publishing Corporation, New York.

Lewan, M.D., Winters, J.C., and McDonald, J.H., 1979, Generation of oil-like pyrolyzates from organic-rich shales, Science, v. 203, p. 897-899.

Leythaeuser, D. and Poelchau, H.S., 1991, Expulsion of petroleum from type III kerogen source rocks in gaseous solution: modelling of solubility fractionation, in England, W.A., & Fleet, A.J., (eds), Petroleum Migration, Geological Society, Special Publication No. 59, pp. 33-46.

Leythaeuser, D., A.S. Mackenzie, R.G. Schaefer, and M. Bjoroy, 1984a, A novel approach for recognition and quantification of hydrocarbon migration effects in shale-sandstone sequences: AAPG Bulletin., v. 68, p. 196-219.

Leythaeuser, D., and R.G. Schaefer, R.G., 1984b, Effects of hydrocarbon expulsion from shale source rocks of high maturity in Upper Carboniferous strata of the Ruhr area, Federal Republic of Germany, in P.A. Schenck, J.W. de Leeuw, and G.W.M. Lijmbach, Advances in org. Geochem. 1983: Org. Geochem. v. 6, Pergamon Press, Oxford, p. 671-681.

Leythaeuser, D., Borromeo, O., Mosca, F., di Primio, R., Radke, M., and Schaefer, R.G., 1994, Pressure solution in carbonate source rocks and its control on petroleum generation and migration, in press.

Leythaeuser, D., Hagemann, H.W, Hollerbach, A., and Schaefer, R.G., 1980, Hydrocarbon generation in source beds as a function of type and maturation of their organic matter. A mass balance approach. Proceedings of the Tenth world Petroleum Congress, V. 2, p. 31-41, Heyden, London.

Leythaeuser, D., M. Radke, and H. Willsch, H., 1989, Geochemical effects of primary migration of petroleum in Kimmeridge source rocks from Brae field area, North Sea, II: Molecular composition of alkylated naphthalenes, phenanthrenes, benzo- and dibenzothiophenes: Geochimica et Cosmochimica Acta, v. 52, p. 2879-2891.

Leythaeuser, D., R. Littke, M. Radke, and R.G. Schaefer, 1988b, Geochemical effects of petroleum migration and expulsion from Toarcian source rocks in the Hils syncline area, MW-Germany, in L. Mattavelli and L. Novelli, eds, Advances in Org. Geochemistry 1987: Oxford, Pergamon Press, Org. Geochem. v. 13, Nos 1-3, p. 489-502.

Leythaeuser, D., R.G. Schaefer, and M. Radke, 1988a, Geochemical effects of primary migration of petroleum in Kimmeridge source rocks from Brae field area, North Sea, I: Gross composition of C15+-saturated hydrocarbons: Geochimica et Cocmochimica Acta v. 52 p. 701-713.

Littke, R., 1993, Deposition, diagenesis and weathering of organic matter-rcih sediments, Lecture Notes in Earth Sciences, v. 47, Springer Verlag, 216 pages.

Mackenzie, A.S., 1984, Applications of biological markers in petroleum geochemistry, in: J. Brooks and D.H. Welte (Eds.) Advances in Petroleum Geochemistry, Vol. 1, p. 115-214, Academic Press.

Mackenzie, A.S., and T.M. Quigley, 1988, Principles of geochemical prospect appraisal: AAPG Bulletin, v. 72, p. 399-415.

Mackenzie, A.S., I. Price, D. Leythaeuser, P. Müller, M. Radke, and R.G. Schaefer, 1987, The expulsion of petroleum from Kimmeridge clay source rocks in the area of the Brae oilfield,

UK continental shelf: *in* J. Brooks and K.W. Glennie, eds., Petroleum Geology of North West Europe: London, Graham and Trotman, p. 865-877.

Mädler, K., 1968, Die figurierten organischen Bestandteile des Posidonienschiefers, Beih. geol. Jb., V. 58, p. 287-406.

Martinez, A.R., 1982, Report of working group on definitions, in The future of heavy crude and tar sands, second international conference, R.F. Meyer, J.C. Wynn, and J.C. Olson (Eds.), McGraw-Hill, Inc.

Matsumoto, G., Torii, T., and Hanya, T., 1982, High abundance of algal 24-ethylcholesterol in Antarctic lake sediment, Nature, Vol. 299, p. 52-54.

Mattavelli, L., Pieri, M. and Groppi, G., 1993, Petroleum exploration in Italy: a review, Marine and Petroleum Geology, Vol. 10, No. 5, p. 410-425.

McAuliffe, C.D., 1978, Role of solubility in migration of petroleum from source, in: Physical and Chemical Constraints on Petroleum Migration, AAPG Continuing Education Course Note Series #8, AAPG Department of Educational Activities.

Meinschein, W.G., 1961, Significance of hydrocarbons in sediments and petroleum, Geochimica et Cosmochimica Acta, V. 22, p. 58-64.

Metzger, P. Berkaloff, C., Casadevall, E., and Coute, A., 1985, Alkadiene- and botryococcene-producing races of wild strains of Botrycoccus braunii, Phytochemistry, Vol. 24, p. 2305-2312

Metzger, P., Templier, J., Largeau, C., and Casadevall, E., 1986, A n-alkatriene and some n-alkadienes from the A race of the green alga Botryococcus braunii, Phytochemistry, Vol. 25, p. 1869.

Moldowan, J.M., Seifert, W.K., and Gallegos, E.J., 1985, Relationship between petroleum composition and depositional environment of petroleum source rocks, AAPG Bulletin, Vol. 69, No. 8, p. 1255-1268.

Moldowan, J.M., Sundararaman, , P., Salvatori, T., Alajbeg, A., Gjukic, B., Lee, C.Y., and Demaison, G.J., 1992, Source correlation and maturity assesment of selected oils and rocks from the Central Adriatic Basin (Italy and Yugoslavia). In: Biological Markers in Sediments and Petroleum (J.M. Moldowan, P. Albrecht, and R.P. Philp, eds.) Prentice Hall, Englewood Cliffs, N.J., p. 370-401.

Momper, J.A., 1978, Oil migraiton limitations suggested by geological and geochemical consideraitons, in: Physical and Chemical Constraints on Petroleum Migration, AAPG Continuing Education Course Note Series #8, AAPG Department of Educational Activities.

Monin, J.C., Connan, J., Oudin, J.L., and Durand, B., 1990, Quantitative and qualitative experimental approach of oil and gas generation: Application to the North Sea source rocks, Organic Geochemistry, 16 Nos. 1-3, pp. 133-142

Monthioux, M., landais, P., and Monin, J.C., 1985, Comparison between natural and artificial maturation series of humic coals from the Mahakam delts, Indonesia, Organic Geochemistry, Vol. 8, No. 4, p. 275-292.

Mullis, J., 1987, Fluid inclusion studies during very low grade metamorphism, in: M.Frey (ed.), Low Temperature Metamorphism, Chap. 5, p. 162-199.

Muscio, G.P.A., 1991, Pyrolyse der makromolecularen organischen Substanz (Kerogene, Asphaltene und Heterokomponenten) einer natürlich gereiften Probenserie des Lias ε der Hils-Mulde, NW-Deutschland, Diplomarbeit, RWTH Aachen.

Nichols, P.D., Palmisano, A.C., Rayner, M.S., Smith, G.A., and White, D.C., 1990, Occurence of novel C30 sterols in Antarctic sea-ice diatom communities during a spring bloom, Organic Geochemistry, Vol. 15, p. 503-508.

Novelli, L., D.H. Welte, L. Mattavelli, M.N. Yalcin, D. Cinelli, and K.J. Schmitt, 1988, Hydrocarbon generation in southern Sicily: A three-dimensional computer aided basin modeling study: *in* L. Mattavelli and L. Novelli, eds., Advances in Organic Geochemistry 1987: Oxford, Pergamon Press, p. 153-164.

Oehler, J.H., 1984, Carbonate source rocks in the Jurassic Smackover Trend of Mississippi, Alabama, and Florida, *in* J.G. Palacas, ed., Petroleum Geochemistry and Source Rock Potential of Carbonate Rocks, AAPG Studies in Geology, v. 18, p.63-70

Orr, W.L., 1986, Kerogen/asphaltene/sulfur relationships in sulfur-rich Monterey oils: Organic Geochemistry, Vol. 10, p 499-516.

Ourisson, G., Albrecht, P., and Rohmer, M., (1987), The Hopanoids, Pure Appl. Chem., Vol. 51, p. 709-729.

Owen, E.W., 1964, Petroleum in carbonate rocks, American Association of Petroleum Geologists Bulletin, V. 45, p. 1727-1730.

Palacas, J.G., 1983, Carbonate rocks as sources of petroleum: Geological and chemical characteristics and oil-source correlations: Proc. 11th World Petroleum Congress, Vol. 2: John Wiley and Sons, Ltd.

Palacas, J.G., 1989, Characteristics of carbonate source rocks of petroleum: *in* L.B. Magoon, ed., Petroleum Systems of the United States: U.S. Geol. Surv Bull. 1870, p. 20-25.

Palacas, J.G., D.E. Anders, and J.D. King, 1984, South Florida Basin - Prime example of carbonate source rocks of petroleum: *in* J.G. Palacas, ed., Petroleum Geochemistry and Source Rock Potential of Carbonate Rocks, AAPG Studies in Geology #18, Tulsa, Oklahoma, p. 71-96.

Palmer, S.E. and Zumberge, J.E., 1981, Organic geochemistry of upper Miocene evaporite deposits in the Sicilian Basin, Sicily, in J. Brooks (ed.) Organic Maturation Studies and Fossil Fuel Exploration, London, Academic Press, p. 393-426.

Peters, K.E. and Moldowan, J.M., 1993, The Biomarker Guide, Prentice Hall Inc.Engelwood Cliffs, New Jersey 07632.

Peters, K.E., 1986, Guidelines for evaluating petroleum source rock using programmed pyrolysis, The American Association of Petroleum Geologists Bulletin, v. 70, No. 3, p.318-329.

Pfeiffer, J.P. and Saal, R.N.J., 1940, Asphaltic bitumen as colloid system, Journal of Physical Chemistry, v. 44, p. 139-149.

Philippi, G.T., 1965, On the depth, time and mechanism of petroleum generation, Geochimica et Cosmochimica Acta, v. 29, p. 1021-1049.

Powell, T.G., 1984, Some aspects of the hydrocarbon geochemistry of a middle Devonian barrier reef complex, western Canada: *in* J.G. Palacas, ed., Petroleum Geochemistry and Source Rock Potential of Carbonate Rocks, AAPG Studies in Geology, v. 18, p. 45-62.

Powell, T.G., 1986, Petroleum geochemistry and depositional setting of lacustrine source rocks, Marine and Petroleum Geology, V. 3, p. 200-219.

Prezbindowski, D.R. and Tapp, J.B., 1991, Dynamics of fluid inclusion alteration in sedimentary rocks: a review and discussion, Organic Geochemistry, Vol. 17, No. 2, p. 131-142.

Price, L.C., and Wenger, L.M., 1992, The influence of pressure on petroleum generation and maturation as suggested by aqueous pyrolysis: Advances in Organic Geochemistry 1991, Organic Geochemistry Vol. 19, Nos. 1-3, p. 141-159, 1992

Quigley, T.M., Mackenzie, A.S., and Gray, J.R., 1987, Kinetic theory of petroleum generation, in: B. Doligez et al. (eds.), Proceedings of the Conference on Migration of Hydrocarbons in Sedimentary Basins, Edition Technip, Paris, p. 649-665.

Radke, M and Welte, D.H., 1983, The methylphenanthrene index (MPI): a maturity parameter based on aromatic hydrocarbons, in: Advances in Organic Geochemistry 1981, M. Bjoroy et al. (eds.), v. 2, p. 141-207, Academic Press, London.

Radke, M., 1981, Class separation of aromatic compounds in rock extracts and crude oils by semipreparative HPLC, KFA-ICH5 report 500581, 34 pages, Jülich.

Radke, M., 1988, Application of aromatic compounds as maturity indicators in source rocks and crude oils: Marine Petroleum Geology v. 5, p. 224-236.

Radke, M., D.H. Welte, and H. Willsch, 1986, Maturity parameters based on aromatic hydrocarbons: Influence of the organic matter type: Organic Geochemistry v. 10 p. 51-63.

Radke, M., H. Willsch, and D.W. Welte, 1980, Preparative hydrocarbon group type determination by automated medium pressure liquid chromatography: Anal. Chem., v. 52, p. 406-411.

Radke, M., H.G. Sittardt, and D.H. Welte, 1978, Removal of soluble organic matter from rock samples with a flow-through extraction cell: Anal. Chem., v. 50, p. 663-665.

Radke, M., Welte, D.H., and Willsch, H., 1982, Geochemical study on a well in the Western Canada Basin: relation of the aromatic distribution pattern to maturity of organic matter, Geochimica et Cosmochimica Acta, V. 46, p. 1-10.

Radke, M., Welte, D.H., and Willsch, H., 1991, Distribution of alkylated aromatic hydrocarbons and dibenzothiophenes in rocks of the Upper Rhine Graben. Chemical Geology, V. 93, p. 325-341.

Richnow, H.H., Jenisch, A., and Michaelis, W., 1991, Structural investigations of sulphur-rich macromolecular oil fractions and a kerogen by sequential chemical degradation, Organic Geochemistry, Vol. 19, Mos 4-6, p. 351-370.

Richnow, H.H., Jenisch, A., and Michaelis, W., 1993, The chemical structure of macromolecular fractions of a sulfur-rich oil, Geochimica et Cosmochimica Acta, Vol. 57, p. 2767-2780.

Ricken, W., 1986, Diagenetic Bedding: Lecture Notes in Earth Sciences, v. 6. Springer Verlag.

Roedder, E., 1984, Fluid Inclusions, Reviews in Mineralogy, Vol. 12, Mineralogical Society of America.

Rohmer, M, Bisseret, P., and Neunlist, S., 1992, The hopanoids, prokaryotic triterpenoids and precursors of ubiquitous molecular fossils, in: Biological Markers in Petroleum and Sediments (ed. J.M. Moldowan, et al.), Prentice Hall.

Ropertz, B., 1994, Wege der primären Migration: Eine Untersuchung über Porennetze, Klüfte und Kerogennetzwercke als Leitbahnen für den Kohlenwasserstoff-Transport, PhD Thesis, RWTH Aachen.

Rowland, J.S., Aareskjold, K., Gou Xuemin, and Douglas, A.G., 1985, Hydrous pyrolysis of sediments: composition and proportions of aromatic hydrocarbons in pyrolysates, Advances in Organic Geochemistry 1985, Organic Geochemistry, V. 10, p. 1033-1040.

Rubinstein, I., Spyckerelle, C., Strausz, O.P., 1979, Pyrolysis of asphaltenes: a source of geochemical information; Geochimica et Cosmochimica Acta, Vol. 43, p. 1-6.

Rullkötter J., D. Leythaeuser, B. Horsfield, R. Littke, U. Mann, P.J. Müller, M. Radke, R.G. Schaefer, H.J. Schenk, K. Schwochau, E.G. Witte, and D.H. Welte, 1988, Organic matter maturation under the influence of a deep intrusive heat source: A natural experiment for quantitation of hydrocarbon generation and expulsion from a petroleum source rock (Toarcian Shale, northern Germany: *in* L. Mattavelli and L. Novelli, eds., Advances in Organic Geochemistry 1987, Oxford, Pergamon Press, p. 847-856.

Rullkötter J., Spiro, B., and Nissenbaum, A., 1985, Biological marker characteristics of oils and asphalts from carbonate source rocks in a rapidly subsiding graben, Dead Sea, Israel; Geochimica et Cosmochimica Acta, Vol. 49, p. 1357-1370.

Rullkötter, J., and Michaelis, W., 1990, The structure of kerogen and related materials. A review of recent progress and future trends, Organic Geochemistry, Vol. 16 Nos. 4-6, p. 829-852.

Rullkötter, J., Littke, R., and Schaefer, R.G., 1990, Characterization of organic matter in sulphur-rich lacustrine sediments of Miocene age (Nördlinger Ries, Southern Germany): in: Geochemistry of Sulphur in Fossil Fuels, Wilson L. Orr and Curt M. White (Eds.), American Chemical Society, Washington DC 1990.

Sandvik, E.I., Young, W.A., and Curry, D.J., 1991, Expulsion from hydrocarbon sources: the role of organic absorption: Advances in Organic Geochemistry 1991, Organic Geochemistry Vol. 19, Nos. 1-3, p. 77-87, 1992

Sassen, R., 1988, Geochemical and carbon isotopic studies of crude oil destruction, bitumen precipitation, and sulfate reduction in the deep Smackover Formation, Organic Geochemistry, Vol. 12, No. 4, p. 351.361.

Sassen, R., 1990, Geochemistry of carbonate source rocks and crude oils in Jurassic salt basins of Gulf Coast: in J, Brooks, ed., Classic Petroleum Provinces Geological Society Special, 1990, Publication No. 50, pp. 265-277, Alden Press, Oxford.

Sassen, R., and Moore, C.H., 1988, Framework of hydrocarbon generation and destruction in Eastern Smackover Trend, AAPG Bulletin, Vol. 72, No. 6, p. 649-663.

Sassen, R., Moore, C.H., and Meendsen, F.C., 1987, Distribution of hydrocarbon source potential in the Jurassic Smackover Formation, Organic Geochemistry, Vol. 11, No. 5, p. 379-383.

Sassen, R., Moore, C.H., Nunn, J.A., Meendsen, F.C., and Hexdari, E., 1987, Geochemical studies of crude oil generation, migration, and destruction in the Mississippi Salt Basin, Gulf Coast Association of Geological Societies, Transactions, Vol. 37, p. 217-224.

Saxby, J.D., 1981, Kerogen genesis and structure - similarities to rubber, Fuel, Vol. 60, p. 994-996.

Schaefer, R.G., H.J. Schenk, H. Hardelauf, and R. Harms, 1990, Determination of gross kinetic parameters for petroleum formation from Jurassic source rocks of different maturity levels by means of laboratory experiments: *in* B. Durand and F. Behar, eds., Advances in Organic Geochemistry 1989, Oxford, Pergamon Press, p. 115-120.

Schenk, H.J., E.G. Witte, R. Littke, and K. Schwochau, 1990, Structural modifications of vitrinite and alginite concentrates during pyrolytic maturation at different heating rates. A combined infrared, ^{13}C NMR and microscopical study: *in* B. Durand and F. Behar, eds., Advances in Organic Geochemistry 1989, Oxford, Pergamon Press, p. 943-950.

Schenk, H.J., Horsfield, B., Richter, A., and Biermans, E., 1992, Comparative characterization of selected shale samples from the Eocene Green River Formation using infrared

spectroscopy, Rock-Eval pyrolysis and kinetic measurements. KFA-ICG-4 Internal Report No. 500692.

Scholle, P.A., and R.B. Halley, 1985, Burial diagenesis: Out of sight, out of mind: *in* Carbonate Cements, SEPM Special Publication 36, p. 135-160.

Schouten, S., van Driel, G.B., Sinninghe Damsté, J.S, and de Leeuw, J.W., 1994, Natural sulphurisation of ketones and aldehydes: A key reaction in the formation of organic sulohur compounds, Geochimica et Cosmochimica Acta, v. 58, p. 5111-5116.

Seifert, W.K. and Moldowan, J.M., 1978, Applications of steranes, terpanes, and monoaromatics to the maturation, migration, and source of crude oils, Geochimica et Cosmochimica Acta, V.42, p. 77-95.

Seifert, W.K. and Moldowan, J.M., 1980, The effect of thermal stress on source rock quality as measured by hopane stereochemistry, in: A.G. Douglas and J.R. Maxwell (eds.) Advances in Organic Geochemistry 1979, Pergamon, Oxford, p. 229-237.

Seifert, W.K. and Moldowan, J.M., 1986, Use of biological markers in petroleum exploration, in: R.B. Johns (ed.), Biological Markers in the Sedimentary Record, Elsevier, p. 261-290.

Sestini, G., and Flores, G., 1984, Petroleum potential of the thrust belt and foretroughs of Sicily. In: M.T. Halbouty, ed., Future Petroleum Provinces of the World, AAPG Memoir No. 40, p. 567-584.

Shinn, E.A., 1983, Tidal Flat Environment, in: P.A. Scholle, D.G. Bebout, and C.H. Moore (Eds.), Carbonate Depositional Environments, AAPG Memoir 33, AAPG Tulsa, Oklahoma 74101, U.S.A.

Sinninghe Damsté, J.S., de las Heras, F.X., van Bergen, P.F., and de Leeuw, J.W., 1993, Characterization of tertiary catalan lacustrine oil shales: Discovery of extremely organic sulphur-rich Type I kerogens, Geochimica et Cosmochimica Acta, Vol. 57, p. 389-415.

Sinninghe Damsté, J.S., Eglington, T.I., de Leeuw, J.W., and Schenck, P.A., 1989, Organic sulphur in macromolecular sedimentary organic matter: I. Structure and origin of sulphur-containing moieties in kerogen, asphaltenes and coal as revealed by flash pyrolysis, Geochimica et Cosmochimica Acta, Vol. 53, p. 873-889.

Sinninghe Damsté, J.S., Eglinton, T.I., Rijpstra, W.I.C., and de Leeuw, J.W., 1990, Characterization of organically bound sulphur in high-molecular-weight, sedimentary organic matter using flash pyrolysis and Raney Ni desulphurization: in: Geochemistry of Sulphur in Fossil Fuels, Wilson L. Orr and Curt M. White (Eds.), American Chemical Society, Washington DC 1990.

Speight, J.G. and Moschopedis, S.E., 1981, On the molecular nature of petroleum asphaltenes, in: J.W. Bunger and N.C. Li (eds.), Chemistry of Asphaltenes, American Chemical Society, Advances in Chemistry Series, v. 195, p.1-16.

Stach, E., Chandra, D., Mackowsky, M.TH., Teichmüller, M., Teichmüller, R., and Taylor, G.H., 1982, Stach's Textbook of Coal Petrology, 3 revised and enlarged edition, Gebrüder Bornträger, Berlin, Stuttgart, 535 pages.

Stainforth, J.G., and J.E.A. Reinders, 1990, Primary migration of hydrocarbons by diffusion through organic matter network, and its effect on oil and gas generation, in B. Durand and F. Behar, eds., Advances in Organic Geochemistry 1989: Oxford, Pergamon Press, v. 16, p. 61-74.

Takeda, N. and Asakawa, T., 1988, Study of petroleum generation by pyrolysis. I. Pyrolysis experiments by Rock-Eval and assumption of molecular structural change of kerogen using ^{13}C-NMR, Applied Geochemistry, Vol. 3, p. 441-453.

Takeda, N., Sato, S., and Machihara, T., 1990, Advances in Organic Geochemistry 1989, Organic Geochemistry, v. 16, Nos. 1-3, p. 143-153.

Talbot, M.R., 1988, The origins of lacustrine oil source rocks: Evidence from the lakes of tropical Africa, in: A.J. Fleet etal. (eds.) Lacustrine Petroleum Source Rocks; Geological Society Special Publication 40, p. 3-26, Blackwell.

Tannenbaum, E., and Aizenshtat, Z., 1984a, Formation of immature asphalt from organic rich carbonate rocks-II. Correlations of maturation indicators, Advances in Organic Geochemistry 1983, P.A.Schenk, J.W. de Leeuw, and G.W.M. Lijmbach (eds.), Organic Geochemistry, v. 6, p. 503-511.

Tannenbaum, E., and Aizenshtat, Z., 1985, Formation of immature asphalt from organic rich carbonate rocks-I. Geochemical correlation, Organic Geochemistry, Vol. 8, No. 2, p. 181-192.

Tegelaar, E.W., de Leeuw, J.W., Derenne, S., and Largeau, C., 1989, A reappraisal of kerogen formation, Geochimica et Cosmochimica Acta, v. 53, p. 3103-3106.

Teichmüller, M. and Ottenjahn, N., 1977, Liptinite und lipoide Stoffe in einem Erdölmuttergestein, Erdöl und Kohle, V. 30, p. 387-398.

ten Haven, H.L., de Leeuw, J.W, Sinninghe Damsté, J.S., Schenck, P.A., Palmer, S.E., and Zumberge, J.E., 1988, Application of biological markers in the recognition of palaeohypersaline environments: in: A.J. Fleet, K. Kelts and M.R. Talbot (eds), 1988, Lacustrine Petroleum Source Rocks, Geological Society Special Publication No. 40, p. 123-130.

Tissot, B.P. and Espitalié, 1975, Thermal evolution of organic matter in sediments: applications of a mathematical simulation, Revue Institut Francais du Petrole, Vol. 30, No. 5, p. 743-777.

Tissot, B.P. and Welte, D.H., 1984, Petroleum formation and occurence, second revised and enlarged edition. -2. Auflage: 699 S.; Berlin-Heidelberg-New York-Tokyo (Springer)

Tissot, B.P., 1981, Connaisances actuelles sur les produits lourds du pétrole, Revue de l'Institut Francais du Pétrole, v. 36, p. 429-446

Tissot, B.P., 1981, Generation of petroleum in carbopate rocks and shales of marine or lacustrine facies and its geochemical characteristics, in: Petroleum Geology in China; Principal Lectures Presented to the United Nations International Meeting on Petroleum Geology, Beijing, China, Pennwell Books, Tulsa, Oklahoma.

Tissot, B.P., 1984, Recent advances in petroleum geochemistry applied to hydrocarbon exploration, The American Association of Petroleum Geologists Bulletin, v. 68, p. 545-563.

Tissot, B.P., Deroo, G., Espitalié, J., 1975, Etude compareé de l'epoque de formation et d'expulsion du pétrole dans diverses provinces géologiques, Proceedings of the 9th World Petroleum Congress Tokyo. London: Applied Science Publications, v. II, p 159-169.

Tissot, B.P., Pelet, R., and Ungerer, PH., 1987, Thermal history of sedimentary basins, maturation indeces, and kinetics of oil and gas generation, AAPG Bulletin, Vol. 71, No. 12, p. 1445-1466.

Ulrich, M.R. and Bodnar, R.J., 1988, Systematics of stretching of fluid inclusions II: barite at 1 atm confining pressure, Economic Geology, Vol. 83, p. 1037-1046.

Ungerer, P., and R. Pelet, 1987, Extrapolation of the kinetics of oil and gas formation from laboratory experiments to sedimentary basins: Nature, v. 327, p. 52-54.

Ungerer, P., Forbes, P., and Rudkiewicz, J.L., 1992, Computer modelling of the interplay between generation and expulsion of petroleum: a new advance in synthesizing geochemical data, Proceedings of the 13th World Petroleum Congress, 1, pp. 1-11

van de Meent, D., Brown, S.C., Philp, R.P., and Simoneit, B.R.T., 1980, Pyrolysis-high resolution gas chromatography and pyrolysis gas chromatography-mass spectrometry of kerogen precursors, Geochimica et Cosmochimica Acta, Vol. 44, p. 999-1014.

Van Graas, G., de Leeuw, J.W., Schenk, P.A., and Haverkamp, J., 1981, Kerogen of Toarcian shales of the Paris Basin. A study of its maturation by flash pyrolysis techniques, Geochimica et Cosmochimica Acta, Vol. 43, p. 281-287.

van Krevelen, D.H., 1961, Coal, Elsevier, Oxford.

Volkman, J.K., 1986, A review of sterol markers for marine and terrigenous organic matter, Organic Geochemistry, Vol. 9, No. 2, p. 83-99.

Volkman, J.K., 1988, Biological marker compounds as indicators of the depositional environments of petroleum source rocks, in: A.J. Fleet, K. Kelts, and M.R. Talbot (Eds.), Lacustrine Petroleum Source Rocks, Oxford, Blackwell, p. 103-122.

Walker, A.L., McCulloh, T.H., Peterson, N.F., and Stewart, R.J., 1983, Anomalously low reflectance of vitrinite in comparison with other petroleum source-rock maturation indeces from the Miocene Modelo-Formation in the Los Angeles basin, California, Pacific Section SEPM, p. 185-190.

Waples, D.W. and Machihara, T., 1991, Biomarkers for Geologists - A Practical Guide to the Application of Steranes and Triterpanes in Petroleum Geology, AAPG Methods in Exploration, No. 9, AAPG Tulsa, Oklahoma, U.S.A.

Welte, D.H., 1987, Migration of hydrocarbons, facts and theories, In: B. Doligez (ed.), Migration of hydrocarbons in sedimentary basins, Paris, Edition Technip, p. 393-413.

Wilhelms, A., Larter, S.R., Leythaeuser, D., and Dypvik, H., 1990, Recognition and quantification of the effects of primary migration in a Jurassic clastic source-rock from the Norwegian continental shelf, Organic Geochemistry, Vol. 16, Nos 1-3, p. 103-113.

Winters, J.C., Williams, J.A., and Lewan, M.D., 1983, A laboratory study of petroleum generation by hydrouspyrolysis, Advances in Organic Geochemistry 1981, p. 524-533, John Wiley & Sons Limited, 1983.

Youngblood, W.W, Blumer, M., Guillard, R.L., Fiore, F., 1971, Saturated and unsaturated hydrocarbons in marine benthic algae, Marine Biology, Vol. 8, p. 190-201.

Zumberge, J.E., 1984, Source rocks of the La Luna Formation (Upper Cretaceous, in the Middle Magdalena Valley, Columbia: *in* J.G. Palacas, ed., Petroleum Geochemistry and Source Rock Potential of Carbonate Rocks, AAPG Studies in Geology #18: Tulsa, Oklahoma, p. 127-134.

6 Appendix 1

Tables 1 to 21

Peak identification of steranes and hopanes

E number	Sub-sample	Well	Sample type	TOC %	TC %	CaCO3 %	TOC St %	S1 mg/g	S2 mg/g	T max C	HI	PI
33353	/1	17	Impregnated	0,85	12,10	93,71		2,19	5,06	425	595	0,30
33354	/1	17	Laminite	1,41	10,10	72,39		0,30	6,36	417	451	0,05
33356	/1	17	Mudstone	0,14	11,85	97,54		0,01	0,19	428	136	0,05
33356	/2	17	Sol. seam	0,50	11,70	93,30	8,41	0,05	1,65	421	330	0,03
33357	/1	17	Mudstone	0,17	11,95	98,13		0,02	0,23	425	135	0,08
33357	/2	17	Sol. seam	2,01	12,75	89,46	21,01	0,64	12,37	418	615	0,05
33357	/3	17	Impregnated	0,20	11,65	95,38		0,05	0,39	424	195	0,11
33360	/1	17	Shale	3,74	3,63	0,00		1,68	11,84	396	317	0,12
33363	/1	4	Laminite	1,68	10,50	73,47		0,35	7,58	415	451	0,04
33366	/1	4	Mudstone	0,16	12,05	99,04		0,01	0,29	423	181	0,03
33366	/2	4	Sol. seam	1,87	12,80	91,05	21,34	0,51	12,40	417	663	0,04
33366	/3	4	Impregnated	0,25	11,95	97,46		0,22	1,96	428	480	0,10
33366	/4	4	Shale	27,60	28,45	7,08		3,27	225,85	417	818	0,01
33369	/1	4	Mudstone	0,07	11,80	97,71		0,00	0,00	0	0	
33369	/2	4	Stylolite	0,34	11,85	95,88	14,47	0,02	0,61	428	179	0,03
33369	/3	4	Impregnated	1,31	12,65	94,46		1,48	8,49	424	648	0,15
33370	/1	4	Impregnated	3,82	12,05	68,56		6,72	29,78	430	783	0,18
33371	/1	4	Mudstone	0,46	12,25	98,21		0,04	1,88	421	409	0,02
33371	/2	4	Sol. seam	2,01	11,85	81,97	9,83	0,23	12,59	418	626	0,02
33372	/1	4	Mudstone	0,42	11,65	93,55		0,16	1,55	429	369	0,09
33372	/2	4	Laminite	0,46	10,75	85,72		0,02	1,48	429	322	0,01
33374	/1	4	Impregnated	0,80	12,60	98,29		1,73	6,15	426	769	0,22
33376	/1	8	Laminite	0,58	10,90	85,97		0,19	2,12	414	366	0,08
33377	/1	8	Laminite	1,63	10,75	75,97		0,54	10,84	408	665	0,05
33381	/1	8	Impregnated	1,81	12,45	88,63		6,90	10,62	415	587	0,39
33384	/1	8	Laminite	1,15	11,65	87,47		0,67	5,12	415	445	0,12
33386	/1	8	Impregnated	0,40	11,50	92,46		1,38	1,49	421	373	0,48
33388	/1	8	Mudstone	0,17	11,90	97,71		0,03	0,32	424	188	0,09
33391	/1	8	Shale	3,86	4,36	4,17		0,70	28,29	412	733	0,02
33393	/1	8	Mudstone	0,81	12,20	94,88		3,18	4,19	420	517	0,43
33393	/2	8	Laminite	0,42	12,15	97,71		0,65	1,47	421	350	0,31
33393	/3	8	Shale	12,10	16,10	33,32		1,30	96,71	412	799	0,01
33398	/1	8	Impregnated	0,69	11,65	91,30		1,05	3,05	422	442	0,26
33399	/1	8	Impregnated	1,84	13,00	93,05		3,64	12,79	417	695	0,22
33400	/1	8	Shale	7,88	8,03	1,25		1,27	57,39	420	728	0,02
33401	/1	8	Shale	8,08	8,57	4,08		1,67	61,54	422	762	0,03
33402	/1	8	Shale	11,00	11,55	4,58		1,66	89,53	422	814	0,02
33403	/1	8	Mudstone	0,10	12,00	99,13		0,01	0,07	432	70	0,13
33403	/2	8	Impregnated	0,38	12,10	97,63		1,06	1,32	426	347	0,45
33404	/1	8	Shale	5,22	5,29	0,58		0,39	33,97	406	651	0,01
33406	/1	8	Shale	7,19	7,41	1,83		1,68	53,34	406	770	0,03
33407	/1	8	Mudstone	0,30	11,75	95,38		0,05	0,80	425	267	0,06
33407	/2	8	Sol. seam	1,91	11,15	76,97	8,64	0,51	12,94	416	677	0,04
33409	/1	8	Laminite	0,80	11,00	85,00		0,31	4,42	411	553	0,07
33411	/1	8	Mudstone	0,32	11,90	96,46		0,17	0,95	426	297	0,15
33411	/2	8	Shale	13,10	16,30	26,66		1,41	109,06	415	833	0,01
33414	/1	8	Laminite	0,48	11,30	90,13		0,09	1,77	426	369	0,05
33416	/1	8	Impregnated							0	0	
33418	/1	8	Mudstone	0,25	11,85	96,63		0,01	0,67	425	268	0,01
33418	/2	8	Sol. seam	0,51	11,80	94,05	9,98	0,03	1,97	423	386	0,02
33421	/1	8	Shale	2,19	7,15	41,32		0,42	13,54	415	618	0,03
33423	/1	8	Shale	7,25	8,55	10,83		1,20	59,12	423	815	0,02
33424	/1	8	Shale	13,70	15,80	17,49		2,18	127,84	411	933	0,02
33425	/1	8	Shale	4,25	4,64	3,25		0,56	30,56	416	719	0,02
33427	/1	8	Impregnated	1,34	13,65	102,54		4,79	7,45	421	556	0,39
33428	/1	8	Impregnated	0,29	12,30	100,04		0,41	0,98	435	338	0,29
33430	/1	24	Impregnated	0,39	11,65	93,80		0,18	1,05	427	269	0,15
33431	/1	24	Mudstone	0,15	11,65	95,80		0,01	0,16	424	107	0,06
33431	/2	24	Stylolite	1,82	13,00	93,13	60,17	0,63	11,58	415	636	0,05
33432	/1	24	Shale	5,99	9,14	26,24		1,22	49,30	417	823	0,02
33433	/1	24	Mudstone	0,45	11,85	94,96		0,06	1,81	427	402	0,03
33433	/2	24	Sol. seam	2,48	11,85	78,05	11,85	0,28	18,10	419	730	0,02
33433	/3	24	Impregnated	0,68	12,00	94,30		0,22	3,25	424	478	0,06

Table 1: Organic carbon, carbonate carbon and Rock-Eval data of all samples analysed.

		TOC	CaCO3	S1	S2	Tmax	HI	PI
		(%)	(%)	(mg HC/g)	mg HC/g)	(°C)	(mg HC/gTOC)	
Impregnated	Average	1,00	93,44	2,13	6,26	424	504	0,25
samples	Maximum	3,82	100,00	6,90	29,78	435	783	0,48
	Minimum	0,20	68,56	0,05	0,39	415	195	0,06
Laminites	Average	0,96	83,76	0,35	4,57	417	441	0,09
	Maximum	1,68	97,71	0,67	10,84	429	665	0,31
	Minimum	0,42	72,39	0,02	1,47	408	322	0,01
Mudstones &	Average	0,28	96,79	0,27	0,94	395	239	0,09
Wackestones	Maximum	0,81	99,13	3,18	4,19	432	517	0,43
	Minimum	0,10	93,55	0,01	0,07	420	70	0,01
Shale	Average	8,88	12,12	1,37	69,86	414	742	0,03
	Maximum	27,60	41,32	3,27	225,85	423	933	0,12
	Minimum	2,19	0,00	0,39	11,84	396	317	0,01
Sol. Seam &	Average	1,49	88,21	0,32	9,36	419	538	0,03
Stylolite	Maximum	2,48	95,88	0,64	18,10	428	730	0,05
	Minimum	0,34	76,97	0,02	0,61	415	179	0,02

Table 2: Average, maximum and minimum TOC, carbonate and Rock Eval data of the sample lithofacies.

E Number	Sample type	TOC %	S2 mg HC/g	HI mg HC/g TOC	OI mg CO2/g TOC	Tmax °C
E 33354	Laminite	5,14	22,58	439	14	404
E 33356/1	Mudstone	7,97	31,73	398	15	416
E 33356/2	Sol. Seam	8,43	36,01	427	25	408
E 33357/2	Sol. Seam	54,90	439,63	801	13	407
E 33363	Laminite	37,50	223,99	597	16	402
E 33366/1	Mudstone	27,30	148,10	542	17	415
E 33366/2	Sol. Seam	51,70	418,76	810	12	408
E 33366/4	Shale	56,00	465,61	831	10	410
E 33369/2	Sol. Seam	46,10	234,73	509	22	410
E 33371/2	Sol. Seam	37,40	235,77	630	18	410
E 33372/2	Sol. Seam	27,00	173,40	642	16	414
E 33376	Laminite	28,00	185,49	662	16	404
E 33377	Shale	36,10	270,90	750	14	406
E 33384	Laminite	44,40	247,59	558	14	398
E 33388	Mudstone	56,20	294,89	525	14	408
E 33402	Shale	30,90	273,78	886	8	420
E 33404	Shale	27,90	230,49	826	10	409
E 33406	Shale	23,40	204,76	875	10	410
E 33407/2	Sol. Seam	40,20	298,02	741	15	409
E 33409	Laminite	36,20	280,16	774	8	411
E 33414	Shale	32,40	229,69	709	16	403
E 33418/1	Mudstone	6,45	30,24	469	18	430
E 33423	Shale	34,30	319,83	932	8	418
E 33424	Shale	44,80	397,95	888	8	411
E 33431/2	Sol. Seam	56,80	400,20	705	10	413
E 33431/1	Mudstone	20,40	77,53	380	20	417
E 33432	Shale	25,50	191,51	751	12	415
E 33433/2	Sol. Seam	52,50	446,46	850	11	416

Table 3: Organic carbon and selected Rock-Eval data of the kerogen concentrates.

E Number	C	H	N	O	S	Fe	S org	O/C	H/C	S/C	N/C
	%	%	%	%	%	%	%				
E 33357/2	57,00	6,80	1,30	9,90	17,20	7,40	8,45	0,13	1,43	0,06	0,0195
E 33363	39,50	4,70	0,80	10,20	26,30	18,30	4,67	0,19	1,43	0,04	0,0174
E 33366/2	56,95	6,25	0,15	n.d.	20,40	8,51	10,34		1,32	0,07	0,0023
E 33366/4	56,30	7,02	0,20	6,80	14,40	2,80	11,09	0,09	1,50	0,07	0,0030
E 33369/2	48,90	5,00	0,70	11,20	19,20	13,10	3,72	0,17	1,23	0,03	0,0123
E 33372/2	28,10	3,40	0,60	7,30	32,50	28,20	-0,83	0,19	1,45	-0,01	0,0183
E 33376	29,70	4,00	0,60	8,30	33,20	25,80	2,71	0,21	1,62	0,03	0,0173
E 33377	37,20	5,00	0,60	7,60	27,30	19,10	4,73	0,15	1,61	0,05	0,0138
E 33402	28,95	3,90	0,25	7,70	13,70	6,77	5,70	0,20	1,62	0,07	0,0074
E 33404	30,50	4,30	0,50	11,90	16,50	9,30	5,51	0,29	1,69	0,07	0,0141
E 33406	25,40	3,90	0,50	8,20	16,70	12,10	2,40	0,24	1,84	0,04	0,0169
E 33407/2	42,10	5,10	0,90	8,60	21,20	14,00	4,65	0,15	1,45	0,04	0,0183
E 33409	37,60	4,70	0,80	7,20	28,70	21,00	3,88	0,14	1,50	0,04	0,0182
E 33414	33,20	3,90	0,60	8,40	26,40	25,50	-3,74	0,19	1,41	-0,04	0,0155
E 33423	36,20	4,35	0,60	7,00	18,10	11,40	4,63	0,15	1,44	0,05	0,0142
E 33424	47,75	5,75	0,15	7,70	18,00	5,03	12,06	0,12	1,45	0,09	0,0027
E 33431-2	62,40	6,85	0,80	9,50	15,80	4,94	9,96	0,11	1,32	0,06	0,0110
E 33432	26,15	3,70	0,30	8,90	15,30	7,32	6,65	0,26	1,70	0,10	0,0098
E 33433/2	54,40	5,95	0,40	8,00	19,90	9,10	9,15	0,11	1,31	0,06	0,0063

Table 4: Elemental composition and atomic ratios of selected kerogen concentrates.

Well 8	T hom	T hom	T hom	Well 24	T hom	T hom	T hom
		Sample Average	Well Average			Sample Average	Well Average
#1	73,30	73,32	75,32	#1	72,10	72,10	72,82
	73,60				71,80		
	73,20				71,80		
	73,20				72,40		
	73,30				72,30		
#2	76,90	76,70		#2	73,20	73,50	
	76,70				73,80		
	76,70				73,40		
	76,30				73,20		
	76,90				73,80		
#3	77,30	77,14		#3	72,40	72,85	
	77,20				72,90		
	77,20				73,10		
	77,00				72,80		
	77,00				73,10		
#4	74,50	74,10					
	74,10						
	74,00						
	74,50						
	73,40						

Table 5: Homogenisation temperatures (°C) determined for the samples described in the text.

E number	Sub-Sample	Well	Sample type	Depth from (m)	Depth to (m)	SOM (mg)	mgSOM/gRock	mgSOM/gTOC
33353	/1	17	Impregnated	1992,30	1992,40	222,86	4,53	532,36
33354	/1	17	Laminite	1994,40	1994,50	300,17	3,00	212,89
33356	/1	17	Mudstone	2020,55	2020,65	9,43	0,09	67,36
33356	/2	17	Sol. Seam	2020,55	2020,65	27,8	0,37	73,88
33357	/1	17	Mudstone	2024,40	2024,50	19,7	0,20	115,88
33357	/2	17	Sol. Seam	2024,40	2024,50	195,53	2,25	112,01
33357	/3	17	Impregnated	2024,40	2024,50	11,54	0,54	271,40
33360	/1	17	Shale	2039,00	2039,20	322,56	6,45	172,49
33363	/1	4	Shale	2532,80	2532,82	82,62	1,65	98,36
33366	/1	4	Mudstone	2541,73	2542,15	21,9	0,22	136,87
33366	/2	4	Sol. Seam	2541,73	2542,15	199,35	2,31	123,54
33366	/3	4	Impregnated	2541,73	2542,15	124,5	2,48	990,26
33366	/4	4	Shale	2541,73	2542,15	944,82	18,90	68,47
33369	/1	4	Mudstone	2552,80	2553,20	14,58	0,15	208,29
33369	/2	4	Stylolite	2552,80	2553,20	21,37	0,21	62,85
33369	/3	4	Impregnated	2552,80	2553,20	158,03	2,90	221,75
33370	/1	4	Impregnated	2553,90	2554,00	2560,14	63,57	1664,25
33371	/1	4	Mudstone	2556,30	2556,40	17,99	0,36	78,22
33371	/2	4	Sol. Seam	2556,30	2556,40	58,49	1,17	58,20
33372	/1	4	Mudstone	2561,05	2561,16	16,65	0,33	79,29
33372	/2	4	Laminite	2561,05	2561,16	22,75	0,23	49,46
33374	/1	4	Impregnated	2613,25	2613,40	317,27	6,48	809,86
33376	/1	8	Laminite	3064,05	3064,15	71,46	0,71	123,21
33377	/1	8	Shale	3064,55	3054,56	168,28	1,80	110,26
33381	/1	8	Impregnated	3073,40	3073,55	449,3	8,71	481,16
33384	/1	8	Laminite	3077,45	3077,50	113,69	2,27	197,72
33386	/1	8	Impregnated	3085,20	3085,30	270,15	6,03	1507,20
33388	/1	8	Mudstone	3092,05	3092,25	29,46	0,29	173,29
33391	/1	8	Shale	3103,20	3103,21	267,09	2,67	69,19
33393	/1	8	Mudstone	3107,00	3107,25	544,38	6,56	809,63
33393	/2	8	Laminite	3107,00	3107,25	313,62	3,14	746,71
33393	/3	8	Shale	3107,00	3107,25	456,29	9,13	75,42
33398	/1	8	Impregnated	3124,65	3124,70	142,95	3,12	451,56
33399	/1	8	Impregnated	3124,70	3124,75	57,93	1,23	66,90
33400	/1	8	Shale	3124,80	3124,85	286,78	5,74	72,79
33401	/1	8	Shale	3124,85	3124,90	390,65	7,81	96,70
33402	/1	8	Shale	3124,95	3125,00	376,15	7,52	68,39
33403	/1	8	Mudstone	3125,00	3125,20	17,36	0,35	347,20
33403	/2	8	Impregnated	3125,00	3125,20	159,3	5,17	1359,31
33404	/1	8	Shale	3127,10	3127,15	437,2	8,74	167,51
33406	/1	8	Shale	3129,30	3129,35	420,75	8,42	117,04
33407	/1	8	Mudstone	3136,45	3136,55	41,99	0,42	139,97
33407	/2	8	Sol. Seam	3136,45	3136,55	254,27	2,54	133,13
33409	/1	8	Laminite	3142,00	3142,05	298,32	2,98	372,90
33411	/1	8	Mudstone	3147,10	3147,20	29,2	1,03	321,30
33411	/2	8	Shale	3147,10	3147,20	643,29	12,87	98,21
33414	/1	8	Shale	3164,50	3164,52	34,77	0,35	72,44
33416	/1	8	Impregnated	3174,30	3174,40	165,6	4,17	
33418	/1	8	Mudstone	3180,70	3180,95	21,91	0,22	87,64
33418	/2	8	Sol. Seam	3180,70	3180,95	43,59	0,44	85,47
33421	/1	8	Shale	3192,65	3192,70	186,18	1,86	85,01
33423	/1	8	Shale	3196,85	3196,90	266,83	5,34	73,61
33424	/1	8	Shale	3202,20	3202,25	366,89	7,34	53,56
33425	/1	8	Shale	3205,60	3205,65	176,51	3,53	83,06
33427	/1	8	Impregnated	3218,25	3218,30	894,12	20,42	1523,76
33428	/1	8	Impregnated	3230,75	3230,90	99,46	1,78	615,18
33430	/1	24	Impregnated	4437,40	4437,45	28,08	0,41	106,37
33431	/1	24	Mudstone	4437,55	4437,65	14,42	0,29	192,27
33431	/2	24	Stylolite	4437,55	4437,65	313,9	3,14	172,47
33432	/1	24	Shale	4439,25	4439,30	286,25	5,73	95,58
33433	/1	24	Mudstone	4439,30	4439,45	46,23	0,46	102,73
33433	/2	24	Sol. Seam	4439,30	4439,45	92,89	1,86	74,91
33433	/3	24	Impregnated	4439,30	4439,45	50,43	0,92	134,59

Table 6: Depth and soluble organic matter content (SOM) of the sample analysed.

E number	Sub-Sample	Well	Sample type	Depth from (m)	Depth to (m)	SOM (mg)	mgSOM/ g rock	mgSOM/ g TOC	Average mgSOM/ g TOC
33357	/3	17	Impregnated	2024,40	2024,50	11,54	0,54	271,40	715,73
33433	/3	24	Impregnated	4439,30	4439,45	50,43	0,92	134,59	
33353	/1	17	Impregnated	1992,30	1992,40	222,86	4,53	532,36	
33366	/3	4	Impregnated	2541,73	2542,15	124,5	2,48	990,26	
33369	/3	4	Impregnated	2552,80	2553,20	158,03	2,90	221,75	
33398	/1	8	Impregnated	3124,65	3124,70	142,95	3,12	451,56	
33399	/1	8	Impregnated	3124,70	3124,75	57,93	1,23	66,90	
33403	/2	8	Impregnated	3125,00	3125,20	159,3	5,17	1359,31	
33430	/1	24	Impregnated	4437,40	4437,45	28,08	0,41	106,37	
33370	/1	4	Impregnated	2553,90	2554,00	2560,14	63,57	1664,25	
33374	/1	4	Impregnated	2613,25	2613,40	317,27	6,48	809,86	
33381	/1	8	Impregnated	3073,40	3073,55	449,3	8,71	481,16	
33386	/1	8	Impregnated	3085,20	3085,30	270,15	6,03	1507,20	
33427	/1	8	Impregnated	3218,25	3218,30	894,12	20,42	1523,76	
33428	/1	8	Impregnated	3230,75	3230,90	99,46	1,78	615,18	
33354	/1	17	Laminite	1994,40	1994,50	300,17	3,00	212,89	283,81
33372	/2	4	Laminite	2561,05	2561,16	22,75	0,23	49,46	
33376	/1	8	Laminite	3064,05	3064,15	71,46	0,71	123,21	
33384	/1	8	Laminite	3077,45	3077,50	113,69	2,27	197,72	
33393	/2	8	Laminite	3107,00	3107,25	313,62	3,14	746,71	
33409	/1	8	Laminite	3142,00	3142,05	298,32	2,98	372,90	
33356	/1	17	Mudstone	2020,55	2020,65	9,43	0,09	67,36	204,28
33357	/1	17	Mudstone	2024,40	2024,50	19,7	0,20	115,88	
33366	/1	4	Mudstone	2541,73	2542,15	21,9	0,22	136,87	
33369	/1	4	Mudstone	2552,80	2553,20	14,58	0,15	208,29	
33371	/1	4	Mudstone	2556,30	2556,40	17,99	0,36	78,22	
33372	/1	4	Mudstone	2561,05	2561,16	16,65	0,33	79,29	
33388	/1	8	Mudstone	3092,05	3092,25	29,46	0,29	173,29	
33393	/1	8	Mudstone	3107,00	3107,25	544,38	6,56	809,63	
33403	/1	8	Mudstone	3125,00	3125,20	17,36	0,35	347,20	
33407	/1	8	Mudstone	3136,45	3136,55	41,99	0,42	139,97	
33411	/1	8	Mudstone	3147,10	3147,20	29,2	1,03	321,30	
33418	/1	8	Mudstone	3180,70	3180,95	21,91	0,22	87,64	
33431	/1	24	Mudstone	4437,55	4437,65	14,42	0,29	192,27	
33433	/1	24	Mudstone	4439,30	4439,45	46,23	0,46	102,73	
33360	/1	17	Shale	2039,00	2039,20	322,56	6,45	172,49	93,23
33363	/1	4	Shale	2532,80	2532,82	82,62	1,65	98,36	
33366	/4	4	Shale	2541,73	2542,15	944,82	18,90	68,47	
33377	/1	8	Shale	3064,55	3054,56	168,28	1,80	110,26	
33391	/1	8	Shale	3103,20	3103,21	267,09	2,67	69,19	
33393	/3	8	Shale	3107,00	3107,25	456,29	9,13	75,42	
33400	/1	8	Shale	3124,80	3124,85	286,78	5,74	72,79	
33401	/1	8	Shale	3124,85	3124,90	390,65	7,81	96,70	
33402	/1	8	Shale	3124,95	3125,00	376,15	7,52	68,39	
33404	/1	8	Shale	3127,10	3127,15	437,2	8,74	167,51	
33406	/1	8	Shale	3129,30	3129,35	420,75	8,42	117,04	
33411	/2	8	Shale	3147,10	3147,20	643,29	12,87	98,21	
33414	/1	8	Shale	3164,50	3164,52	34,77	0,35	72,44	
33421	/1	8	Shale	3192,65	3192,70	186,18	1,86	85,01	
33423	/1	8	Shale	3196,85	3196,90	266,83	5,34	73,61	
33424	/1	8	Shale	3202,20	3202,25	366,89	7,34	53,56	
33425	/1	8	Shale	3205,60	3205,65	176,51	3,53	83,06	
33432	/1	24	Shale	4439,25	4439,30	286,25	5,73	95,58	
33356	/2	17	Sol. Seam	2020,55	2020,65	27,8	0,37	73,88	99,61
33357	/2	17	Sol. Seam	2024,40	2024,50	195,53	2,25	112,01	
33366	/2	4	Sol. Seam	2541,73	2542,15	199,35	2,31	123,54	
33371	/2	4	Sol. Seam	2556,30	2556,40	58,49	1,17	58,20	
33407	/2	8	Sol. Seam	3136,45	3136,55	254,27	2,54	133,13	
33418	/2	8	Sol. Seam	3180,70	3180,95	43,59	0,44	85,47	
33433	/2	24	Sol. Seam	4439,30	4439,45	92,89	1,86	74,91	
33369	/2	4	Stylolite	2552,80	2553,20	21,37	0,21	62,85	
33431	/2	24	Stylolite	4437,55	4437,65	313,9	3,14	172,47	

Table 7: Average and absolute SOM yields of the samples analysed sorted according to their lithofacies.

E Number	Sub-Sample	Sample type	Sat (%)	Aro (%)	Het (%)	Asph (%)
33352	/1	Mudstone	26,75	12,77	39,88	20,60
33353	/1	Impregnated				
33354	/1	Laminite	20,80	7,07	21,37	50,76
33356	/1	Mudstone	14,84	12,65	53,89	18,62
33356	/2	Sol. Seam	10,80	12,16	43,91	33,12
33357	/3	Impregnated	11,66	25,91	35,74	26,70
33357	/1	Mudstone	12,10	12,88	48,63	26,39
33357	/2	Sol. Seam	10,59	16,00	41,61	31,80
33360	/1	Shale	101,89	4,90	22,04	-28,84
33363	/1	Laminite				
33366	/4	Shale				
33366	/3	Impregnated	2,56	8,82	24,73	63,89
33366	/1	Mudstone	5,66	10,08	42,62	41,64
33366	/2	Sol. Seam	3,82	14,84	43,95	37,39
33369	/3	Impregnated	3,39	9,32	30,41	56,89
33369	/1	Mudstone	18,93	4,09	23,13	53,85
33369	/2	Stylolite	9,56	11,06	49,87	29,52
33370	/1	Impregnated	0,27	0,90	3,61	95,22
33371	/1	Mudstone				
33371	/2	Sol. Seam				
33372	/2	Laminite	9,67	20,25	55,59	14,49
33372	/1	Mudstone				
33374	/1	Impregnated	1,46	4,68	12,95	80,90
33376	/1	Laminite	14,96	13,54	58,87	12,62
33377	/1	Shale	8,98	13,59	55,15	22,28
33381	/1	Impregnated	16,48	13,05	27,33	43,14
33384	/1	Laminite				
33386	/1	Impregnated	18,03	13,36	38,24	30,37
33388	/1	Mudstone	7,37	13,13	51,53	27,96
33391	/1	Shale	12,08	11,53	62,00	14,39
33393	/3	Shale	3,52	3,63	16,39	76,46
33393	/2	Laminite	11,70	10,30	26,51	51,49
33393	/1	Mudstone	18,19	18,09	35,69	28,03
33398	/1	Impregnated	16,99	17,00	39,19	26,82
33399	/1	Impregnated	19,61	17,75	36,18	26,46
33400	/1	Shale	2,24	6,47	54,13	37,17
33401	/1	Shale	0,97	3,28	31,31	64,44
33402	/1	Shale	2,75	9,92	48,76	38,56
33403	/2	Impregnated	17,26	18,49	40,91	23,34
33403	/1	Mudstone				
33404	/1	Shale	4,38	17,99	53,67	23,95
33406	/1	Shale	3,28	12,09	48,23	36,40
33407	/1	Mudstone	3,25	12,14	55,04	29,57
33407	/2	Sol. Seam				
33409	/1	Laminite	2,99	15,49	59,62	21,91
33411	/2	Shale	0,54	3,82	19,23	76,40
33411	/1	Mudstone	3,73	16,29	59,31	20,67
33414	/1	Shale	13,92	16,93	61,04	8,11
33416	/1	Impregnated	4,41	14,85	49,52	31,22
33418	/1	Mudstone	7,54	13,18	64,70	14,58
33418	/2	Sol. Seam	6,10	12,68	57,36	23,87
33421	/1	Shale	13,71	21,87	58,04	6,37
33423	/1	Shale	7,79	9,90	52,35	29,96
33424	/1	Shale				
33425	/1	Shale	8,25	18,25	47,28	26,22
33427	/1	Impregnated	3,95	4,45	9,97	81,63
33428	/1	Impregnated	8,09	11,84	28,87	51,21
33430	/1	Impregnated	4,60	7,57	35,11	52,73
33431	/1	Mudstone	4,69	6,85	34,45	54,00
33431	/2	Stylolite				
33432	/1	Shale				
33433	/3	Impregnated	5,19	10,68	41,68	42,46
33433	/1	Mudstone	6,26	13,39	53,88	26,47
33433	/2	Sol. Seam	3,05	9,88	44,55	42,51

Table 8: Compound class distribution of the sampes analysed. Samples without data are those where quantification was impossible due to oxidation for aromatic analysis.

E number	Sub-Sample	Sample type	Sat (%)	Aro (%)	Het (%)	Asph (%)	Sat Av.	Aro Av.	Het Av.	Asph Av.
33357	/3	Impregnated	11,66	25,91	35,74	26,70	8,93	11,91	30,30	48,86
33416	/1	Impregnated	4,41	14,85	49,52	31,22				
33433	/3	Impregnated	5,19	10,68	41,68	42,46				
33353	/1	Impregnated								
33366	/3	Impregnated	2,56	8,82	24,73	63,89				
33369	/3	Impregnated	3,39	9,32	30,41	56,89				
33398	/1	Impregnated	16,99	17,00	39,19	26,82				
33399	/1	Impregnated	19,61	17,75	36,18	26,46				
33403	/2	Impregnated	17,26	18,49	40,91	23,34				
33430	/1	Impregnated	4,60	7,57	35,11	52,73				
33370	/1	Impregnated	0,27	0,90	3,61	95,22				
33374	/1	Impregnated	1,46	4,68	12,95	80,90				
33381	/1	Impregnated	16,48	13,05	27,33	43,14				
33386	/1	Impregnated	18,03	13,36	38,24	30,37				
33427	/1	Impregnated	3,95	4,45	9,97	81,63				
33428	/1	Impregnated	8,09	11,84	28,87	51,21				
33354	/1	Laminite	20,80	7,07	21,37	50,76	12,02	13,33	44,39	30,25
33363	/1	Laminite								
33372	/2	Laminite	9,67	20,25	55,59	14,49				
33376	/1	Laminite	14,96	13,54	58,87	12,62				
33384	/1	Laminite								
33393	/2	Laminite	11,70	10,30	26,51	51,49				
33409	/1	Laminite	2,99	15,49	59,62	21,91				
33352	/1	Mudstone	26,75	12,77	39,88	20,60	10,78	12,13	46,90	30,20
33356	/1	Mudstone	14,84	12,65	53,89	18,62				
33357	/1	Mudstone	12,10	12,88	48,63	26,39				
33366	/1	Mudstone	5,66	10,08	42,62	41,64				
33369	/1	Mudstone	18,93	4,09	23,13	53,85				
33371	/1	Mudstone								
33372	/1	Mudstone								
33388	/1	Mudstone	7,37	13,13	51,53	27,96				
33393	/1	Mudstone	18,19	18,09	35,69	28,03				
33403	/1	Mudstone								
33407	/1	Mudstone	3,25	12,14	55,04	29,57				
33411	/1	Mudstone	3,73	16,29	59,31	20,67				
33418	/1	Mudstone	7,54	13,18	64,70	14,58				
33431	/1	Mudstone	4,69	6,85	34,45	54,00				
33433	/1	Mudstone	6,26	13,39	53,88	26,47				
33360	/1	Shale	101,89	4,90	22,04	-28,84	6,34	11,48	46,74	35,44
33366	/4	Shale								
33377	/1	Shale	8,98	13,59	55,15	22,28				
33391	/1	Shale	12,08	11,53	62,00	14,39				
33393	/3	Shale	3,52	3,63	16,39	76,46				
33400	/1	Shale	2,24	6,47	54,13	37,17				
33401	/1	Shale	0,97	3,28	31,31	64,44				
33402	/1	Shale	2,75	9,92	48,76	38,56				
33404	/1	Shale	4,38	17,99	53,67	23,95				
33406	/1	Shale	3,28	12,09	48,23	36,40				
33411	/2	Shale	0,54	3,82	19,23	76,40				
33414	/1	Shale	13,92	16,93	61,04	8,11				
33421	/1	Shale	13,71	21,87	58,04	6,37				
33423	/1	Shale	7,79	9,90	52,35	29,96				
33424	/1	Shale								
33425	/1	Shale	8,25	18,25	47,28	26,22				
33432	/1	Shale								
33356	/2	Sol. Seam	10,80	12,16	43,91	33,12	7,32	12,77	46,88	33,03
33357	/2	Sol. Seam	10,59	16,00	41,61	31,80				
33366	/2	Sol. Seam	3,82	14,84	43,95	37,39				
33371	/2	Sol. Seam								
33407	/2	Sol. Seam								
33418	/2	Sol. Seam	6,10	12,68	57,36	23,87				
33433	/2	Sol. Seam	3,05	9,88	44,55	42,51				
33369	/2	Stylolite	9,56	11,06	49,87	29,52				
33431	/2	Stylolite								

Table 9: Average (av.) and absolute compound class distributions of the samples analysed sorted according to their lithofacies.

E Number	CPI 1	CPI 2	CPI 3	CPI 4	CPI 5	LHCPI	ISO 1	ISO 2	ISO 3
E 33353	1,15	1,21	1,34	1,47	1,28	1,05	1,28	2,87	0,42
E 33354	0,97	1,05	1,06	1,07	1,03	0,04	1,86	3,81	0,69
E 33356/1	0,92	1,04	1,06	1,10	1,04	2,22	0,67	0,72	1,14
E 33356/2	0,96	1,05	1,08	1,10	1,05	1,37	0,71	0,88	0,99
E 33357/1	1,01	1,07	1,09	1,10	1,07	2,61	0,85	1,50	0,61
E 33357/2	1,12	1,18	1,31	1,44	1,24	1,75	1,00	2,34	0,49
E 33357/3	0,93	1,04	1,06	1,08	1,04	0,19	0,89	1,53	0,58
E 33363	2,44	2,92	2,67	2,35	2,53	0,30	4,01	7,64	0,71
E 33366/1	1,16	1,22	1,32	1,42	1,22	0,85	0,83	1,36	0,69
E 33366/2	1,16	1,25	1,34	1,44	1,27	1,76	0,69	1,16	0,65
E 33366/3	1,17	1,26	1,31	1,36	1,24	1,56	0,73	0,89	0,62
E 33366/4	1,17	1,79	1,93	2,08	1,40	0,79	3,68	2,59	1,80
E 33369/1	0,99	1,01	1,02	1,04	1,02	0,25	0,52	0,79	0,69
E 33369/2	1,02	1,01	1,03	1,06	1,01	1,64	0,62	0,79	0,98
E 33369/3	1,05	1,07	1,13	1,20	1,10	1,68	0,41	0,79	0,44
E 33370	1,05	1,09	1,15	1,20	1,13	1,68	0,34	0,96	0,40
E 33371/1	1,06	1,08	1,13	1,19	1,14	2,33	1,15	0,85	1,61
E 33371/2	1,23	1,18	1,43	1,65	1,42	0,85	1,76	1,27	1,78
E 33372/1	1,81	1,96	1,95	1,94	1,90	0,44	0,89	3,14	0,36
E 33372/2	1,05	1,22	1,48	1,71	1,35	1,79	2,12	1,35	1,92
E 33374	1,01	1,04	1,09	1,14	1,08	1,43	0,33	0,78	0,37
E 33376	2,19	2,67	2,58	2,50	2,30	0,45	1,71	13,14	0,18
E 33377	2,02	2,33	2,28	2,23	2,28	0,40	3,75	20,31	0,24
E 33381	1,16	1,32	1,50	1,65	1,34	1,49	1,48	4,06	0,44
E 33384	1,15	1,28	1,53	1,73	1,33	1,65	1,36	4,08	0,46
E 33386	1,17	1,26	1,46	1,65	1,33	1,39	1,41	3,87	0,42
E 33388	1,52	1,67	1,76	1,82	1,74	1,79	0,88	2,00	0,55
E 33391	1,74	2,90	2,60	2,32	2,21	1,17	0,90	5,92	0,25
E 33393/1	1,15	1,26	1,41	1,55	1,19	1,43	1,46	4,13	0,45
E 33393/2	1,14	1,25	1,42	1,56	1,31	1,29	1,48	4,22	0,41
E 33393/3	1,14	1,28	1,48	1,67	1,31	1,75	1,24	3,55	0,45
E 33398	1,22	1,36	1,57	1,75	1,39	1,58	1,43	3,72	0,45
E 33399	1,20	1,33	1,57	1,77	1,38	1,99	1,17	2,17	0,46

Table 10: CPI and ISO data of all samples. Page 1

E Number	CPI 1	CPI 2	CPI 3	CPI 4	CPI 5	LHCPI	ISO 1	ISO 2	ISO 3
E 33400	1,31	1,37	1,59	1,74	1,18	3,60	1,24	4,01	0,50
E 33401	1,35	1,40	1,61	1,78	1,17	3,00	1,32	4,61	0,47
E 33402	1,28	1,30	1,58	1,81	1,31	3,68	1,25	4,00	0,51
E 33403/1	1,05	0,98	1,21	1,62	1,11	4,20	1,13	2,56	0,58
E 33403/2	1,17	1,30	1,50	1,68	1,26	1,17	1,49	3,67	0,41
E 33404	1,62	1,79	2,12	2,42	1,82	1,29	2,72	5,42	0,74
E 33406	1,87	1,96	2,16	2,36	1,90	0,98	2,33	4,84	0,64
E 33407/1	1,67	2,19	2,35	2,52	2,04	0,71	2,87	5,87	0,61
E 33407/2	1,48	1,92	2,46	2,99	2,83	0,96	2,79	4,22	0,83
E 33409	1,63	1,36	1,33	1,31	1,46	1,09	2,65	7,40	0,43
E 33411/1	1,43	1,85	1,86	1,87	1,72	0,62	1,79	3,83	0,55
E 33411/2	1,36	1,53	1,81	2,11	1,40	1,84	1,39	3,26	0,63
E 33414	1,50	1,76	1,85	1,93	1,68	1,10	1,69	7,32	0,30
E 33418/1	1,14	1,11	1,21	1,30	1,18	2,07	0,92	1,12	1,28
E 33418/2	1,09	1,07	1,20	1,33	1,35	1,87	1,01	1,22	1,41
E 33421	1,62	1,72	1,79	1,86	1,80	1,13	1,44	3,64	0,56
E 33423	1,79	1,92	2,06	2,21	1,97	0,96	2,35	5,31	0,61
E 33424	1,64	2,32	2,24	2,15	1,82	1,22	3,04	8,85	0,48
E 33425	1,90	1,87	1,93	2,00	1,81	1,07	1,96	3,95	0,66
E 33427	1,03	1,04	1,20	1,39	1,07	2,48	0,45	1,04	0,46
E 33428	0,99	1,01	1,03	1,04	1,02	1,46	0,29	0,51	0,51
E 33430	1,46	1,78	1,92	2,04	1,71	1,74	0,79	0,55	0,74
E 33431/1	1,04	1,03	1,17	1,32	1,21	4,54	0,68	0,99	0,59
E 33431/2	1,60	1,82	1,93	2,04	1,75	0,97	1,53	3,41	0,54
E 33432	1,13	1,16	1,36	1,54	1,21	1,26	5,26	9,12	0,64
E 33433/1	1,42	1,42	1,51	1,60	1,45	1,95	1,16	2,29	0,70
E 33433/2	1,20	1,39	1,53	1,65	1,33	1,20	3,20	6,10	0,64
E 33433/3	1,55	1,54	1,65	1,75	1,60	1,33	0,81	1,14	0,61

CPI 1 =	CPI (23-25)		CPI 4 =	CPI (29)			ISO 1 =	Pristane/n-C17H36
CPI 2 =	CPI (27)		CPI 5 =	CPI (25-31)			ISO 2 =	Phytane/n-C18H38
CPI 3 =	CPI (27-29)		LHCPI =	LHCPI (17, 18, 19/27, 28, 29)			ISO 3 =	Pristane/Phytane

Table 10: CPI and ISO data of all samples. Page 2

Sample	E 33352/1-EC_MPLC-1/1	E 33353/2-EC_MPLC-1/1	E 33354/2-EC_MPLC-1/1	E 33356/1-EC_MPLC-1/1	E 33356/1-EC_MPLC-2/1	E 33357/1-EC_MPLC-1/1	E 33357/3-EC_MPLC-2/1	E 33357/1-EC_MPLC-3/1
Depth in m	851.000 - 853.000	1992.300 - 1992.400	1994.400 - 1994.500	2020.550 - 2020.650	2020.550 - 2020.650	2024.400 - 2024.500	2024.400 - 2024.500	2024.400 - 2024.500
C-org (%)	0.20	0.85	1.41	0.14	0.50	0.17	2.01	0.20
n-Alkanes	Concentration in microgram / gram C-org							
15	323.35	398.37	129.46	158.69	119.19	88.06	83.80	62.49
16	466.47	693.62	126.50	239.62	138.93	155.01	88.88	115.87
17	521.44	1221.04	134.47	277.12	149.73	225.54	111.33	174.12
18	415.82	1316.48	95.77	225.58	120.96	208.77	97.62	172.99
19	275.24	1357.68	93.96	150.17	87.07	168.59	87.46	121.88
20	173.74	1276.80	179.81	95.23	60.81	131.60	74.52	98.76
21	110.13	1305.66	524.15	66.25	47.92	108.35	70.50	96.89
22	60.76	1312.37	852.40	50.14	41.26	92.40	66.39	125.82
23	32.28	1380.50	1143.03	44.81	41.16	83.33	67.23	210.53
24	20.46	1196.50	1385.05	50.03	45.09	74.39	56.42	313.41
25	18.28	1347.13	1759.09	62.48	56.16	77.28	61.41	426.77
26	16.31	1053.77	2382.39	82.57	72.02	77.65	49.62	611.38
27	17.80	1223.44	2947.24	95.36	84.97	82.59	56.23	758.44
28	14.90	967.94	3209.99	101.62	89.70	76.62	45.63	847.60
29	16.28	1513.73	3039.80	97.65	87.35	71.89	67.26	840.02
30	10.63	1092.23	2476.80	76.74	68.41	53.68	47.55	701.08
31	9.97	1317.63	1815.06	58.76	53.41	41.22	54.01	560.74
32	6.08	1045.17	1004.08	34.41	31.84	25.20	44.28	327.25
33	4.89	891.78	417.78	24.84	24.84	29.36	41.43	181.67
34	-	-	-	-	-	-	-	-
35	-	-	-	-	-	-	-	-
36	-	-	-	-	-	-	-	-
Sum n-Alkanes	2514.83	21911.84	23716.80	1992.06	1420.83	1871.53	1271.57	6747.70
Pristane	218.41	1568.55	250.70	186.60	105.91	192.09	111.60	154.20
Phytane	206.03	3778.02	364.51	163.38	106.58	313.04	227.96	264.21

Table 11: Yields of individual n-alkanes and selected isoprenoids

Sample	E 33370/1-EC_MPLC-1/1	E 33371/3-EC_MPLC-1/1	E 33371/2-EC_MPLC-2/1	E 33372/3-EC_MPLC-1/1	E 33372/1-EC_MPLC-2/1	E 33374/1-EC_MPLC-1/1
Depth in m	2553.900 - 2554.000	2556.300 - 2556.400	2556.300 - 2556.400	2561.050 - 2561.160	2561.050 - 2561.160	2613.250 - 2613.400
C-org (%)	3.82	0.46	2.01	0.46	0.46	0.80
n-Alkanes	Concentration in microgram / gram C-org					
15	338.75	28.54	19.18	20.62	34.93	88.56
16	422.99	43.39	22.29	25.86	35.94	137.02
17	512.75	58.26	27.25	37.35	39.98	215.56
18	461.52	49.08	21.17	29.30	32.89	245.16
19	449.90	37.03	17.08	37.33	28.53	234.94
20	417.80	28.08	14.18	35.76	30.43	225.47
21	403.98	23.89	12.80	74.44	28.21	217.41
22	373.62	19.98	12.53	49.67	21.18	203.73
23	355.32	19.55	15.53	87.36	15.90	190.49
24	308.11	18.16	13.48	54.26	11.10	168.16
25	306.68	20.00	18.69	110.38	12.94	162.68
26	276.34	18.58	16.03	60.78	11.45	156.39
27	283.96	20.53	21.87	106.28	16.11	157.83
28	244.33	19.52	21.06	47.69	14.90	147.92
29	318.16	21.95	34.24	81.84	25.79	179.75
30	284.83	17.44	20.40	36.82	15.33	166.58
31	289.58	18.57	29.65	58.13	24.52	159.80
32	212.74	12.76	19.37	31.10	24.82	118.68
33	266.39	31.73	28.23	46.11	26.47	138.21
34	-	-	-	-	-	-
35	-	-	-	-	-	-
36	-	-	-	-	-	-
Sum n-Alkanes	6527.75	507.04	385.02	1031.08	451.42	3314.34
Pristane	176.82	67.13	48.00	33.30	84.93	70.42
Phytane	440.86	41.63	26.92	91.87	44.32	190.93

Table 11 continued

Sample	E 33363/1-EC_MPLC-1/1	E 33366/1-EC_MPLC-1/1	E 33366/1-EC_MPLC-2/1	E 33366/1-EC_MPLC-3/1	E 33366/1-EC_MPLC-4/1	E 33369/1-EC_MPLC-1/1	E 33369/1-EC_MPLC-2/1	E 33369/1-EC_MPLC-3/1
Depth in m	2532.800 - 2532.820	2541.730 - 2542.150	2541.730 - 2542.150	2541.730 - 2542.150	2541.730 - 2542.150	2552.800 - 2553.200	2552.800 - 2553.200	2552.800 - 2553.200
C-org (%)	1.68	0.16	1.87	0.25	27.60	0.07	0.34	1.31
n-Alkanes	Concentration in microgram / gram C-org							
15	26.10	25.54	32.56	69.10	1.97	22.21	29.99	19.41
16	24.11	41.84	43.78	110.42	2.27	51.21	46.21	41.90
17	26.36	55.15	57.03	198.62	2.37	88.44	61.69	78.39
18	19.36	49.15	52.11	264.23	1.87	83.28	49.10	92.54
19	21.04	37.84	50.76	209.26	1.55	53.83	29.75	83.32
20	18.01	32.28	45.89	186.87	1.26	47.65	19.85	73.84
21	24.95	30.69	46.45	188.75	1.13	65.91	18.23	69.47
22	21.79	29.08	41.04	168.48	1.02	92.68	23.09	65.54
23	47.03	36.73	42.34	175.27	1.23	113.37	25.21	63.83
24	27.15	30.73	33.18	141.09	0.84	157.25	25.08	56.41
25	93.03	38.68	36.67	160.14	1.46	217.29	26.48	55.75
26	38.60	38.97	28.26	123.60	1.87	261.89	28.33	49.95
27	113.35	53.98	32.63	148.06	2.96	287.77	29.28	50.31
28	39.03	49.44	23.77	111.87	1.43	310.19	29.72	44.49
29	72.59	63.35	34.21	171.99	2.93	289.23	26.44	56.68
30	22.76	40.32	23.62	141.76	1.38	247.63	20.36	50.25
31	38.06	33.73	24.89	142.24	2.12	175.43	15.46	46.05
32	22.53	23.78	18.61	108.38	4.10	101.49	11.53	36.08
33	24.92	36.46	27.14	153.72	3.34	51.42	18.46	47.39
34	-	-	-	-	-	-	-	-
35	-	-	-	-	-	-	-	-
36	-	-	-	-	-	-	-	-
Sum n-Alkanes	720.75	747.93	694.91	2973.84	37.10	2718.19	534.27	1081.57
Pristane	105.65	46.01	39.39	145.76	8.74	45.72	38.01	32.15
Phytane	148.01	66.85	60.49	235.57	4.85	65.82	38.89	73.55

Table 11 continued

Sample	E 33376/1-EC_MPLC-1/1	E 33377/1-EC_MPLC-1/1	E 33381/1-EC_MPLC-1/1	E 33384/2-EC_MPLC-1/1	E 33386/1-EC_MPLC-1/1	E 33388/1-EC_MPLC-1/1	E 33391/1-EC_MPLC-1/1	E 33393/1-EC_MPLC-1/1
Depth in m	3064.050 - 3064.150	3064.550 - 3064.560	3073.400 - 3073.550	3077.450 - 3077.500	3085.200 - 3085.300	3092.050 - 3092.250	3103.200	3107.000 - 3107.250
C-org (%)	0.58	1.63	1.81	1.15	0.40	0.17	3.86	0.81
n-Alkanes	Concentration in microgram / gram C-org							
15	127.93	31.31	271.54	163.73	811.41	87.03	97.41	658.45
16	119.10	26.64	303.26	146.51	965.96	103.28	60.43	704.66
17	148.64	38.40	431.54	172.93	1442.62	144.84	109.62	942.11
18	104.96	30.01	358.82	123.76	1246.83	116.38	66.97	743.82
19	114.70	38.50	332.10	107.27	1139.42	109.75	91.45	684.95
20	103.00	29.10	274.18	85.19	980.57	74.61	71.51	587.85
21	136.56	62.75	269.91	83.18	976.18	85.96	67.70	578.54
22	127.13	59.86	276.18	82.39	1014.58	57.24	46.02	592.19
23	213.79	102.77	289.29	86.40	1045.03	69.90	58.74	616.90
24	97.15	44.70	244.85	73.11	902.56	39.36	32.73	537.54
25	257.20	88.04	268.07	78.44	1029.04	61.02	66.08	595.95
26	108.41	39.91	191.19	58.66	735.54	36.40	32.07	443.01
27	327.78	99.97	238.06	70.87	873.37	68.27	102.87	529.67
28	137.41	45.88	170.15	51.76	653.02	45.35	38.87	394.48
29	349.12	118.81	342.81	121.84	1237.65	93.85	87.97	737.81
30	142.22	60.47	244.90	89.46	846.52	57.62	37.04	560.18
31	177.82	170.28	304.74	108.85	1096.04	96.23	71.35	491.16
32	93.39	84.62	270.85	102.02	1013.73	48.21	49.75	640.64
33	113.23	49.93	186.52	67.89	678.65	83.57	60.33	443.03
34	-	-	-	-	-	-	-	-
35	-	-	-	-	-	-	-	-
36	-	-	-	-	-	-	-	-
Sum n-Alkanes	2999.56	1221.95	5268.96	1874.25	18688.73	1478.87	1248.91	11482.95
Pristane	254.81	144.09	636.59	234.63	2036.19	126.90	98.54	1372.09
Phytane	1379.61	609.47	1456.92	504.93	4823.08	232.65	396.45	3072.28

Table 11 continued

Sample	E 33393/1-EC_MPLC-2/1	E 33393/1-EC_MPLC-3/1	E 33398/1-EC_MPLC-1/1	E 33399/1-EC_MPLC-1/1	E 33400/1-EC_MPLC-1/1	E 33401/1-EC_MPLC-1/1	E 33402/1-EC_MPLC-1/1	E 33403/2-EC_MPLC-1/1
Depth in m	3107.000 - 3107.250	3107.000 - 3107.250	3124.650 - 3124.700	3124.700 - 3124.750	3124.800 - 3124.850	3124.850 - 3124.900	3124.950 - 3125.000	3125.000 - 3125.200
C-org (%)	0.42	12.10	0.69	1.84	7.88	8.08	11.00	0.10
n-Alkanes	Concentration in microgram / gram C-org							
15	220.33	16.93	251.50	32.80	14.99	17.49	13.81	31.91
16	288.30	16.63	297.56	38.65	10.93	13.52	10.59	59.00
17	434.57	21.15	401.43	61.73	10.75	13.51	10.81	74.53
18	369.11	16.36	340.78	72.97	6.66	8.22	6.61	56.09
19	356.85	14.76	298.13	56.59	5.81	7.33	5.52	46.69
20	317.09	12.11	243.09	42.29	3.56	4.80	3.67	38.79
21	316.81	11.62	246.15	40.14	3.54	4.95	3.55	48.97
22	323.81	11.51	233.24	36.65	2.63	3.71	2.70	46.06
23	336.91	11.85	253.63	38.16	2.94	4.25	2.94	39.71
24	298.53	10.06	199.19	29.87	1.90	2.68	1.84	35.24
25	323.57	10.70	230.07	33.63	2.10	3.18	2.02	34.34
26	241.38	7.97	161.80	23.47	1.29	1.97	1.35	25.03
27	285.62	9.49	207.49	29.44	1.81	2.88	1.78	16.88
28	214.39	6.90	143.74	20.85	1.36	2.14	1.39	9.59
29	402.69	13.56	307.38	46.02	3.28	4.68	3.07	15.75
30	300.72	9.37	208.27	31.19	2.39	3.14	2.01	9.85
31	392.06	11.86	279.04	40.57	4.35	3.55	3.98	5.61
32	340.33	11.18	243.42	36.10	11.33	8.73	6.35	10.67
33	229.07	8.47	177.65	26.09	14.19	19.57	4.25	14.34
34	-	-	-	-	-	-	-	-
35	-	-	-	-	-	-	-	-
36	-	-	-	-	-	-	-	-
Sum n-Alkanes	5992.14	232.45	4723.56	737.21	105.79	130.31	88.22	619.05
Pristane	644.71	26.15	572.97	72.36	13.29	17.83	13.53	83.95
Phytane	1557.14	58.14	1267.30	158.18	26.70	37.88	26.45	143.74

Table 11 continued

Sample	E 33403/1-EC_MPLC-2/1	E 33404/1-EC_MPLC-1/1	E 33406/1-EC_MPLC-1/1	E 33407/1-EC_MPLC-1/1	E 33407/1-EC_MPLC-2/1	E 33409/1-EC_MPLC-1/1	E 33411/1-EC_MPLC-1/1	E 33411/1-EC_MPLC-2/1
Depth in m	3125.000 - 3125.200	3127.050 - 3127.100	3129.300 - 3129.350	3136.450 - 3136.550	3136.450 - 3136.550	3141.900 - 3142.000	3147.100 - 3147.200	3147.100 - 3147.200
C-org (%)	0.38	5.22	7.19	0.30	1.91	0.80	0.32	13.10
n-Alkanes	Concentration in microgram / gram C-org							
15	417.70	64.12	23.22	35.70	21.27	68.99	47.41	4.89
16	622.06	51.00	20.35	36.40	19.89	69.20	86.09	4.65
17	1032.12	65.84	27.48	36.09	21.11	77.18	106.55	4.40
18	1010.31	44.93	20.81	28.67	16.75	64.52	90.40	2.99
19	913.47	59.44	30.99	21.65	12.96	66.45	78.94	2.21
20	781.95	46.40	24.75	20.77	11.24	54.68	73.59	1.81
21	798.62	60.77	36.54	19.48	10.39	68.63	77.42	1.71
22	831.73	41.86	21.17	18.28	9.43	54.97	78.35	1.57
23	881.83	56.55	32.96	23.38	11.40	79.14	94.29	1.63
24	760.79	27.93	14.68	18.42	8.88	47.55	75.43	1.10
25	864.84	40.31	28.16	38.65	14.43	81.94	133.18	1.69
26	630.79	22.15	14.74	19.08	7.70	47.87	88.19	1.08
27	788.51	43.65	29.74	46.01	16.80	67.70	171.66	1.74
28	585.34	26.50	15.54	22.92	9.81	51.90	97.59	1.19
29	1150.16	62.02	35.62	53.28	26.48	71.68	174.77	2.29
30	782.13	24.78	14.70	19.43	7.90	57.58	88.92	0.98
31	787.94	38.18	20.69	25.00	48.26	77.65	127.34	1.75
32	948.83	27.93	15.88	18.47	15.76	47.44	79.09	3.67
33	670.21	51.14	22.42	38.75	11.01	21.60	144.50	16.52
34	-	-	-	-	-	-	-	-
35	-	-	-	-	-	-	-	-
36	-	-	-	-	-	-	-	-
Sum n-Alkanes	15259.34	855.52	450.44	540.43	301.48	1176.68	1913.70	57.86
Pristane	1532.93	179.15	64.16	103.44	58.97	204.26	190.82	6.12
Phytane	3705.20	243.53	100.70	168.37	70.77	477.19	346.02	9.77

Table 11 continued

Sample	E 33414/1-EC_MPLC-1/1	E 33418/1-EC_MPLC-1/1	E 33418/1-EC_MPLC-2/1	E 33421/1-EC_MPLC-1/1	E 33423/1-EC_MPLC-1/1	E 33424/1-EC_MPLC-1/1	E 33425/1-EC_MPLC-1/1	E 33427/1-EC_MPLC-1/1
Depth in m	3164.500 - 3164.520	3180.700 - 3180.950	3180.700 - 3180.950	3192.650 - 3192.700	3196.850 - 3196.900	3202.200 - 3202.250	3205.600 - 3205.650	3218.250 - 3218.300
C-org (%)	0.48	0.25	0.51	2.19	7.25	13.70	4.25	1.34
n-Alkanes	Concentration in microgram / gram C-org							
15	90.67	60.16	60.12	122.87	55.40	15.15	70.43	1040.93
16	75.76	50.84	41.46	75.42	36.90	12.18	52.56	1179.31
17	107.59	39.35	29.35	107.20	57.13	17.03	67.38	1334.59
18	83.20	25.31	17.21	76.28	41.22	12.19	50.28	1246.05
19	87.55	18.19	11.64	70.26	58.00	12.74	54.15	1182.32
20	72.33	14.42	9.77	51.53	41.01	9.61	38.01	1042.58
21	89.02	14.28	10.37	63.80	61.89	13.00	58.02	931.47
22	92.28	14.47	10.53	68.61	53.20	10.59	47.81	816.81
23	105.36	15.05	10.73	88.86	85.76	14.73	77.43	747.24
24	58.13	12.58	9.23	46.93	43.42	7.47	34.88	660.54
25	88.14	14.39	9.62	80.84	70.62	11.57	66.69	629.43
26	49.98	12.10	8.42	47.41	34.26	6.62	34.23	528.66
27	91.02	13.24	9.67	82.94	62.91	14.98	63.82	493.78
28	53.17	11.78	9.63	48.90	31.40	6.31	34.09	424.94
29	108.16	15.05	11.90	93.18	67.88	13.18	63.26	599.60
30	59.00	11.23	8.27	51.27	29.97	5.96	29.32	439.78
31	97.85	11.65	15.95	135.24	61.80	8.62	50.27	380.02
32	76.31	9.14	8.08	99.11	32.86	7.99	39.04	496.95
33	105.96	38.24	39.21	89.83	42.38	6.15	38.09	433.28
34	-	-	-	-	-	-	-	-
35	-	-	-	-	-	-	-	-
36	-	-	-	-	-	-	-	-
Sum n-Alkanes	1591.50	401.54	331.16	1500.48	968.01	206.08	969.75	14608.27
Pristane	181.30	36.15	29.69	154.26	134.16	51.83	131.96	595.97
Phytane	609.04	28.33	21.01	277.52	218.75	107.85	198.76	1297.63

Table 11 continued

Sample	E 33428/1- EC_MPLC-1/1
Depth in m	3230.750 - 3230.900
C-org (%)	0.29
n-Alkanes	Concentration in microgram / gram C-org
15	345.30
16	495.57
17	638.49
18	708.86
19	635.15
20	584.92
21	550.76
22	517.06
23	513.08
24	514.61
25	516.62
26	529.22
27	499.22
28	455.07
29	406.49
30	327.58
31	265.98
32	208.68
33	196.39
34	-
35	-
36	-
Sum n-Alkanes	8909.03
Pristane	183.63
Phytane	362.11

Table 11 continued

Sample	E 33430/1-EC_MPLC-1/1	E 33431/1-EC_MPLC-1/1	E 33431/1-EC_MPLC-2/1	E 33432/1-EC_MPLC-1/1	E 33433/1-EC_MPLC-1/1	E 33433/1-EC_MPLC-2/1	E 33433/1-EC_MPLC-3/1
Depth in m	4437.400 - 4437.450	4437.550 - 4437.650	4437.550 - 4437.650	4439.250 - 4439.300	4439.300 - 4439.450	4439.300 - 4439.450	4439.300 - 4439.450
C-org (%)	0.39	0.15	1.82	5.99	0.45	2.48	0.68
n-Alkanes	Concentration in microgram / gram C-org						
15	5.40	25.31	51.43	14.05	78.86	10.60	31.08
16	16.91	61.17	56.08	13.72	89.58	11.09	54.92
17	49.46	106.31	77.31	15.19	114.51	12.99	102.27
18	95.17	122.60	63.87	13.73	82.41	10.64	118.91
19	43.58	95.34	58.09	12.03	66.64	9.31	75.71
20	26.72	66.96	48.38	9.54	50.11	7.45	52.57
21	23.80	51.62	56.45	10.57	56.62	8.35	62.02
22	23.45	41.69	53.24	12.61	51.23	8.86	58.96
23	29.27	35.67	74.47	11.86	61.66	9.23	82.14
24	19.71	28.20	44.82	8.42	36.64	6.64	48.52
25	30.31	27.38	72.50	8.99	49.11	7.81	75.20
26	18.59	23.69	41.08	7.59	31.78	6.22	46.56
27	36.90	22.95	76.79	9.60	46.57	8.98	76.79
28	22.81	20.87	43.51	8.98	34.02	6.69	53.44
29	48.65	27.62	85.56	13.91	54.89	11.71	92.47
30	24.89	20.82	40.21	9.06	34.53	7.47	52.15
31	34.46	20.85	59.13	10.27	46.12	9.30	85.62
32	23.11	6.58	41.97	11.43	33.19	9.48	59.36
33	34.99	2.67	78.21	8.86	58.43	10.91	44.43
34	-	-	-	-	-	-	-
35	-	-	-	-	-	-	-
36	-	-	-	-	-	-	-
Sum n-Alkanes	608.19	808.31	1123.11	210.40	1076.88	173.71	1273.11
Pristane	39.19	71.86	117.95	79.92	132.76	41.60	83.11
Phytane	52.77	121.69	217.60	125.19	189.02	64.92	135.43

Table 11 continued

Sample	Well	Lithofacies	C34/(C33+C35)	C32 S/(S+R)	Tm/(Tm+Ts)
E 33353	17	Impregnated	0,72	0,44	0,74
E 33354	17	Laminite	0,61	0,16	0,93
E 33356/1	17	Mudstone	0,85	0,40	0,80
E 33356/2	17	Sol. Seam	0,78	0,31	0,87
E 33357/1	17	Mudstone	1,06	0,43	0,84
E 33357/2	17	Sol. Seam	0,74	0,52	0,73
Oil Well 17	17	E 33436	0,50	0,49	0,69
E 33363	4	Laminite	0,44	0,24	0,91
E 33366/2	4	Sol. Seam	0,51	0,52	0,95
E 33366/4	4	Shale	0,77	0,18	0,98
E 33369/2	4	Stylolite	1,93	0,26	0,91
E 33370	4	Impregnated	0,43	0,56	0,96
E 33371/2	4	Sol. Seam	1,35	0,35	0,77
E 33372/2	4	Laminite	0,41	0,23	0,94
E 33374	4	Impregnated	0,36	0,57	0,99
E 33376	8	Laminite	1,07	0,29	0,67
E 33377	8	Laminite	0,53	0,39	0,77
E 33381	8	Impregnated	0,65	0,46	0,66
E 33384	8	Laminite	0,70	0,49	0,66
E 33386	8	Impregnated	0,50	0,62	0,68
E 33388	8	Mudstone	1,48	0,45	0,81
E 33393/2	8	Laminite	0,56	0,48	0,68
E 33402	8	Shale	0,44	0,27	0,82
E 33403/2	8	Impregnated.	0,48	0,47	0,64
E 33404	8	Shale	0,57	0,18	0,87
E 33406	8	Shale	0,56	0,20	0,95
E 33407/2	8	Sol. Seam	0,81	0,34	0,89
E 33409	8	Laminite	0,88	0,31	0,83
E 33411/2	8	Shale	0,81	0,39	0,97
E 33414	8	Laminite	0,37	0,22	0,82
E 33418/1	8	Mudstone	1,07	0,18	0,93
E 33418/2	8	Sol. Seam	1,00	0,39	0,91
E 33423	8	Shale	0,46	0,15	0,92
E 33424	8	Shale	0,54	0,24	0,90
E 33427	8	Impregnated	0,72	0,52	0,71
Oil Well 8	8	E 33435	0,37	0,59	0,85
E 33430	24	Impregnated.	0,96	0,39	0,84
E 33431/1	24	Mudstone	1,28	0,37	0,92
E 33431/2	24	Stylolite	1,31	0,40	0,85
E 33432	24	Shale	0,50	0,20	0,95
E 33433/1	24	Mudstone	0,93	0,28	0,89
E 33433/2	24	Sol. Seam	0,57	0,22	0,99
E 33433/3	24	Impregnated.	0,54	0,40	0,89

Table 12: Biomarker ratios and percentual concentrations calculated from GC/MS results. Page 1

Sample	C35/C31-C35	C27 S/S+R	C28 S/S+R	C29 S/S+R	C27 aa/bb	DiaC27/Dia+reg
E 33353	0,10	0,29	0,18	0,24	0,32	0,24
E 33354	0,09	0,15	0,06	0,11	0,25	0,28
E 33356/1	0,07	0,35	0,29	0,30	0,61	0,34
E 33356/2	0,17	0,19	0,22	0,17	0,39	0,18
E 33357/1	0,08	0,24	0,17	0,28	0,40	0,18
E 33357/2	0,07	0,29	0,16	0,31	0,31	0,22
Oil Well 17	0,23	0,34	0,17	0,24	0,46	0,26
E 33363	0,06	0,19	0,07	0,14	0,50	0,37
E 33366/2	0,06	0,32	0,26	0,39	0,46	0,01
E 33366/4	0,04	0,16	0,15	0,12	0,09	0,10
E 33369/2	0,06	0,23	0,13	0,19	0,34	0,14
E 33370	0,15	0,35	0,31	0,39	0,49	0,00
E 33371/2	0,04	0,32	0,25	0,18	0,47	0,28
E 33372/2	0,26	0,14	0,08	0,10	0,15	0,30
E 33374	0,25	0,38	0,35	0,37	0,44	0,00
E 33376	0,10	0,22	0,07	0,16	0,12	0,09
E 33377	0,29	0,19	0,06	0,09	0,09	0,12
E 33381	0,05	0,28	0,11	0,19	0,25	0,21
E 33384	0,05	0,25	0,09	0,21	0,28	0,17
E 33386	0,18	0,26	0,15	0,19	0,20	0,24
E 33388	0,05	0,29	0,25	0,21	0,30	0,15
E 33393/2	0,18	0,27	0,14	0,19	0,38	0,17
E 33402	0,11	0,34	0,16	0,22	0,37	0,15
E 33403/2	0,18	0,24	0,13	0,19	0,07	0,23
E 33404	0,09	0,18	0,13	0,14	0,22	0,09
E 33406	0,06	0,20	0,03	0,08	0,15	0,11
E 33407/2	0,11	0,16	0,12	0,18	0,00	0,00
E 33409	0,06	0,21	0,10	0,15	0,24	0,14
E 33411/2	0,05	0,21	0,06	0,17	0,23	0,08
E 33414	0,26	0,20	0,01	0,12	0,15	0,11
E 33418/1	0,04	0,28	0,31	0,18	0,70	0,21
E 33418/2	0,15	0,20	0,16	0,12	0,28	0,07
E 33423	0,04	0,17	0,05	0,08	0,30	0,20
E 33424	0,05	0,20	0,10	0,23	0,45	0,16
E 33427	0,05	0,34	0,18	0,27	0,49	0,19
Oil Well 8	0,21	0,47	0,37	0,44	0,66	0,32
E 33430	0,11	0,20	0,16	0,24	0,35	0,27
E 33431/1	0,06	0,32	0,18	0,27	0,48	0,14
E 33431/2	0,04	0,23	0,18	0,26	0,40	0,12
E 33432	0,16	0,13	0,07	0,08	0,00	0,39
E 33433/1	0,08	0,17	0,16	0,18	0,29	0,24
E 33433/2	0,14	0,19	0,05	0,07	0,19	0,42
E 33433/3	0,26	0,14	0,10	0,09	0,16	0,30

Table 12: Biomarker ratios and percentual concentrations calculated from GC/MS results. Page 2

Sample	C28 aa/bb	C27a/C29a	Ster/Hop	C30 Hop/Gam
E 33353	0,49	0,61	0,43	0,47
E 33354	0,45	1,53	0,25	0,24
E 33356/1	0,68	1,19	1,71	0,08
E 33356/2	0,63	0,26	0,27	0,12
E 33357/1	0,64	0,49	0,26	0,21
E 33357/2	0,55	1,54	1,97	0,28
Oil Well 17	0,58	0,79	0,18	0,45
E 33363	0,70	2,24	0,99	0,19
E 33366/2	0,72	1,20	1,02	0,18
E 33366/4	0,51	3,95	0,17	0,36
E 33369/2	0,61	0,96	2,90	0,05
E 33370	0,72	0,65	0,10	0,30
E 33371/2	0,67	1,29	1,77	0,07
E 33372/2	0,48	1,26	0,12	0,05
E 33374	0,70	0,43	0,17	0,34
E 33376	0,47	3,64	4,51	0,38
E 33377	0,31	2,73	0,34	1,04
E 33381	0,44	1,50	2,90	0,30
E 33384	0,47	1,17	1,89	0,40
E 33386	0,44	0,75	0,30	0,28
E 33388	0,67	1,33	1,65	0,19
E 33393/2	0,49	0,79	0,25	0,39
E 33402	0,63	2,05	0,13	0,23
E 33403/2	0,44	0,70	0,33	0,53
E 33404	0,72	7,37	1,10	0,08
E 33406	0,75	5,64	0,09	0,15
E 33407/2	0,66	0,96	0,11	0,24
E 33409	0,64	1,36	0,24	0,40
E 33411/2	0,61	1,64	0,03	0,64
E 33414	0,60	2,23	0,24	0,12
E 33418/1	0,77	0,51	0,22	0,13
E 33418/2	0,62	0,70	0,15	0,06
E 33423	0,56	2,36	0,46	0,12
E 33424	0,62	1,37	0,25	0,13
E 33427	0,63	0,84	0,43	0,28
Oil Well 8	0,70	0,88	0,10	0,22
E 33430	0,59	0,68	0,08	0,20
E 33431/1	0,78	0,66	0,54	0,11
E 33431/2	0,70	1,74	0,63	0,17
E 33432	0,44	2,79	0,08	0,11
E 33433/1	0,65	1,03	0,15	0,24
E 33433/2	0,43	1,65	0,14	0,14
E 33433/3	0,51	1,20	0,24	0,08

Table 12: Biomarker ratios and percentual concentrations calculated from GC/MS results. Page 3

Sample	C30Hop/C27St	C27 %	C28 %	C29 %
E 33353	2,77	26,56	22,05	51,39
E 33354	3,33	39,44	23,80	36,76
E 33356/1	0,42	38,20	23,34	38,46
E 33356/2	7,21	16,95	11,09	71,96
E 33357/1	4,69	30,15	18,06	51,80
E 33357/2	0,44	44,84	27,91	27,24
Oil Well 17	5,03	28,51	19,98	51,51
E 33363	0,85	50,96	18,68	30,36
E 33366/2	0,66	50,71	14,86	34,43
E 33366/4	3,15	58,91	20,32	20,78
E 33369/2	0,26	38,43	13,83	47,75
E 33370	7,90	37,11	11,47	51,42
E 33371/2	0,40	35,25	14,09	50,67
E 33372/2	6,60	40,27	14,84	44,90
E 33374	5,89	25,72	12,96	61,32
E 33376	0,21	53,35	26,37	20,28
E 33377	4,32	34,81	39,94	25,26
E 33381	0,42	38,08	25,30	36,63
E 33384	0,59	38,90	22,61	38,49
E 33386	4,70	26,90	22,29	50,81
E 33388	0,67	41,18	16,51	42,31
E 33393/2	4,99	28,99	21,02	49,99
E 33402	6,57	44,43	22,27	33,31
E 33403/2	4,53	28,30	20,52	51,18
E 33404	0,31	74,35	12,98	12,67
E 33406	4,84	56,64	17,01	26,35
E 33407/2	12,47	40,82	20,80	38,38
E 33409	3,27	37,31	26,04	36,66
E 33411/2	21,40	34,97	38,83	26,20
E 33414	2,58	45,56	20,37	34,07
E 33418/1	3,55	20,44	18,71	60,84
E 33418/2	8,52	27,71	9,63	62,66
E 33423	0,94	45,53	14,28	40,18
E 33424	2,52	47,38	22,09	30,52
E 33427	2,53	33,00	18,13	48,87
Oil Well 8	7,27	36,13	20,17	43,71
E 33430	16,16	34,25	22,84	42,91
E 33431/1	1,67	31,49	11,51	56,99
E 33431/2	1,07	54,76	16,79	28,45
E 33432	6,68	52,77	14,52	32,70
E 33433/1	3,42	45,82	11,66	42,52
E 33433/2	5,57	32,38	15,98	51,64
E 33433/3	3,17	40,11	8,17	51,72

Table 12: Biomarker ratios and percentual concentrations calculated from GC/MS results. Page 4

E number	Well	Depth (m)	MNR	ENR	DNR	TNR	MPR	DPR	MPI I	MPI II	RC (%)	MDR	MDR 1	MDR 2,3	MDR 4
E 33354	17	1994,5	0,90	0,70	2,67	0,63	0,94	0,34	0,43	0,47	0,66	0,46	0,97	0,74	0,45
E 33357	17	2024,5	0,92	0,71	2,10	0,60	0,90	0,30	0,40	0,47	0,64	0,64	0,74	0,83	0,48
E 33363	4	2532,8	1,25	0,65	2,28	0,49	1,07	0,30	1,09	0,98	1,05	0,37	1,58	1,31	0,59
E 33371	4	2556,4	1,02	0,69	1,94	0,54	1,06	0,29	0,48	0,57	0,69	0,52	1,05	0,78	0,54
E 33384	8	3077,5	1,11	1,00	2,39	0,68	0,70	0,22	0,64	0,71	0,78	0,63	1,20	1,04	0,76
E 33402	8	3125,0	1,34	0,65	3,06	0,64	1,16	0,31	0,92	0,99	0,95	0,56	1,25	1,52	0,70
E 33424	8	3202,2	93,00	0,47	1,36	0,42	0,87	0,39	0,84	0,95	0,90	0,41	1,60	1,55	0,66
E 33431	24	4437,6	0,96	0,44	1,39	0,54	0,97	0,28	0,85	0,98	0,91	0,55	1,44	1,50	0,79
E 33432	24	4439,3	0,58	0,30	0,99	0,49	0,69	0,30	0,63	0,65	0,78	0,38	1,87	1,28	0,72

Table 13: aromatic maturity ratios of selected samples from all wells.

E Number	mple ty	TOC	S2	OI	Tmax	HI
		%	mg/g	CO2/g	°C	HC/g TOC
E 33366/4	Asphalt	61,1	785,8	18	409	1286
E 33427	Asphalt	61,0	651,9	8	424	1069
E 33435	Asphalt	65,3	493,7	2	436	756
E 33436	Asphalt	63,2	729,9	10	425	1155

Table 14: Organic carbon and selected Rock-Eval data of the asphaltene samples analysed.

E Number	C	H	N	O	S	S org	O/C	H/C	S/C	N/C
	%	%	%	%	%	%				
E 33427	73,20	7,50	0,80	2,90	9,40	9,40	0,03	1,23	0,05	0,0094
E 33435	77,10	6,90	1,00	1,70	10,50	10,50	0,02	1,07	0,05	0,0111
E 33436	73,90	7,60	0,80	2,00	10,20	10,20	0,02	1,23	0,05	0,0093

Table 15: Elemental composition of the asphaltene samples analysed.

E Number	Temp. range	C1-C5	C6-C14	C15+	n-Alkanes	Aromatics	Sulphur	S/C5+
		%	%	%	%	%	%	
E 33384	300-600	64,45	25,18	10,38	85,35	8,25	6,40	
E 33431/1	300-600	60,29	27,28	12,44	87,24	7,76	5,00	
E 33431/2	300-600	61,00	27,71	11,29	86,17	7,56	6,27	0,28
E 33366/4	300-600	65,70	26,80	7,50	81,76	8,29	9,95	0,35
E 33402	300-600	52,60	32,14	15,26	85,98	7,40	6,62	0,30
E 33424	300-600	60,44	26,32	13,24	78,49	8,79	12,72	0,41
E 33357/2	300-600	71,41	19,95	8,64	85,79	7,25	6,97	
E 33363	300-600	69,76	19,80	10,44	85,75	6,87	7,38	
E 33377	300-600	68,78	20,81	10,41	84,29	7,12	8,59	
E 33388	300-600	69,26	20,68	10,06	86,99	6,85	6,16	
E 33404	300-600	63,08	24,02	12,90	81,93	8,19	9,88	
E 33406	300-600	68,66	20,01	11,33	84,52	7,40	8,09	
E 33414	300-600	67,22	20,68	12,10	86,92	6,73	6,35	
E 33423	300-600	54,73	29,01	16,26	85,60	7,30	7,10	
E 33432	300-600	57,92	27,26	14,81	86,04	7,13	6,84	
E 33402 As	300-600	59,26	25,23	15,50	87,56	6,26	6,18	0,17
E 33366/4 As	300-600	57,04	31,25	11,71	84,76	8,15	7,09	0,19
E 33431/2 As	300-600	56,25	28,33	15,41	86,98	6,77	6,26	0,16
E 33424 As	300-600	61,14	27,05	11,81	83,19	9,24	7,57	0,23
E 33427 As	300-600	57,27	32,34	10,39	88,21	9,14	2,65	
E 33435 As	300-600	68,32	20,78	10,90	92,36	6,35	1,29	
E 33436 As	300-600	60,10	28,74	11,16	87,35	8,14	4,51	

Table 16: Alkane/alkene distribution and percentual yields of alkanes, aromatics and sulphur compounds of the Kerogen concentrates and asphaltenes (As) analysed by PyGC. S/C5+ shows ratios of sulphur compounds to C5+ compounds.

PyGC		
Sample	Resolved	Total
E 33357/2	0,59	0,20
E 33363	0,56	0,18
E 33366/4	0,55	0,16
E 33377	0,41	0,12
E 33384	0,69	0,21
E 33388	0,51	0,17
E 33402	0,56	0,16
E 33404	0,39	0,11
E 33406	0,40	0,12
E 33414	0,44	0,13
E 33423	0,36	0,11
E 33424	0,50	0,13
E 33431/1	0,64	0,22
E 33431/2	0,66	0,19
E 33432	0,42	0,12

Multistep PyGC			
Sample	Temp. (°C)	Resolved	Total
E 33366/4	300-375	0,32	0,10
	375-450	0,42	0,12
	450-600	1,66	0,66
E 33431/2	300-375	0,27	0,08
	375-450	0,48	0,13
	450-600	1,85	0,88
E 33384	300-375	0,31	0,08
	375-450	0,50	0,15
	450-600	1,92	0,98

Asphaltene PyGC		
Sample	Resolved	Total
E 33366/4	0,45	0,10
E 33431/2	0,48	0,11
E 33424	0,44	0,10

Asphaltene Multistep PyGC			
Sample	Temp. (°C)	Resolved	Total
E 33366/4	300-375	0,24	0,04
	375-450	0,35	0,08
	450-600	1,91	0,35
E 33431/2	300-375	0,22	0,04
	375-450	0,34	0,09
	450-600	1,41	0,42

MSSV Kerogen concentrates			
Sample	Temp. (°C)	Resolved	Total
E 33366/4	270	0,22	0,07
	290	0,20	0,07
	310	0,20	0,08
	330	0,23	0,11
	350	0,32	0,19

MSSV Asphaltenes			
Sample	Temp. (°C)	Resolved	Total
E 33366/4	270	0,17	0,06
	290	0,21	0,07
	310	0,23	0,09
	330	0,26	0,10
	350	0,32	0,18

Table 17: Gas/oil ratios of the samples analysed by PyGC, multistep PyGC and MSSV.

	TOC	CaCO3	S1	S2	S3	Tmax	PI	HI	OI
	%	%	mgHC/g	mgHC/g	mgCO2/g	°C		mgHC/gTOC	mg CO2/gTOC
Before OSHP	7,00	10,75	0,98	54,08	0,52	406	0,02	773	7
After OSHP	2,11	4,25	0,27	0,39	0,26	445	0,41	18	12

Table 18: Organic carbon, carbonate carbon and Rock-Eval data of the source rock sample prior and after Open System Hydrous Pyrolysis.

Experiment: R. di Primio		Start:	05.04.1995	08:34					
Sample:	Limestone								
Sample thickness	*11,5*	mm							
Sample diameter	28,5	mm							
Sample cross-section	6.379E-07	m²							
Temperature	*23*	°C	296,15	K					
Water viscosity	9,50E-01	cP	9,50E-04	Pa s					
Pressure difference	3.200E+03	Pa	32	bar					
Pressure gradient	2.783E+05	Pa/m							
Calculation of flowrate									
Start of exp.:	29. Sep 92	13:00				V			
Date	**Time**	**Volume / [ml]**	**Time [h]**	**Flow Rate/[m³/s]**	**Confining Pressure / [MPa]**	**Flux / [m/s]**	**Permeability/ [m²]**	**Darcy**	**nDarcy**
29. 09	13:00	0,80	0,0		6				
29. 09	17:20	1,70	4,3	5,76923E-11	6	9,04354E-08	**3,08592E-19**	3,09E-07	309
30. 09	8:50	5,20	19,8	6,2724E-11	6	9,83228E-08	**3,35506E-19**	3,36E-07	336
30. 09	10:50	5,50	21,8	4,16667E-11	6	6,53144E-08	**2,22872E-19**	2,23E-07	223
30. 09	14:20	5,90	25,3	3,1746E-11	6	4,97634E-08	**1,69807E-19**	1,70E-07	170
01. 10	7:45	7,00	42,8	1,75439E-11	6	2,75008E-08	**9,38408E-20**	9,38E-08	94
01. 10	12:15	7,30	47,3	1,85185E-11	10	2,90286E-08	**9,90542E-20**	9,91E-08	99
01. 10	17:00	7,50	52,0	1,16959E-11	10	1,83339E-08	**6,25605E-20**	6,26E-08	63
01. 10	20:00	7,50	55,0	0	10	0	**0**	0,00E+00	0
02. 10	8:15	8,00	67,3	1,13379E-11	10	1,77726E-08	**6,06454E-20**	6,06E-08	61

Table 19: Permeability data calculated in the course of the experiment at 23° and 84.5°C. Page 1

Experiment: R. di Primio		Start:	05.04.1995	08:34					
Sample:	Limestone								
Sample thickness	*11,5*	mm							
Sample diameter	28,5	mm							
Sample cross-section	6.379E-07	m²							
Temperature	*84,5*	°C	357,65	K					
Water viscosity	3,43E-01	cP	3,43E-04	Pa s					
Pressure difference	3.200E+03	Pa	32	bar					
Pressure gradient	2.783E+05	Pa/m							
Calculation of flowrate									
Start of exp.:	29. Sep 92	13:00		D		V			
Date	**Time**	**Volume / [ml]**	**Time [h]**	**Flow Rate/[m³/s]**	**Confining Pressure / [MPa]**	**Flux / [m/s]**	**Permeability/ [m²]**	**Darcy**	**nDarcy**
07.10.1992	9:40	0	0		10				
07.10.1992	16:10	0,45	6,5	1,92308E-11	10	3,01451E-08	3,71946E-20	3,72E-08	37
08.10.1992	8:05	1,82	22,4	2,39092E-11	10	3,74789E-08	4,62433E-20	4,62E-08	46
08.10.1992	17:00	2,85	31,3	3,20872E-11	10	5,02982E-08	6,20605E-20	6,21E-08	62
09.10.1992	8:10	4,75	46,5	3,47985E-11	10	5,45483E-08	6,73045E-20	6,73E-08	67
09.10.1992	8:15	0	0		10	0	0	0,00E+00	0
09.10.1992	14:00	0,84	5,8	4,05797E-11	10	6,36106E-08	7,8486E-20	7,85E-08	78
09.10.1992	15:30	1,00	7,3	2,96296E-11	10	4,64458E-08	5,73072E-20	5,73E-08	57

Table 19: Permeability data calculated in the course of the experiment at 23° and 84.5°C. Page 2

E 33365		320°C	300 bar	
Experiment #1				
	mg	Expulsion Efficiency (%)	Generated (mg)	Expelled (mg)
Soxhlet-Extract	57,06			
Upper reservoir	41,85	30,23	327,15	98,91
Lower reservoir	43,88			
E 33422/3		320°C	150 bar	
Experiment #2				
	mg	Expulsion Efficiency (%)	Generated (mg)	Expelled (mg)
Soxhlet-Extract	169,82			
Upper reservoir	1,37	1,59	172,56	2,74
Lower reservoir	1,37			
E 33422/4		320°C	500 bar	
Experiment #3				
	mg	Expulsion Efficiency (%)	Generated (mg)	Expelled (mg)
Soxhlet-Extract	54,74			
Upper reservoir	14,72	27,91	75,93	21,19
Lower reservoir	6,47			
E 33434/1		320°C	300 bar	
Experiment #4				
	mg	Expulsion Efficiency (%)	Generated (mg)	Expelled (mg)
Soxhlet-Extract	453,78			
Upper reservoir	73,61	13,96	527,39	73,61
E 33434/2		320°C	300 bar	
Experiment #5				
	mg	Expulsion Efficiency (%)	Generated (mg)	Expelled (mg)
Soxhlet-Extract	181,52			
Upper reservoir	366,92	66,90	548,44	366,92

Table 20: SOM yields generated and expelled during each high pressure high temperature experiment

		CPI 1	CPI 2	CPI 3	CPI 4	LHCPI	ISO 1	ISO 2	ISO 3
expelled oil E 33393		1,17	1,28	1,41	1,52	3,19	1,43	4,04	0,48
expelled oil E 33407		1,84	2,39	2,28	2,18	1,03	2,97	8,19	0,46
expelled oil E 33418		1,27	1,22	1,22	1,22	5,56	0,65	0,90	0,88
expelled oil E 33433		1,47	1,42	1,51	1,59	4,27	0,90	1,73	0,73
Oil Well 8	E 33435	0,98	0,97	0,99	1,03	29,89	0,80	1,99	0,52
Oil Well 17	E 33436	1,10	1,16	1,23	1,30	3,60	1,24	2,91	0,51

Table 21: CPI and ISO data of the calculated expelled oils as compared to data measured on the oils of wells 17 and 8. Column heading descriptions are given in table 10.

Peak identification of the steranes (m/z 217)

Peak	Compound
a	13β(H), 17α(H)-diacholestane (20S)
b	13β(H), 17α(H)-diacholestane (20R)
c	13α(H), 17β(H)-diacholestane (20S)
d	13α(H), 17β(H)-diacholestane (20R)
e	24-methyl-13β(H), 17α(H)-diacholestane (20S)
f	24-methyl-13β(H), 17α(H)-diacholestane (20R)
g	24-methyl-13α(H), 17β(H)-diacholestane (20S) + 14α(H), 17α(H)-cholestane (20S)
h	24-ethyl-13β(H), 17α(H)-diacholestane (20S) + 14β(H), 17β(H)-cholestane (20R)
i	14β(H), 17β(H)-cholestane (20S) + 24-methyl-13α(H), 17β(H)-diacholestane (20R)
j	14α(H), 17α(H)-cholestane (20R)
k	24-ethyl-13β (H), 17α(H)-diacholestane (20R)
l	24-ethyl-13α (H), 17β(H)-diacholestane (20S)
m	24-methyl-14α (H), 17α(H)-cholestane (20S)
n	24-ethyl-13α (H), 17β(H)-diacholestane (20R) + 24-methyl-14β (H), 17β(H)-cholestane (20R)
o	24-methyl-14β (H), 17β(H)- cholestane (20S)
p	24-methyl-14α (H), 17α(H)- cholestane (20R)
q	24-ethyl-14α (H), 17α(H)- cholestane (20S)
r	24-ethyl-14β (H), 17β(H)- cholestane (20R)
s	24-ethyl-14β (H), 17β(H)- cholestane (20S)
t	24-ethyl-14α (H), 17α(H)- cholestane (20R)

Peak identification of the hopanes (m/z 191)

Peak	Compound
A	18α(H)-Trisnorneohopane
B	17α(H)- Trisnorhopane
C	17α(H)-Norhopane
D	Normoretane
E	17α(H)-Hopane
F	Moretane
G	17α(H)-Homohopane (22S)
H	17α(H)-Homohopane (22R)
I	Homomoretane
J	17α(H)-Bishomohopane (22S and 22R)
K	17α(H)-Trishomohopane (22S and 22R)
L	17α(H)-Tetrakishomohopane (22S and 22R)
M	17α(H)-Pentakishomohopane (22S and 22R)
Gam	Gammacerane

7 Appendix 2

Plates 1 to 4

Plate 1a: Sample E 33365, Wackestone with solution seams, Well 4, 2538.40 m. Core of a typical wackestone with solution seams. Scale bar is in cm.

1b: Sample E 33376, laminite, Well 8, 3064.05 m. Core of a typical carbonate laminite. Scale bar is in cm.

1c: Sample E 33411, mudstone-shale contact, Well 8, 3147.10 m. Core showing the abrupt change from a pure carbonate mud to shale lithofacies. Scale bar is in cm.

1d: Sample E 33426, oil impregnated dolostone, Well 8, 3216.20 m. Core of one of the typical intraformational reservoir zones. Scale bar is in cm.

Plate 1

a

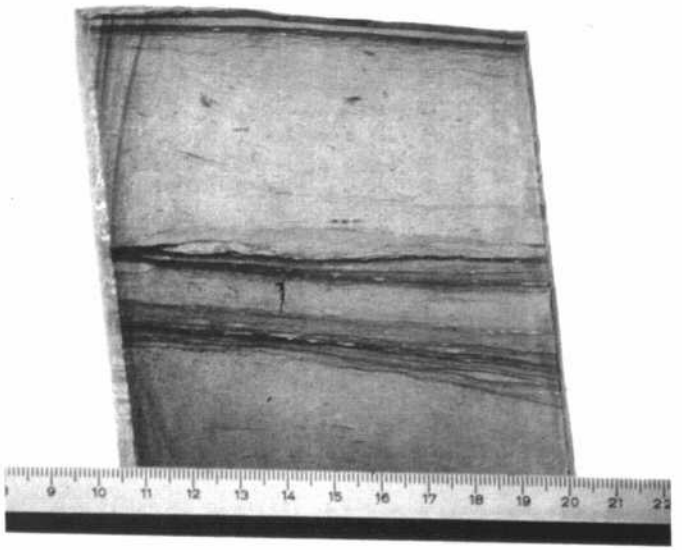

b

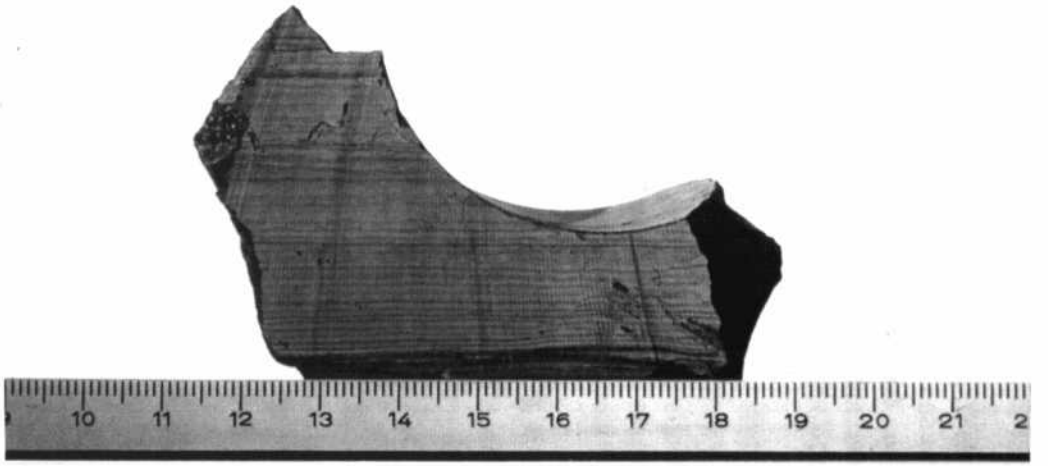

c

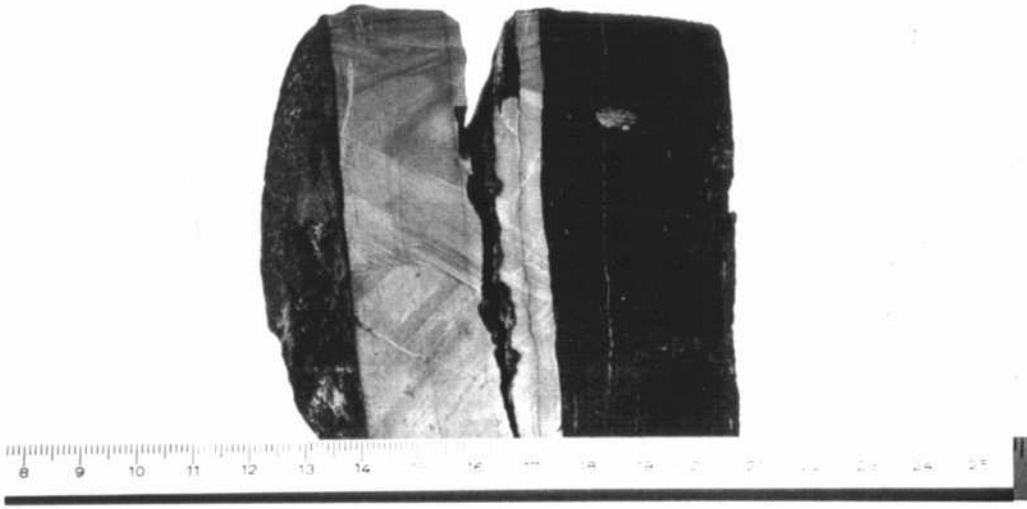

d

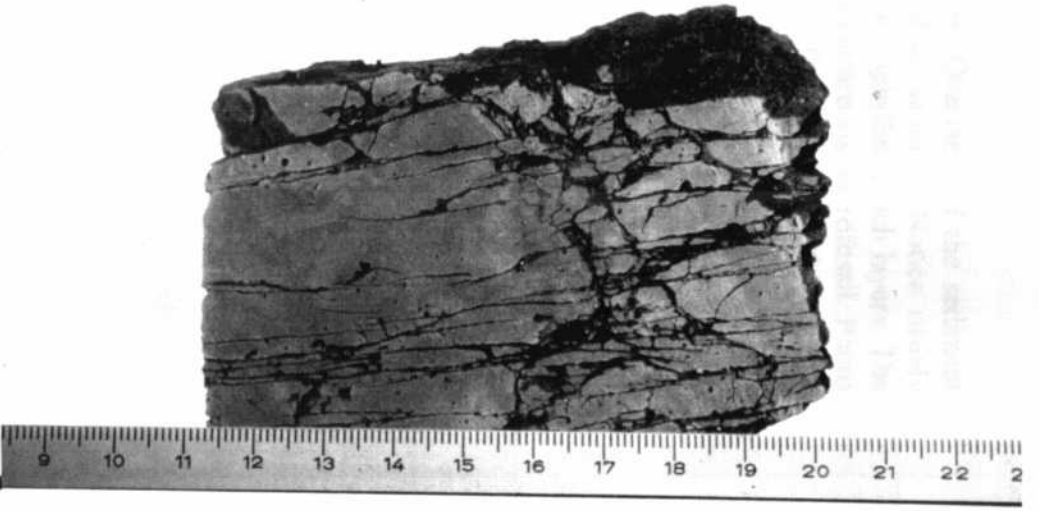

Plate 2a: Sample E 33411, shale lithofacies, Well 8, 3147.10 m. Overview of the sediment structure and typical fluorescence colours found in shale samples. Notice mainly yellow-brown bituminous groundmass and blood-red chlorophyllinite-rich layers. The green particle in the centre of the photomicrograph is a calcareous microfossil. Photo width corresponds to 1 mm. Whole rock polished section, fluorescence mode.

2b: Sample E 33401, shale lithofacies, Well 8, 3124.85 m. Detail of a thick chlorophyllinite-rich layer. In this photomicrograph the oxydised rims of the particle are clearly visible. Internal structure of the particle shows no recognisable characteristics which could be compared to known macerals. Photo width corresponds to 200 µm. Whole rock polished section, fluorescence mode.

2c: Sample E 33401, shale lithofacies, Well 8, 3124.85 m. Three individual algae are embedded in a yellow fluorescing groundmass, where liptodetrinite is quite common (lighter yellow colour). Photo width corresponds to 100 µm. Whole rock polished section, fluorescence mode.

2d: Sample E 33401, shale lithofacies, Well 8, 3124.85 m. In the upper right portion of this photomicrograph two blood-red fluorescing algae can be seen. Slightly left of the center an orange-yellow fluorescing sporinite is visible. Photo width corresponds to 100 µm. Whole rock polished section, fluorescence mode.

2e: Sample E 33402, shale lithofacies, Well 8, 3124.95 m. Fibrous structures resembling those observed in the sediment (plate 2b) but with clearly darker fluorescence colours can be seen in this photo. White and green fluorescence colours are characteristic of the epoxy resin used. Photo width corresponds to 200 µm. Extracted kerogen concentrate, polished section, fluorescence mode.

2f: Sample E 33402, shale lithofacies, Well 8, 3124.95 m. Detail of the fibrous structures mentioned above. Notice similar distribution of lighter fluorescence colours as in the chlorophyllinite-rich particle of plate 2b. White and green fluorescence colours are characteristic of the epoxy resin used. Photo width corresponds to 200 µm. Extracted kerogen concentrate, polished section, fluorescence mode.

2g: Sample E 33424, shale lithofacies, Well 8, 3202.20 m. Semifusinite particle embedded in a chlorophyllinite-rich laminae. Photo width corresponds to 100 µm. Whole rock polished section, fluorescence mode.

2h: Sample E 33424, shale lithofacies, Well 8, 3202.20 m. Semifusinite particle embedded in a chlorophyllinite-rich laminae. Photo width corresponds to 100 µm. Whole rock polished section, reflected white light.

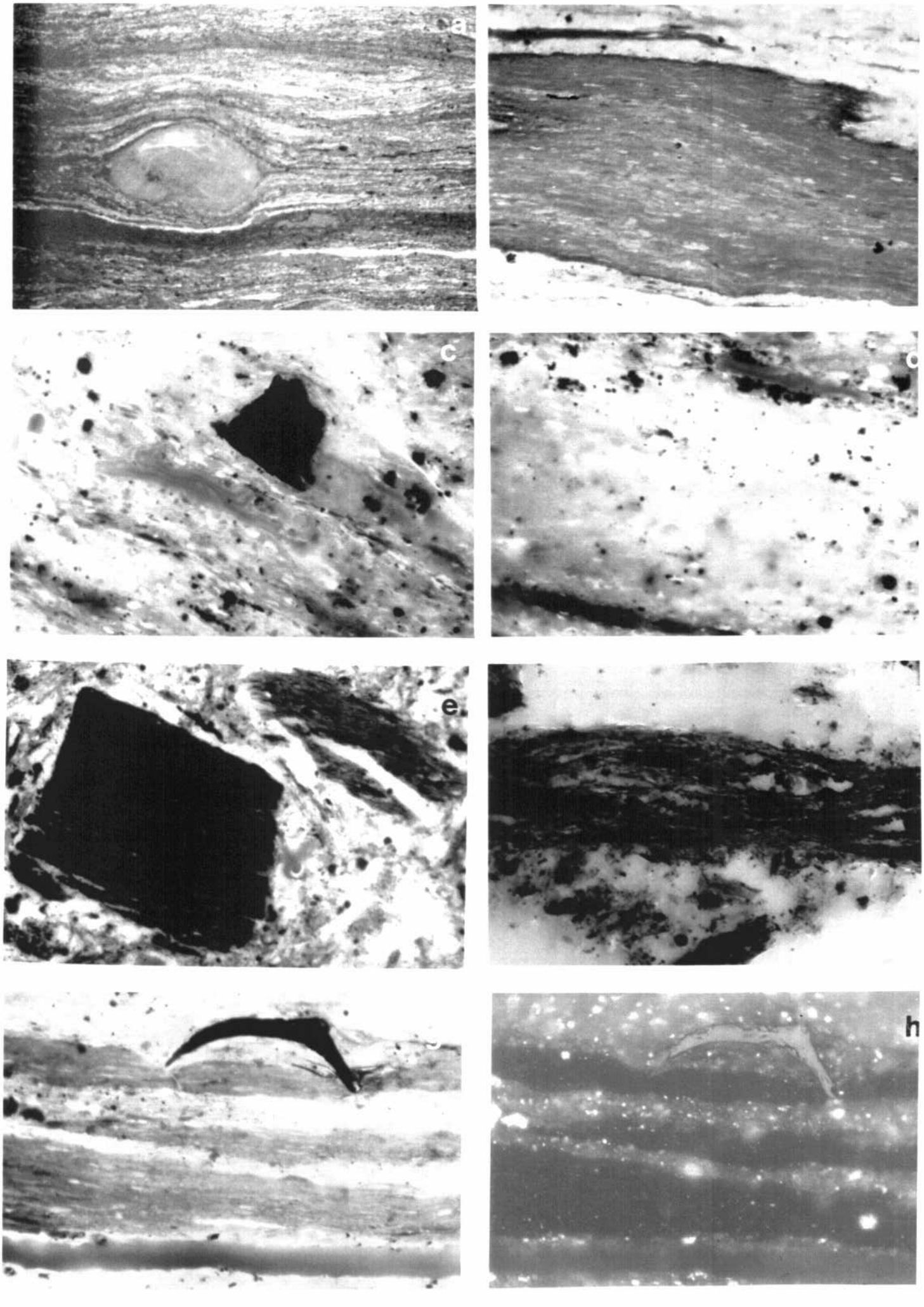

Plate 2

Plate 3a: Sample E 33357/2, solution seam, well 17, 2024.40 m. Two solution seams at the bottom of this photograph are cut by a clacite healed fracture (left). Several oil impregnated fractures originate in the upper solution seams. Red colour is due to thin section staining. Photo width corresponds to 1 mm. Whole rock polished thin-section, transmitted white light.

3b: Sample E 33418/2, solution seam, well 8, 3180.70 m. Several oil impregnated fractures originate in the thick solution seam on the left side of the photograph and cross through the carbonate matrix. Photo width corresponds to 500 µm. Whole rock polished section, fluorescence mode.

3c: Sample E 33416, solution seam, Well 8, 3174.30 m. The solution seam on the left side of this picture was cut by a calcite healed fracture. The fracture wall is impregnated by bright yellow fluorescing hydrocarbons. Photo width corresponds to 1 mm. Whole rock polished section, fluorescence mode.

3d: Sample E 33401, shale lithofacies, Well 8, 3124.85 m. Bitumen filled fractures in a shale sample. Photo width corresponds to 1 mm. Whole rock polished section, fluorescence mode.

3e: Sample E 33401, shale lithofacies, Well 8, 3124.85 m. Bitumen impregnated fracture leading to the porous zone of plate 3d. Photo width corresponds to 200 µm. Whole rock polished section, fluorescence mode.

3f: Sample E 33433/3, mudstone with clay flakes, Well 24, 4439.30 m. This sample was impregnated with the crude oil produced from well 17 during the experiment. The oil intruded from the top border of the sample shown in the upper part of the photomicrograph along the, now fluorescing, fractures and clay flakes. The oil impregnation reached the lower border of the photograph (half the sample thickness) after 3 days. Photo width corresponds to 4 mm. Whole rock polished section, fluorescence mode.

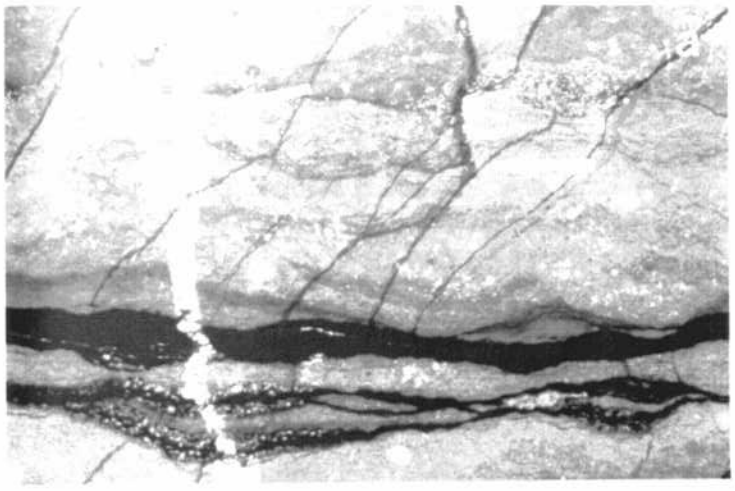

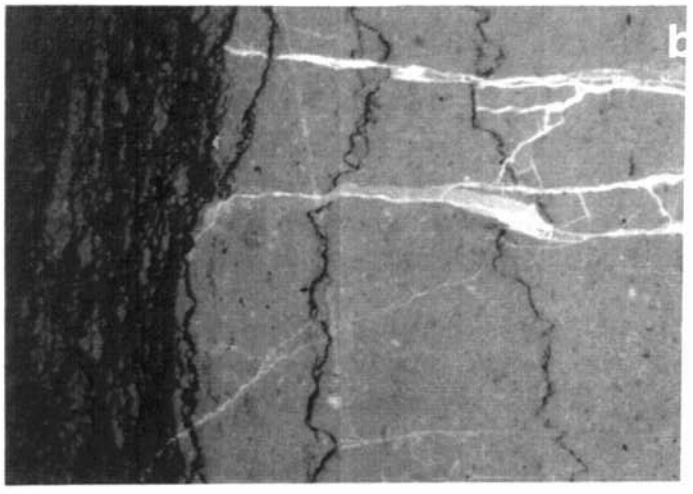

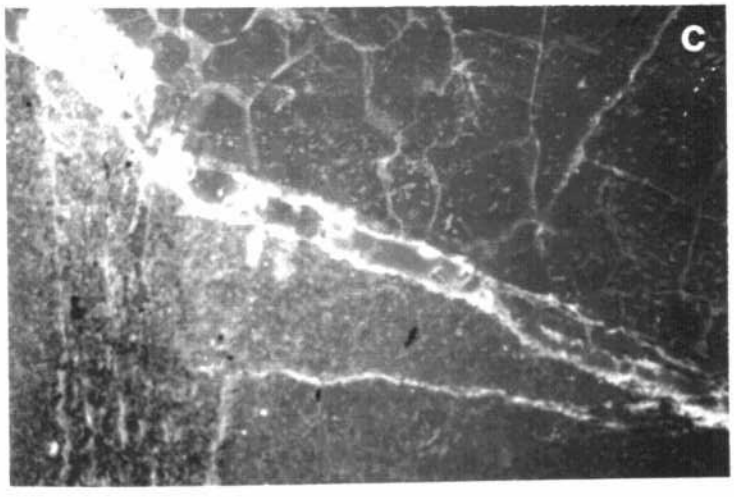

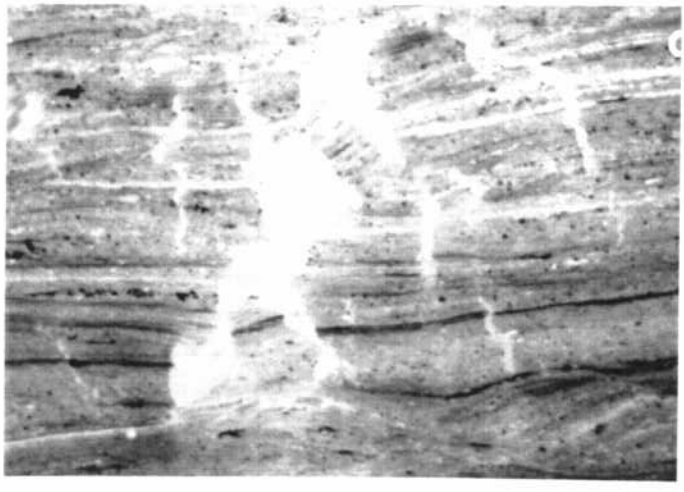

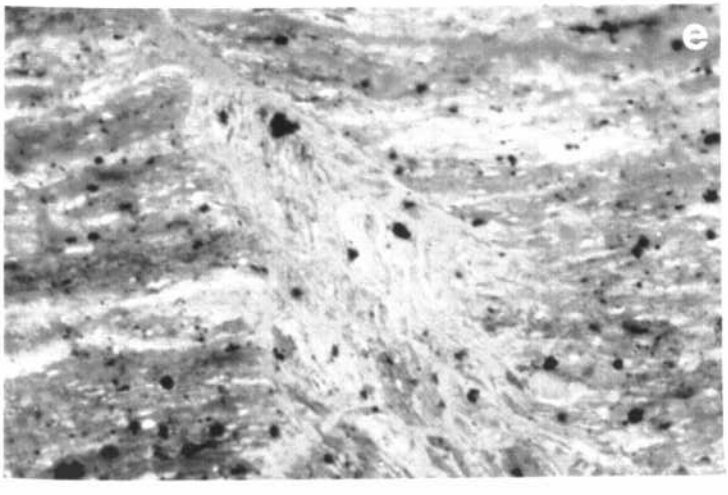

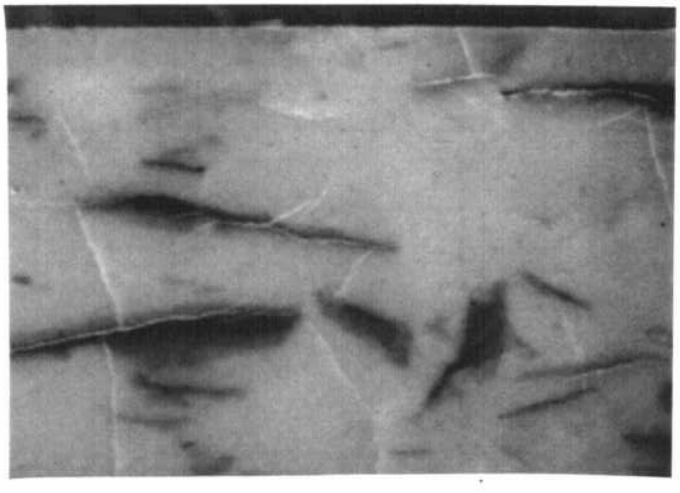

Plate 3

Plate 4a: Sample E 33422/3, solution seam, Well 8, 3194.50 m. Yellow fluorescing bitumen in one of the solution seams and staining a microfracture in the adjoining mudstone. Photo width corresponds to 4 mm. Whole rock polished section, fluorescence mode.

4b: Sample E 33422/4, solution seam, Well 8, 3194.50 m. Same organic rich layer as in plate 4a, but now in the centre of the sample. No fluorescence is noticeable. Photo width corresponds to 1 mm. Whole rock polished section, fluorescence mode.

4c: Sample E 33434/1, stylolites and solution seams connected by a vertical fracture, Well 24, 4440.30 m. Oil stained calcite healed fracture after the generation and expulsion of hydrocarbons during experiment # 4. Photo width corresponds to 4 mm. Whole rock polished section, fluorescence mode.

4d: Sample E 33422/4, solution seam, Well 8, 3194.50 m. Organic rich layer at the border of the sample which was in direct contact to the reservoir during the experiment. Notice yellow fluorescence and horizontal fractures in the layer. Photo width corresponds to 1 mm. Whole rock polished section, fluorescence mode.

4e: Sample E 33434/2, shale lithofacies, Well 24, 4441.30 m. This sample was analysed microscopically before the HPHT experiment # 5 and was characterised by yellow to red fluorescing organic matter concentrated in the intergranular space of the sample. Photo width corresponds to 500 µm. Whole rock polished section, fluorescence mode

4f: Sample E 33434/2, shale lithofacies, Well 24, 4441.30 m. After experiment # 5 no fluorescing organic matter can be observed in the sample. Photo width corresponds to 500 µm. Whole rock polished section, fluorescence mode.

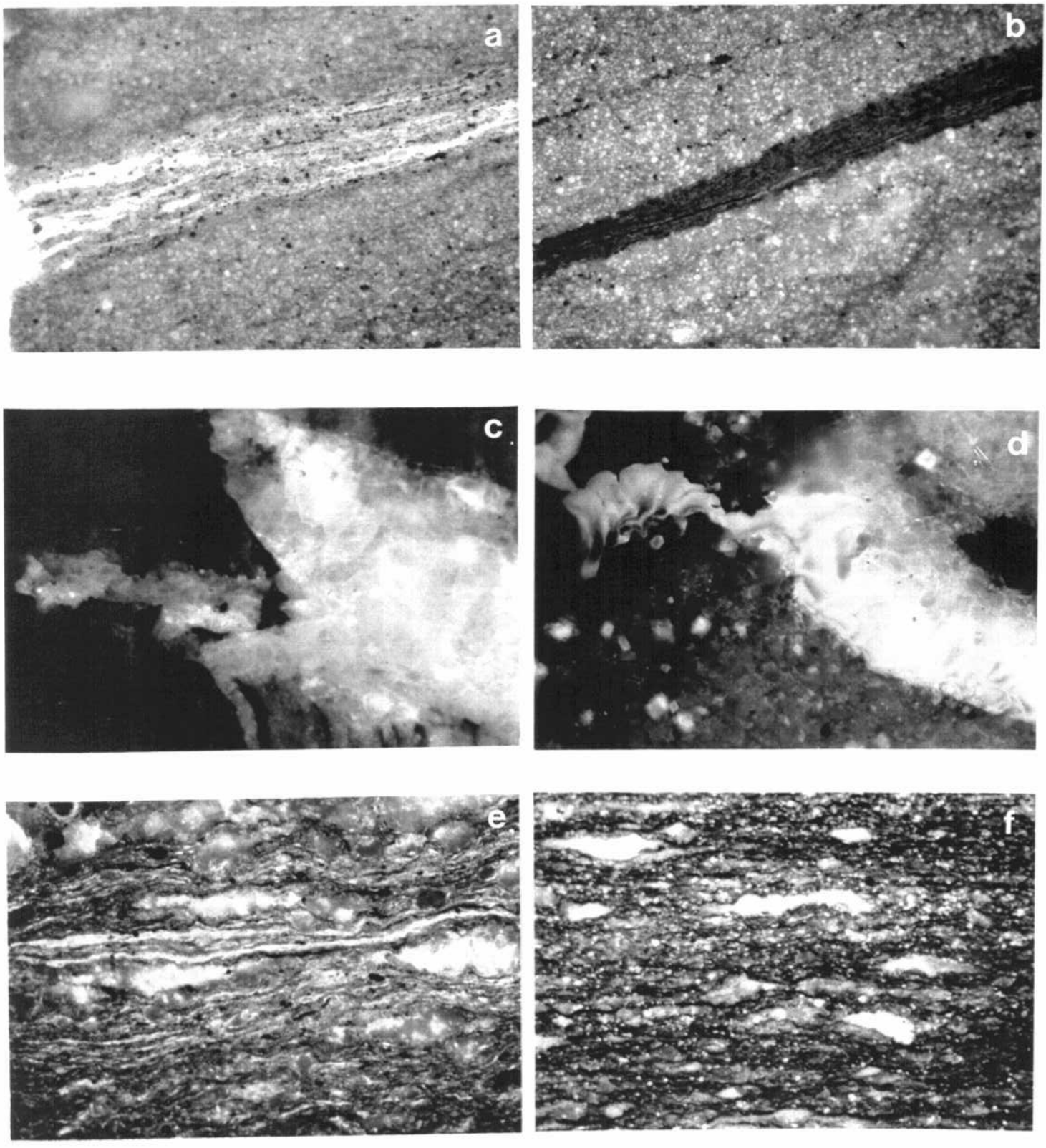

Plate 4

FORSCHUNGSZENTRUM JÜLICH GmbH

KFA

Jül-3110
September 1995
ISSN 0944-2952